Numerical Model of Interaction and Behavior of Short Span High Speed Rail Bridge on Viscoelastic Supports

BY

SAID IBRAHIM NOUR
B.Eng., Ryerson Polytechnic University, Toronto, Ontario, Canada, 1998
M.S., University of Windsor, Windsor, Ontario, Canada, 2001

DISSERTATION

Submitted as partial fulfillment of the requirements
for the degree of Doctor of Philosophy in Civil Engineering
in the Graduate College of the
University of Illinois at Chicago, 2016

Chicago, Illinois

Defense Committee:

Dr. Mohsen A. Issa, Chair and Advisor, Civil and Materials Engineering
Dr. Alexander Chudnovsky, Civil and Materials Engineering
Dr. Craig D. Foster, Civil and Materials Engineering
Dr. Krishna R. Reddy, Civil and Materials Engineering
Dr. Ahmed A. Shabana, Mechanical and Industrial Engineering

DEDICATION

In memory of my mother HAWA HASSAN GALEB

~ R.I.P ~

ACKNOWLEDGMENTS

I would like to extend my thanks to the National University Rail Center (NURail) for the partial sponsor of this research.

I am deeply grateful to Professor Mohsen A. Issa for his valuable guidance throughout this research. I am particularly thankful for the professor's wise advices in academic, professional and personal matters. Without his constant support this work would not have been possible. I would also like to thank the members of the committee: Professor Craig Foster, Professor Krishna Reddy, Professor Ahmed Shabana and professor Chudnovsky; their patience and advice are greatly appreciated.

I would like to thank also the following colleagues for their assistance and thoughtful discussions: Ibrahim Lotfi, Maen Farhat, Mustafa Al-Obadi, Mustafa Ibrahim, Aiman Shibli and Momenur Rahman. Thank you all.

I am grateful to University of Illinois at Chicago, Department of Civil and Materials Engineering, to the faculty, staff and students for their teaching, help and cooperation. I would like to particularly thank Sara Arevalo, the Graduate Program Coordinator, for her professionalism and assistance throughout the years of my studies at the University.

Lastly, I would like to extent my gratitude to my family and friends for their encouragement, support and patience over the years.

Said Ibrahim Nour

CONTRIBUTION OF AUTHORS

Chapter 3 includes parts of a previously published conference paper (Nour and Issa, 2016) for which I was the primary author. My research advisor, Dr. Mohsen A. Issa, contributed to the writing of the paper. Chapter 4 includes parts of a previously published conference paper (Nour and Issa, 2015) for which I was the primary author. My research advisor, Dr. Mohsen A. Issa, contributed to the writing of the paper.

TABLE OF CONTENTS

CHAPTER PAGE

1 INTRODUCTION 1
1.1 Background 1
1.2 Research Motivation 5
1.3 Research Objectives and Scope 8
1.4 Dissertation Outline 9

2 STATE OF THE ART 10
2.1 Historical Background 10
2.2 Relevant Contributions of Previous Researchers 15
2.3 Train-Track-Bridge System Identification and Modelling 20
2.3.1 Bridge modelling 21
2.3.2 Railway track structure 24
2.3.2.1 Characteristics of ballasted track 24
2.3.2.1.1 Rails 25
2.3.2.1.2 Railway fastening systems 27
2.3.2.1.3 Sleepers/crossties 28
2.3.2.1.4 Ballast materials 29
2.3.2.2 Characteristics of ballastless track 30
2.3.3 Modeling of ballasted track-bridge system 32
2.3.4 Modeling of ballastless track-bridge system 37
2.3.5 Railway track irregularities 37
2.3.6 Train vehicle modelling 38
2.3.6.1 Moving force models 38
2.3.6.2 Moving mass models 40
2.3.6.3 Moving sprung mass models 41
2.3.6.4 Moving system models 42
2.3.7 Solution methods of vehicle-track-bridge interaction problems 44
2.3.7.1 Iterative solution method 45
2.3.7.2 Dynamic condensation method 48
2.3.7.3 Direct solution method 50
2.4 Review of International Codes and Standards 53
2.4.1 Requirements for dynamic analysis 54
2.4.2 Requirements for dynamic models 59
2.4.2.1 Train and load models 60
2.4.2.2 Bridge models 64
2.4.2.3 Track models 66
2.4.3 Serviceability limit state criteria 67

3 NUMERICAL MODEL OF A TRAIN-TRACK-BRIDGE INTERACTION 69
3.1 Introduction 69
3.2 Mathematical Formulation of the Train-Track-Bridge Interaction Problem 72
3.2.1 Equations of motion of the vehicle subsystem 75

TABLE OF CONTENTS (Continued)

CHAPTER		PAGE
3.2.2	Equations of motion of the track-bridge subsystem	81
3.2.3	Equations of the random vertical track irregularities	85
3.3	Numerical Integration Method	91
3.4	Solutions of the Train-Track-Bridge Interaction Problem	94
3.4.1	Solutions of the vehicle responses and contact forces	95
3.4.2	Constraint equations at the contact points	99
3.4.3	Solutions of the coupled track-bridge problem	104
3.5	Working Procedure of Dynamic Simulation	105
3.6	Model Verifications by Numerical Examples	107
3.6.1	Verification by semi-analytical method	108
3.6.2	Verification by finite element method with results in literature	110
4	**INVESTIGATION OF NATURAL FREQUENCIES**	114
4.1	Introduction	114
4.2	Effects of Bridge Support Vertical Stiffness	115
4.2.1	Case of simply supported Euler-Bernoulli beam	117
4.2.2	Case of elastically supported Euler-Bernoulli Beam	118
4.2.2.1	Development of empirical equations	119
4.2.3	Case of elastically supported Timoshenko beam	122
4.2.3.1	Fundamental frequency of elastically supported Timoshenko beam	125
4.3	Natural Frequency of Ballasted Track-Bridge System	130
4.4	Vibration Mode Shapes of Elastically Supported Bridge	136
4.5	Natural Frequency of Bridge with Vertical and Rotational Springs	138
4.6	Concluding Remarks	141
5	**NUMERICAL STUDIES OF SHORT SPAN HIGH SPEED RAIL BRIDGES**	142
5.1	Dynamic Simulation Methodology	142
5.2	Description of Study Cases	145
5.2.1	Bridge models	145
5.2.2	Track structure	150
5.2.3	Real high speed trains models	151
5.3	Effects of Shear Deformations and Rotational Inertia on Bridge Response	157
5.4	Effects of Vehicle Interaction and Track Structure	161
5.5	Conditions of Resonance and Effects of Service Speed	163
5.6	Effects of Track Vertical Stiffness and Damping	167
5.6.1	Bridge dynamic responses	167
5.6.2	Track dynamic responses	169
5.6.3	Vehicle dynamic responses	170
5.7	Influence of Different Trainsets on Bridge and Vehicle Responses	171
5.8	Effects of Track Irregularities on Bridge and Vehicle Responses	173

TABLE OF CONTENTS (Continued)

CHAPTER PAGE

5.9 Influence of Elastic Boundary Conditions on Dynamic Responses 176
5.9.1 Case of free end rotations with no damping at bridge supports.....177
5.9.2 Case of partial end rotations with no damping at bridge supports.....179
5.9.3 Case of fixed end rotations with no damping at bridge supports.....181
5.9.4 Case of free rotation with very soft springs and damping at supports.....184
5.9.5 Case of partial rotation with very soft springs and damping at supports.....186
5.9.6 Case of free rotation with soft springs and damping at supports.....188
5.9.7 Case of partial rotation with soft springs and damping at supports.....190

6 CONCLUSIONS 192
6.1 General Conclusions 192
6.2 Practical Recommendations.....200
6.3 Suggestions for Further Research 202

CITED LITERATURE 204

APPENDICES.....213
Appendix A.....214
Appendix B 218

VITA.....219

LIST OF TABLES

TABLE PAGE

I TYPICAL RAILS MATERIAL PROPERTIES....27

II TRACK PROPERTIES OF SINGLE-LAYER CONTINUOUS MODEL....34

III TRACK PROPERTIES OF TWO-LAYER DISCRETE MODEL....35

IV TRACK PROPERTIES OF THREE-LAYER DISCRETE MODEL....36

V MAXIMUM VALUE $(v/n_0)_{lim}$ FOR BEAM OR PLATE ON SIMPLE SUPPORTS AND WITH A MAXIMUM PERMISSIBLE ACCELERATION SMALLER THAN 3.50 m/s^2....57

VI MAXIMUM VALUE $(v/n_0)_{lim}$ FOR BEAM OR PLATE ON SIMPLE SUPPORTS AND WITH A MAXIMUM PERMISSIBLE ACCELERATION SMALLER THAN 5 m/s^2....58

VII HSLM-A HIGH SPEED TRAIN LOAD MODEL....61

VIII DAMPING VALUES FOR DESIGN PURPOSES....65

IX TRACK-BRIDGE SUBSYSTEM PARAMETERS NOTATIONS....74

X TRACK CLASS QUALITY AND SPEED LIMITS....86

XI TRACK CLASS ROUGHNESS PARAMETERS AND QUALITY....88

XII TRACK IRREGULARITIES MODEL PARAMETER VALUES....89

XIII PROPERTIES OF VEHICLE IN MODEL VERIFICATION....107

XIV PROPERTIES OF BRIDGE IN MODEL VERIFICATION....108

XV PROPERTIES OF TRACK IN MODEL VERIFICATION....108

XVI VALUES OF $f_n(\kappa)$ FOR FIRST SIX NATURAL FREQUENCIES OF ELASTICALLY SUPPORTED EULER-BERNOULLI BEAM....119

XVII PROPERTIES OF LOW MASS SHORT SPAN RAILWAY BRIDGES....145

XVIII PROPERTIES OF MODIFIED ERRID D214 BRIDGE PROTOTYPES....146

XIX FREQUENCY, SLENDERNESS AND DAMPING OF BRIDGE MODELS....147

LIST OF TABLES (Continued)

TABLE PAGE

XX PROPERTIES OF THE AREMA RE141 RAIL AND TRACK MODEL.....150

XXI HIGH SPEED TRAINS DISTRIBUTED TRACTION CONFIGURATION 152

XXII PROPERTIES OF HIGH SPEED TRAIN MOTORIZED COACHES.....153

XXIII PROPERTIES OF HIGH SPEED TRAIN TRAILER COACHES 154

XXIV AXLE DISTANCE FROM THE FRONT AXLE (INCHES).....155

XXV AXLE DISTANCE FROM THE FRONT AXLE (METERS).....156

LIST OF FIGURES

FIGURE		PAGE
1.1	Japan High Speed Rail Network Map	2
1.2	Europe High Speed Rail Network Map	3
1.3	Chinese High Speed Rail Network Map	4
1.4	United States Planned High Speed Rail Map	5
2.1	View of River Dee bridge collapse	11
2.2	Early theoretical model of a locomotive over ballasted bridge	14
2.3	Elastic supports of a bridge	22
2.4	Triangular falsework system	22
2.5	Double beam system	23
2.6	Double string system	23
2.7	Ballasted track	24
2.8	Typical flat-bottomed UIC 60 rail used in high speed line	25
2.9	Sketches of AREMA 136RE (left) and 141RE (right) rail profiles	26
2.10	Fastening systems: rubber rail pad (top left), Pandrol Fastclip (top right), Vossloh Clip (bottom left), Pandrol Clip (bottom right)	28
2.11	Monoblock crosstie (left), twin-block concrete crosstie (right)	29
2.12	Typical Rheda 2000® ballastless track	31
2.13	Continuous single-layer model with distributed vertical spring-dampers	33
2.14	Continuous single-layer model with vertical and horizontal spring-dampers	33
2.15	Two-layer discrete model for ballasted track-bridge system	35
2.16	Three-layer discrete model for ballasted track-bridge system	36

LIST OF FIGURES (Continued)

FIGURE		PAGE
2.17	Schematic of a ballastless track model	37
2.18	Vertical profile of track irregularities	38
2.19	Moving force model	39
2.20	Moving mass model	40
2.21	Moving sprung mass model	41
2.22	Two-dimensional 10-DOF train vehicle model	43
2.23	Three-dimensional 27-DOF train vehicle model	44
2.24	Vehicle-bridge interaction element without pitching effect	48
2.25	Vehicle-bridge interaction element with pitching effect	49
2.26	Vehicle-bridge interaction model with higher degree of complexity	50
2.27	Vehicle-structure interaction: (a) schematic and (b) free body diagram	51
2.28	Flow chart for dynamic analysis requirement check	55
2.29	Limits of first natural frequency in relation to span length	56
2.30	Types of high speed trains according to Eurocode 1	60
2.31	HSLM-B high speed train load model	62
2.32	Number of N points forces and d spacing of HSLM-B model	63
2.33	Train model according to European Code	63
2.34	Additional damping to account for effects of vehicle-bridge interaction	66
2.35	Dynamic train-track-bridge model	67
2.36	Maximum allowable vertical deflection of bridge corresponding to a vertical Acceleration in the vehicle of 1 m/s^2	68

LIST OF FIGURES (Continued)

FIGURE		PAGE
3.1	Vehicle-track-bridge interaction model	72
3.2	Ten degrees of freedom of the train vehicle	75
3.3	Free-body diagram of train vehicle	76
3.4	Finite element of track-bridge subsystem	82
3.5	Sample of random vertical track irregularity profile, N=2000	90
3.6	1st order derivative of random vertical track irregularity profile, N=2000	91
3.7	2nd order derivative of random vertical track irregularity profile, N=2000	91
3.8	Train-track-bridge interaction elements	99
3.9	Results comparison of vehicle carbody vertical responses: deflection (left), acceleration (right)	109
3.10	Results Comparison of bridge mid-span vertical responses: deflection (left), acceleration (right)	110
3.11	Result comparisons of vehicle carbody vertical displacement: present study results (left graph); reference model results (right graph)	111
3.12	Result comparisons of vehicle carbody vertical acceleration: present study results (left graph); reference model results (right graph)	111
3.13	Result comparisons of bridge vertical displacement: present study results (left graph); reference model results (right graph)	112
3.14	Result comparisons of bridge vertical acceleration: present study results (left graph); reference model results (right graph)	112
3.15	Results comparison for track vertical displacement: present study results (left graph); reference model results (right graph)	113
4.1	Elastically supported beam	116
4.2	Plots of $f_n(\kappa)$ for the first six natural frequencies of Euler-Bernoulli beam	120

LIST OF FIGURES (Continued)

FIGURE PAGE

4.3 Ratio R of fundamental frequency for elastically supported Timoshenko beam with $\gamma = 1$ 126

4.4 Ratio R of fundamental frequency for elastically supported Timoshenko beam with $\gamma = 2$ 126

4.5 Ratio R of fundamental frequency for elastically supported Timoshenko beam with $\gamma = 3$ 127

4.6 Ratio R of fundamental frequency for elastically supported Timoshenko beam with $\gamma = 4$ 127

4.7 Ratio R of fundamental frequency for elastically supported Timoshenko beam with $\gamma = 5$ 128

4.8 Density plot of ratio R as a function of κ and ϕ 129

4.9 Contour plots of ratio R as a function κ and ϕ 130

4.10 Ballasted track-bridge system with vertical flexible supports 131

4.11 Fundamental frequency of elastically supported Bernoulli type of bridge: (a) $\bar{R}$ values for low mass ratio; (b) $\bar{R}$ values for high mass ratio 134

4.12 Fundamental frequency of elastically supported Timoshenko type of bridge: (a) $\bar{\bar{R}}$ values for low mass ratio; (b) $\bar{\bar{R}}$ values for high mass ratio....135

4.13 Plots of 1st mode shape for different ratios of κ....136

4.14 Plots of 2nd mode shape for different ratios of κ....137

4.15 Plots of 3rd mode shape for different ratios of κ 137

4.16 Bridge with vertical and rotational spring supports....138

4.17 Frequency ratio R_{ω_1} for bridge with vertical and rotational spring supports 140

5.1 Frequency (left) and mass (right) versus span length of group A bridges....148

5.2 Frequency (left) and mass (right) versus span length of group B bridges....148

5.3 Typical EMU high speed train with 8-car convoy configuration 151

LIST OF FIGURES (Continued)

FIGURE PAGE

5.4 Effects of Shear deformations and rotational inertia on mid-span acceleration of simply supported Group A (a-f) and Group B (g-l) bridge models.....158

5.5 Effects of Shear deformations and rotational inertia on mid-span deflection of simply supported Group A (a-f) and Group B (g-l) bridge models.....159

5.6 Ratio R_y of bridge mid-span static deflection for different shear factors k_s.....160

5.7 Mid-span vertical deflections of simply supported bridges B1 through B6 162

5.8 Mid-span vertical accelerations of simply supported bridges B1 through B6...163

5.9 Mid-span vertical acceleration time-histories of bridge models B1, B2, B4 and B5 due to ICE-3 running at service and resonance speeds 164

5.10 Mid-span vertical deflection time-histories of bridges B1 (top), B2 (middle) and B4 (bottom) due to ICE-3 train running at crawling and service speeds....166

5.11 Effects of track Low Stiffness (LS), Low Damping (LD), High Stiffness (HS) and High Damping (HD) on vertical deflections of bridges B1 through B6.....168

5.12 Effects of track Low Stiffness (LS), Low Damping (LD), High Stiffness (HS) and High Damping (HD) on rail accelerations of bridges B1 through B6 169

5.13 Effects of track Low Stiffness (LS), Low Damping (LD), High Stiffness (HS) and High Damping (HD) on vehicle deflections over bridges B1 through B6..170

5.14 Effects of trainset type on vertical deflections of bridges B1 through B6.....171

5.15 Effects of trainset type on leading car vertical accelerations over the mid-span of bridges B1 through B6.....172

5.16 Effects of track irregularities on the dynamic response at mid-span of bridge B4 with ICE-3 at service speed: (a) deflection; (b) acceleration 174

5.17 Effects of track irregularities on the vertical response of leading car over bridge B4 with ICE-3 at service speed: (a) deflection; (b) acceleration....175

5.18 Mid-span vertical deflections of bridges B1 through B6 with vertical support stiffness ratios η_{sv} from 1.5 to 3 and SS for cases $\eta_{s\theta}$ = -3 and c_{sv} = 0.....177

LIST OF FIGURES (Continued)

FIGURE PAGE

5.19 Maximum vertical accelerations of bridges B1 through B6 with vertical support stiffness ratios η_{sv} from 1.5 to 3 and SS for cases $\eta_{s\theta}$ = -3 and c_{sv} = 0.....178

5.20 Mid-span vertical deflections of bridges B1 through B6 with vertical support stiffness ratios η_{sv} from 1.5 to 3 and SS for cases $\eta_{s\theta}$ = 0 and c_{sv} = 0.....179

5.21 Maximum vertical accelerations of bridges B1 through B6 with vertical support stiffness ratios η_{sv} from 1.5 to 3 and SS for cases $\eta_{s\theta}$ = 0 and c_{sv} = 0.....181

5.22 Mid-span vertical deflections of bridges B1 through B6 with vertical support stiffness ratios η_{sv} from 1.5 to 3 and SS for cases $\eta_{s\theta}$ = 3 and c_{sv} = 0.....182

5.23 Maximum vertical accelerations of bridges B1 through B6 with vertical support stiffness ratios η_{sv} from 1.5 to 3 and SS for cases $\eta_{s\theta}$ = 3 and c_{sv} = 0.....183

5.24 Mid-span vertical deflection of bridges B1 through B6 with different vertical supports damping ratios $\zeta_d(\%)$ for cases η_{sv} = 1.5 and $\eta_{s\theta}$ = -3.....184

5.25 Maximum vertical acceleration of bridges B1 through B6 with different vertical supports damping ratios $\zeta_d(\%)$ for cases η_{sv} = 1.5 and $\eta_{s\theta}$ = -3.....185

5.26 Mid-span vertical deflection of bridges B1 through B6 with different vertical supports damping ratios $\zeta_d(\%)$ for cases η_{sv} = 1.5 and $\eta_{s\theta}$ = 0.....186

5.27 Maximum vertical acceleration of bridges B1 through B6 with different vertical supports damping ratios $\zeta_d(\%)$ for cases η_{sv} = 1.5 and $\eta_{s\theta}$ = 0.....187

5.28 Mid-span vertical deflection of bridges B1 through B6 with different vertical supports damping ratios $\zeta_d(\%)$ for cases η_{sv} = 2 and $\eta_{s\theta}$ = -3.....188

5.29 Maximum vertical acceleration of bridges B1 through B6 with different vertical supports damping ratios $\zeta_d(\%)$ for cases η_{sv} = 2 and $\eta_{s\theta}$ = -3.....189

5.30 Mid-span vertical deflection of bridges B1 through B6 with different vertical supports damping ratios $\zeta_d(\%)$ for cases η_{sv} = 2 and $\eta_{s\theta}$ = 0.....190

5.31 Maximum vertical acceleration of bridges B1 through B6 with different vertical supports damping ratios $\zeta_d(\%)$ for cases η_{sv} = 2 and $\eta_{s\theta}$ = 0.....191

LIST OF ABBREVIATIONS

AREA	American Railway Engineering Association
AREMA	American Railway Engineering and Maintenance-of-Way Association
AVE	Alta Velocidad Española
CHSTP	California High-Speed Train Project
CRH	China Railway High-Speed
DOF	Degree Of Freedom
ERRI	European Rail Research Institute
FEM	Finite Element Method
HSLM	High Speed Load Model
HSR	High-Speed Rail
ICE	Inter-City Express
KTX	Korea Train eXpress
ORE	Office de Recherches et d'Essais
PSD	Power Spectral Density
TGV	Trains à Grande Vitesse
THSRC	Taiwan High Speed Rail Corporation
TTBI	Train-Track-Bridge Interaction
UIC	Union Internationale des Chemins de Fer
VBTI	Vehicle-Bridge-Track Interaction

SUMMARY

Currently in the United States, the National University Rail (NuRail) Center is leading a federally funded renewed interest in railway engineering that includes research on high speed rail networks and increase of speeds on shared corridors. Assessment of existing railroad bridges and construction of new high speed rail bridges would require adequate theoretical modeling to predict their dynamic behavior. Single span short bridges over roads, rivers, wildlife trails or other environmental features are usually considered to have a relatively low budget compared to larger structures. Consequently, they are assigned a correspondingly low budget for engineering often requiring the use of simple methods for dynamic calculations. Although this philosophy may be acceptable for highway bridges which are mostly governed by the ultimate limit state criteria, this approach becomes problematic particularly for short span high speed rail bridges where resonance may occur resulting in excessive vertical accelerations of the bridge deck. These serviceability problems are real as experienced in France during the early stage of the high speed rail program when some retrofitted existing short span bridges had to be shut down temporarily. Facing similar challenges, the United States could benefit from the past experiences gained in Europe and Asia. The literature review during this research has shown that simple models consisting of simply supported beams subjected to a series of moving point loads grossly overestimate results by as much as 50% in some short span bridges; and complex numerical models of fully coupled vehicle-bridge systems are computational expensive. The effects of the track-bridge interaction and the influence of boundary conditions on bridge responses are not yet well studied. Motivated by the above statements, this research focuses on the formulation of a numerical model for train-track-bridge interactions; investigation of the free vibration problems; and parametric studies of short span high speed rail bridges through dynamic simulations.

SUMMARY (Continued)

In the first part of this dissertation, a 2D numerical model is developed that takes into account the interaction of the train moving at a constant speed as well as the track structure and boundary conditions. The Train-Track-Bridge Interaction (TTBI) system is treated as two separate subsystems. The equations of the train vehicle as a moving subsystem and the equations of the stationary underlying track-bridge subsystem are formulated independently, thus decoupling the whole system. The interaction between the two subsystems is assumed to occur at the wheel-rail interface where constant contact is enforced through constraint equations. The track-bridge finite elements are assumed to consist of contact elements and non-contact elements. Using dynamic condensation and Hermitian cubic interpolation functions, the degrees of freedom of the wheels at the contact points are related to the nodal displacement vector of the rail. Vectors of velocity and acceleration of contact points are computed from the first two derivatives respectively of the vector of displacement. The equations of motion of the vehicle are solved using modified Newmark finite difference schemes based on the HHT alpha method. Contact forces are obtained from the equations of the vehicle which are then used to solve the equations of the track-bridge subsystem in a step-by-step direct time integration algorithm. The boundary conditions of the bridge are incorporated using linear viscoelastic elements whose values are added to the diagonals of global matrices at their corresponding degrees of freedom. The result accuracy of the proposed numerical model is validated against results from a semi-analytical method of a fully coupled vehicle-bridge interaction problem using modal superposition and against results from other studies using different finite element models found in the literature. Results comparisons show excellent agreement indicating accuracy of the proposed model.

In the second part of this dissertation, the effects of key model aspects in the free vibrations of a track-bridge system are investigated. It is found that natural frequencies of the bridge decrease when shear deformations and rotational inertia are considered. The decrease is more significant when the slenderness ratio decreases and at the same time the shear deformation parameter increases. The vertical stiffness of the bridge supports has a significant effect on the natural frequencies of the bridge. The vertical stiffness ratio, defined as the ratio of support vertical stiffness to bridge flexural stiffness, determines the degree of flexibility at the boundary conditions. The natural frequencies of the bridge are reduced when this ratio decreases. For a given value of this ratio, the decrease is more significant in the frequencies of higher modes. Also, for constant bridge support conditions, the decrease is more significant for short span bridges. The additional mass of the ballast decreases the natural frequencies of short span bridges with rigid supports. However, for support vertical stiffness ratio less than 100, the ballast mass has no significant effect on the fundamental frequency. The vertical stiffness of the track has negligible effects on the natural frequencies of short span bridges modeled with rigid supports but has noticeable effects as the bridge supports become more flexible.

In the third part of this dissertation, numerical simulations of bridges with spans ranging from 5 m (16.4 ft) to 40 m (131.2 ft) are performed. The influence on the bridge vertical accelerations and deflections of several key parameters and aspects of the numerical model are investigated. Results show that shear deformations and rotational inertia can be ignored in the dynamic analysis of short span high speed rail bridges when the slenderness ratio is greater than 50. As the slenderness ratio decreases, the magnitude of the dynamic response is increased and the speed at which resonance occurs is smaller because the natural frequencies are reduced.

Both the vehicle interaction and the track structure reduce dynamic peak responses at resonance speeds. This reduction is more significant for shorter bridges. For example, for the cases investigated in this study, reductions of about 30-50% in the vertical acceleration were observed. The elastic properties of the boundary conditions have significant effects on bridge dynamic responses. The logarithmic value of the support vertical stiffness to bridge flexural stiffness (η_{sv}) and the logarithmic value of the support rotational stiffness to bridge rotational stiffness ($\eta_{s\theta}$) are found to be two important non-dimensional parameters that can be used to determine whether the boundary conditions should be considered and their impacts on the bridge responses. Generally, bridge dynamic responses increase when η_{sv} decreases and they decrease when $\eta_{s\theta}$ increases. However, the ratio η_{sv} is more critical than the ratio $\eta_{s\theta}$. For values of $\eta_{sv} > 3$ the bridge can be modeled as a simply supported structure since there are no significant differences in dynamic responses. For values of $\eta_{sv} \leq 3$ the fundamental frequency is reduced and the mode shapes become a combination of rigid modes and flexural modes. For very soft vertical supports with values of $\eta_{sv} < 2$, rigid mode dominates. For $\eta_{sv} \leq 2.5$, dynamic responses are significantly amplified and the damping at the supports becomes necessary and even more effective as this ratio is further reduced. It is not recommended to have $\eta_{sv} \leq 1.5$ for short span high speed rail bridges even with damping at supports. For soft supports with $\eta_{sv} \leq 2$, the available structural damping in elastomeric bearings and/or soil foundation may not be sufficient to reduce the vertical bridge vibrations to acceptable levels. In that case, additional damping in the form of external devices, such as Fluid Viscous Dampers (FVD), installed at the supports may be an efficient method to control theses high vertical accelerations in short span high speed rail bridges.

CHAPTER 1

INTRODUCTION

1.1 Background

The rapid economic and technological development in the second half of the twentieth century has led to a growing demand for a convenient and expeditious means of transport. Expectations of continuously increasing standards of living have driven and continue to drive the evolution of air, road and of course rail transportation networks.

The era of rail transport at high speeds began in 1964 when, during the Olympic Games of Tokyo, Japan started circulating the first "bullet train" of the Tōkaidō Shinkansen that travelled from Tokyo to Osaka at a speed of 210 km/h (130 mph). The success of the bullet train was so overwhelming it prompted Japan to expand the Shinkansen lines to other hubs of the country creating a network of more than 2000 km (1243 mi.) that connects the different islands of the Japanese archipelago. Today the world's pioneer in modern high speed rail has an established and still growing network as shown in Figure 1.1 (Shinkansen Route Map, 2016).

Seventeen years after the Shinkansen first high speed train, France became the first European country entering the high speed rail market in 1981 with the TGV (Trains à Grande Vitesse) line connecting Paris and Lyon at a speed of 260 km/h (162 mph). At the same time, Germany began building its first high speed rail lines but, due to legal battles, has not deployed the first generation of ICE (Inter-City Express) trains until 10 years later in 1991. A year later, on the occasion of the Universal Exhibition that took place in Seville, Spain launched its first AVE (Alta Velocidad Española) high speed train connecting the city to the capital.

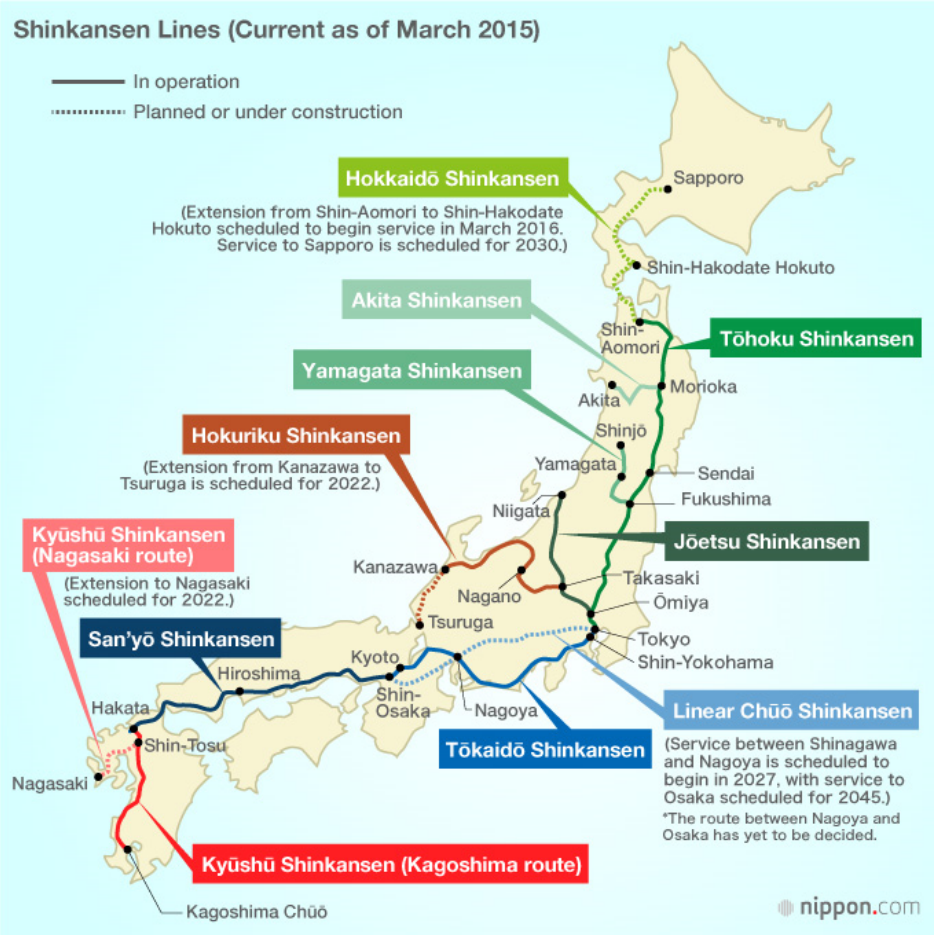

Figure 1.1 Japan High Speed Rail Network Map

Currently Europe has an extensive high speed rail network linking various parts of the continent as shown in Figure 1.2 (High Speed Rail in Europe, Wikipedia, 2016).

Besides the Japanese, the first country in East Asia implementing a high speed rail program was South Korea. The Korea Train eXpress (KTX), operated by Korail, began construction of a high speed line from Seoul to Busan in 1992 and started services on April 1, 2004. Shortly after, in January 2007, Taiwan High Speed Rail Corporation (THSRC) has opened its first high speed line running approximately 345 km (214 mi.) along the west coast of the island.

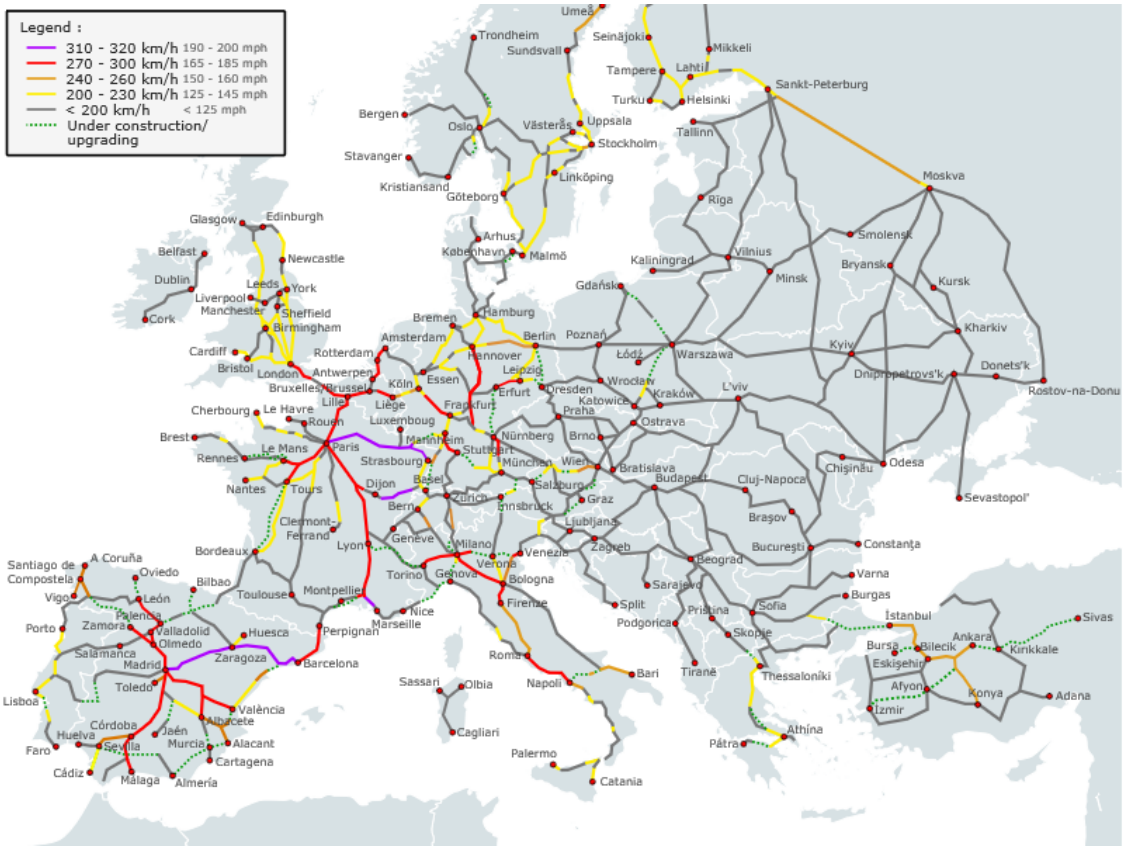

Figure 1.2 Europe High Speed Rail Network Map

China has drawn extensively on the Japanese and European experience and introduced its first China Railway High-Speed (CRH) train in April 2007. As shown in Figure 1.3, in a very short period of time, the CRH has become the longest High Speed Rail network in the world with over 19000 km (12000 mi.) in service as of January 2016 according to Wikipedia (High Speed Rail in China, Wikipedia, 2016) and an additional network of 30000 km (19000 mi.) planned for the year 2020.

Figure 1.3 Chinese High Speed Rail Network Map

The United States has not experienced a similar boom in High Speed Rail (HSR) construction as in Europe and South East Asia primarily due to funding. The lack of investment in HSR upgrades and development of new networks resulted in The HSR system being limited to one line along the east coast. The California project has been in planning for over a decade and the construction work is yet to begin. The proposed California project consists of new HSR tracks that will eventually handle traffic speeds of 241 km/h (150 mph), which will be unprecedented for HSR corridors in the U.S. The Boston to Washington HSR line uses conventional rail systems. It is the only high speed system in operation in the U.S. However, there is a new interest in HSR. Figure 1.4 (US High Speed Rail, 2016) shows the proposed plans for the HSR systems in the United States.

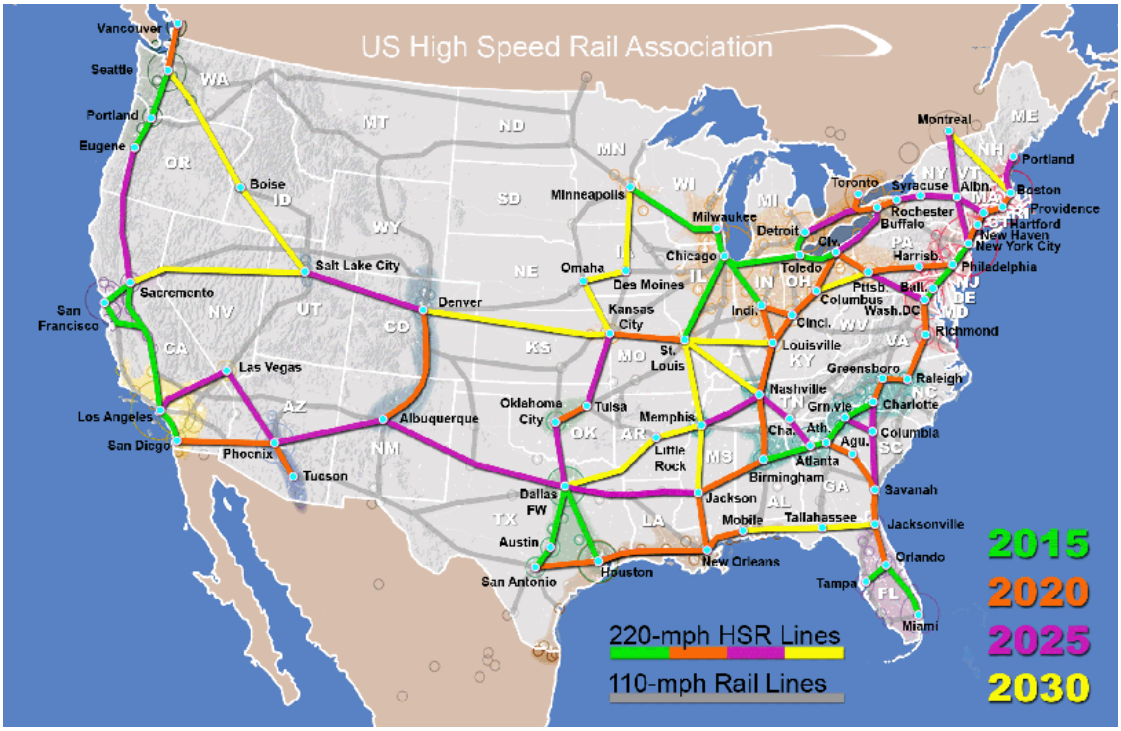

Figure 1.4 United States Planned High Speed Rail Map

1.2 Research Motivation

In the United States, the National University Rail (NuRail) Center is currently leading a federally funded renewed interest in railway engineering which includes research on potential high speed rail networks and possible increase of traffic speeds on shared corridors. Railroad bridges in the U.S. have not been designed for true high speed trains. The assessment of existing bridges or construction of new high speed rail bridges would therefore require proper theoretical models to predict their dynamic behavior.

Bridges crossed by moving vehicles have been the subject of much research work. Accurate evaluation of the interaction between trains and structures is an important aspect of bridge dynamics. Most recent research projects are confined to a small number of models for the vehicle or the bridge which necessitate complicated and computationally expensive dynamic

analyses. Hence, a model of a general nature and capable of incorporating the interactions of the vehicle, track system, bridge structure as well as the viscoelastic elements at the bridge supports will improve the analysis procedure.

Dynamic response of the bridge without vehicle interaction was the focus in the majority of research in this area. For cases where the bridge response only is of interest, the moving vehicles are generally represented by a number of moving loads. This type of approximation however overestimates significantly the actual dynamic response of the bridge. Moreover, depending on the application under consideration, the vehicle response may be also important. The vertical acceleration of the vehicle is a design criterion regarding the passenger comfort and should be computed as accurately as possible.

In urban areas as well as over rivers, creeks or other environmental features, short distance grade separation for the railway track usually necessitates the use of short span bridges. This class of underpasses presents its own challenges in evaluating the dynamic responses with the mostly used simplified models. In that context, most engineering design codes for railway bridges have adopted the approach of a dynamic factor which takes into account the dynamic effect of a single moving load. This approach does not cover the possibility of resonant response of the bridge due to the periodic array of wheel loads moving at high speed which may surpass largely that of a single moving load. Furthermore, the issue of dynamic analysis becomes more important in the capacity assessment of an existing short span bridge that was not originally designed for fast moving trains but planned for use in an upcoming new high speed rail line. The consequences of waiving accurate dynamic calculations for existing short span bridges are such that an underestimation of bridge responses will impact the safety and an overestimation will

impact the retrofit or rehabilitation budget. In that sense, it is desirable to use appropriate models that include the interaction effects and other key parameters or system aspects.

The vast majority of research on the dynamic analysis of short span bridges assumes the boundary conditions to be simply supported. However, to minimize damages caused by violent seismic events to bridges, elastic isolators are used as bearings in most cases. These are typically located at the ends of the bridge for the purpose of isolating the transmission of energy from the ground. These isolators may significantly alter the dynamic responses of the bridge due to the moving train loads. The degree of soil compressibility in the foundation may also have an effect.

In light of the shortcomings related to simple models and the challenges still presented by short span high speed rail bridges, it is the motivation of the author of this dissertation to carry out a research on the dynamic behavior of short span high speed rail bridges considering the various sources of dynamic loading that include vehicle interaction, track irregularities and the viscoelasticity of the bridge supports. For that purpose, a Train-Track-Bridge Interaction (TTBI) model is introduced. The TTBI analysis is suitable for the types of analysis where the mutual effects of the vehicle, the track and the bridge are important. An effective method of the TTBI analysis involves the use of the concept of "dynamic condensation" methods which *condense* the degrees of freedom of the vehicle to those of the supporting subsystem. One of these methods includes the application of the TTBI elements referring to rail beam elements which are directly in contact with the wheels of the moving train. Other non-contact rail elements are therefore modeled as conventional elements. Subsequent interaction of rail beam elements with bridge beam elements are treated through coupling actions via the elastic layers in the track structure. Therefore there is still a need for further research to address the shortcomings of available

theoretical models and gain more knowledge in the quest of better understanding the dynamic behavior of short span high speed rail bridges.

1.3 Research Objectives and Scope

The first goal of this study is to provide procedures within the frame work of analytical and finite element methods for the dynamic calculations in the Train-Track-Bridge Interaction problem related to short span high speed rail bridges with flexible support conditions and subjected to various types of train loading and traffic speeds. The formulation of the numerical model will remain as general as possible for use in most practical cases. At the same time the effects of various parameters on the dynamic response of the vehicle, the track and the bridge will be identified. The second objective of this research is to evaluate the influence of model aspects and system parameters on the modal characteristics of short span bridges. The third and final objective of this research is to use the developed model to investigate the dynamic behavior of short span high speed rail bridges through numerical simulations of bridge prototypes and evaluate the significance of key parameters influencing the dynamic results.

With the purpose of achieving these objectives, the scope of the research is to:

1. Develop a 2D model for Train-Track-Bridge Interaction (TTBI) problems considering the predominantly vertical loadings and with the assumption of constant traffic speed.
2. Establish the mathematical formulations of the TTBI model identifying the governing equations of motion of each subsystem and their solution algorithms.
3. Verify the validity and accuracy of the developed model with numerical examples and compare results against those from other models.

4. Investigate the free vibration problem with an emphasis on the fluctuations of natural frequencies resulting from changes in the model aspects or system parameters. The effects of elasticity in bridge supports, track parameters and adopted beam theories are examined.
5. Carry out parametric studies through numerical simulations of short span high speed rail bridges with the objective of investigating the influence of key parameters on the critical dynamic responses.

1.4 Dissertation Outline

The dissertation is organized in six chapters as outlined below:

- Chapter 2 presents a comprehensive review of previous studies available in the literature and that are closely related to the subject matter of this research.
- Chapter 3 deals with the modeling of the interactions between the train and track-bridge subsystems. Mathematical formulation of equations governing the dynamic behavior of each subsystem is established. This chapter also discusses the solution methods of the TTBI problem and presents two examples to validate the model.
- Chapter 4 investigates the effects of flexibility in the boundary conditions on the natural frequencies of the bridge. The influence of shear deformations and rotational inertia on the free vibrations is also investigated. The impact of the track structure on the bridge fundamental frequency is examined.
- Chapter 5 includes numerical simulations of several short span high speed rail bridges. Parametric studies are carried and a discussion of results is provided.
- Chapter 6 presents the important outcome and conclusions of this research as well as practical recommendations and suggested work for future research.

CHAPTER 2

STATE OF THE ART

2.1 Historical Background

Problems that usually faced the engineering field rose from the desire of societies to reach higher levels of development and welfare. This desire to overcome barriers imposed by nature has always promoted the development of numerous disciplines that make up the now very broad fields of science and technology. Rail transport, of course, is no exception. Since the times of the industrial revolution railway has brought numerous advantages to societies such as movements of heavy freights, reduced travel times, and the pursuit of safety and comfort for travelers.

The construction of the first railway lines could be traced back to the first half of the 19th century in England. On the 24th day of May 1847, in the outskirts of Chester, England, the Stephenson's cast and wrought-iron girder bridge over the Dee River suddenly collapsed while being crossed by a passenger train, killing five people and injuring a dozen more (Taylor, 2013). An illustration of the collapse is shown in Figure 2.1. The railway line was linking London to Holyhead. This event happened only six months after the opening inauguration of the bridge which was made of riveted iron beams. This incident raised safety questions related to all other structures of the British Railway Network which was then in full expansion. By the order of

Queen Victoria, a Royal Commission was created with the task of investigating the cause of the fatal accident and to avoid similar tragedies in existing or new structures.

Figure 2.1 View of River Dee bridge collapse
(From Illustrated London News, June 12 1847, Courtesy of John Weedy)

Among the numerous problems faced by the new railway lines emerged an important debate related to the construction of bridges. The debate divided the discussions into two schools of thought. One group of engineers believed that the movement of the railway locomotive over the bridge would generate an impact, while the other group believed the structure would not have enough time to deform during the passage of the engine (Frýba, 1996). For this reason, Stokes

was the first scientist who tried to tackle the issue in his theoretical studies (Stokes, 1847). Neglecting the mass of the bridge with respect to the locomotive, he showed that the solution was half-way between the two opposing ideas among engineers. Stokes' solution, presented in the form of series development, was later simplified by Willis (Willis, 1849) who performed the first experiment and obtained a formula that increased the static response to cover the dynamic effects. This approach to the problem can be regarded as the first attempt to obtain a coefficient of impact.

In his doctoral work, Alvarez (Alvarez, 1984) included an introductory chapter which provided facts and interesting data on the initial period of the development of dynamic calculation in railway bridges. He summarized that no problem due to dynamic effects manifested itself in the massive structures that were used until the beginning of the 19th century but were soon suspected following the disasters that occurred in steel bridges. In fact, it was likely that those disasters were also due to poor designs and construction of the structures. However it became evident that dynamic effects, due to the profound ignorance about the issue at that time, were valid reasons to blame.

During the rest of the century other authors have worked on the railway bridge dynamic problems, but a definitive theoretical formulation was not reached until the beginning of the 20th century with the work of (Bleich, 1924) and, mainly, (Timoshenko, 1955) and (Inglis, 1934), whose approaches decisively influenced the further development of the discipline. In parallel with the attempts to find a theoretical basis that would deal with the problem, early experimental works were carried out to support the analytical results and obtain practical formulas. In reality, poor correlations between theoretical and experimental results led to the development and use of empirical formulas during the 19th century. Tests carried out by Robinson in 1887, as well as

various campaigns undertaken by the American Railway Engineering Association (AREA) in the first half of the 20th century are mentioned in the literature (Chu et al., 1979). Some of the empirical formulas proposed during the nineteenth and early twentieth centuries are compiled in (Alvarez, 1984), showing also the curious experimental apparatus system designed and built by Professor Willis, Captain James and Lieutenant Galton in 1849 to support the hypothesis that the dynamic deflection of girders due to rolling loads can grow larger than the static deflection; an inquiry that was prompted by the collapse of the Chester railway bridge in the United Kingdom.

In the middle of the 1950's, a new momentum was created in the field of railway bridge dynamics when the *Office de Recherches et d'Essais* (O.R.E.) of the *Union Internationale des Chemins de Fer* (U.I.C.) launched in 1955 the committee D23, a group of experts, in order to lay a firm foundation for the dynamic calculations of railway bridges. The works of the ORE and its successor, the ERRI (European Rail Research Institute), dealing with both the experimental and the theoretical field, have become the standards in the field of Railway Engineering.

According to (Alvarez, 1984), Arne Hilleborg published the first attempt to model the railway vehicle-track interaction using systems of masses and springs. This approach was later followed by Biggs, Fleming and Romualdi in proposing the first models which took into account the interaction between the vehicle and the structure. These models are some of the most used approaches to this day.

The research carried out by the committee D23 and its successor D128 established a solid framework that has been the basis for bridge dynamic calculation methods until the emergence of high speed trains. In the work of both committees various types of numerical models were used; from the most simple model based on constant moving forces to complex models of interaction

which took into account track irregularities, wheel flats and a large number of factors that could not be addressed until the development of computers in the second half of the last century. Frýba (Frýba, 1999) has made an early contribution with the first theoretical model in the field of railway vehicle-track-bridge interaction. As shown in Figure 2.2, he studied the responses of a simple beam traversed by a multi-axle system representing a locomotive of a train including significant parameters like suspensions and track irregularities.

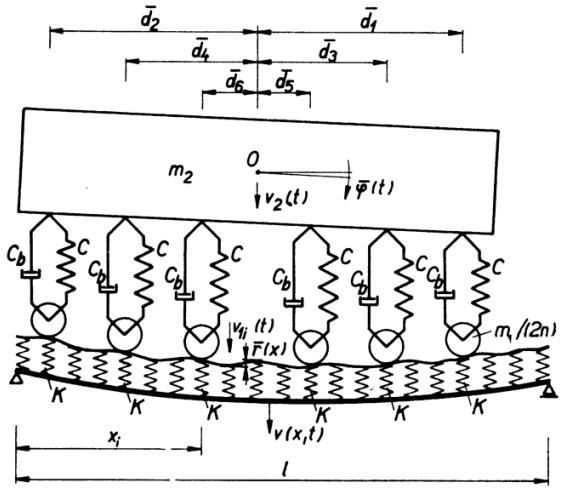

Figure 2.2 Early theoretical model of a locomotive over ballasted bridge (Frýba, 1999)

The progressive increase in the speed of trains, mostly during the years 1960's and 1970's, culminated, a decade later, with the appearance of the first high speed line in passenger trains. Since then, the adopted approach in the dynamic calculation of railway bridges changed significantly and the focus shifted to the problems associated with the passenger comfort. With this new scenario, the ORE launched in 1983 the committee D160, dedicated to the study of the conditions that should prevail in the construction of new bridges to ensure the comfort of

travelers. The studies of the committee D160 resulted in some new criteria for the maximum admissible deflection of the bridge, requirements that went on to become, in most cases, the most restrictive condition imposed on the structure.

2.2 Relevant Contributions of Previous Researchers

In this section of the chapter, a brief summary is presented regarding the research contributions from the most current references that the author of this dissertation has had the opportunity to review during the course of this research. The available literature with the most relevance to the subject matter of this study is only selected and discussed below.

In the paper of (Maunder, 1960), the author discussed the Timoshenko paradox from the point of view of the physical conditions required to transmit a purely vertical force to a beam, which implied the need for tangential forces (friction slip or rotation) to develop. The paradox arises when checking that the net work done by a force to traverse a beam is zero, while the beam is in a state of free vibration (and therefore with a certain kinetic energy) when the load leaves the beam. The author explained the paradox imagining a small disc of negligible mass transmitting power to the beam. But after reading this paper, it is rather difficult to not have the impression that the energy balance should be met equally without having to explicitly define the nature of force transmission.

According to the authors of (Chu et al., 1979), this was the first study in which the vertical motion of a train wagon was realistically modeled with a carriage having three degrees of freedom (vertical displacement, pitch and rotation). Forces and masses were applied at the nodes of the bridge model. The variations of displacements, velocities and accelerations were assumed to be linear between consecutive nodes. The authors analyzed several cases with non-

zero initial conditions of vehicles and obtained higher impact coefficients than the case with zero initial conditions.

In the paper of (Chu et al., 1980), the researchers used the same numerical model as in their work of the year before (Chu et al., 1979) for the purpose of confirming mainly their previous conclusions. In addition, the authors found that the impact coefficients were much lower than those proposed by the American Railway Engineering Association (AREA). Furthermore, they observed that the impact coefficients in all members of the bridge did not increase when using non-zero initial conditions of the vehicle or when the structural damping was decreased from 2% to 0%.

The paper of (Vu-Quoc and Olsson, 1989) presented a comprehensive and rigorous formulation of the equations of motion of a vehicle-structure system, as well as efficient algorithms for its solution. The treatment of the energy balance in the system focused from the perspective discussed by (Maunder, 1960). The study contained several original contributions, among which few should be mentioned as follows: 1) the vehicle does not travel at a constant speed but enters the bridge at a given speed and evolves freely in accordance with the laws of motion; 2) the authors presented numerical examples demonstrating that the vehicle speed decreased, and that the loss in kinetic energy equaled the energy that kept the beam in its free vibration; 3) the decrease in speed with respect to the nominal speed was significant only for low speeds, approximately less than about 10 m/s (32.8 ft/s); 4) the numerical examples demonstrated that, even in the absence of dissipative mechanisms (viscous or friction), the vehicle would end up stopping if the bridge was sufficiently long; 5) the formulation included velocity and acceleration terms associated with the slope and curvature of the deformed shape of the beam, claiming that they were significant, which may have been largely due to the ratio of

span to static deflection which were of the order of 150/200 (i.e. some 10 times smaller than typical high speed rail bridges).

In the work of (Klasztorny and Langer, 1990), the authors made some contributions to the issue of a series of moving loads crossing a single-span beam bridge. Their basic load models included moving forces with constant amplitudes as well as un-sprung masses and spring-damper oscillators. The system's equations of motion were established in matrix form. The issue "of dynamic stability and steady-state response of a bridge carrying a periodic stream of inertial loads" was discussed including the problem formulation and solution. The authors also studied vibrations of a bridge beam "subjected to a uniform stream of moving loads, of a limited or unlimited number of load cycles."

The researcher (Olsson, 1991) presented the basic approach to the problem of moving constant loads over a simply supported bridge, with special emphasis on the assumptions and their implications. The author concluded that when the non-dimensional speed parameter, defined by $K = vt/2L$, was greater than one the maximum response occurred after the load has left the bridge which implies an impact (i.e. the period of the forcing load begins to be small compared to the period of the bridge).

The authors (Yang and Yau, 1997a) contributed a vehicle-bridge interaction element for use in the analysis of railway bridges carrying high speed trains. Their paper was an improvement of the work presented by (Yang and Lin, 1995). In their study, the authors modeled the train vehicle as sprung masses concentrated at the bogie (truck) level; and the bridge, including track irregularities, as beam elements. They established a pair of coupled equations of

motion. The sprung mass was discretized and condensed to that of the bridge element at the contact point. They demonstrated the applicability of their element with numerical studies.

The researchers (Yang et al., 1997b) carried out an interesting analytical study on the condition of speed, bridge span and train length that favor the appearance or cancellation of resonance. The train was broken down into two series of equidistant loads corresponding to the front and rear axles of the bogies (trucks) respectively. They demonstrated the relationship that must be met between the bridge span and the distance between the loads for the resonance cancellation of the first mode of vibration to occur.

The authors (Tartary and Fournol, 1999) presented a description of the Prony-Pisarenko auto-regressive method and its application in estimating the damping ratio of real railway bridges. The most interesting conclusion was that the damping ratio depended on the vibration amplitude in some cases, while in other cases it was not. This result was indicative of the difficulty involved in trying to get the damping ratio for use in projects.

The researchers (Le et al., 1999) discussed the possibility of placing rubber mat under the ballast in order to reduce the degradation of high speed rail bridges. Using numerical simulations, they concluded that: 1) this elastic layer reduces the pressure on the ballast but increases the vertical accelerations unless special sleepers (crossties) with elastic fasteners are used; 2) the maximum accelerations of the ballast at mid-span of the bridge are due to the first frequency of the bridge vibration while the maximum ballast vibration at the ends of the bridge are caused by higher frequency modes; 3) trial tests conducted in Switzerland showed that these higher frequency components detected at the bridge ends were responsible for the degradation of the transition zone; 4) the neoprene bearings at the ends of the bridge considerably affect the

third mode lowering its frequency of vibration, so it is necessary to take these elements into account in the model in order to assess realistically the vibrations at the ends of the bridge.

The authors (Zhang et al., 2001) proposed a three-dimensional formulation for bridge dynamic analysis taking into account the vehicle-structure interaction and track irregularities. The most significant conclusions of their work were: 1) the residual forces in the integration tend to be negligible if a small time step is used; 2) results from a separate two-dimensional model were similar to those from the three-dimensional model.

Frýba (Frýba, 2001) undertook the development of some simple expressions to evaluate the critical speed, maximum deflection, maximum bending moment and maximum vertical acceleration due to the passage of a freight train. The author used a model with point loads and assumed, as in his previous work (Frýba, 1998), that the maximum amplitude of displacement and acceleration occur when the last load leaves the bridge. The expressions proposed by this author were later used to develop criteria for interoperability of rail networks in Europe. The author also included results of measurements carried out with the TGV train composition that showed a good agreement with those obtained from the simple expressions, even though the ERRI D214 committee reports indicated that such expressions are generally conservative estimates.

In 2003, Song proposed in (Song et al., 2003) a new three-dimensional finite element model for the study of vehicle-structure interaction in high speed rail line bridges. Lagrange equations were used to formulate the equations of motion of the vehicle-structure system. Global system matrices were constructed by derivation of the equations of the interaction forces. The

study was accompanied by numerical examples in which comparison of results obtained with the new model were made against those obtained with previous models and experimental results.

The excellent book of (Yang et al., 2004) was entirely dedicated to the dynamics of vehicle-bridge interaction in high speed rail bridges. Finite element models were developed to address complex problems and at the same time analytical solutions of typical cases were investigated, enabling the identification of the key parameters affecting the vehicle-bridge system. Experimental results were also provided to compare performances of the proposed different models. However, models of vehicle-bridge interaction in this book are based on simply supported bridges.

2.3 Train-Track-Bridge System Identification and Modeling

Research endeavors in the study of dynamic responses of bridges carrying moving vehicles have gone through two distinct stages. The appearance of modern computers can be seen as the transition between these two stages. Simplified or approximate analytical methods were used to solve basic and elementary problems before the age of computers. As those simplified analyses used in earlier research work are not adequate for the study of complex Train-Track-Bridge Interaction (TTBI) problems, this review will be focusing mostly on the relatively recent published work.

The spread of digital computations allowed researchers to incorporate more realistic models of train vehicles, tracks and bridges in their analysis. Previous work carried out by (Timoshenko and Young, 1955) and later by (Biggs, 1964) considered the bridge analysis using moving loads only with no track or vehicle interaction. Further studies on the moving load analysis were performed by (Frýba, 1972) who was one of the first researchers to introduce

analytical approach of the train-track-bridge interaction. Comprehensive studies on the dynamics of railway bridges were later undertaken by (Garg and Dukkipati, 1984) and (Frýba, 1996). Today, the modeling and analysis of the train-track-bridge interaction problems can be tackled with more realistic characterization of the system components as discussed in the follow sections.

2.3.1 Bridge modeling

Different types of models have been considered in the dynamic analysis of railway bridges. The choice of the model is determined by the procedure of the analysis and objectives. A few of the models relevant to the subject matter of this research are discussed in the following.

Previous research work on the TTBI Interaction analysis considered continuum models described by Bernoulli beam theory equations. Such models are useful mainly for prismatic bridges having a simple span. The benefit of such models, besides being simple, is the fact that they provide closed-form solutions. These types of theoretical models are still used by researchers whose objective is to solve the Vehicle-Bridge Interaction problem with closed-form equations (Biondi et al., 2005). In some cases, the inherent simplifications of the Euler-Bernoulli beam theory may not be adequate and models based on Timoshenko beam theory may be a good choice, thus taking into account shear deformations and rotary inertia.

Models using the continuum beam models are satisfactory for simple structures only. Combined continuum-discrete models were proposed for more complex bridges. This concept was applied to model a continuous bridge with three spans having an internal hinge and uniform cross-section (Veletsos and Huang, 1970), “double-I-girder bridges” (Chu et al., 1979), and “truss bridge with rigid, semi-rigid or pinned joints” (Garg and Dukkipati, 1984).

Very recently, in their quest to diminish the dynamic response of bridges, researchers have introduced different types of models intended to include additional properties of the bridge system or to approach the bridge dynamic issues from different perspectives. For example, the authors of (Yang et al., 2004) have inserted spring elements at the ends of the bridge, as shown in Figure 2.3, to represent elastomeric bearings. However, this type of model can be extended to take into account the flexibility of boundary conditions characterizing any type of elastic supports at bridge ends, including soft soil conditions.

Figure 2.3 Elastic supports of a bridge (Yang et al., 2004)

Reckmann (Reckmann, 2002) proposed a control system for the triangular falsework using the model shown in Figure 2.4, suitable for short span bridges.

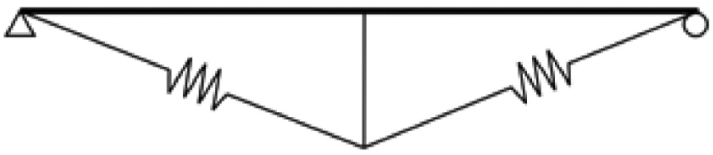

Figure 2.4 Triangular falsework system

Even the so-called double systems were considered by some researchers. For instance, the authors of (Kawazoe et al., 1998) have proposed the double beam system as shown in Figure 2.5 which may be suitable for short and medium span bridges, while the author of (Oniszczuk, 2000) considered the double string system as shown in Figure 2.6 which is too soft for railway bridges according to Frýba (Frýba, 2009).

Figure 2.5 Double beam system

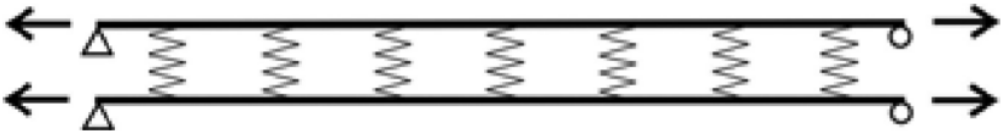

Figure 2.6 Double string system

Further improvements in computer capabilities made it possible to use discrete models in the study of any complex structures. These models also allow sound programming capability for program codes to perform step-by-step dynamic calculations. In the majority of recent works, one of these methods, namely the Finite Element Method (FEM), has been used extensively to model various types of bridges in 2D or 3D. For example, the authors of (Majka and Hartnett, 2008) have modeled a railway bridge using 3D, two-node finite beam element. However, a formulation based on the Euler-Bernoulli theory was adopted resulting in an element capable of

capturing the torsional, axial and bi-directional bending displacements. The six degrees of freedom at each node make an element with twelve degrees of freedom sufficient to simulate different types of motions.

2.3.2 Railway track structure

Generally the railway track guides the trains in an economic and safe manner. It is designed according to various criteria such as comfort, resistance, construction speed and maintenance costs. The railway tracks can be categorized into two groups; ballasted tracks and ballastless tracks. The track behavior when subjected to train loading depends on the properties of its layers as well as their interaction with each other and with the supporting structure. The track is an integral part of the railway bridge and for this reason it is necessary to include its contribution in the modeling of the high speed rail bridges. The physical and mechanical properties of each track types and their modeling techniques are discussed in the following sections.

2.3.2.1 Characteristics of ballasted track

The ballasted track as shown in Figure 2.7 (Proença et al., 2011) is a solution that has been in existence for over two centuries and used in the majority of high speed rail tracks.

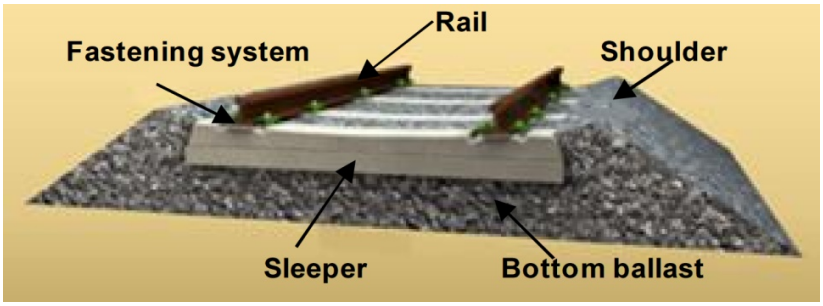

Figure 2.7 Ballasted track

In railroad bridges, this configuration consists of the superstructure including the rails, crossties (sleepers) and fastening systems as well as the ballast as a substructure. Despite the fact that this track arrangement is frequently adopted these days, its geometric definition and elements' properties have some variations as discussed in the following subsections.

2.3.2.1.1 Rails

The rails are the first components that are in contact with the wheels of the train vehicle and their main functions are the transfer and distribution of vertical and horizontal forces through the sleepers (crossties). They also serve to guide the wheels. In Europe, the commonly used rail profile in high speed lines is the UIC60 for which a photo is shown on the left side and dimensions on the right side in Figure 2.8 (Araujo, 2011).

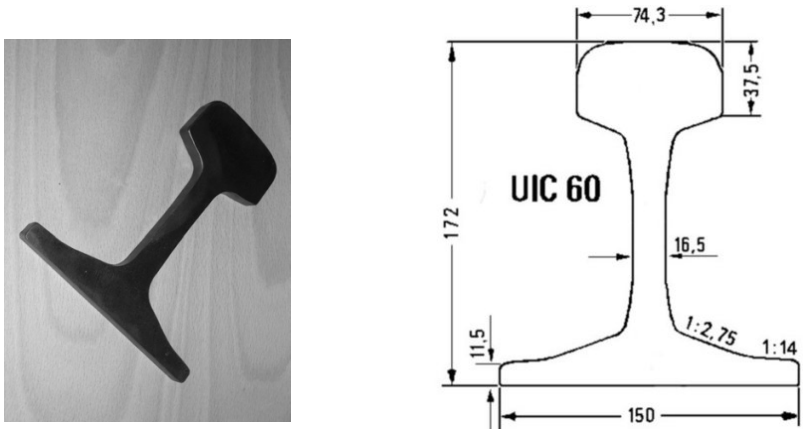

Figure 2.8 Typical flat-bottomed UIC 60 rail used in high speed line

In the United States, the relatively heavier AREMA 136RE rail profile is typical for the Amtrak Acela lines, the only high speed line currently working in the North-East corridor. The planned California high speed rail projects specify the even heavier AREMA 141RE rail profile. The AREMA 136RE and 141RE rails are shown on the left side and right side of Figure 2.9 respectively. They are 12% and 16% heavier than the European UIC60 rail respectively.

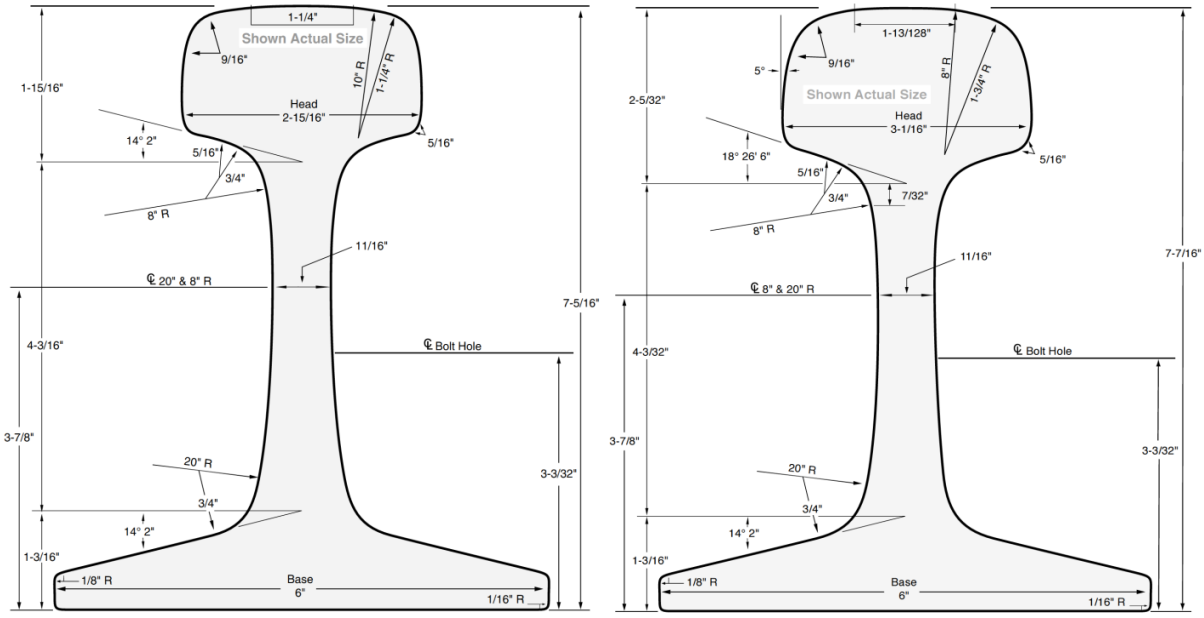

Figure 2.9 Sketches of AREMA 136RE (left) and 141RE (right) rail profiles

The mechanical and physical properties of the UIC60, AREMA 136RE and AREMA 141RE rails are shown in TABLE I (Rail Technical Guide, 2016), including their Poisson's ratio and shear correction factors.

TABLE I
TYPICAL RAILS MATERIAL PROPERTIES

Notation	Units	Value		
		UIC60	AREMA 136RE	AREMA 141RE
E_r	Ib_f/in^2 (MPa)		30 x 10^6 (206000)	
I_r	in^4 (cm^4)	73 (3038.3)	94.20 (3920.9)	100.44 (4180.5)
A_r	in^2 (cm^2)	11.89 (76.7)	13.32 (85.94)	13.80 (89.03)
m_r	Ib_m/ft (kg/m)	40.46 (60.21)	45.26 (67.36)	46.96 (69.88)
ν_r	-		0.3	
k_{sr}	-		0.4	

2.3.2.1.2 Railway fastening systems

The selection of the fastening system is essentially determined by the railway track and the sleeper (crosstie) that are being used as well as the stiffness of the granular layers supporting the sleepers (crossties). Figure 2.10 (Araujo, 2011) shows typical rail pads (see top left photo), proprietary Pandrol Fastclip (See top right photo), Vossloh Clip (see bottom left photo), and Pandrol Clip (see bottom right photo) mostly used in current high speed rail tracks. These components should guarantee a good connection between the rail and the sleepers (crossties). Pads consisting of rubber elements and placed under the rail may also be included to control the railway track stiffness for the purpose of decreasing the dynamic impact resulting from the train traffic. Rail pads provide resiliency for the rail/sleeper system, provide damping of vibrations induced by the wheels, reduce the contact friction between the rail and the sleeper, and provide electrical insulation. Teixeira (Teixeira, 2003) reported that the stiffness of rail pads used in high speed railways is between 171,305 Ib_f/in (30 kN/mm) and 2,855,079 Ib_f/in (500 kN/mm).

Figure 2.10 Fastening systems: rubber rail pad (top left), Pandrol Fastclip (top right), Vossloh Clip (bottom left), Pandrol Clip (bottom right)

2.3.2.1.3 Sleepers/crossties

The crosstie (sleeper) is an important component of the railway track and has a considerable stiffness. The crossties (sleepers) distribute the stresses from the rails to the track layer that supports them. The most common types are the concrete monoblock crossties and the twin-block crossties as shown in Figure 2.11 (Araujo, 2011).

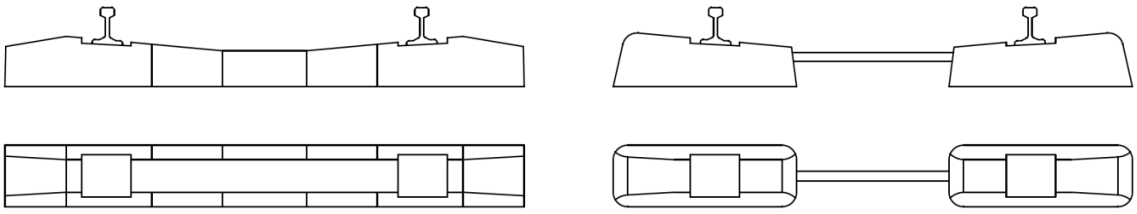

Figure 2.11 Monoblock crosstie (left), twin-block concrete crosstie (right)

These elements are usually placed at a spacing of between approximately 19.7 inches (50 cm) and 27.6 inches (70 cm). The weight of the monoblock crosstie is typically taken between 600 Ibs (272 kg) to 750 Ibs (340 kg) according to California High-Speed Train Project (CHSTP) Design Criteria Manual (California High Speed Train Project, 2014).

Although wood crossties are lighter, have better elasticity and easier to handle than concrete crossties, their disadvantage is their short lifespan due to deterioration.

2.3.2.1.4 Ballast materials

The ballast is the well compacted granular material supporting the sleepers (crossties). It is evenly graduated with angular shape and made of granite or limestone. The ballast should not be affected by frost and should not inhibit vegetation growth. Its functions are to absorb airborne noise, reduce pressure from the sleepers (crossties), allow drainage, and serve as a resilient material to absorb track energy.

The ballast layer is proportioned to ensure the proper distribution and transmission of the forces to the supporting structure. The European code EN 1991-2 (Eurocode 1, 2003) requires

that, in order to distribute the stresses without damaging the surface of the bridge or the eventual ballast mats, the ballast depth should not be less than 10 inches (250 mm). Generally however the ballast depth is chosen to be around 13.75 inches (350 mm) which permits an efficient maintenance of the track. The California High-Speed Train Project specifies a minimum ballast depth of 12 inches (305 mm) on at-grade tracks and 15 inches (381 mm) on short span bridges (California High Speed Train Project, 2014)

2.3.2.2 Characteristics of ballastless track

The ballastless track is a relatively newer development that was introduced in the late 1960's. The first ballastless track was used on a 700 meter (2296.6 ft) long segment in the Rheda Station in Germany. The so-called Rheda Solution 2000, as shown in Figure 2.12, is used nowadays in high speed railway bridges and is made of pre-compressed crossties (sleepers) embedded in a layer of reinforced concrete. The fastening system is made of materials having elastic properties. The ballastless track is already gaining popularity in the railway engineering field, offering many advantages in contrast to the ballasted track. The increasing and higher demands of HSR traffic have created opportunities for new innovative tracks with higher levels of performance. It is particularly in high speed rail lines that the ballastless track offers some real benefits. The ballastless track becomes attractive primarily for its performance, resulting in significant reduction of costs in maintenance as well as work such as tamping, cleaning of the ballast or lining of the track.

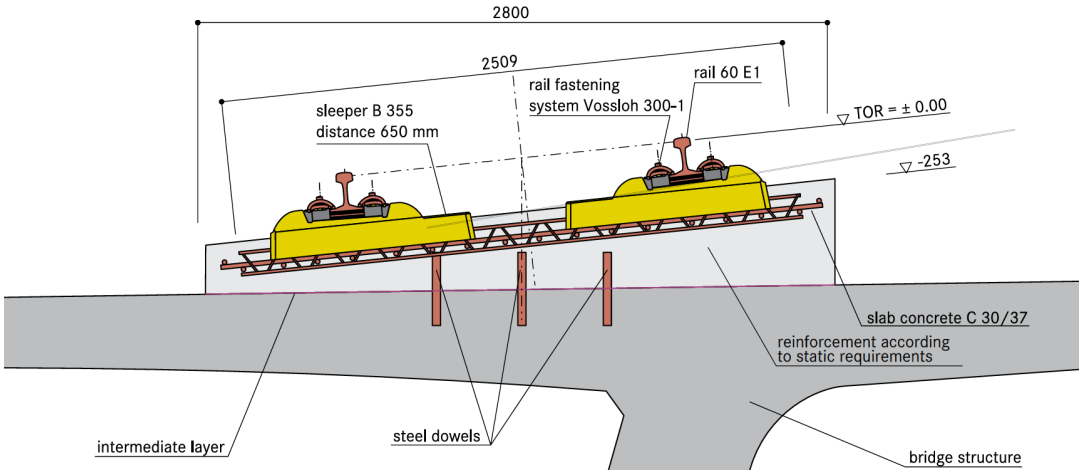

Figure 2.12 Typical Rheda 2000® ballastless track (Source: rail.One, n.d)

The higher initial construction costs may be offset by the maintenance savings over the service life of the track, therefore providing a more economical and competitive solution. In addition, the problem of forces of drag in ballasted track due to high speed traffic is not a concern anymore. This benefit, along with others, has been producing incentives for the use of ballastless tracks on HSR lines. There are many different types of ballastless developed by many countries, such as Germany, Japan or even the Netherlands, that may overwhelm a designer during the selection process. In fact, there exist higher functional, economical and technical ambiguities associated with the different available solutions. However the Rheda® system is generally considered as the solution that proved its efficiency and performance for a long time since it has been used in many projects since its origin.

According to the work of (Tünnissen, 2007), the slab of the ballastless track is “anchored to the bridge structure in pre-designated free-drilling zones by means of stainless steel dowels”,

of high quality having a diameter of 1.5 in (40 mm). An interesting characteristic of this type of connection is that it allows some movements in the longitudinal direction. Therefore, the overstressing of dowels due to such movements of the bridge or even track slab can be eliminated (Infraspeed, 2006). The ballastless track is typically made of slab segments having a length of 11.5 feet (3.50 meters) to 21 feet (6.40 meters).

2.3.3 Modeling of ballasted track-bridge system

Researchers studying ballasted high speed rail bridges interested in including the effects of the track have proposed and used several different types of models depending on the levels of complexities required to achieve their objectives. Typically these models can be categorized as continuous models or discrete models. Generally for the investigation of bridge vertical responses, 2D continuous models were found to be sufficient. However for studies intended to investigate the torsional behavior of the bridge deck, 3D models would be necessary. Discrete models have become a better choice for the evaluation of track-bridge interaction where the effects of the track on the bridge and the effects of the bridge on the track are equally important. In the Finite Element Analysis (FEM) discrete models usually involve discretization of the track-bridge system with nodal points coinciding with the positions of the sleepers (crossties). Brief discussions are provided below related to most relevant 2D and 3D models dealing with the vertical track-bridge interaction.

The earliest simplest continuous model that has been used in the study of track behavior or track-bridge interaction is the one-layer Winkler model. The rails are modeled as an infinite beam resting on uniformly distributed spring-damper systems characterizing the ballast as shown

in Figure 2.13. The introduction of the viscoelastic damping of the track is an improvement of the original Winkler foundation model with only distributed springs.

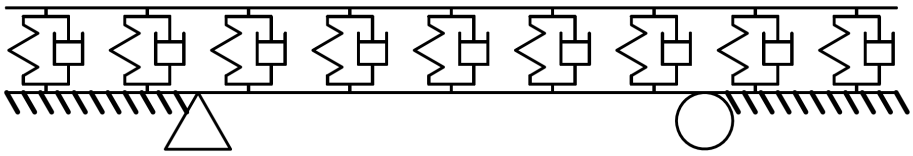

Figure 2.13 Continuous single-layer model with distributed vertical spring-dampers

Some researchers have also used a different continuous single-layer model as shown in Figure 2.14. Similarly, with this model the rails are represented as infinite beams with in-plane and out-plane flexural stiffness as well as axial stiffness. Linear spring-dampers in the vertical and horizontal directions represent the ballast. This model is adequate for the vertical behavior of railway ballasted bridge traversed by an accelerating or decelerating high speed trains as the frictional effects of the ballast layer are taken into account.

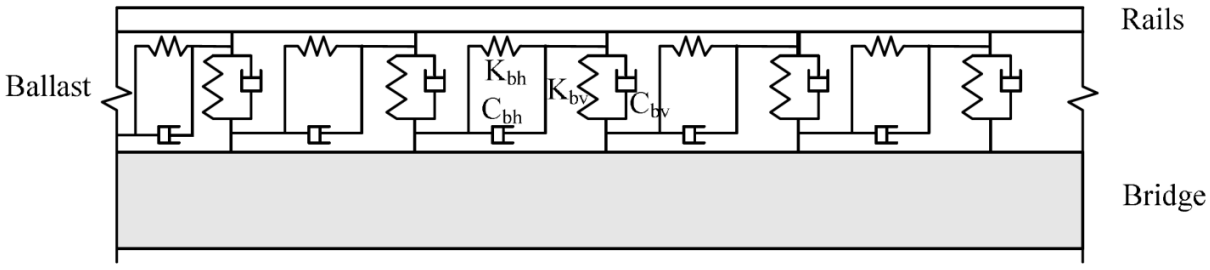

Figure 2.14 Continuous single-layer model with vertical and horizontal spring-dampers

The properties of the track in a track-bridge single-layer continuous model as shown in Figure 2.14 are given in TABLE II (Yang et al., 2004).

TABLE II
TRACK PROPERTIES OF SINGLE-LAYER CONTINUOUS MODEL

Description	Notation	Value	
Vertical stiffness	K_{bv}	104000 kN/m^2	(15084 Ib$_f$/in^2)
Vertical damping	C_{bv}	50 kN.s/m^2	(7.25 Ib$_f$.s/in^2)
Horizontal stiffness	K_{bh}	10400 kN/m^2	(1508.4 Ib$_f$/in^2)
Horizontal damping	C_{bh}	50 kN.s/m^2	(7.25 Ib$_f$.s/in^2)

The continuous single-layer models as described above would be sufficient for the 2D dynamic studies of vertical behavior of track-bridge system. The drawback is in their inability to provide the tools to analyze the response of other individual components of the track such as the crossties (sleepers) and ballast mass for which the 2D discrete models may be better alternatives.

A discrete 2D model as shown in Figure 2.15 is categorized as a two-layer model providing the ability to capture the vertical dynamic behavior of the rail, sleepers and bridge deck separately. This model considers the rail pads as linear spring-damper elements acting in parallel and connecting the rails and the crossties. The crossties are included as rigid bodies with point mass. The ballast bed is incorporated as discrete linear springs and viscous dampers. In this model, the spacing of the discrete elements is defined by the spacing of the crossties (sleepers). The ballast is assumed to be a non-vibrating material and its mass is usually added to the mass of the bridge.

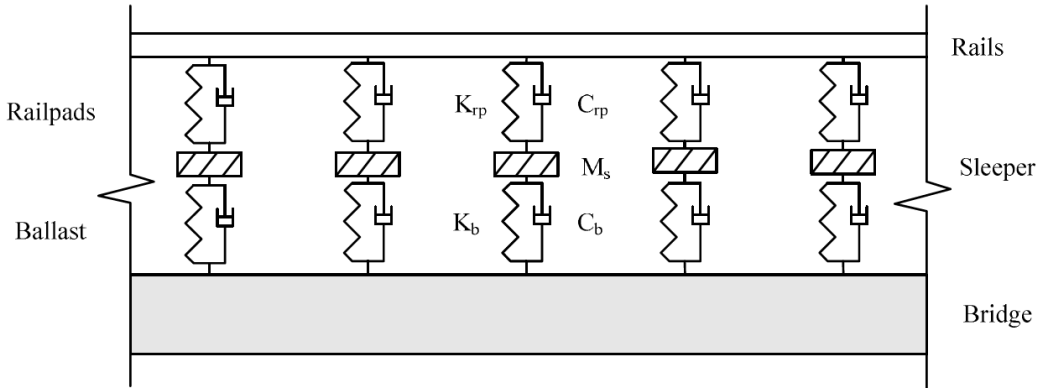

Figure 2.15 Two-layer discrete model for ballasted track-bridge system

The properties of track in a track-bridge two-layer discrete model as shown in Figure 2.15 are given in TABLE III (Man, 2002).

TABLE III
TRACK PROPERTIES OF TWO-LAYER DISCRETE MODEL

Description	Notation	Value	
Vertical stiffness (rail/sleeper)	K_{rp}	300,000 kN/m	(1,713,047 Ib_f/in)
Vertical damping (rail/sleeper)	C_{rp}	80 kN.s/m	(457 Ib_f.s/in)
Crosstie/sleeper mass	M_s	300 kg	(1.713 Ib_f-s^2/in)
Crossties/sleeper spacing	L_s	0.6 m	(23.62 in)
Vertical stiffness of ballast	K_b	120,000 kN/m	(685,219 Ib_f/in)
Vertical damping of ballast	C_b	114 kN.s/m	(651 Ib_f.s/in)

Studies that require the inclusion of the ballast as a vibrating material may use the 2D discrete three-layer model as shown in Figure 2.16. In this model, in addition to the two-layer discrete model, the ballast is considered as suspended masses. These masses are connected to the crossties (sleepers) and to the bridge deck through spring-dampers elements.

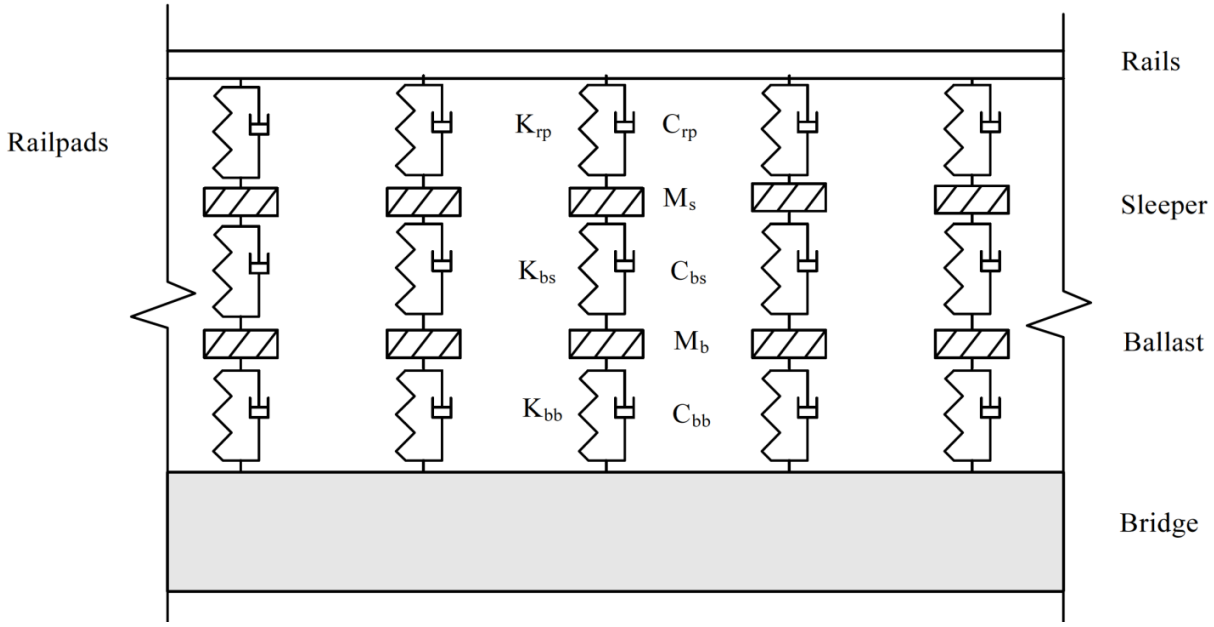

Figure 2.16 Three-layer discrete model for ballasted track-bridge system

The properties of track in a track-bridge three-layer discrete model as shown in Figure 2.16 are given in TABLE IV (ERRI, 1999).

TABLE IV
TRACK PROPERTIES OF THREE-LAYER DISCRETE MODEL

Description	Notation	Value	
Vertical stiffness (rail/sleeper)	K_{rp}	500,000 kN/m	(2,855,079 Ib_f/in)
Vertical damping (rail/sleeper)	C_{rp}	200 kN.s/m	(1142 Ib_f.s/in)
Crosstie/sleeper mass	M_s	290 kg	(1.656 Ib_f-s^2/in)
Crossties/sleeper spacing	L_s	0.6 m	(23.62 in)
Vertical stiffness (ballast/sleeper)	K_{bs}	538,000 kN/m	(3,072,065 Ib_f/in)
Vertical damping (ballast/sleeper)	C_{bs}	120 kN.s/m	(685 Ib_f.s/in)
Ballast mass	M_{ba}	412 kg	(2.353 Ib_f-s^2/in)
Vertical stiffness (bridge/ballast)	K_{bb}	1,000,000 kN/m	(5,710,157 Ib_f/in)
Vertical damping (bridge/ballast)	C_{bb}	50 kN.s/m	(286 Ib_f.s/in)

2.3.4 Modeling of ballastless track-bridge system

Some researchers (Casal, 2010; Proença, 2011) used the model shown in Figure 2.17 to study dynamic behavior of high speed railway bridges with a Rheda type track.

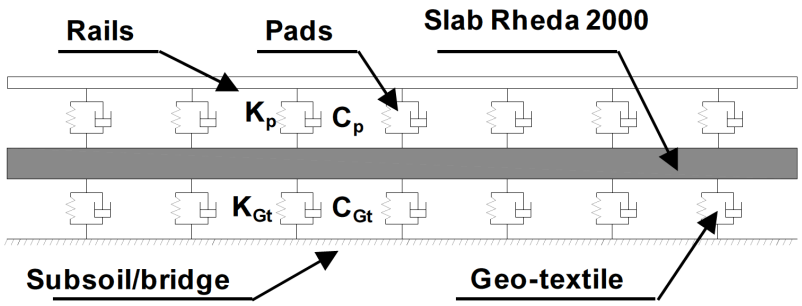

Figure 2.17 Schematic of a ballastless track model

A geotextile is placed under the slab. The main function of the geotextile is to reduce the effects of the interaction between the support structure and the Rheda slab 2000 preventing the breakdown between them, due to the cyclical effects of the use of the trains. Casal (Casal, 2010) adopted a value of $2x10^{10}$ kN/m (1.14×10^{11} Ib_f/in) for vertical stiffness of the geotextile.

2.3.5 Railway track irregularities

An important parameter in the railway bridge and vehicle dynamic responses is the track irregularities. These are deviations from the ideal and perfectly smooth geometry. The rail surface profile may have different conditions due to initial constructions, weather conditions and maintenance. The track irregularities are naturally in three dimensions and the two rails of the track can have two different irregularity profiles independent from each other. However, for the studies of vertical responses of the structure, a mean value of rail irregularities is assumed and they are generally modeled in two dimensions as shown in Figure 2.18.

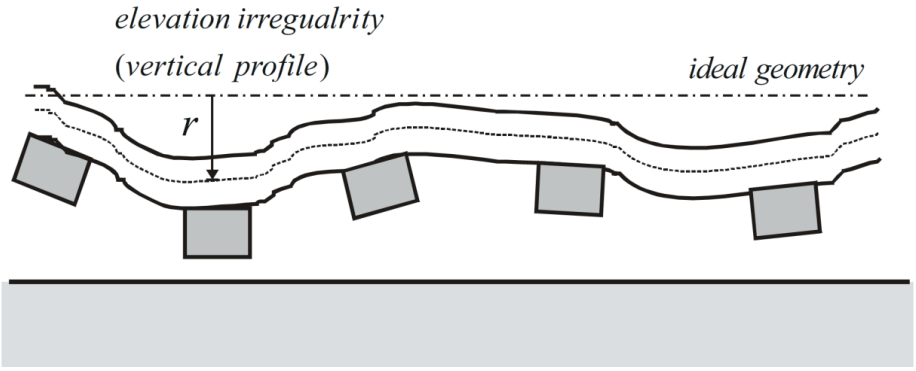

Figure 2.18 Vertical profile of track irregularities

The Track irregularity of railway bridges is typically a random parameter that is fundamentally modeled by functions called Power Spectral Density (PSD). For that purpose, functions are randomly generated depending on the conditions of the track and used to construct a profile over the bridge.

2.3.6 Train vehicle modeling

A variety of models for train vehicles are available depending on applications and goals. The choice of vehicle modeling has a significant impact on the amount of the analysis time and required computational efforts. They should be chosen carefully. This section discusses several different types of traffic loads on railway bridges via simple or complex vehicle models.

2.3.6.1 Moving force models

The most basic and straightforward model used to analyze the dynamic problem of bridges is the moving force (or moving load) model as shown in Figure 2.19.

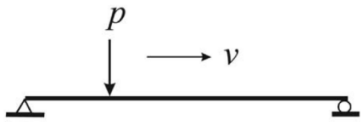

Figure 2.19 Moving force model

In this model, train axle loads are represented by constant vertical forces *p* crossing the bridge at a speed *v* equal to that of the vehicle. Therefore, the interaction effects of bridge and vehicle as well as the vehicle's inertia are all ignored. This is a satisfactory approach in situations where the ratio of the mass of the vehicle to the mass of the bridge is negligible and therefore the behavior of the bridge only is being studied (Yang et al., 2004). In addition, this approach may be considered when certain dynamic sources (such as track irregularities, rail joints, wheel flat, etc.) are not needed in the analysis. Furthermore, this model may be of interest for problems where a closed-form solutions are sought or in the approximate evaluation of the bridge dynamic responses as applied by the authors of (Frýba, 2001; Brady et al., 2006).

Despite providing approximate results the moving force model is the most used in the design and analysis of bridges because it is simple. Extensive previous research efforts in this area can be found in the literature (Frýba, 1972; Wu and Dai, 1987; Weaver et al., 1990; Gbadeyan and Oni, 1995; Wang, 1997; Zheng et al., 1998; Rao, 2000; Chen and Li, 2000; Dugush and Eisenberger, 2002). One more argument for the widespread applications of simple methods like the moving force model is the fact that the important controlling parameters can be ascertained with closed-form solutions; therefore, rational simplified formulas could be written for adoption in codes of design (Humar and Kasif, 1993).

2.3.6.2 Moving mass models

The subsequent straightforward model after the one described in the previous section is the moving mass model as shown in Figure 2.20.

Figure 2.20 Moving mass model

This model may be suitable for problems where the ratio of the mass of the vehicle, *M*, to the mass of the bridge as well as the vehicle's inertia effects on the bridge are not negligible. A vast amount of research has been carried out on the development of numerical and analytical solutions of bridge dynamic problems using moving mass models. Fourier series expansion was utilized by the authors of (Stanišić and Hardin, 1969) to compute "the response of a simple beam" subjected to an "arbitrary" number "of moving masses." Also, in the work of (Ting et al., 1974; Sadiku and Leipholz, 1987), the authors used Green's function to examine the problem of the moving mass. For this model, a closed form solution was initially proposed by (Stanišić, 1985) while investigating the dynamic response of a simple beam crossed by a single mass. The authors of (Akin and Mofid, 1989) utilized the same closed-form solution in an analytical-numerical method to investigate the problem of a moving mass crossing beams having different boundary conditions.

Despite the fact that this model can take into consideration the moving vehicle's inertia effects, it does not however include the effect of relative displacement between the bridge and

the vehicle. This could have considerable impact on the response of the bridge where the track irregularities are to be added to the analysis and also for high-speed vehicles. Moreover, the moving mass model is not adequate for cases where the vehicle's response is also important since the moving mass vibration is usually taken at the point of contact on the bridge surface assuming no-jump of the moving mass.

2.3.6.3 Moving sprung mass models

A model that is simple and takes into consideration the effect of suspension system is the so-called moving sprung mass model as shown in Figure 2.21. In this type of model, the moving mass M_v is supported by a spring and dashpot having a vertical stiffness k_v and a damping constant c_v respectively thus representing the suspensions system of the train vehicle.

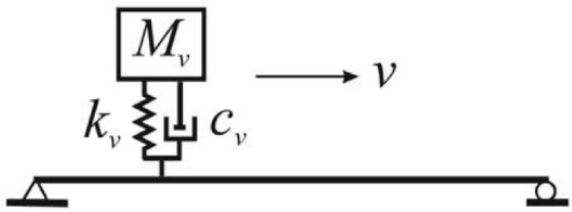

Figure 2.21 Moving sprung mass model

This type of model may be used as a generic system to carry out studies of the interaction between the bridge and the train. The solution of problems involving a sprung mass crossing a simple beam was proposed by Biggs (Biggs, 1964) using an approach based on a semi-analytical method. Later, Frýba (Frýba, 1972) considered various types of vehicle modeling including

moving sprung mass, moving mass and moving load. He investigated the key parameters and the sensitivity as well as impact of different variables on the response of the bridge. He then proposed solutions based on numerical and analytical methods. Other researchers (Pesterev et al., (2001; Pesterev et al., 2003) also investigated the case of an elastic continuum subjected to multiple moving oscillators using the technique of series expansion.

2.3.6.4 Moving system models

In contrast to sprung mass models, more complex models consisting of many degrees of freedom are generally called moving system models. The different components of the train vehicle are treated as discrete masses which are attached to each other by suspension systems. The suspension systems are usually modeled using spring-dampers. Some researchers modeled the stiffness of the suspension systems as springs with linear properties; and the damping of the suspension system and air cushions as linear dashpots (Humar and Kashif, 1993; Green and Cebon, 1994; Xia et al., 2003; Majka and Hartnett, 2008). Nevertheless, other researchers have used nonlinear models for forces in the suspension systems (Hwang and Nowak, 1991; Zhai et al., 2009).

Due to the important dynamic interactions between trains and railway bridges, numerous models have been used to characterize the train. A rather simple model that is able to include the carbody pitching effect was used by some researchers (Yang et al., 1999). Such a model has 4 degrees of freedom: one rotational (or pitching) and three vertical. The car body is assumed to be a rigid bar connected to wheels by two suspension systems assumed to be linear spring-dampers. Other more intricate models with several physical components of a train such as wheelset, truck (bogie), and with the car body having linear suspension properties have been adopted greatly by

many researchers (Zhang et al., 2001; Xia et al., 2001; Xia et al., 2003; Majka and Hartnett, 2008).

This type of advanced train models are mainly used for the analysis of the train-track-bridge interaction systems in high speed rail lines. An example of a two-dimensional train model used by the authors in (Wu and Yang, 2003) is shown in Figure 2.22. This type of 2D model, with 10 degrees of freedom, consists of the carbody, front and rear truck (bogie), and four wheelsets. All bodies are modeled as rigid; and linked by linear springs and dampers as shown. Rotational (or pitching) and vertical degrees of freedom are retained for the carbody and trucks (bogies), and only vertical degrees of freedom are considered for wheels.

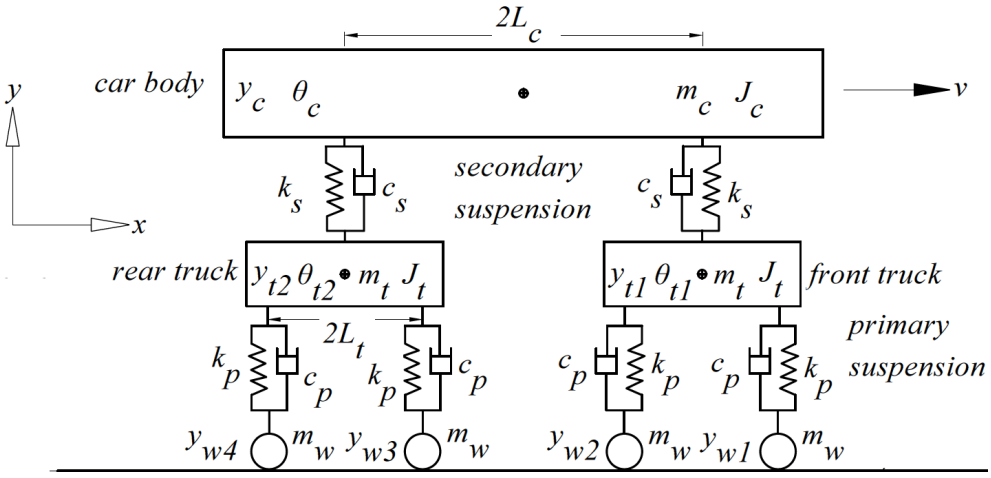

Figure 2.22 Two-dimensional 10-DOF train vehicle model

Other researchers (Majka and Hartnett, 2008) have adopted the 3D vehicle model shown in Figure 2.23. Comparable parts as in the 2D model are assumed for the train vehicle with

additional degrees of freedom. For the carbody and the two trucks (bogies), the total number of degrees of freedom is assumed to be 5.

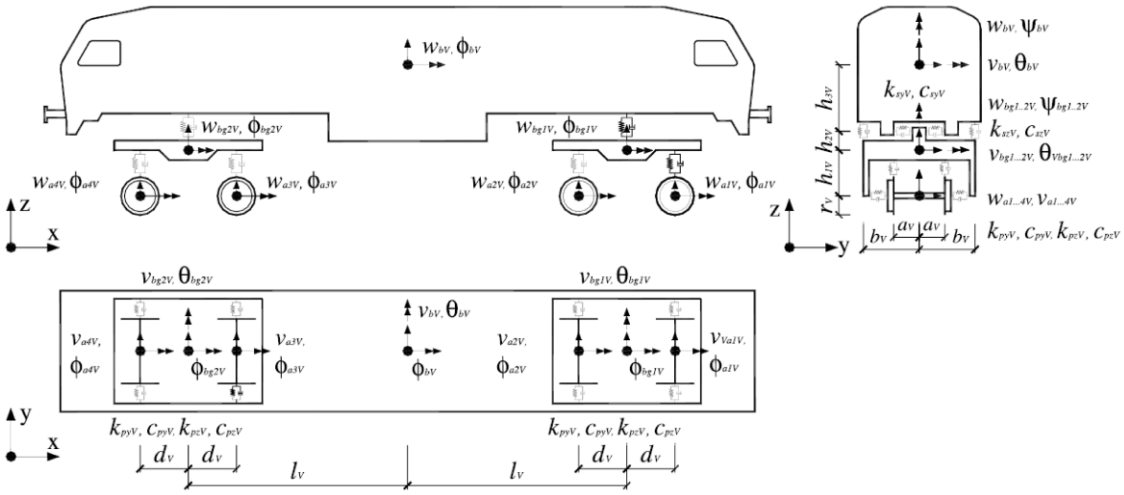

Figure 2.23 Three-dimensional 27-DOF train vehicle model

Two translational degrees of freedom for lateral and vertical displacements and three rotational degrees of freedom for rolling (about x-axis), yawning (about z-axis) and pitching motions are used. For the wheelsets, only 3 degrees of freedom are used including the vertical, lateral and rolling motions. Therefore, a total of 27 degrees of freedom are considered to represent one car of a moving train using a 3D model.

2.3.7 Solution methods of vehicle-track-bridge interaction problems

This section of the chapter discusses the state-of-the-art solution methods used to solve the vehicle-track-bridge interaction problems. For simple and elementary cases in which the

moving force model and the moving mass model are used in conjunction with the bare beam models, closed-form solutions can be found in the literature (Frýba, 1972; Stanišić, 1985). These basic models do not consider the interaction phenomenon. Another method used by many researchers since 1960 is the modal superposition technique (Frýba, 1967; Frýba, 1972; Richardson and Wormley, 1974; Ting and Genin, 1980; Genin et al., 1982; Xia et al., 2001; Xia et al., 2003). However, this latter method is not versatile enough to include some additional effects in the analysis, such as track irregularities. Therefore, this section of the literature review will focus only on recently developed methods having enough complexity and versatility; and of significant relevance to the research of this dissertation.

2.3.7.1 Iterative solution method

The iterative method is a widespread technique that has been used by many researchers to solve the interaction problem between the vehicle and the underlying structure (Hwang and Nowak, 1991; Yang and Fonder, 1996; Delgado and Santos, 1997; Lei and Noda, 2002; Xia et al., 2008; Lee and Kimb, 2010). This method consists of establishing the equilibrium of forces acting on the contact interface and uses successive iterations to impose the constraint equations that relate the vehicle's wheel displacement at the contact point with the corresponding displacement of the structure.

The two subsystems, namely the vehicle and the structure, are treated as two separate entities whose decoupled governing equilibrium equations may be expressed as

$$\begin{bmatrix} \boldsymbol{M}_v & \boldsymbol{0} \\ \boldsymbol{0} & \boldsymbol{M}_s \end{bmatrix} \begin{bmatrix} \ddot{\boldsymbol{a}}_v \\ \ddot{\boldsymbol{a}}_s \end{bmatrix} + \begin{bmatrix} \boldsymbol{C}_v & \boldsymbol{0} \\ \boldsymbol{0} & \boldsymbol{C}_s \end{bmatrix} \begin{bmatrix} \dot{\boldsymbol{a}}_v \\ \dot{\boldsymbol{a}}_s \end{bmatrix} + \begin{bmatrix} \boldsymbol{K}_v & \boldsymbol{0} \\ \boldsymbol{0} & \boldsymbol{K}_s \end{bmatrix} \begin{bmatrix} \boldsymbol{a}_v \\ \boldsymbol{a}_s \end{bmatrix} = \begin{bmatrix} \boldsymbol{F}_v \\ \boldsymbol{F}_s \end{bmatrix} \tag{2.1}$$

where quantities $\boldsymbol{M}$, $\boldsymbol{C}$ and $\boldsymbol{K}$ are the mass, damping and stiffness matrices, respectively. Vector quantities $\boldsymbol{a}$, $\dot{\boldsymbol{a}}$ and $\ddot{\boldsymbol{a}}$ are the nodal displacements, velocities and accelerations respectively. The vector $\boldsymbol{F}$ contains the loads and the subscripts *v* and *s* indicate vehicle and structure, respectively.

According to this iterative method developed by the authors of (Delgado and Santos, 1997), each time step involves the following operations at each iteration j+1: 1) The action of the moving forces, corresponding to the wheelsets of the train, is subjected to the structure. Each moving force F_s^{j+1} is described by

$$F_s^{j+1} = F_{st} + F_{dyn}^{j} \tag{2.2}$$

where F_{st} is the static load of the wheelset and F_{dyn}^{j} is the dynamic component of the interaction force resulting from the previous iteration *j*. At each time step, the forces F_{dyn}^{j} in the first iteration are equal to those calculated in the previous time step. The nodal displacements a_s^{j+1} of the structure are computed by solving its corresponding system of equations, and, from the shape functions of the finite elements, the displacements of the structure under the contact nodes a_y^{j+1} are calculated; 2) At the same time, the displacements a_v^{j+1}, corresponding to the displacements of the structure under the contact nodes a_y^{j+1} plus any track irregularity *r* between the wheel and the rail, are applied at the contact nodes of the vehicle. The reaction forces at the contact nodes are then computed by solving the system of equations corresponding to the vehicle. These reactions are the dynamic components of the interaction force F_{dyn}^{j+1} that is to be applied to the

structure in the next iteration; and 3) a convergence criterion is verified (after each iteration) as described by the following

$$\frac{\left\| F_{dyn}^{j+1} - F_{dyn}^{j} \right\|}{\left\| F_{dyn}^{j} \right\|} \leq \varepsilon \tag{2.3}$$

The parameter ε represents a desired tolerance. If the desired degree of convergence is obtained, the procedure may move to the next time step, otherwise, the process continues to the next iteration.

A comparable approach is proposed by the authors of (Yang and Fonder, 1996) which considers an acceleration scheme, namely the relaxation and Aitken techniques to make the convergence rate better. The researchers in (Lei and Noda, 2002) also adopted a similar scheme, in which the contact forces are computed using the Hertz formula with allowance of penetrations or separations between the wheel and the rail.

These above described iterative methods are limited to the vertical interaction between the vehicle and the structure. However, other authors have developed alternative iterative methods to include the lateral interaction. For example, the researchers in (Nguyen et al., 2009a; Nguyen et al., 2009b) developed a 3D dynamic interaction model that can incorporate the loss of contact between the wheel and the rail, considering tensionless stiffness springs in the vertical direction. In the lateral direction, the contact is characterized by a spring-dashpot in order to model both the normal contact, due to the impact between wheel and rail, and the tangential contact due to the creep forces. Despite the fact this approach accounts for the lateral dynamics

of the vehicle, its scope is limited to ordinary operation scenarios in which the movement of the vehicle does not experience significant lateral disturbances caused by external sources, such as earthquakes or crosswinds.

2.3.7.2 Dynamic condensation method

The authors in (Yang and Yau, 1997) developed a finite element called vehicle-bridge interaction element as shown in Figure 2.24. According to the researchers, this element is both accurate and efficient for modeling the vehicle-bridge interaction.

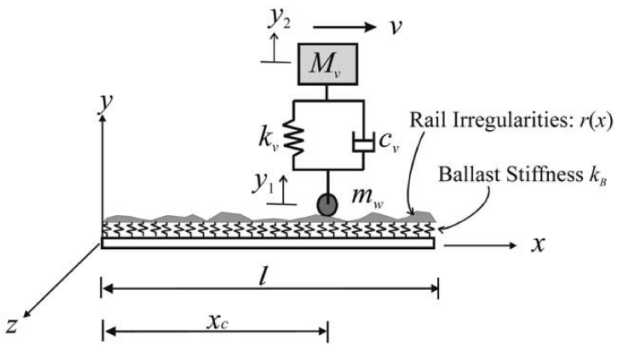

Figure 2.24 Vehicle-bridge interaction element without pitching effect

In their work, the vehicle is modeled as a sequence of lumped sprung masses; the bridge as beam elements; and the track as lumped masses, springs and dashpot elements to represent the ballast. The method is based on the formulation of two equations of motion of the system, one for the bridge and one for the lumped sprung masses representing the vehicle. The equation of the vehicle is then discretized using Newmark's finite difference formulas, resulting in the condensation of its degrees of freedom into the bridge elements that are in contact. As the

vehicle is modeled as a series of sprung masses, the developed interaction element ignores the pitching effect of the vehicle, which may considerably affect the response of the whole system. Therefore, the same authors (Yang et al., 1999) proposed an improved interaction element, in which the vehicle is modeled with a rigid beam supported by two spring-dampers as shown Figure 2.25.

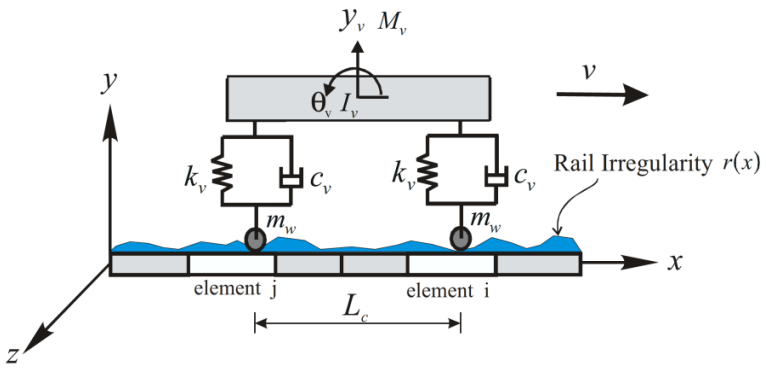

Figure 2.25 Vehicle-bridge interaction element with pitching effect

Despite the fact this improved element considers the pitching effect of the vehicle; it does not include in the model the bogies (trucks). To resolve this drawback, the authors of (Yang and Wu, 2001; Wu et al., 2001) later developed a model and procedure that can simulate vehicle-bridge systems of varying complexity as shown in Figure 2.26.

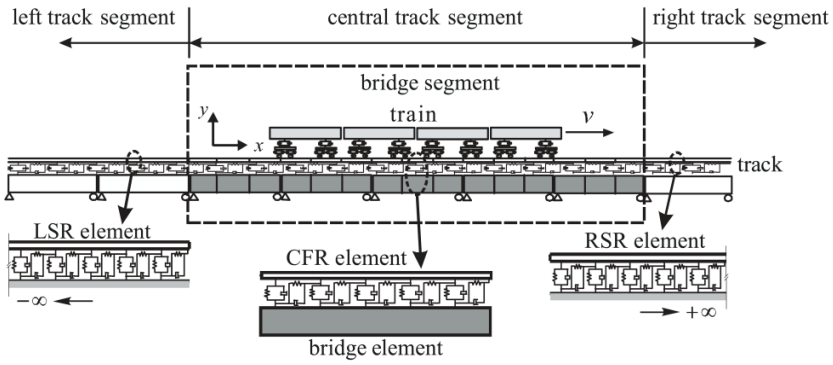

Figure 2.26 Vehicle-bridge interaction model with higher degree of complexity

In depth formulation of the different versions of the interaction element and a number of applications on high-speed railway bridges may be found in (Yang et al., 2004).

The vehicle-bridge interaction element based on the condensation techniques preserve the properties of symmetry and bandwidth. However, as the position of each contact point changes over time, the matrices of the system in this method are time-dependent and must be updated and factorized at each time step, which requires a considerable amount of computational effort.

2.3.7.3 Direct solution method

The author of (Neves et al., 2012) developed a new algorithm, referred to as the direct method; in which additional constraint equations complement the governing equilibrium equations of the vehicle and structure. With no separation between the vehicle and the structure, these “constraint equations relate the displacements of the” vehicle’s contact nodes with “the corresponding nodal displacements of the structure.” The track irregularities at the contact

interface can be included in the constraint equations; and the vehicle and structure subsystems can be modeled using various types of finite elements having any degree of complexity, such as beams, springs, shells, and solids, as shown in Figure 2.27.

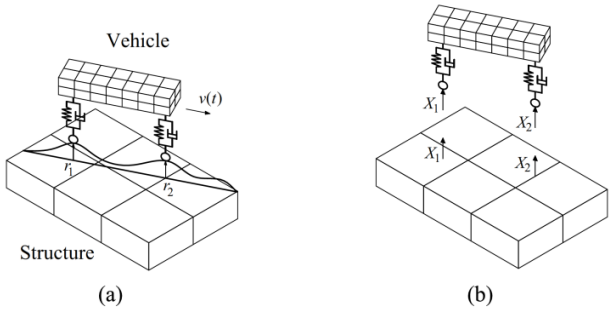

Figure 2.27 Vehicle-structure interaction: (a) schematic and (b) free body diagram

According to the authors of this method, “the equations of motion and the” constraint “equations” represent “a single system, with displacements and contact forces as unknowns.” The equations of the system are then solved directly using an optimized block factorization algorithm, therefore avoiding the iterative procedure to satisfy the constraint equations. In this case, the single system of linear equations is given in matrix form as

$$\begin{bmatrix} \overline{\boldsymbol{K}}_{FF} & \overline{\boldsymbol{D}}_{FX} \\ \overline{\boldsymbol{H}}_{XF} & \boldsymbol{0} \end{bmatrix} \begin{bmatrix} \boldsymbol{a}_F^{t+\Delta t} \\ \boldsymbol{X}^{t+\Delta t} \end{bmatrix} = \begin{bmatrix} \overline{\boldsymbol{F}}_F \\ \overline{\boldsymbol{r}} \end{bmatrix} \tag{2.4}$$

In the above equation, $\overline{\boldsymbol{K}}_{FF}$ represents the “effective stiffness matrix of the vehicle-structure” system. The quantity $\overline{\boldsymbol{D}}_{FX}$ is a transformation “matrix that relates the contact forces” in the local

coordinate to the "nodal forces in the global coordinate." The quantity $\bar{\boldsymbol{H}}_{XF}$ is a "transformation matrix" that associates the global coordinate "nodal displacements" to the local coordinate displacements of auxiliary points. The quantities $\boldsymbol{a}_F^{t+\Delta t}$ and $\boldsymbol{X}^{t+\Delta t}$ are the current time step's nodal displacements and contact forces respectively. The quantity $\bar{\boldsymbol{F}}_F$ is the load vector and the quantity $\bar{\boldsymbol{r}}$ represents the track irregularities at the contact interface.

In a later publication in 2014, the authors of (Neves et al., 2014) extended their formulation to include the case of a separation between the wheel and the rail. These researchers developed a contact search algorithm that aims to detect which elements are in contact and therefore the constraint is only imposed only when contact occurs. As a frictionless contact only is considered in this formulation, the constraint equations are rather geometric and relate the displacements of the contact node to the displacements of the corresponding target element. Because of the nonlinear nature of the contact problem, an iterative algorithm based on the Newton method (Owen and Hinton, 1980; Bathe, 1996) is considered to solve the equation of motion of the vehicle-structure system, and therefore the system of equations is given in an incremental form as

$$\begin{bmatrix} \bar{\boldsymbol{K}}_{FF} & \bar{\boldsymbol{D}}_{FX} \\ \bar{\boldsymbol{H}}_{XF} & \boldsymbol{0} \end{bmatrix} \begin{bmatrix} \Delta \boldsymbol{a}_F^{j+1} \\ \Delta \boldsymbol{X}^{j+1} \end{bmatrix} = \begin{bmatrix} \Psi(\boldsymbol{a}_F^{t+\Delta t,j}, \boldsymbol{X}^{t+\Delta t,j}) \\ \bar{\boldsymbol{r}} \end{bmatrix} \tag{2.5}$$

In the above equation, the quantities $\Delta \boldsymbol{a}_F^{j+1}$ and $\Delta \boldsymbol{X}^{j+1}$ at the current iteration represent the incremental displacements and contact forces respectively. The quantity Ψ represents the

residual force vector and depends on the nodal displacements and contact forces computed in the previous iteration. The iterative process continues until the following condition is satisfied.

$$\frac{\left\|\Psi(\boldsymbol{a}_F^{t+\Delta t,j+1}, \boldsymbol{X}^{t+\Delta t,j+1})\right\|}{\|P_F^{t+\Delta t}\|} \leq \varepsilon \tag{2.6}$$

In the above equation, the quantity $P_F^{t+\Delta t}$ represents the vector of applied external loads at the current time step. The parameter ε represents a desired tolerance. It should be noted that the iteration procedure of this improved direct method is not related to the compatibility of displacements between the vehicle and the underlying structure, as described in the iterative solution method of section 2.3.7.1, but rather to the nonlinear nature of the contact due to the consideration of contact loss.

2.4 Review of International Codes and Standards

The objective of this section of the dissertation is to provide an overview of the various current international codes and technical standards dealing with the dynamic analysis of railway bridges used in high speed train lines. In Europe, “Eurocodes for construction” of the new European standards are now the basis for designing high speed railway bridges. Rules and recommendations related to Serviceability Limit States (SLS), actions and calculations are available in two major documents: Eurocode European Norm (EN) 1990 Annex A2 and European Norm (EN) 1991, Part 2, Section 6. These two documents summarize study efforts based on collective experience of different European railway companies. These works have been compiled and published into the so-called UIC leaflets which serve as technical guidelines in

many parts of the world, including the standards of the California High-Speed Train Project (CHSTP, 2014) in the United States. As a result, this section focuses on the dynamic analysis of railway bridges as outlined in the rules of Eurocodes and provides some background information about those rules.

2.4.1 Requirements for dynamic analysis

The current state-of-the art in the evaluation of dynamic effects in high speed rail bridges is, first of all, to make a determination whether dynamic analysis is required or not. For this purpose, the ERRI D214 committee, appointed by the *Union International de Chemin de fer* (UIC), proposed a flow chart as shown in Figure 2.28 adopted from (UIC Leaflet 776-2, 2nd edition, 2009) that should be used for such a determination but also gives guidance concerning dynamic analysis methodologies.

The parameters of the flow chart depend on: i) the maximum speed of the high speed rail line; ii) the simplicity of the structure, iii) the span; and iv) the first natural bending and torsional frequencies.

The “simplicity” of the structure refers to high speed railway bridges that may be considered to be simply supported and modeled with longitudinal line beam or simple plate with negligible skew. The flow chart implies that, for simple structures of high speed railway bridges with a span L > 40 m (131.23 ft) and with first natural bending frequency n_o within the limits shown in Figure 2.29 (UIC Leaflet 776-2, 2nd edition, 2009), no dynamic analysis is required.

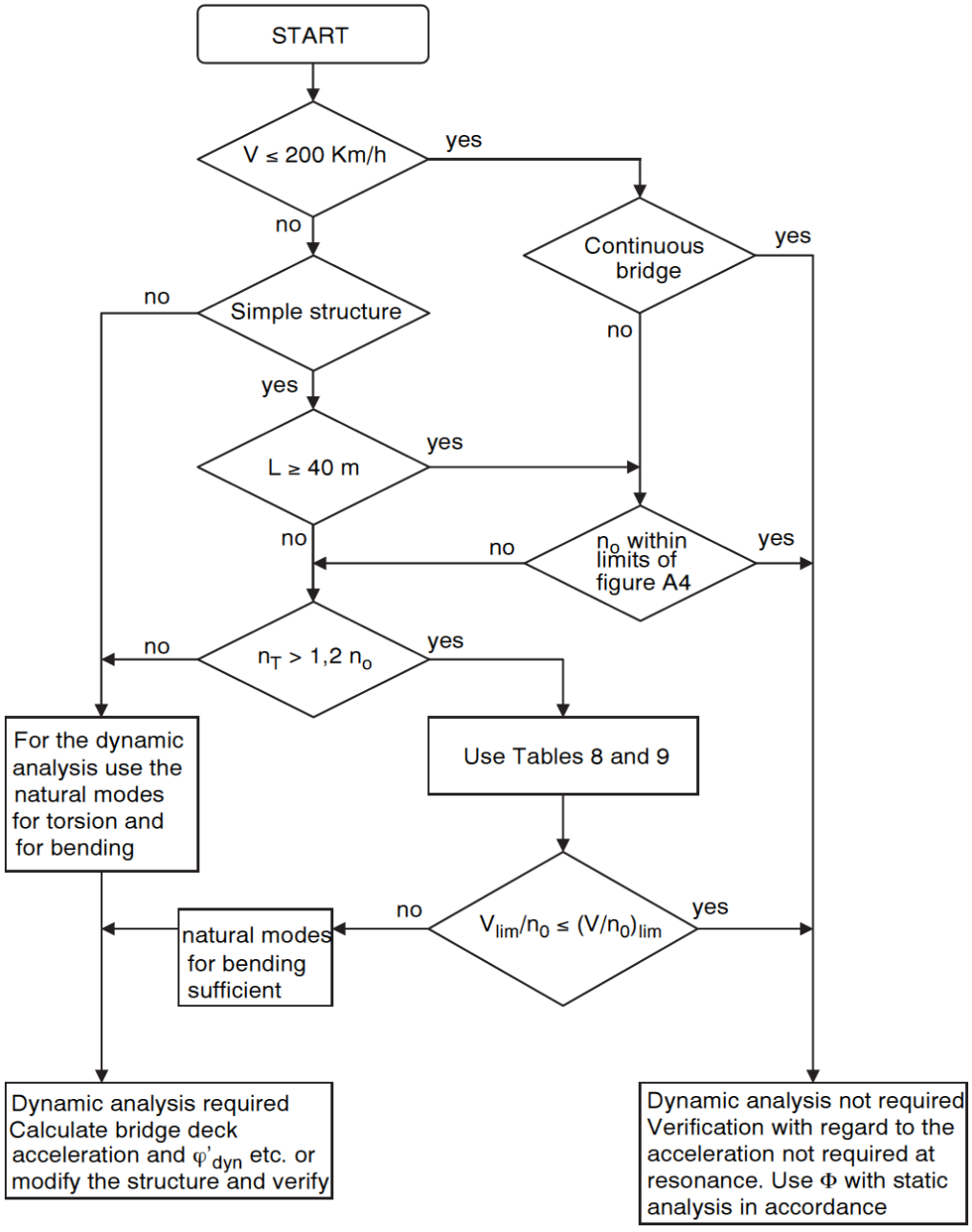

Figure 2.28 Flow chart for dynamic analysis requirement check

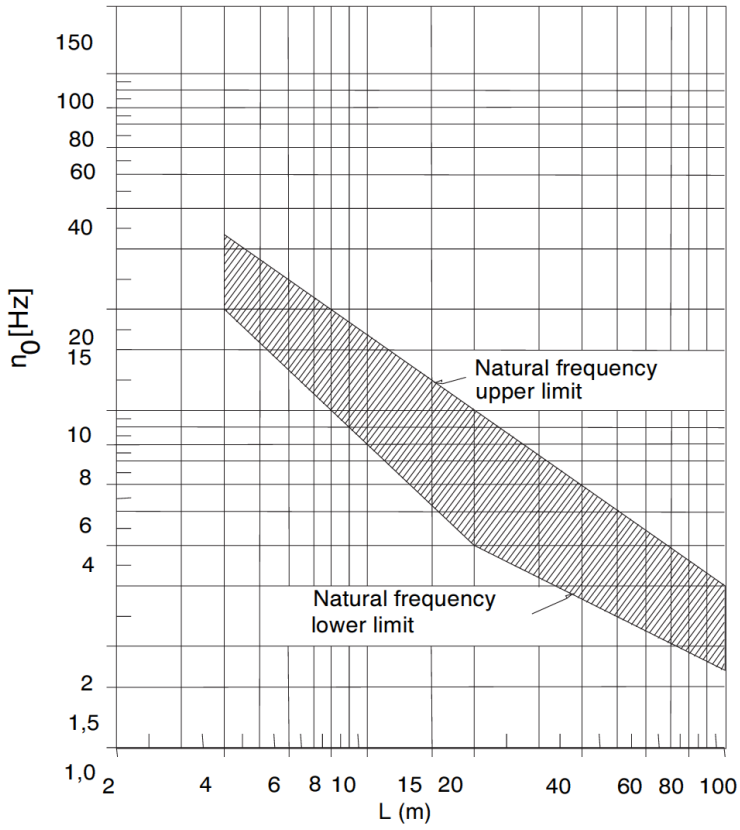

Figure 2.29 Limits of first natural frequency in relation to span length

The limits of Figure 2.29 define the range of spans and first natural bending frequencies for which the dynamic effects are obtained by multiplying the static effects with a dynamic amplification factor *Φ*. According to the flow chart, the use of this dynamic amplification factor is also valid for short span railway bridges of a span L< 40 m (131.23ft) with an unlikely coupling of bending and torsion, and where the ratio v_{lim}/n_0 is lower than the ratio $(v/n_0)_{lim}$ given in TABLE V (referred to table 8 in Figure 2.29) for ballasted track and TABLE VI (referred to table 9 in Figure 2.29) for ballastless track. Both tables are adopted from (UIC Leaflet 776-2, 2nd edition, 2009).

TABLE V
MAXIMUM VALUE $(v/n_0)_{lim}$ FOR BEAM OR PLATE ON SIMPLE SUPPORTS AND WITH A MAXIMUM PERMISSIBLE ACCELERATION SMALLER THAN 3.50 m/s^2

Mass m 10^3 kg/m		≥ 5,0 < 7,0	≥ 7,0 < 9,0	≥ 9,0 < 10,0	≥ 10,0 < 13,0	≥ 13,0 < 15,0	≥ 15,0 < 18,0	≥ 18,0 < 20,0	≥ 20,0 < 25,0	≥ 25,0 < 30,0	≥ 30,0 < 40,0	≥ 40,0 < 50,0	≥ 50,0 -
Span L ∈ m [a]	ζ	v/n_o	v/n_o	v/n_o	v/n_o	v/n_o	v/n_o	v/n_o	v/n_o	v/n_o	v/n_o	v/n_o	v/n_o
	%	m	m	m	m	m	m	m	m	m	m	m	m
[5,00 ; 7,50)	2	1,71	1,78	1,88	1,88	1,93	1,93	2,13	2,13	3,08	3,08	3,54	3,59
	4	1,71	1,83	1,93	1,93	2,13	2,24	3,03	3,08	3,38	3,54	4,31	4,31
[7,50 ; 10,0)	2	1,94	2,08	2,64	2,64	2,77	2,77	3,06	5,00	5,14	5,20	5,35	5,42
	4	2,15	2,64	2,77	2,98	4,93	5,00	5,14	5,21	5,35	5,62	6,39	6,53
[10,0 ; 12,5)	1	2,40	2,50	2,50	2,50	2,71	6,15	6,25	6,36	6,36	6,45	6,45	6,57
	2	2,50	2,71	2,71	5,83	6,15	6,25	6,36	6,36	6,45	6,45	7,19	7,29
[12,5 ; 15,0)	1	2,50	2,50	3,58	3,58	5,24	5,24	5,36	5,36	7,86	9,14	9,14	9,14
	2	3,45	5,12	5,24	5,24	5,36	5,36	7,86	8,22	9,53	9,76	10,36	10,48
[15,0 ; 17,5)	1	3,00	5,33	5,33	5,33	6,33	6,33	6,50	6,50	6,50	7,80	7,80	7,80
	2	5,33	5,33	6,33	6,33	6,50	6,50	10,17	10,33	10,33	10,50	10,67	12,40
[17,5 ; 20,0)	1	3,50	6,33	6,33	6,33	6,50	6,50	7,17	7,17	10,67	12,80	12,80	12,80
[20,0 ; 25,0)	1	5,21	5,21	5,42	7,08	7,50	7,50	13,54	13,54	13,96	14,17	14,38	14,38
[25,0 ; 30,0)	1	6,25	6,46	6,46	10,21	10,21	10,21	10,63	10,63	12,75	12,75	12,75	12,75
[30,0 ; 40,0)	1				10,56	18,33	18,33	18,61	18,61	18,89	19,17	19,17	19,17
≥ 40,0	1				14,73	15,00	15,56	15,56	15,83	18,33	18,33	18,33	18,33

a. L ∈ [a, b) means a ≤ L < b

It can be observed from the above flow chart that the use of dynamic amplification factor is rather limited because the cases for which a dynamic analysis is required are many such as:

- non-simple bridges with continuous deck, skew decks, portal and frame bridges;
- simply supported structures with span greater than 40 m (131.23 ft) and first natural bending frequency outside the specified limits; and
- simply supported bridges with span smaller than 40 m (131.23 ft) and $n_T < 1.2n_0$.

TABLE VI
MAXIMUM VALUE $(v/n_0)_{lim}$ FOR BEAM OR PLATE ON SIMPLE SUPPORTS AND WITH A MAXIMUM PERMISSIBLE ACCELERATION SMALLER THAN 5 m/s^2

Mass 10^3 kg/m		≥ 5,0 < 7,0	≥ 7,0 < 9,0	≥ 9,0 < 10,0	≥ 10,0 < 13,0	≥ 13,0 < 15,0	≥ 15,0 < 18,0	≥ 18,0 < 20,0	≥ 20,0 < 25,0	≥ 25,0 < 30,0	≥ 30,0 < 40,0	≥ 40,0 < 50,0	≥ 50,0 -
Span $L \in$ m [a]	ζ	v/n_o	v/n_o	v/n_o	v/n_o	v/n_o	v/n_o	v/n_o	v/n_o	v/n_o	v/n_o	v/n_o	v/n_o
	%	m	m	m	m	m	m	m	m	m	m	m	m
[5,00 ; 7,50)	2	1,78	1,88	1,93	1,93	2,13	2,13	3,08	3,08	3,44	3,54	3,59	4,13
	4	1,88	1,93	2,13	2,13	3,08	3,13	3,44	3,54	3,59	4,31	4,31	4,31
[7,50 ; 10,0)	2	2,08	2,64	2,78	2,78	3,06	5,07	5,21	5,21	5,28	5,35	6,33	6,33
	4	2,64	2,98	4,86	4,93	5,14	5,21	5,35	5,42	6,32	6,46	6,67	6,67
[10,0 ; 12,5)	1	2,50	2,50	2,71	6,15	6,25	6,36	6,36	6,46	6,46	6,46	7,19	7,19
	2	2,71	5,83	6,15	6,15	6,36	6,46	6,46	6,46	7,19	7,19	7,75	7,75
[12,5 ; 15,0)	1	2,50	3,58	5,24	5,24	5,36	5,36	7,86	8,33	9,14	9,14	9,14	9,14
	2	5,12	5,24	5,36	5,36	7,86	8,22	9,53	9,64	10,36	10,36	10,48	10,48
[15,0 ; 17,5)	1	5,33	5,33	6,33	6,33	6,50	6,50	6,50	7,80	7,80	7,80	7,80	7,80
	2	5,33	6,33	6,50	6,50	10,33	10,33	10,50	10,50	10,67	10,67	12,40	12,40
[17,5 ; 20,0)	1	6,33	6,33	6,50	6,50	7,17	10,67	10,67	12,80	12,80	12,80	12,80	12,80
[20,0 ; 25,0)	1	5,21	7,08	7,50	7,50	13,54	13,75	13,96	14,17	14,38	14,38	14,38	14,38
[25,0 ; 30,0)	1	6,46	10,20	10,42	10,42	10,63	10,63	12,75	12,75	12,75	12,75	12,75	12,75
[30,0 ; 40,0)	1				18,33	18,61	18,89	18,89	19,17	19,17	19,17	19,17	19,17
≥ 40,0	1				15,00	15,56	15,83	18,33	18,33	18,33	18,33	18,33	18,33

a. $L \in$ [a, b) means $a \leq L < b$

A significant drawback of the flow chart is that, for small high speed railway bridges made of reinforced concrete, models to be used in dynamic analysis are not given in European Norms standards. Also, the stiffness for concrete in flexure or tension obtained using those standards is underestimated. Deflections obtained with static actions are always lower than those obtained with the rules of the standards.

This is due to the fact that:

- the effects of the flexural track rigidity in small structures are more significant for shorter span bridges;
- very high loads are used to estimate cracking in concrete;
- boundary conditions of the structure are often different from those assumed in the modeling; and
- the dynamic modulus of the concrete is larger than the static modulus and the actual static modulus may be larger than the assumed modulus.

2.4.2 Requirements for dynamic models

Dynamic problems where analytical procedure may be used to solve the equations describing the effects of trains traversing a beam are confined to simply supported beams. Approximations are made even when computer software is utilized. Nowadays, many Finite Element Method (FEM) programs are able to correctly calculate dynamic response of trains running over any kind of bridge.

In both cases, however, train loading, geometrical and mechanical data as well as track parameters have to be defined by the designer. The standards provide a specific guidance to determine the input values for the computations despite recommendations are lacking for the type of bridge models to be used.

2.4.2.1 Train and load models

The types of high speed train described in the standards vary broadly in terms of distance between axles, coach lengths, etc. They can be classified into three categories as shown in Figure 2.30 (European Committee of Standardization, 2003): trains with articulated configuration (one truck/bogie between coaches), trains with conventional configuration (two trucks/bogies per coach) and trains of the regular type (one axle between coaches).

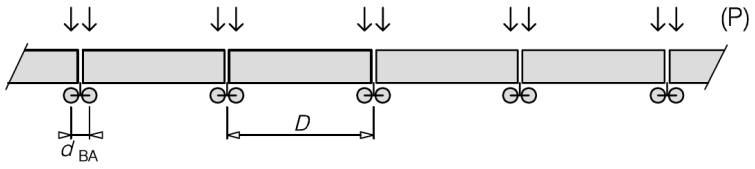

Figure E1 - Articulated train

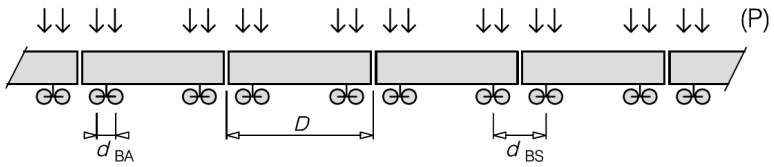

Figure E2 - Conventional train

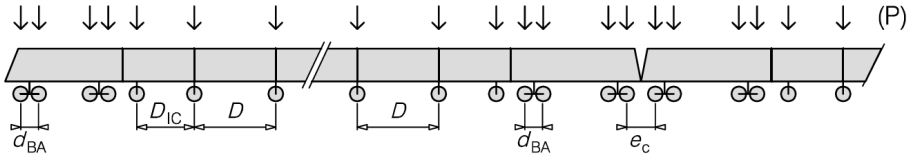

Figure E3 - Regular train

Figure 2.30 Types of high speed trains according to Eurocode 1

The approach of performing dynamic analysis for all train types is cumbersome and time consuming. To limit the number of computations to be performed and standardize loading models, the committee ERRI D214 has established the so-called High Speed Load Model

(HSLM) which is made of a family of fictitious trainsets for which dynamic effects have been shown to be an envelope of all current and future trainsets.

The family of HSLM load models comprises of two separate models of trains with variable coach lengths, HSLM-A and HSLM-B. The load model HSLM-A constitutes of 10 universal trains as shown in TABLE VII (European Committee of Standardization, 2003), and intended to be used for continuous and complex structures as well as bridges with a span greater than 7 m (23 ft). The load model HSLM-B is intended to be used for very short bridges with spans smaller than 7 m (23 ft).

TABLE VII
HSLM-A HIGH SPEED TRAIN LOAD MODEL

Universal train	Number of intermediate coaches N	Length of coach D [m]	Axle spacing in the bogie d [m]	Localised force P [kN]
A1	18	18	2,0	170
A2	17	19	3,5	200
A3	16	20	2,0	180
A4	15	21	3,0	190
A5	14	22	2,0	170
A6	13	23	2,0	180
A7	13	24	2,0	190
A8	12	25	2,5	190
A9	11	26	2,0	210
A10	11	27	2,0	210

The HSLM-B load model (European Committee of Standardization, 2003) comprises of N number of point forces of 170 kN (38,218 Ib_f) with uniform spacing d. The parameters N and d are obtained from Figures 2.31 and 2.32.

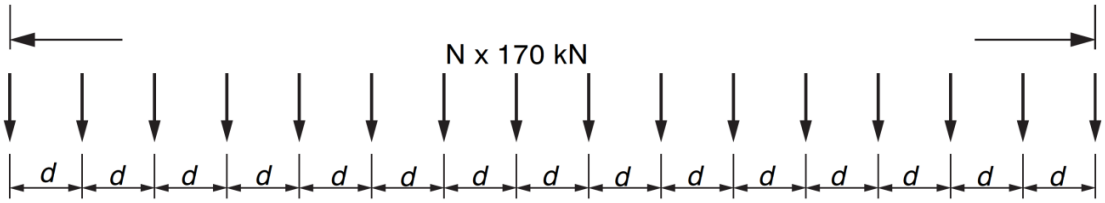

Figure 2.31 HSLM-B high speed train load model

It should be noted however that the HSLM load models imply running vertical point forces representing maximum axle loads applied to the axis of the track on the bridge. Therefore, the distribution of the wheel load by the rail and the ballast is not considered. This may be acceptable for long span bridges but it is not acceptable for small short span bridges. Moreover, these types of load models are not suitable for train-track-bridge interaction problems nor can they be used for studying passenger comfort problems.

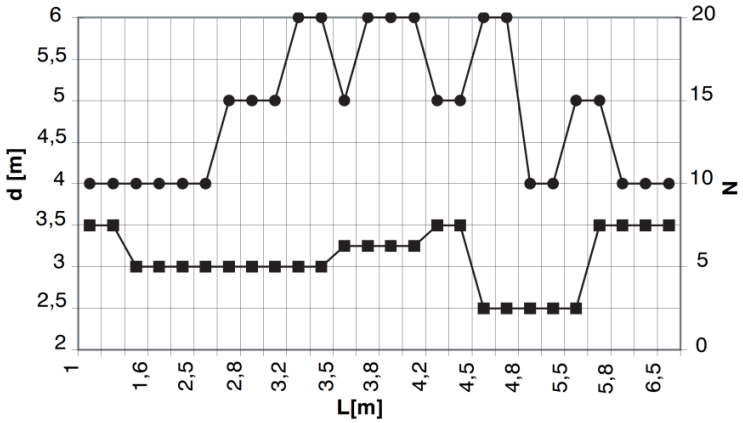

Figure 2.32 Number of N point forces and d spacing of HSLM-B model

The HSLM universal trains are the simplest form of live load models and provide less accurate results than the complex models, particularly for short span high speed railway bridges. Consequently, the UIC leaflet 776-2 recommends the use of the load model shown in Figure 2.33 where the coupling between the wheel and the rail is modeled by means of a Hertzian contact model.

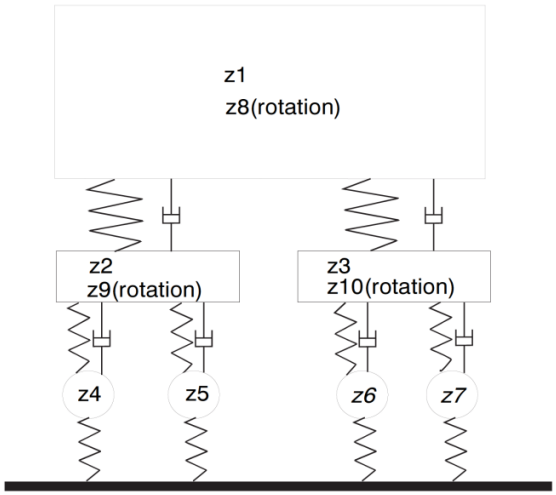

Figure 2.33 Train model according to European Code

2.4.2.2 Bridge models

The international codes and standards require that the bridge be modeled as accurately as possible using two or three dimensional elements. In fact, the relevant codes recognize that modeling methods that utilize beam elements are the most appropriate to evaluate the dynamic behavior of bridges and structures mainly composed of bars. There exists some flexibility for designers to use proven and efficient models provided in technical papers and text books. However, regardless of whether modal analysis method or analysis by direct integration methods are used, most international codes provide guidelines for model inputs like mass, stiffness, damping and boundary conditions of the structure.

The mass of the bridge changes during the life of the structure. The distribution of the mass along the bridge may also vary. The maximum acceleration of the structure at resonance is typically proportional to its mass. Therefore, the European Norms EN1991-2 recommends that a minimum and maximum value of the mass of the bridge be taken into account. The minimum estimate of the mass is intended to predict the maximum deck acceleration with a minimum likely dry clean density and minimum ballast thickness. The maximum estimate of the mass is intended to predict the lowest resonance speeds likely to occur with maximum saturated density of dirty ballast.

The stiffness of the bridge changes also during the life of the structure. Generally, at the beginning of the life of the bridge, the stiffness is high and the mass is at its minimum. At the end of the bridge's life, the opposite is true. This implies that the natural frequency of the bridge decreases with time and resonance may occur with proportionally lower train speeds. A maximum stiffness corresponds to a section free of cracks, for example, or without any reduction

of stiffness from its original design. A minimum stiffness corresponds to cracked sections, for example, or additional effects leading to reduction in stiffness such as effects of differential settlement, contraction and temperature. Consequently the codes recommends that a lower bound of stiffness be considered in conjunction with a maximum value of the mass; and a upper bound of the stiffness in conjunction with a minimum values of the mass.

The damping of the bridge is a parameter that is difficult to quantify. Yet, the peak responses of the bridge at train speeds corresponding to resonant loading depends highly on the damping. So, the codes adopted by most international high speed rail authorities provide some guidance as to the damping to be used for consistency during the design. For example in Europe, the damping values to be assumed for different types of high speed rail bridges during the design is shown in TABLE VIII (UIC Leaflet 776-2, 2nd edition, 2009).

TABLE VIII
DAMPING VALUES FOR DESIGN PURPOSES

Type of bridge	**Lower limit of the percentage of critical damping ζ [%]**	
	Span length L < 20 m	Span length L ≥ 20 m
Metal and mixed	ζ = 0,5 + 0,125 (20 - L)	ζ = 0,5
Encased steel girders and reinforced concrete	ζ = 1,5 + 0,07 (20 - L)	ζ = 1,5
Pre-stressed concrete	ζ = 1,0 + 0,07 (20 - L)	ζ = 1,0

According to the European Norms (EN), real trains may be represented by a series of travelling point forces and the vehicle/bridge mass interaction may be neglected. At the same time these

codes indicate that for short bridges with spans less than 30 m (98.43 ft) the dynamic vehicle-bridge interaction reduces the peak responses at resonance. To account for these effects a dynamic vehicle-bridge interactive analysis may be carried, or the moving force model may be used with an increase of the assumed bridge damping as shown in Figure 2.34. This additional damping, however, was calibrated for the Inter-City Express 2 (ICE-2) and Eurostar real trains only and its use may not be justified for other real trains.

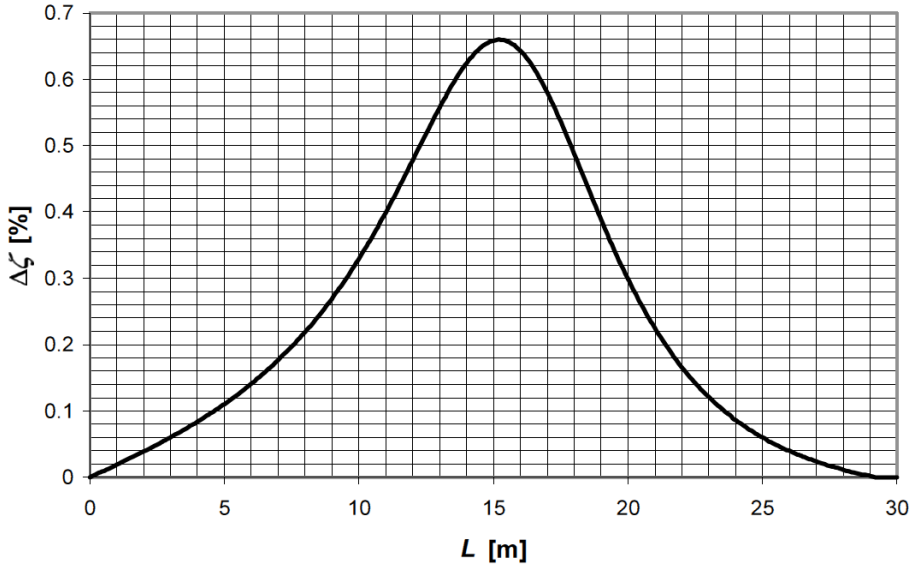

Figure 2.34 Additional damping to account for effects of vehicle-bridge interaction

2.4.2.3 Track models

According to the UIC Leaflet 776-2, the track may be modeled with Timoshenko beam elements for the rails and the rail/sleeper fastening characteristics as well as the ballast (if applicable) may be taken into consideration. Sleepers and ballast are represented by concentrated

masses. As shown Figure 2.35, parallel spring and damper systems are used to link the rail, sleeper, ballast and bridge or subgrade. Any length on both sides of the bridge may be included. This model provides better results especially for short span bridges where the stiffening effect of the structure has to be included. However, the effects of track distribution are not added with this model.

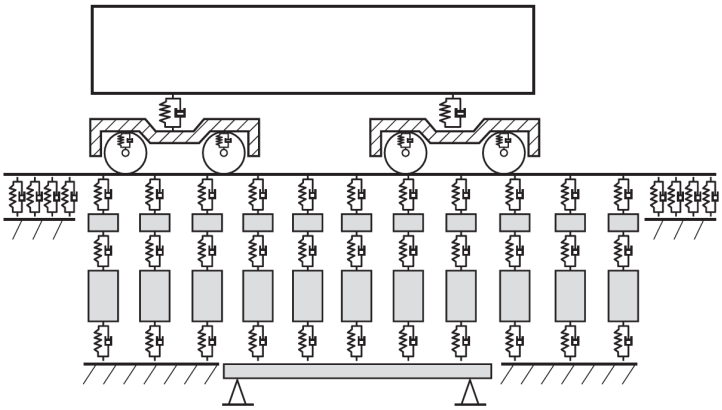

Figure 2.35 Dynamic train-track-bridge model

Each train vehicle is capable of absorbing the kinetic energy of the bridge. Consequently at resonance, the bridge deflections and accelerations using this model are lower than those obtained from the moving force model. It should be noted, however, that in cases where the ultimate goal is not to study behavior of sleepers and ballast, this model may be modified by replacing the track's three layers of elastic elements in series with an equivalent spring and damper.

2.4.3 Serviceability limit state criteria

An important code requirement for high speed rail bridges is a set of criteria related to Serviceability Limit State (SLS). One of the critical criterions to check in a dynamic analysis is

the bridge deck vertical acceleration. For ballasted tracks, the maximum value of bridge deck vertical acceleration limited to 3.5 m/s^2 (11.5 ft/s^2). This limitation is to provide a safety factor of 2 against ballast liquefaction. For ballastless track and for track stability and wheel/rail contact, this value is limited to 5.0 m/s^2 (16.4 ft/s^2).

Another important criterion in international standards and codes is to guarantee the passenger comfort by limiting the vertical acceleration in the vehicle. It is generally stated that a vertical acceleration in the train vehicle of 2 m/s^2 (6.6 ft/s^2) is acceptable and a value of 1.0 m/s^2 (3.3 ft/s^2) is very good as far as the passenger comfort is concerned. This criterion of passenger comfort is directly related to the maximum allowable vertical deflection of the bridge deck. In order to achieve the 1.0 m/s^2 (3.3 ft/s^2) vertical acceleration in the vehicle, the maximum permissible deflection of the bridge deck should be according to the values given in Figure 2.36 (UIC Leaflet 776-2, 2nd edition, 2009). This limit value of L/δ depends on the bridge span and the train speed.

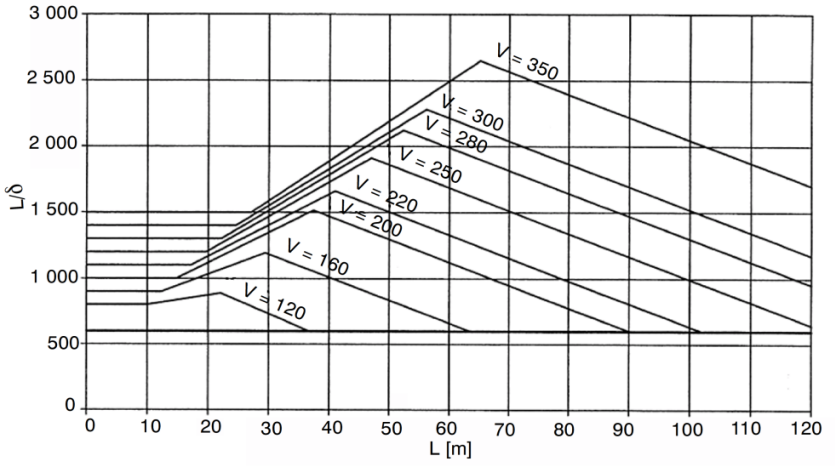

Figure 2.36 Maximum allowable vertical deflection of bridge corresponding to a vertical acceleration in the vehicle of 1 m/s^2

CHAPTER 3

NUMERICAL MODEL OF A TRAIN-TRACK-BRIDGE INTERACTION

Parts of the material presented in this chapter are published in (Nour and Issa, 2016) and reproduced in this dissertation with permission which is listed in Appendix B. The author of this dissertation is a contributing co-author.

3.1 Introduction

The study of dynamic responses of a railway bridge traversed by a train has been a topic of interest for engineers and researchers since the end of the 19th century. In earlier studies, the moving force model was used where the vehicle inertia was believed to be small compared to that of the bridge (Timoshenko, 1922) and the moving mass model was used where the mass of the vehicle was significant in relation to that of the bridge (Frýba, 1999). With the increase of train speeds and axle loads as well as expansion of high speed rail networks, the interaction problem between the vehicles and bridge structures has gained much more attention in the last several decades. Some previous studies have entirely excluded the effects of the track structure (Yang et al., 1997; Cheung et al, 1999; Yang et al., 1999). Other previous research partially accounted for the effects of the track in the interaction investigations (Wiriyachai et al, 1982; Chu et al, 1986; Yang and Yau, 1997). The dynamic response of track structures under moving loads has been often studied by modeling the railway track system as either a beam on a Winkler foundation (Duffy, 1990; Thambiratnam and Zhuge, 1996) or a beam supported on a

series of discrete springs and dampers (Clark et al., 1982; Zhai and Cai, 1997; Oscarsson and Dahlberg, 1998). Analytical methods of bridge analysis were limited to moving forces where closed forms of the solution could be derived. Semi-analytical methods of the vehicle-track-bridge problem were used by a number of researchers (Hutton and Cheung, 1979; Frýba, 1999) by solving numerically the coupled second order differential equations of the system using modal superposition for the bridge and treating the vehicle as a sprung mass. For the vehicle-track-bridge interaction problems of higher complexities, numerical methods based on the finite element formulation were found to be more versatile by the authors in (Lin and Trethewey, 1990; Cheng et al., 2001; Lou, 2005; Lou and Zeng, 2005) who treated the entire system as a coupled whole system for simply supported bridges and solved using Newmark integration scheme with time-dependent matrices. These techniques have a drawback in computational efforts or convergence issues requiring iterations. Furthermore, a literature review carried out by the author of this dissertation has found that limited research studies have dealt with the train-track-bridge interaction problem considering a train convoy or including the flexibility in the bridge supports. The authors of (Yau et al., 2001) have studied the dynamic responses of bridges with elastic bearings but have not taken into consideration the train vehicle interaction and track effects. The work of (Fournol and Dieleman, 2005) consisted of calibrating a theoretical model to match the field measured fundamental frequency of short span bridges. Their approach was to select values of a pair of vertical spring stiffness and rotational spring stiffness inserted at the bridge ends of their theoretical model to match the calculated fundamental frequency to the measured one. They then performed numerical simulations without any damping of the bridge supports and without vehicle interaction.

In this chapter of the dissertation, a 2D train-track-bridge model is developed for use in dynamic simulations of short span high speed rail bridges. The interaction between the train and the track-bridge is considered as an interaction between two decoupled subsystems. A first subsystem is assumed to be the train vehicle treated as a four-wheelset mass-spring-damper system with two-layer of suspension systems possessing 10 degrees of freedom. The eccentricities of the masses are ignored. A second subsystem is assumed to be the underlying track-bridge system treated as a top rail beam and a bottom bridge beam coupled by continuous springs and dampers representing the elastic properties of the trackbed smeared over the spacing of the sleepers (crossties). The bridge supports are assumed to be flexible characterizing elastomeric bearings and/or soft foundation. Linear viscoelastic elements are used to model the boundary conditions. Two sets of equations of motion of the finite element form are derived for each subsystem independently by means of the Newton's second law. The dynamic interaction between the moving vehicle of the first subsystem and the underlying stationary track-bridge structure of the second subsystem is established by means of a no-separation constraint equation at the contact points where the degrees of freedom of the wheels are condensed to those of the rails. Numerical solutions of the decoupled equations of motion for both subsystems are obtained with the step-by-step direct time integration using HHT alpha method with a special scheme at the contact interface. The solution accuracy of the proposed method is validated at the end of the chapter against responses obtained from a semi-analytical method of a single train car travelling over a simply supported bridge. The numerical model thus synthesized in this chapter is used to examine modal characteristics of bridges in Chapter 4 and to investigate the dynamic behavior of short span high speed rail bridges through parametric studies in Chapter 5.

3.2 Mathematical Formulation of the Train-Track-Bridge Interaction Problem

The 2D model of the train-track-bridge interaction problem of this study is shown in Figure 3.1.

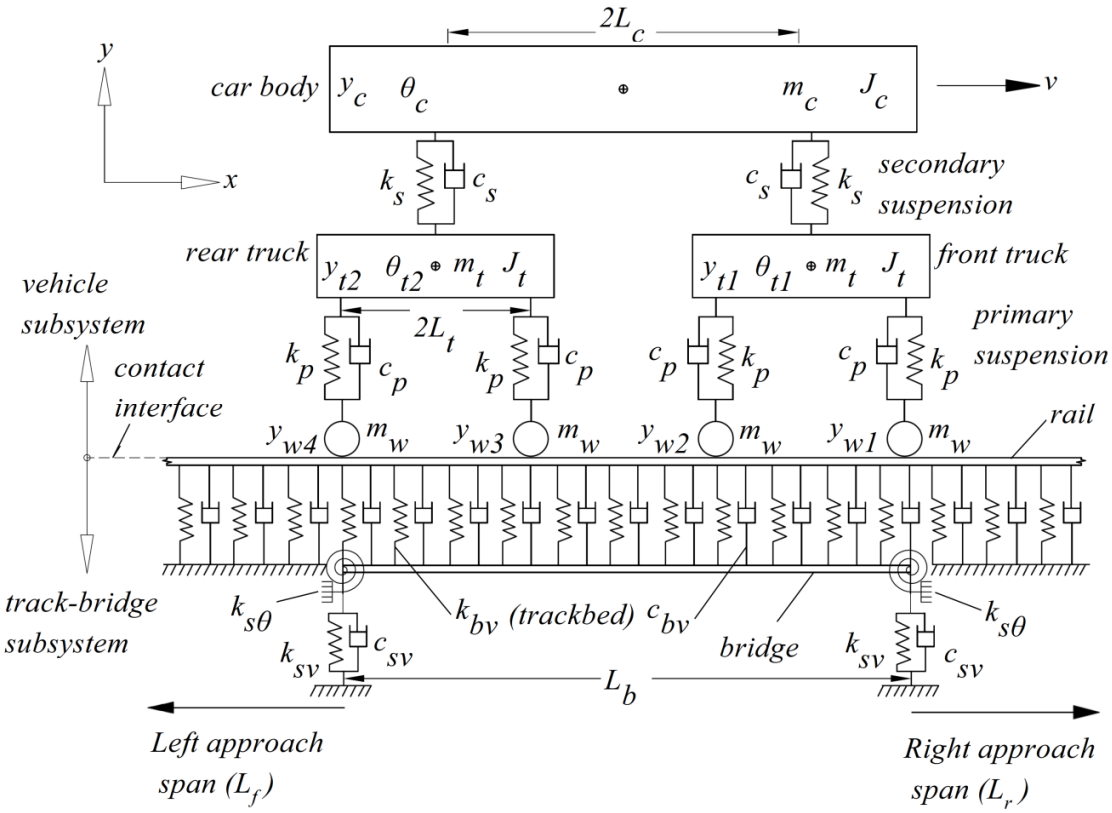

Figure 3.1 Vehicle-track-bridge interaction model

The train vehicle and the underlying track-bridge structure are treated as two separate subsystems. The interaction between the two subsystems occurs at the contact interface between the rails and the wheelsets. It is assumed that each wheelset of the vehicle is always in contact

with the rails. The vehicle is modeled as a mass-spring-damper system and consists of a carbody, two trucks (bogies) spaced at $2L_c$ and two wheelsets per truck (bogie) spaced at $2L_t$. The carbody is modeled as a rigid body with a mass m_c and a moment of inertia J_c about the transverse horizontal axis through its center of gravity. Similarly, each truck (bogie) is considered as a rigid body having a mass m_t and a moment of inertia J_t about the transverse horizontal axis through its center of gravity. Each wheelset is also assumed to be a rigid body having a mass m_w. The primary suspensions between the truck (bogie) and each wheelset are characterized by a spring stiffness k_p and a damping coefficient c_p respectively. Likewise, the secondary suspensions between the carbody and the truck (bogie) are characterized by a spring stiffness k_s and a damping coefficient c_s respectively. As the carbody is assumed to be rigid, its motions may be described by the vertical displacement y_c and rotation θ_c at its center of gravity. Similarly, the motions of the front truck (bogie) may be described by the vertical displacement y_{t1} and rotation θ_{t1} at its center of gravity; the motions of the rear truck (bogie) may be described by the vertical displacement y_{t2} and rotation θ_{t2} at its center of gravity. The motions of the four wheelsets may be described by the vertical displacements y_{w1}, y_{w2}, y_{w3} and y_{w4} respectively. Therefore, the total number of degrees of freedom for one vehicle is 10. The vertical displacement of each wheelset is however constrained by the displacement of rails. Consequently, the independent degrees of freedom for one vehicle become 6. It is assumed that the upward vertical displacement and clockwise rotation of the vehicle are taken positive and that they are measured with reference to their respective static equilibrium positions coming onto the track-bridge subsystem. The vehicle proceeds with a constant velocity v in the longitudinal direction from left to right.

The two rails of the typical railway track are combined into one upper beam of the same properties in this research. An upper beam modeling the rails and an elastically supported lower

beam modeling the bridge deck are interconnected by continuous springs and dampers characterizing the properties of the track bed. Based on the discretization with the finite element method, the upper beam is divided into N_r elements of equal length l, and the lower beam is divided into N_b elements of equal length l. The beam elements are assumed to be of the Bernoulli or Timoshenko type. It is assumed that the damping of the rails is negligible, and the lower beam has a linear viscous damping of the Rayleigh type. The stiffness and damping coefficients of the spring-damper system between the upper and lower beams are k_{bv} and c_{bv} respectively, thus representing the effective vertical stiffness and damping of the rail support components (i.e. rail pads, fastening system, ballast, etc.) smeared over the spacing of the crossties (sleepers). A section of the left approach track of length L_f and a section of the right approach track of length L_r are included in the numerical model. The mass of the crossties (sleepers) is included in the mass per unit length of the upper beam (i.e. rails). The mass of the ballast is included in the mass per unit length of the lower beam (i.e. bridge). Additional notations of the material and physical parameters of the track-bridge subsystem are described in Table IX.

TABLE IX TRACK-BRIDGE SUBSYSTEM PARAMETERS NOTATIONS

Parameter	Upper beam	Lower beam
Mass per unit length	m_r	m_b
Modulus of Elasticity	E_r	E_b
Cross-sectional area	A_r	A_b
Moment of Inertia	I_r	I_b
Shear modulus	G_r	G_b
Timoshenko shear coefficient	k_{sr}	k_{sb}
Shear deformation parameter	ϕ_r	ϕ_b
Bridge support vertical stiffness	-	k_{sv}
Bridge support vertical damping	-	c_{sv}

3.2.1 Equations of motion of the vehicle subsystem

The objective of this section is to derive the equations of motion that describe the behavior of the train vehicle for which the degrees of freedom are shown in Figure 3.2. The vehicle is assumed to be composed of two parts: an upper noncontact part consisting of the carbody, suspension systems and trucks (bogies); and a lower part in contact with the rails consisting of the wheelsets.

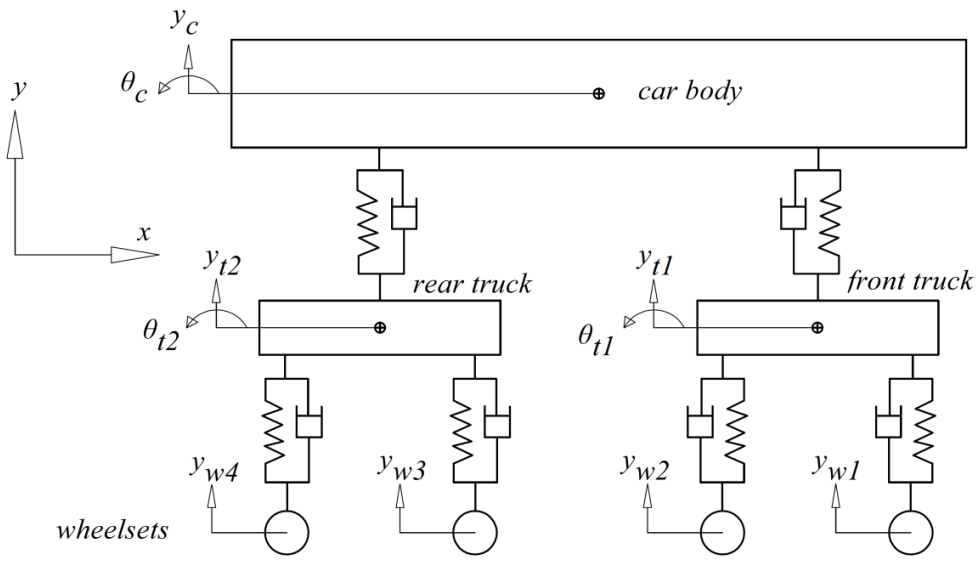

Figure 3.2 Ten degrees of freedom of the train vehicle

The vehicle is treated as a whole subsystem and is acted upon by the contact forces V_{c1}, V_{c2}, V_{c3} and V_{c4} through the four wheelsets considered to be external forces; and the additional internal forces as shown in the free body diagram of Figure 3.3.

In relation to the free body diagram of the vehicle, all internal dynamic forces in the spring-dampers of the suspension systems are given by the set of 12 equations (3.1.1) through (3.1.12) where an over-dot denotes differentiation with respect to time.

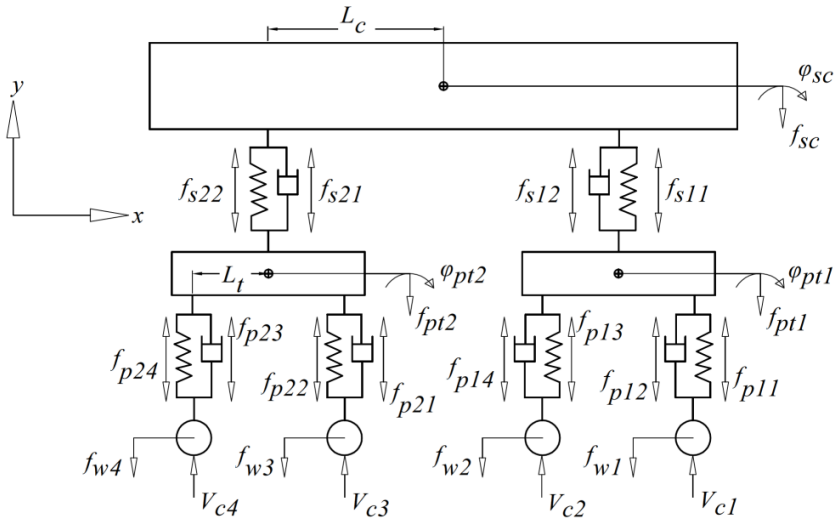

Fig.3.3 Free body diagram of train vehicle

$$f_{s11} = k_s(y_{t1} - y_c - L_c\theta_c) \tag{3.1.1}$$

$$f_{s12} = c_s(\dot{y}_{t1} - \dot{y}_c - L_c\dot{\theta}_c) \tag{3.1.2}$$

$$f_{s21} = c_s(\dot{y}_{t2} - \dot{y}_c + L_c\dot{\theta}_c) \tag{3.1.3}$$

$$f_{s22} = k_s(y_{t2} - y_c + L_c\theta_c) \tag{3.1.4}$$

$$f_{p11} = k_p(y_{w1} - y_{t1} - L_t\theta_{t1}) \tag{3.1.5}$$

$$f_{p12} = c_p(\dot{y}_{w1} - \dot{y}_{t1} - L_t\dot{\theta}_{t1}) \tag{3.1.6}$$

$$f_{p13} = k_p(y_{w2} - y_{t1} + L_t\theta_{t1}) \tag{3.1.7}$$

$$f_{p14} = c_p(\dot{y}_{w2} - \dot{y}_{t1} + L_t\dot{\theta}_{t1}) \tag{3.1.8}$$

$$f_{p21} = c_p(\dot{y}_{w3} - \dot{y}_{t2} - L_t\dot{\theta}_{t2}) \tag{3.1.9}$$

$$f_{p22} = k_p(y_{w3} - y_{t2} - L_t\theta_{t2}) \tag{3.1.10}$$

$$f_{p23} = c_p(\dot{y}_{w4} - \dot{y}_{t2} + L_t\dot{\theta}_{t2}) \tag{3.1.11}$$

$$f_{p24} = k_p(y_{w4} - y_{t2} + L_t\theta_{t2}) \tag{3.1.12}$$

Balancing all external and internal forces acting on the vehicle, the equations of equilibrium corresponding to the 10 degrees of freedom are obtained as follows.

$$f_{s11} + f_{s12} + f_{s21} + f_{s22} = f_{sc} = m_c \ddot{y}_c \tag{3.2.1}$$

$$L_c(f_{s11} + f_{s12} - f_{s21} - f_{s22}) = \varphi_{sc} = J_c \ddot{\theta}_c \tag{3.2.2}$$

$$f_{p11} + f_{p12} + f_{p13} + f_{p14} - f_{s11} - f_{s12} = f_{pt1} = m_t \ddot{y}_{t1} \tag{3.2.3}$$

$$L_t(f_{p11} + f_{p12} - f_{p13} - f_{p14}) = \varphi_{pt1} = J_t \ddot{\theta}_{t1} \tag{3.2.4}$$

$$f_{p21} + f_{p22} + f_{p23} + f_{p24} - f_{s21} - f_{s22} = f_{pt2} = m_t \ddot{y}_{t2} \tag{3.2.5}$$

$$L_t(f_{p21} + f_{p22} - f_{p23} - f_{p24}) = \varphi_{pt2} = J_t \ddot{\theta}_{t2} \tag{3.2.6}$$

$$V_{c1} - f_{p11} - f_{p12} = f_{w1} = m_w \ddot{y}_{w1} \tag{3.2.7}$$

$$V_{c2} - f_{p13} - f_{p14} = f_{w2} = m_w \ddot{y}_{w2} \tag{3.2.8}$$

$$V_{c3} - f_{p21} - f_{p22} = f_{w3} = m_w \ddot{y}_{w3} \tag{3.2.9}$$

$$V_{c4} - f_{p23} - f_{p24} = f_{w4} = m_w \ddot{y}_{w4} \tag{3.2.10}$$

Inserting equations (3.1.1) through (3.1.12) into equations (3.2.1) through (3.2.10) and after re-arranging, a system of 10 second order differential equations describing the dynamic behavior of the vehicle is obtained as given by the following equations (3.3.1) through (3.3.10).

$$m_c \ddot{y}_c + 2c_s \dot{y}_c - c_s \dot{y}_{t1} - c_s \dot{y}_{t2} + 2k_s y_c - k_s y_{t1} - k_s y_{t2} = 0 \tag{3.3.1}$$

$$J_c \ddot{\theta}_c + 2c_s L_c^2 \dot{\theta}_c - c_s L_c \dot{y}_{t1} + c_s L_c \dot{y}_{t2} + 2k_s L_c^2 \theta_c - k_s L_c y_{t1} + k_s L_c y_{t2} = 0 \tag{3.3.2}$$

$$m_t\ddot{y}_{t1} - c_s\dot{y}_c - c_sL_c\dot{\theta}_c + (c_s + 2c_p)\dot{y}_{t1} - k_sy_c - k_sL_c\theta_c + (k_s + 2k_p)y_{t1} - c_p\dot{y}_{w1} - c_p\dot{y}_{w2} - k_py_{w1} - k_py_{w2} = 0 \quad (3.3.3)$$

$$J_t\ddot{\theta}_{t1} + 2c_pL_t^2\dot{\theta}_{t1} + 2k_pL_t^2\theta_{t1} - c_pL_t\dot{y}_{w1} + c_pL_t\dot{y}_{w2} - k_pL_ty_{w1} + k_pL_ty_{w2} = 0 \quad (3.3.4)$$

$$m_t\ddot{y}_{t2} - c_s\dot{y}_c + c_sL_c\dot{\theta}_c + (c_s + 2c_p)\dot{y}_{t2} - k_sy_c + k_sL_c\theta_c + (k_s + 2k_p)y_{t2} - c_p\dot{y}_{w3} - c_p\dot{y}_{w4} - k_py_{w3} - k_py_{w4} = 0 \quad (3.3.5)$$

$$J_t\ddot{\theta}_{t2} + 2c_pL_t^2\dot{\theta}_{t2} + 2k_pL_t^2\theta_{t2} - c_pL_t\dot{y}_{w3} + c_pL_t\dot{y}_{w4} - k_pL_ty_{w3} + k_pL_ty_{w4} = 0 \quad (3.3.6)$$

$$m_w\ddot{y}_{w1} - c_p\dot{y}_{t1} - c_pL_t\dot{\theta}_{t1} - k_py_{t1} - k_pL_t\theta_{t1} + c_p\dot{y}_{w1} + k_py_{w1} = V_{c_1} \quad (3.3.7)$$

$$m_w\ddot{y}_{w2} - c_p\dot{y}_{t1} + c_pL_t\dot{\theta}_{t1} - k_py_{t1} + k_pL_t\theta_{t1} + c_p\dot{y}_{w2} + k_py_{w2} = V_{c_2} \quad (3.3.8)$$

$$m_w\ddot{y}_{w3} - c_p\dot{y}_{t2} - c_pL_t\dot{\theta}_{t2} - k_py_{t2} - k_pL_t\theta_{t2} + c_p\dot{y}_{w3} + k_py_{w3} = V_{c_3} \quad (3.3.9)$$

$$m_w\ddot{y}_{w4} - c_p\dot{y}_{t2} + c_pL_t\dot{\theta}_{t2} - k_py_{t2} + k_pL_t\theta_{t2} + c_p\dot{y}_{w4} + k_py_{w4} = V_{c_4} \quad (3.3.10)$$

In the remainder of this dissertation, matrices, column vectors and row vectors are represented by quantities enclosed in [ ], { } and ⟨ ⟩ respectively. Let $\{\ddot{d}_u\}$, $\{\dot{d}_u\}$ and $\{d_u\}$ denote vectors containing the accelerations, velocities and displacements respectively of the vehicle upper part given by the following expressions of equation (3.4),

$$\begin{aligned}\{\ddot{d}_u\} &= \langle \ddot{y}_c\ \ddot{\theta}_c\ \ddot{y}_{t1}\ \ddot{\theta}_{t1}\ \ddot{y}_{t2}\ \ddot{\theta}_{t2}\rangle^T \\ \{\dot{d}_u\} &= \langle \dot{y}_c\ \dot{\theta}_c\ \dot{y}_{t1}\ \dot{\theta}_{t1}\ \dot{y}_{t2}\ \dot{\theta}_{t2}\rangle^T \\ \{d_u\} &= \langle y_c\ \theta_c\ y_{t1}\ \theta_{t1}\ y_{t2}\ \theta_{t2}\rangle^T\end{aligned} \tag{3.4}$$

where the superscript T denotes the transpose of the vector

and let $\{\ddot{d}_w\}$, $\{\dot{d}_w\}$ and $\{d_w\}$ denote vectors containing the accelerations, velocities and displacements respectively of the wheelsets given by the following expressions of equation (3.5),

$$\begin{aligned}\{\ddot{d}_w\} &= \langle \ddot{y}_{w1}\ \ddot{y}_{w2}\ \ddot{y}_{w3}\ \ddot{y}_{w4}\rangle^T \\ \{\dot{d}_w\} &= \langle \dot{y}_{w1}\ \dot{y}_{w2}\ \dot{y}_{w3}\ \dot{y}_{w4}\rangle^T \\ \{d_w\} &= \langle y_{w1}\ y_{w2}\ y_{w3}\ y_{w4}\rangle^T\end{aligned} \tag{3.5}$$

and let $\{f_{dy}\}$ denote the vector containing the time-dependent dynamic contact forces between the four wheelsets and the rails given by the following expression.

$$\{f_{dy}\} = \langle V_{c1}\ V_{c2}\ V_{c3}\ V_{c4}\rangle^T \tag{3.6.1}$$

The constant static contact force $\{f_{st}\}$ is given by the following expression.

$$\{f_{st}\} = \left(\frac{1}{4}m_c + \frac{1}{2}m_t + m_w\right) g\langle 1\ 1\ 1\ 1\rangle^T \tag{3.6.2}$$

where the parameter g is the gravitational constant.

The resultant contact force $\{f_c\}$ is the sum of the static component and dynamic component, and given by the following expression.

$$\{f_c\} = \{f_{st}\} + \{f_{dy}\} \tag{3.6}$$

Therefore making use of equations (3.3) through (3.6), the equations of motion of the vehicle can be assembled into a semi-compact matrix form given by the following equation (3.7).

$$\begin{bmatrix}[m_{uu}] & [m_{uw}]\\ [m_{wu}] & [m_{ww}]\end{bmatrix}\begin{Bmatrix}\{\ddot{d}_u\}\\ \{\ddot{d}_w\}\end{Bmatrix} + \begin{bmatrix}[c_{uu}] & [c_{uw}]\\ [c_{wu}] & [c_{ww}]\end{bmatrix}\begin{Bmatrix}\{\dot{d}_u\}\\ \{\dot{d}_w\}\end{Bmatrix} + \begin{bmatrix}[k_{uu}] & [k_{uw}]\\ [k_{wu}] & [k_{ww}]\end{bmatrix}\begin{Bmatrix}\{d_u\}\\ \{d_w\}\end{Bmatrix} = \begin{Bmatrix}\{0\}\\ \{f_c\}\end{Bmatrix} \tag{3.7}$$

The vehicle matrices in the left-hand side of equation (3.7) are summarized as follows

$$[m_{uu}] = \begin{bmatrix} m_c & 0 & 0 & 0 & 0 & 0\\ 0 & J_c & 0 & 0 & 0 & 0\\ 0 & 0 & m_t & 0 & 0 & 0\\ 0 & 0 & 0 & J_t & 0 & 0\\ 0 & 0 & 0 & 0 & m_t & 0\\ 0 & 0 & 0 & 0 & 0 & J_t \end{bmatrix} \tag{3.7.1}$$

$$[m_{ww}] = \begin{bmatrix} m_w & 0 & 0 & 0\\ 0 & m_w & 0 & 0\\ 0 & 0 & m_w & 0\\ 0 & 0 & 0 & m_w \end{bmatrix} \tag{3.7.2}$$

$$[m_{uw}] = [m_{wu}]^T = [0] \tag{3.7.3}$$

$$[c_{uu}] = \begin{bmatrix} 2c_s & 0 & -c_s & 0 & -c_s & 0\\ 0 & 2c_sL_c^2 & -c_sL_c & 0 & c_sL_c & 0\\ -c_s & -c_sL_c & c_s + 2c_p & 0 & 0 & 0\\ 0 & 0 & 0 & 2c_pL_t^2 & 0 & 0\\ -c_s & c_sL_c & 0 & 0 & c_s + 2c_p & 0\\ 0 & 0 & 0 & 0 & 0 & 2c_pL_t^2 \end{bmatrix} \tag{3.7.4}$$

$$[c_{ww}] = \begin{bmatrix} c_p & 0 & 0 & 0 \\ 0 & c_p & 0 & 0 \\ 0 & 0 & c_p & 0 \\ 0 & 0 & 0 & c_p \end{bmatrix} \tag{3.7.5}$$

$$[k_{uu}] = \begin{bmatrix} 2k_s & 0 & -k_s & 0 & -k_s & 0 \\ 0 & 2k_sL_c^2 & -k_sL_c & 0 & k_sL_c & 0 \\ -k_s & -k_sL_c & k_s + 2c_p & 0 & 0 & 0 \\ 0 & 0 & 0 & 2k_pL_t^2 & 0 & 0 \\ -k_s & k_sL_c & 0 & 0 & k_s + 2k_p & 0 \\ 0 & 0 & 0 & 0 & 0 & 2k_pL_t^2 \end{bmatrix} \tag{3.7.6}$$

$$[k_{uw}] = \begin{bmatrix} 0 & 0 & 0 & 0 \\ 0 & 0 & 0 & 0 \\ -k_p & -k_p & 0 & 0 \\ -k_pL_t & k_pL_t & 0 & 0 \\ 0 & 0 & -k_p & -k_p \\ 0 & 0 & -k_pL_t & k_pL_t \end{bmatrix} \tag{3.7.7}$$

$$[k_{wu}] = [k_{uw}]^T = \begin{bmatrix} 0 & 0 & -k_p & -k_pL_t & 0 & 0 \\ 0 & 0 & -k_p & k_pL_t & 0 & 0 \\ 0 & 0 & 0 & 0 & -k_p & -k_pL_t \\ 0 & 0 & 0 & 0 & -k_p & k_pL_t \end{bmatrix} \tag{3.7.8}$$

Matrix $[k_{ww}]$ is obtained by replacing c_p with k_p in $[c_{ww}]$. Matrix $[c_{uw}]$ is obtained by replacing k_p with c_p in $[k_{uw}]$, and keeping in mind that $[c_{wu}] = [c_{uw}]^T$

3.2.2 Equations of motion of the track-bridge subsystem

In the finite element framework, the track-bridge subsystem is discretized into a number of simple elements of equal length. The model of this interaction element consists of rail element and bridge element connected by continuous viscoelastic supports as shown in Figure 3.4. The track-bridge interaction element consists of two nodes *i* and *i*+1. If the longitudinal displacements are neglected, each of the top rail element and bottom bridge element has 4 degrees of freedom.

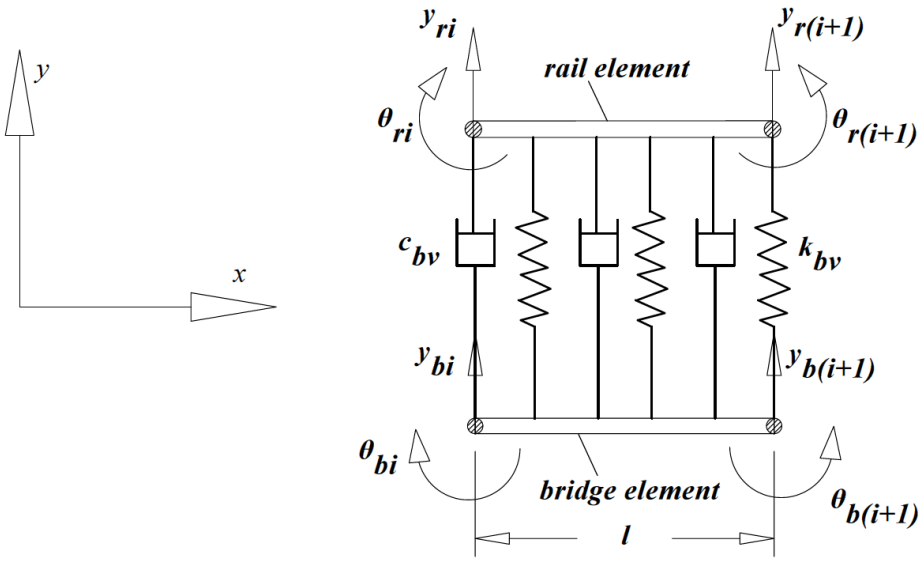

Figure 3.4 Finite element of track-bridge subsystem

The vertical displacement y_r^e and bending rotation θ_r^e of the rail element at an arbitrary point taken at x distance from the left node i can be expressed as in the following equations (3.8) and (3.9) respectively

$$y_r^e = \left[N_{yr1}N_{yr2}N_{yr3}N_{yr4}\right]\langle y_{ri}\ \theta_{ri}\ \ y_{r(i+1)}\ \theta_{r(i+1)}\rangle^T \tag{3.8}$$

$$\theta_r^e = \left[N_{\theta r1}N_{\theta r2}N_{\theta r3}N_{\theta r4}\right]\langle y_{ri}\ \theta_{ri}\ \ y_{r(i+1)}\ \theta_{r(i+1)}\rangle^T \tag{3.9}$$

Similarly, the vertical displacement y_b^e and bending rotation θ_b^e of the bridge element at an arbitrary point taken at x distance from the left node i can be expressed as in the following equations (3.10) and (3.11) respectively

$$y_b^e = \left[N_{yb1}\ N_{yb2}\ N_{yb3}\ N_{yb4}\right]\langle y_{bi}\ \theta_{bi}\ \ y_{b(i+1)}\ \theta_{b(i+1)}\rangle^T \tag{3.10}$$

$$\theta_b^e = [N_{\theta b1}\ N_{\theta b2}\ N_{\theta b3}\ N_{\theta b4}]\langle y_{bi}\ \theta_{bi}\ \ y_{b(i+1)}\ \theta_{b(i+1)}\rangle^T \tag{3.11}$$

The quantity $\{d_r\} = \langle y_{ri}\ \theta_{ri}\ \ y_{r(i+1)}\ \theta_{r(i+1)}\rangle^T$ in equations (3.8) and (3.9) is the nodal displacement vector of the rail element. The quantity $\{d_b\} = \langle y_{bi}\ \theta_{bi}\ \ y_{b(i+1)}\ \theta_{b(i+1)}\rangle^T$ in equations (3.10) and (3.11) is the nodal displacement vector of the bridge element.

The matrices $[N_{yr}]$, $[N_{\theta r}]$, $[N_{yb}]$ and $[N_{\theta b}]$ in equations (3.8) through (3.11) are derived from the general expression of matrices $[N_y] = [N_{y1}\ N_{y2}\ N_{y3}\ N_{y4}]$ and $[N_\theta] = [N_{\theta 1}\ N_{\theta 2}\ N_{\theta 3}\ N_{\theta 4}]$ whose entries are the Hermite interpolation functions given by the following set of equations (3.12.1) through (3.12.8).

$$N_{y1} = (2\bar{x}^3 - 3\bar{x}^2 - \phi\bar{x} + 1 + \phi)/(1 + \phi) \tag{3.12.1}$$

$$N_{y2} = l(\bar{x}^3 - (2 + \phi/2)\bar{x}^2 + (1 + \phi/2)\bar{x})/(1 + \phi) \tag{3.12.2}$$

$$N_{y3} = (-2\bar{x}^3 + 3\bar{x}^2 + \phi\bar{x})/(1 + \phi) \tag{3.12.3}$$

$$N_{y4} = l(\bar{x}^3 - (1 - \phi/2)\bar{x}^2 - \phi\bar{x}/2)/(1 + \phi) \tag{3.12.4}$$

and,

$$N_{\theta 1} = (6\bar{x}^2 - 6\bar{x})/l(1 + \phi) \tag{3.12.5}$$

$$N_{\theta 2} = (3\bar{x}^2 - (4 + \phi)\bar{x} + 1 + \phi)/(1 + \phi) \tag{3.12.6}$$

$$N_{\theta 3} = (-6\bar{x}^2 + 6\bar{x})/l(1 + \phi) \tag{3.12.7}$$

$$N_{\theta 4} = (3\bar{x}^2 - (2 - \phi)\bar{x})/(1 + \phi) \tag{3.12.8}$$

For the rail beam element, quantities [N_{yr}] and [$N_{\theta r}$] are obtained from [N_y] and [N_θ] respectively by replacing ϕ with ϕ_r. Similarly, in the case of the bridge beam element, quantities [N_{yb}] and [$N_{\theta b}$] are obtained from [N_y] and [N_θ] respectively by replacing ϕ with ϕ_b.

The shear deformation parameters ϕ_r and ϕ_b can be expressed as

$$\phi_r = \frac{12E_rI_r}{k_{sr}G_rA_rl^2} \tag{3.12.9a}$$

$$\phi_b = \frac{12E_bI_b}{k_{sb}G_bA_bl^2} \tag{3.12.9b}$$

It is worth noting that if the Euler-Bernoulli beam theory is adopted in the track-bridge elements, the shear deformation parameters are zero and the interpolation functions are the same for the rail element and the beam element.

In the track-bridge finite element model, $\bar{x}$ is the local coordinate along the longitudinal axis of the element and is given by

$$0 \leq \bar{x} = \frac{x}{l} \leq 1 \tag{3.12.10}$$

Making use of the mathematical expressions of equations (3.8) through (3.12.10), the equations of motion of the track-bridge interaction element subjected to the wheels' contact forces $\{f_c\}$ resulting from equation (3.7) can now be further derived and written in a semi-compact form as

$$\begin{bmatrix}[m_{rr}] & [0] \\ [0] & [m_{bb}]\end{bmatrix}\begin{Bmatrix}\{\ddot{d}_r\} \\ \{\ddot{d}_b\}\end{Bmatrix}+\begin{bmatrix}[c_{rr}] & [c_{rb}] \\ [c_{br}] & [c_{bb}]\end{bmatrix}\begin{Bmatrix}\{\dot{d}_r\} \\ \{\dot{d}_b\}\end{Bmatrix}+\begin{bmatrix}[k_{rr}] & [k_{rb}] \\ [k_{br}] & [k_{bb}]\end{bmatrix}\begin{Bmatrix}\{d_r\} \\ \{d_b\}\end{Bmatrix} = \begin{Bmatrix}-[N_{yr}]\{f_{rc}\} \\ \{0\}\end{Bmatrix} \tag{3.13}$$

When the track effects are ignored, the equations of motion of the bridge element subjected to the wheels' contact forces can be reduced to the expression given by

$$[m_{bb}]\{\ddot{d}_b\}+[c_{bb}]\{\dot{d}_b\}+[k_{bb}]\{d_b\}=-[N_{yb}]\{f_{bc}\} \tag{3.14}$$

It is worth nothing that loading vectors $\{f_{rc}\}$ and $\{f_{bc}\}$ in equations (3.13) and (3.14) are directly related to the vector of the contact force $\{f_c\}$ of the vehicle as will be demonstrated later. The vectors in the left-hand side of equations (3.13) and (3.14) with a single-overdot and double-overdot represent the velocity and acceleration vectors respectively. All matrices in the left-hand side can be easily derived by integrating the product of the shape functions and their transposed over the element length; and are readily available in the literature (Yang et al., 2004; Lou et al., 2006).

3.2.3 Equations of the random vertical track irregularities

Researchers and engineers dealing with the train-track-bridge interaction problems in the high speed rail lines commonly consider the railway track irregularities to be one of the main factors affecting the dynamic response of the system. This section of the dissertation discusses the mathematical models and relevant parameters of random vertical irregularities in high speed rail tracks. Some of the causes of track irregularities are mechanical maintenance, construction

variations, wear, clearances, ground subsidence, or settlement. Track irregularities may be either measured experimentally for a particular track or analytically generated using Monte-Carlo methods. For the purposes of formulating the mathematical model of the high speed rail track irregularities, the following assumptions are adopted in this research: i) random vertical track irregularities are identical for both rails; ii) no consideration is made for the short wavelength, corrugation irregularities in rail, and design geometry irregularities; and iii) the track is assumed to be straight horizontally.

With these assumptions, vertical track irregularities having wavelengths of between 0.1 m (0.328 feet) to 70 m (229.7 feet) are considered, which, according to (Podworna, 2015) induce vertical vibrations in the train-track-bridge system at frequencies of about 1.1 Hz to 800 Hz for operating speeds up to 186.4 mph (300 km/h).

Track irregularities are defined by railway administrations in different countries, depending on the operating train speeds. The U.S. Federal Railroad Administration (FRA) track class quality and speed limits are shown in Table X (Fries and Coffey, 1990). The track class 1 is the worst and unacceptable on high speed rail lines. The track class 6 is the best and considered to be a very good quality track.

TABLE X TRACK CLASS QUALITY AND SPEED LIMITS

Track Class	Speed Limit		Track Quality
	Passenger	Freight	
1	15 mph (24 km/h)	10 mph (16 km/h)	Very Poor
2	30 mph (48 km/h)	25 mph (40 km/h)	Poor
3	60 mph (97 km/h)	40 mph (64 km/h)	Poor
4	80 mph (129 km/h)	60 mph (97 km/h)	Average
5	90 mph (145 km/h)	80 mph (129 km/h)	Good
6	110 mph (177 km/h)	110 mph (177 km/h)	Very Good

A common model of railway track irregularities in the vertical profile is a stationary ergodic Gaussian process in space that is described by the random function $r(x)$ of zero expectance and constant variance, and for which random samples to the function are determined from the inverse Fourier Transform (Zhang et al., 2001). The function $r(x)$ can be written as

$$r(x) = 2\sum_{n=1}^{N}\sqrt{G_{rr}(\Omega_n)\Delta\Omega}\cos(\Omega_n x + \phi_n) \tag{3.15}$$

These track irregularities are characterized by one-sided Power Spectral Density (PSD) function $G_{rr}(\Omega_n)$. In this dissertation, the PSD function of the random variable $r(x)$ corresponds to track class 1 to 6 according to the American Railway Standard developed by the U.S. Federal Railroad Administration (FRA) and has the following form (Wiriyachai et al, 1982).

$$G_{rr}(\Omega_n) = kA\frac{\Omega_c^2}{\Omega_n^2(\Omega_n^2 + \Omega_c^2)} \tag{3.15.1}$$

The units of $G_{rr}(\Omega_n)$ are mm^2.m/rad (in^2.in/rad). The parameter A is a roughness coefficient of the vertical track irregularity and is dependent on the quality of the track class as shown in Table XI (Lei and Noda, 1982). The value of the coefficient k is usually taken as 0.25. The critical frequency Ω_c does not depend on the quality of the track class.

TABLE XI TRACK CLASS ROUGHNESS PARAMETERS AND QUALITY

Track Class	A [mm^2.rad/m]	A [in^2.rad/in]
1	121.07	0.00477
2	101.81	0.00401
3	68.16	0.00268
4	53.76	0.00212
5	20.95	0.00082
6	3.39	0.00013

The variable Ω_n is the frequency of the n^{th} random sample of the PSD function and is given by

$$\Omega_n = \Omega_L + (n - 1/2)\Delta\Omega \tag{3.15.2}$$

where the frequency increment $\Delta\Omega$ is defined by

$$\Delta\Omega = (\Omega_U - \Omega_L)/N \tag{3.15.3}$$

The quantities Ω_L and Ω_U are the lower and upper limits respectively of the spatial frequency that defines the range in which the PSD function is included. The integer N is the total number of frequency increments between the lower and upper frequencies. The parameter ϕ_n in equation (3.15) is a random phase angle that is distributed uniformly between 0 and 2π.

In order to generate vertical track irregularity profiles that are close to the actual field conditions of the railway track, the total number of samples N should be large enough. In this study, a total number of $N = 2000$ samples are considered.

Table XII summarizes relevant parameters adopted in this dissertation for the vertical track irregularities using the model discussed in this section.

TABLE XII TRACK IRREGULARITIES MODEL PARAMETER VALUES

k	Ω_c		Ω_L		Ω_U		$\Delta\Omega$	N
	(rad/m)	(rad/in)	(rad/m)	(rad/in)	(rad/m)	(rad/in)		
0.25	0.8245	0.02094	0.08976	0.0028	62.832	1.596	0.001594	2000

As it will be shown later in this chapter, the first derivative and second derivative of the track irregularities given by the following equations (3.16) and (3.17) also play important roles in the dynamic behavior of the interaction between the train vehicle and the underlying track structure.

$$r'(x) = -2\sum_{n=1}^{N}\sqrt{G_{rr}(\Omega_n)\Delta\Omega}\;\Omega_n \sin(\Omega_n x + \phi_n) \tag{3.16}$$

$$r''(x) = -2\sum_{n=1}^{N}\sqrt{G_{rr}(\Omega_n)\Delta\Omega}\;\Omega_n^2 \cos(\Omega_n x + \phi_n) \tag{3.17}$$

Inserting the expressions of equations (3.15.1) through (3.15.3) into equations (3.15), (3.16) and (3.17), the amplitude function $r(x)$ of the track vertical random irregularity, and its first and second order derivatives with respect to the global horizontal axis of the track-bridge system may be expressed in a more useful form as shown in the following equations.

$$r(x) = 2\sum_{n=1}^{N}\sqrt{\frac{kA\Omega_c^2\Delta\Omega}{[\Omega_L+(n-1/2)\Delta\Omega]^2\{[\Omega_L+(n-1/2)\Delta\Omega]^2+\Omega_c^2\}}} \quad (3.18)$$

$$* \cos\{[\Omega_L+(n-1/2)\Delta\Omega]x+\phi_n\}$$

$$r'(x) = -2\sum_{n=1}^{N}\sqrt{\frac{kA\Omega_c^2\Delta\Omega}{[\Omega_L+(n-1/2)\Delta\Omega]^2\{[\Omega_L+(n-1/2)\Delta\Omega]^2+\Omega_c^2\}}} \quad (3.19)$$

$$* [\Omega_L+(n-1/2)\Delta\Omega] * \sin\{[\Omega_L+(n-1/2)\Delta\Omega]x+\phi_n\}$$

$$r''(x) = -2\sum_{n=1}^{N}\sqrt{\frac{kA\Omega_c^2\Delta\Omega}{[\Omega_L+(n-1/2)\Delta\Omega]^2\{[\Omega_L+(n-1/2)\Delta\Omega]^2+\Omega_c^2\}}} \quad (3.20)$$

$$* [\Omega_L+(n-1/2)\Delta\Omega]^2 * cos\{[\Omega_L+(n-1/2)\Delta\Omega]x+\phi_n\}$$

Generated random samples of vertical track irregularity profiles as well as profiles of their first and second order derivatives for track classes 1, 4 and 6 are shown in Figures 3.5 through 3.7.

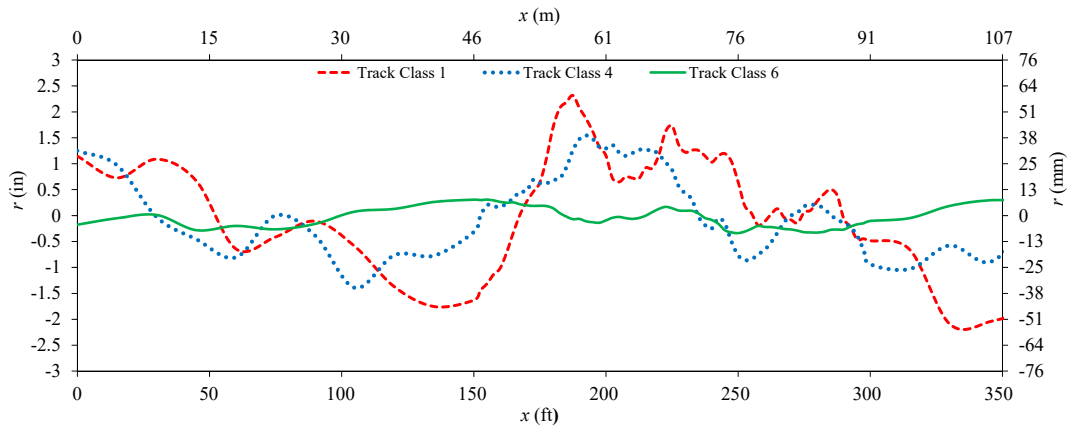

Figure 3.5. Sample of random vertical track irregularity profile, N=2000.

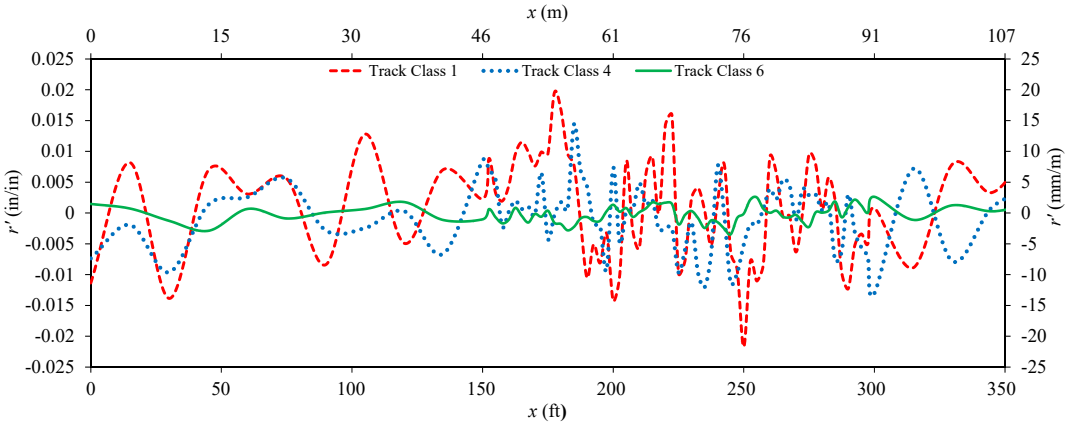

Figure 3.6. 1st order derivative of random vertical track irregularity profile, N=2000.

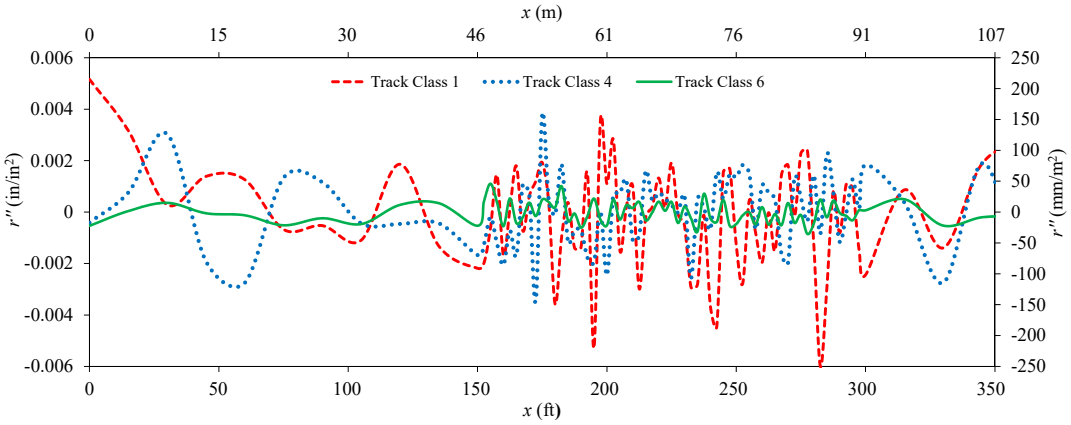

Figure 3.7. 2nd order derivative of random vertical track irregularity profile, N=2000.

3.3 Numerical Integration Method

In this section of the dissertation, a review is made of the numerical integration method used in this research to solve the train-track-bridge interaction problem. Consider the general equation of motion of a damped dynamic system described by the following equation (3.21).

$$[M]\{\ddot{u}\} + [C]\{\dot{u}\} + [K]\{u\} = \{F\} \tag{3.21}$$

$[M]$, $[C]$, and $[K]$ are the mass, damping, and stiffness matrices; $\{F\}$ is the time-dependent load vector; vectors $\{\ddot{u}\}$, $\{\dot{u}\}$ and $\{u\}$ are vectors containing the acceleration, velocity, and displacement responses respectively. The solutions of the equation can be obtained through a direct step-by-step numerical integration in the time domain. For that purpose, the response of the system within the time incremental step from t to $t + \Delta t$ can be obtained with the method developed by Hilber, Hughes and Taylor (Hilber et al., 1977), the so-called HHT α method, for which the algorithmic form of equation (3.21) can be expressed as

$$[M]\{\ddot{u}\}^c + (1+\alpha)[C]\{\dot{u}\}^c + (1+\alpha)[K]\{u\}^c = (1+\alpha)\{F\}^c - \alpha\{F\}^p + \alpha[C]\{\dot{u}\}^p + \alpha[K]\{u\}^p \tag{3.22}$$

The superscripts c and p in equation (3.22) indicate the current time step $t + \Delta t$ and the previous time step t respectively. The HHT α integration method is a generalization of the Newmark β method (Newmark, 1959) and uses the same two basic equations proposed by Newmark for determining the displacement and velocity at the current time step as given by

$$\{u\}^c = \{u\}^p + \{\dot{u}\}^p \Delta t + [(1/2 - \beta)\{\ddot{u}\}^p + \beta\{\ddot{u}\}^c](\Delta t)^2 \tag{3.23.1}$$

$$\{\dot{u}\}^c = \{\dot{u}\}^p + \{\dot{u}\}^p \Delta t + [(1-\gamma)\{\ddot{u}\}^p + \gamma\{\ddot{u}\}^c](\Delta t) \tag{3.23.2}$$

The parameter β denotes the variation of acceleration during the time step. The γ parameter relates to the property of numerical or artificial damping introduced into the system by

discretization in the time domain. The only combination of β and γ that leads to an unconditionally stable solution of a second order accuracy in the Newmark algorithm is β = 1/4 and γ = 1/2 which is the trapezoidal method. However, the drawback is that the trapezoidal method of Newmark β method does not generate any numerical damping in the solution, which makes it impractical for problems that have high-frequency oscillations of no interest or parasitic high-frequency oscillations that are a byproduct of the finite element discretization (Negrut et al., 2007). The HHT α method is intended to be an improvement of the Newmark β method to overcome this drawback with the introduction of the α parameter. When α is zero the HHT α method is the same as the Newmark β method. The most numerical damping of the spurious higher modes is obtained with a value of α equal to - 1/3.

In further deriving the HHT α method, the accelerations and velocities of the system at the current time step can be solved from equations (3.23.1) and (3.23.2); and expressed as

$$\{\ddot{u}\}^c = b_0(\{u\}^c - \{u\}^p) - b_1\{\dot{u}\}^p - b_2\{\ddot{u}\}^p \tag{3.24.1}$$

$$\{\dot{u}\}^c = b_5(\{u\}^c - \{u\}^p) - b_6\{\dot{u}\}^p - b_7\{\ddot{u}\}^p \tag{3.24.2}$$

where the coefficients b_0 to b_7, β, γ and α are given by

$$b_0 = \frac{1}{\beta\Delta t^2} \;;\quad b_1 = \frac{1}{\beta\Delta t} \;;\quad b_2 = \frac{1}{2\beta} - 1$$

$$b_5 = \frac{\gamma}{\beta\Delta t} \;;\quad b_6 = \frac{\gamma}{\beta} - 1 \;;\quad b_7 = \frac{\Delta t}{2}\left(\frac{\gamma}{\beta} - 2\right) \tag{3.24.3}$$

$$\beta = \frac{(1-\alpha)^2}{4} \;;\quad \gamma = \frac{(1-2\alpha)}{2} \;;\quad -1/3 \le \alpha \le 0$$

Substituting equations (3.24.1) and (3.24.2) into equation (3.22) leads to the equivalent stiffness equation given by

$$[K_e]\{u\}^c = \{F_e\}^c \tag{3.25}$$

where the effective stiffness matrix $[K_e]$ and the effective load vector $\{F_e\}^c$ are defined as follows

$$[K_e] = b_0[M] + (1+\alpha)b_5[C] + (1+\alpha)[K] \tag{3.25.1}$$

$$\begin{aligned}\{F_e\}^c = (1+\alpha)\{F\}^c - \alpha\{F\}^p + [M](b_0\{u\}^p + b_1\{\dot{u}\}^p + b_2\{\ddot{u}\}^p) \\ + (1+\alpha)[C](b_5\{u\}^p + b_6\{\dot{u}\}^p + b_7\{\ddot{u}\}^p) + \alpha[C]\{\dot{u}\}^p + \alpha[K]\{u\}^p\end{aligned} \tag{3.25.2}$$

From equation (3.25), the system displacements $\{u\}^c$ at the current time $t + \Delta t$ can be solved as

$$\{u\}^c = [K_e]^{-1}\{F_e\}^c \tag{3.25.3}$$

Finally, the accelerations and velocities for the current time $t + \Delta t$ can then be solved using equations (3.24.1) and (3.24.2) respectively.

3.4 Solutions of the Train-Track-Bridge Interaction Problem

The approach in tackling the train-track-bridge interaction problem consists of separately solving the decoupled equations of motion of the train vehicle subsystem and the track-bridge subsystem in a step-by-step direct integration in the time domain using numerical integration. A special mathematical formulation at the contact interface between wheels and rails is used to transfer responses of one subsystem to the other as excitation inputs. In the next section 3.4.1, methods for solving vehicle's responses and contact forces are presented. In the subsequent section 3.4.2, constraint equations at the contact points between the two subsystems are

formulated describing the interaction phenomenon. To verify the efficiency of the proposed model and solution procedure in handling rapid transient event, a validation study is presented in section 3.4.3 with a vehicle travelling at high speed over a short bridge.

3.4.1 Solutions of the vehicle responses and contact forces

In this section of the dissertation, a general approach is developed for solving the train vehicle's vertical responses as well as the wheel contact forces using an algorithm similar to the one presented in the previous section 3.3. In the same context as equation (3.22), the master equation of motion of the vehicle as given by equation (3.7) can be algorithmically expressed using the HHT α method as in the following equation (3.26).

$$\begin{aligned}
&\begin{bmatrix}[m_{uu}]\,[m_{uw}]\\ [m_{wu}][m_{ww}]\end{bmatrix}\begin{Bmatrix}\{\ddot{d}_u\}\\ \{\ddot{d}_w\}\end{Bmatrix}^c + (1+\alpha)\begin{bmatrix}[c_{uu}]\,[c_{uw}]\\ [c_{wu}][c_{ww}]\end{bmatrix}\begin{Bmatrix}\{\dot{d}_u\}\\ \{\dot{d}_w\}\end{Bmatrix}^c \\
&+(1+\alpha)\begin{bmatrix}[k_{uu}]\,[k_{uw}]\\ [k_{wu}][k_{ww}]\end{bmatrix}\begin{Bmatrix}\{d_u\}\\ \{d_w\}\end{Bmatrix}^c \\
&=(1+\alpha)\begin{Bmatrix}\{0\}\\ \{f_c\}\end{Bmatrix}^c - \alpha\begin{Bmatrix}\{0\}\\ \{f_c\}\end{Bmatrix}^p + \alpha\begin{bmatrix}[c_{uu}]\,[c_{uw}]\\ [c_{wu}][c_{ww}]\end{bmatrix}\begin{Bmatrix}\{\dot{d}_u\}\\ \{\dot{d}_w\}\end{Bmatrix}^p \\
&+\ \alpha\begin{bmatrix}[k_{uu}]\,[k_{uw}]\\ [k_{wu}][k_{ww}]\end{bmatrix}\begin{Bmatrix}\{d_u\}\\ \{d_w\}\end{Bmatrix}^p
\end{aligned} \tag{3.26}$$

To formulate the solutions of the vehicle's vertical responses, the first row of equation (3.26) is first expanded, re-arranged and can be compacted into the following equation (3.27).

$$\begin{aligned}
&[m_{uu}]\{\ddot{d}_u\}^c + (1+\alpha)[c_{uu}]\{\dot{d}_u\}^c + (1+\alpha)[k_{uu}]\{d_u\}^c \\
&\qquad = -\{q_{uc}\}^c + \{Q_{u\alpha}\}^p + \{Q_{w\alpha}\}^p
\end{aligned} \tag{3.27}$$

The loading vector terms in the right-hand side of equation (3.27) are given by

$$\{q_{uc}\}^c = [m_{uw}]\{\ddot{d}_w\}^c + (1+\alpha)[c_{uw}]\{\dot{d}_w\}^c + (1+\alpha)[k_{uw}]\{d_w\}^c \tag{3.27.1}$$

$$\{Q_{u\alpha}\}^p = \alpha\Big([c_{uu}]\{\dot{d}_u\}^p + [k_{uu}]\{d_u\}^p\Big) \tag{3.27.2}$$

$$\{Q_{w\alpha}\}^p = \alpha\Big([c_{uw}]\{\dot{d}_w\}^p + [k_{uw}]\{d_w\}^p\Big) \tag{3.27.3}$$

Using the procedure of the HHT α method described in Section 3.3, vectors containing the displacements, velocities and accelerations of the vehicle upper part can be readily solved and are summarized as follows after skipping the tedious algebraic intermediate steps.

$$\{d_u\}^c = [\Psi_{uu}]^{-1}\{\Delta d_u\} + \{d_u\}^p \tag{3.27.4}$$

$$\{\dot{d}_u\}^c = b_5[\Psi_{uu}]^{-1}\{\Delta d_u\} - b_6\{\dot{d}_u\}^p - b_7\{\ddot{d}_u\}^p \tag{3.27.5}$$

$$\{\ddot{d}_u\}^c = b_0[\Psi_{uu}]^{-1}\{\Delta d_u\} - b_1\{\dot{d}_u\}^p - b_2\{\ddot{d}_u\}^p \tag{3.27.6}$$

The vehicle effective matrix $[\Psi_{uu}]$ and the vehicle's upper part incremental displacement $\{\Delta d_u\}$ are given by

$$[\Psi_{uu}] = b_0[m_{uu}] + (1+\alpha)b_5[c_{uu}] + (1+\alpha)[k_{uu}] \tag{3.27.7}$$

$$\begin{aligned}\{\Delta d_u\} = &-[m_{uw}]\{\ddot{d}_w\}^c - (1+\alpha)[c_{uw}]\{\dot{d}_w\}^c - (1+\alpha)[k_{uw}]\{d_w\}^c \\ &+ \alpha[c_{uu}]\{\dot{d}_u\}^p + \alpha[k_{uu}]\{d_u\}^p + \alpha[c_{uw}]\{\dot{d}_w\}^p + \alpha[k_{uw}]\{d_w\}^p \\ &+ [m_{uu}]\Big(b_1\{\dot{d}_u\}^p + b_2\{\ddot{d}_u\}^p\Big) + (1+\alpha)[c_{uu}]\Big(b_6\{\dot{d}_u\}^p + b_7\{\ddot{d}_u\}^p\Big) \\ &- (1+\alpha)[k_{uu}]\{d_u\}^p\end{aligned} \tag{3.27.8}$$

It should be noted that in all expressions of equations (3.27) through (3.27.8), the responses of the vehicle at the end of the current time step depend on known quantities from the previous time step and also on the unknown quantities of the wheel responses $\{d_w\}^c$, $\{\dot{d}_w\}^c$ and $\{\ddot{d}_w\}^c$ at the beginning of the current time step which will be condensed to the responses of the underlying track-bridge structure as explained in the forthcoming section 3.4.2.

In a similar way, the contact forces $\{f_c\}$ can be obtained by expanding the second row of equation (3.26) which can be initially expressed as follows

$$\begin{aligned}[m_{wu}]\{\ddot{d}_u\}^c + (1+\alpha)[c_{wu}]\{\dot{d}_u\}^c + (1+\alpha)[k_{wu}]\{d_u\}^c + [m_{ww}]\{\ddot{d}_w\}^c \\ + (1+\alpha)[c_{ww}]\{\dot{d}_w\}^c + (1+\alpha)[k_{ww}]\{d_w\}^c \\ = (1+\alpha)\{f_c\}^c - \alpha\{f_c\}^p + \alpha[c_{wu}]\{\dot{d}_u\}^p + \alpha[c_{ww}]\{\dot{d}_w\}^p \\ + \alpha[k_{wu}]\{d_u\}^p + \alpha[k_{ww}]\{d_w\}^p\end{aligned} \tag{3.28}$$

Now, inserting the vehicle's upper part response quantities of equations (3.27.4) through (3.27.6) into equation (3.28) and using again the numerical integration procedure described in section 3.3, the contact force vector $\{f_c\}^c$ at the current time step can be readily solved and is summarized in a compact form given by equation (3.28.1) after skipping intermediate algebraic steps.

$$\begin{aligned}\{f_c\}^c = \frac{1}{1+\alpha}\left([\bar{m}_c]\{\ddot{d}_w\}^c + [\bar{c}_c]\{\dot{d}_w\}^c + [\bar{k}_c]\{d_w\}^c\right) \\ + \frac{1}{1+\alpha}([\Psi_{wu}][\Psi_{uu}]^{-1}\{q_u\}^p - \{q_w\}^p) - \frac{\alpha}{1+\alpha}\{q_{wc}\}^p \\ + \frac{\alpha}{1+\alpha}\{f_c\}^p\end{aligned} \tag{3.28.1}$$

The matrices in equation (3.28.1) depend on known vehicle matrices and are given by

$$[\bar{m}_c] = [m_{ww}] - [\Psi_{wu}][\Psi_{uu}]^{-1}[m_{uw}] \tag{3.28.2}$$

$$[\bar{c}_c] = (1+\alpha)([c_{ww}] - [\Psi_{wu}][\Psi_{uu}]^{-1}[c_{uw}]) \tag{3.28.3}$$

$$[\bar{k}_c] = (1+\alpha)([k_{ww}] - [\Psi_{wu}][\Psi_{uu}]^{-1}[k_{uw}]) \tag{3.28.4}$$

$$[\Psi_{wu}] = b_0[m_{wu}] + (1+\alpha)b_5[c_{wu}] + (1+\alpha)[k_{wu}] \tag{3.28.5}$$

The previous time step response quantities in equation (3.28.1) are also known and given by

$$\{q_u\}^p = [m_{uu}]\left(b_1\{\dot{d}_u\}^p + b_2\{\ddot{d}_u\}^p\right) + (1+\alpha)[c_{uu}]\left(b_6\{\dot{d}_u\}^p + b_7\{\ddot{d}_u\}^p\right) - (1+\alpha)[k_{uu}]\{d_u\}^p \tag{3.28.6}$$

$$\{q_w\}^p = [m_{wu}]\left(b_1\{\dot{d}_u\}^p + b_2\{\ddot{d}_u\}^p\right) + (1+\alpha)[c_{wu}]\left(b_6\{\dot{d}_u\}^p + b_7\{\ddot{d}_u\}^p\right) - (1+\alpha)[k_{wu}]\{d_u\}^p \tag{3.28.7}$$

$$\{q_{wc}\}^p = [\bar{c}_{cu}]\{\dot{d}_u\}^p + [\bar{k}_{cu}]\{d_u\}^p + [\bar{c}_{cw}]\{\dot{d}_w\}^p + [\bar{k}_{cw}]\{d_w\}^p \tag{3.28.8}$$

The matrices in equation (3.28.8) are due to the HHT α method algorithm and are given by

$$[\bar{c}_{cu}] = \alpha([c_{wu}] - [\Psi_{wu}][\Psi_{uu}]^{-1}[c_{uu}]) \tag{3.28.9}$$

$$[\bar{k}_{cu}] = \alpha([k_{wu}] - [\Psi_{wu}][\Psi_{uu}]^{-1}[k_{uu}]) \tag{3.28.10}$$

$$[\bar{c}_{cw}] = \alpha([c_{ww}] - [\Psi_{wu}][\Psi_{uu}]^{-1}[c_{uw}]) \tag{3.28.11}$$

$$[\bar{k}_{cw}] = \alpha([k_{ww}] - [\Psi_{wu}][\Psi_{uu}]^{-1}[k_{uw}]) \tag{3.28.12}$$

It should be equally noted that in all expressions of equations (3.28) through (3.28.12), the contact forces $\{f_c\}^c$ at the end of the current time step depend on known quantities from the previous time step and also on the unknown quantities of the wheel responses $\{d_w\}^c$, $\{\dot{d}_w\}^c$ and $\{\ddot{d}_w\}^c$ at the beginning of the current time step.

In summary, to solve for the dynamic responses of the train vehicle in equation (3.27) and contact forces in equation (3.28.1), the only needed inputs are the wheel responses which are obtained from the global deformations of the underlying track-bridge subsystem through constraint equations at the contact points.

3.4.2 Constraint equations at the contact points

The key aspect in solving the train-track-bridge interaction lies in the contact interface between the two subsystems. Figure 3.8 shows a train vehicle travelling over an underlying structure discretized in space with some beam finite elements of length *l*.

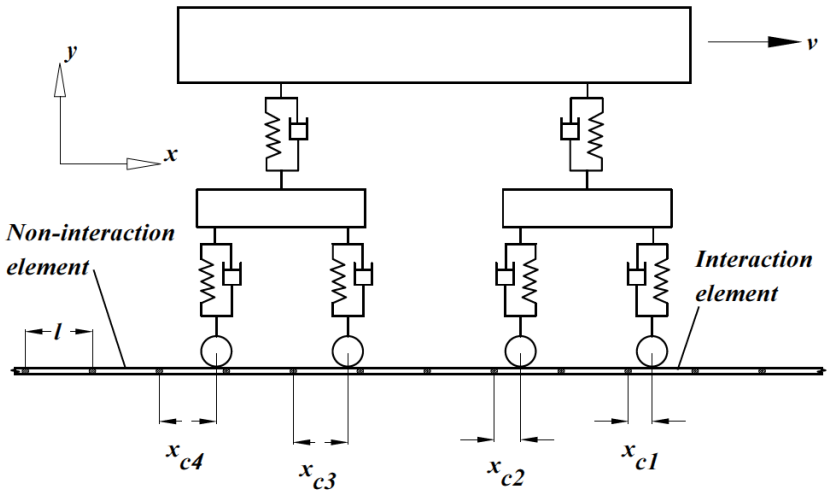

Figure 3.8 Train-track-bridge interaction elements

At any given time, wheels are assumed to be in contact with the structure. There exists some contact elements and some non-contact elements of the underlying structure called "interaction element" and "non-interaction element" respectively. As the train vehicle moves across the structure, the interaction elements move with the wheels. Let x_{cj} denote the local coordinate of the wheel j from the left node of the interaction element e_j and let y_{cj} denote the vertical deflection of the underlying structure at the contact point. The vector containing the vertical deflections of the contact points can be written as

$$\{d_c\} = \langle y_{c1}\ y_{c2}\ \ y_{c3}\ y_{c4)}\rangle^T \tag{3.29}$$

The wheel displacement $\{d_w\}$ can be related to the contact displacement $\{d_c\}$ of the underlying structure by the following constraint equation (3.30)

$$\{d_w\} = \{d_c\} + \{r\} \tag{3.30}$$

The vector $\{r\}$ representing the effect of the railway track irregularities and usually defined based on the power spectral density functions, is formulated in section 3.2.3 of this dissertation. The vector $\{r\}$ contains the vertical coordinates of the track irregularities at the points of contact between the wheels and the rails. It should be noted that the functions of the power spectral density are some functions of the global location *X* of the wheel on the bridge in relation to an origin taken as one end of the physical model. The wheel velocity $\{\dot{d}_w\}$ and acceleration $\{\ddot{d}_w\}$ as functions of the contact points and irregularities can be obtained with a first and second order differentiations of equation (3.30). Before differentiating equation (3.30), it is necessary to explain the meanings of the global coordinate *X* and the local coordinate *x*, and their effect on the

derivation process. For any track-bridge element, a relationship can be written between x and X making use of a constant as shown in the following equation,

$$X = x + Constant \tag{3.31}$$

With the chain rule, it can be shown that taking the derivative of a function of *X*, such as $\{r\}$, with respect to *X* is the same as taking the derivative of that function with respect to *x*. Because of the expression of equation (3.31), the following can be written

$$\frac{dX}{dx} = \frac{dx}{dX} = 1 \tag{3.31a}$$

where d(·)/d(·) is considered to be derivative operator with respect to the variable in the denominator. By the chain rule, the following equation holds true

$$\frac{d(\{r\})}{dX} = \frac{d(\{r\})}{dx}\frac{dx}{dX} = \frac{d(\{r\})}{dx} \tag{3.31b}$$

Equation (3.31b) implies that taking the differentiation of the irregularities function with respect to local coordinate *x* is the same as taking the differentiation of the irregularities with respect to the global coordinate *X*, which is easier to be computed.

Taking the first derivative of equation (3.30), the wheel velocity $\{\dot{d}_w\}$ can be obtained as follows

$$\{\dot{d}_w\} = \{\dot{d}_c\} + \frac{dx}{dt}\{r'\} = \{\dot{d}_c\} + v\{r'\} \tag{3.32}$$

In equation (3.32), the over-dot means differentiating with respect to time, and the prime means differentiating with respect to local coordinate. The parameter v is the speed of the train.

By taking another derivative of equation (3.32), the wheel acceleration $\{\ddot{d}_w\}$ can be obtained as follows

$$\{\ddot{d}_w\} = \{\ddot{d}_c\} + a\{r'\} + v^2\{r''\} \tag{3.33}$$

In equation (3.33), the parameter a is the change in train speed which is zero in this study since the vehicle's speed is assumed to be constant.

Equations (3.30), (3.32) and (3.33) relate the response of the wheels to those of the contact points on the rails.

In the context of the step-by-step direct time integration of the numerical solution algorithms, the vectors containing the responses of the wheels and the vectors containing the responses of the contact points at the beginning of the current time step $t + \Delta t$ are related by the following

$$\{d_w\}^c = \{d_c\}^c + \{r\}^c \tag{3.34}$$

$$\{\dot{d}_w\}^c = \{\dot{d}_c\}^c + v\{r'\}^c \tag{3.35}$$

$$\{\ddot{d}_w\}^c = \{\ddot{d}_c\}^c + v^2\{r''\}^c \tag{3.36}$$

However, the contact displacement vector $\{d_c\}^c$ at the beginning of the current time step is obtained from the nodal displacement of the underlying structure at the end of the previous time step and is given by

$$\{d_c\}^c = \langle N_c \rangle^c_{x=x_{cj}} \{d_r\}^p \quad \text{(Track-Bridge)} \quad (3.37)$$

$$\{d_c\}^c = \langle N_c \rangle^c_{x=x_{cj}} \{d_b\}^p \quad \text{(Bridge only)} \quad (3.38)$$

The interpolation function $\langle N_c \rangle$ calculated at the contact position x_{cj} for the current time step is given by

$$\langle N_c \rangle^c_{x=x_{cj}} = \langle N_{y_r}(x_{cj}) \rangle^c \quad \text{(Track-Bridge)} \quad (3.39)$$

$$\langle N_c \rangle^c_{x=x_{cj}} = \langle N_{y_b}(x_{cj}) \rangle^c \quad \text{(Bridge only)} \quad (3.40)$$

Similarly, vectors containing the velocities and accelerations of the wheels can be obtained taking the first and second derivatives of equations (3.37) or (3.38) and expressed as follows for the case of the track-bridge subsystem

$$\{\dot{d}_c\}^c = v\langle N'_{yr}(x_{cj}) \rangle^c \{d_r\}^p + \langle N_{y_r}(x_{cj}) \rangle^c \{\dot{d}_r\}^p \quad (3.41)$$

$$\{\ddot{d}_c\}^c = \langle N_{y_r}(x_{cj}) \rangle^c \{\ddot{d}_r\}^p + 2v\langle N'_{yr}(x_{cj}) \rangle^c \{\dot{d}_r\}^p + v^2 \langle N''_{yr}(x_{cj}) \rangle^c \{d_r\}^p \quad (3.42)$$

or

as follows for the case when the track effects are ignored

$$\{\dot{d}_c\}^c = v\langle N'_{yb}(x_{cj}) \rangle^c \{d_b\}^p + \langle N_{y_b}(x_{cj}) \rangle^c \{\dot{d}_b\}^p \quad (3.43)$$

$$\{\ddot{d}_c\}^c = \langle N_{y_b}(x_{cj}) \rangle^c \{\ddot{d}_b\}^p + 2v\langle N'_{yb}(x_{cj}) \rangle^c \{\dot{d}_b\}^p + v^2 \langle N''_{yb}(x_{cj}) \rangle^c \{d_b\}^p \quad (3.44)$$

The interpolation quantities with a prime or double-prime are simply first and second derivative respectively of equations (3.12.1) through (3.12.4) taken at the contact point x_{cj}.

3.4.3 Solutions of the coupled track-bridge problem

The global track-bridge subsystem can be solved by assembling the contact elements and non-contact elements together into a master equation of motion given by

$$\begin{bmatrix}[M_{rr}] & [0] \\ [0] & [M_{bb}]\end{bmatrix}\begin{Bmatrix}\{\ddot{D}_r\} \\ \{\ddot{D}_b\}\end{Bmatrix}+\begin{bmatrix}[C_{rr}] & [C_{rb}] \\ [C_{br}] & [C_{bb}]\end{bmatrix}\begin{Bmatrix}\{\dot{D}_r\} \\ \{\dot{D}_b\}\end{Bmatrix}+\begin{bmatrix}[K_{rr}] & [K_{rb}] \\ [K_{br}] & [K_{bb}]\end{bmatrix}\begin{Bmatrix}\{D_r\} \\ \{D_b\}\end{Bmatrix}=\begin{Bmatrix}\{F_c\} \\ \{0\}\end{Bmatrix} \quad (3.45)$$

The bridge supports viscoelastic elements are added to the diagonal of the global stiffness $[K_{bb}]$ and damping $[C_{bb}]$ matrices at their corresponding degrees of freedom at end nodes of the bridge finite element model. The global damping matrix is based on the Rayleigh damping. It can be obtained from the damping ratio and the first two natural frequencies of the bridge in the conventional manner.

The quantity $\{F_c\} = 0$ for the non-interaction elements and $\{F_c\} = -[N_{yr}]\{f_c\}$ for the interaction elements. The key in solving the train-track-bridge interaction problem is to solve for the contact forces $\{f_c\}$ from equation (3.28.1) and apply them at the corresponding track-bridge interaction elements in equation (3.45).

3.5 Working Procedure of Dynamic Simulation

In the following, a summary procedure is provided for the time-history step-by-step incremental analysis proposed in this dissertation:

(1) Gather the fundamental data of the train vehicle and the track-bridge structure.

(2) Construct a spatial discretization of the track-bridge subsystem using finite beam elements, either Bernoulli or Timoshenko beam types.

(3) Assemble the global mass matrices $[M_{rr}]$ and $[M_{bb}]$; and global stiffness matrices $[K_{rr}]$, $[K_{rb}]$, $[K_{br}]$ and $[K_{bb}]$ of the track-bridge system free of any traffic load. Solve the eigenvalue problem to extract the first two natural frequencies for use in constructing the damping matrices $[C_{rr}]$ and $[C_{bb}]$.

(4) Set the initial conditions of the track-bridge subsystem and vehicle subsystem to zero at time $t = 0$. Position the first wheel of the trainset at the beginning of the track-bridge finite element model. Specify the dynamic analysis parameters such as time-step Δt and constant speed v.

(5) Self-start the analysis with the first time-step $t = \Delta t$. Compute the positions x_{cj} of each wheelset on the track-bridge subsystem. Assume the load to be the static force f_{st} for the first time-step with equation (3.6.2). Use interpolation functions to compute nodal forces. Solve the global track-bridge subsystem equation (3.45) using HHT α method. Obtain all nodal displacement vectors $\{\{D_r\}\ \{D_b\}\}^T$, velocity vectors $\{\{\dot{D}_r\}\ \{\dot{D}_b\}\}^T$ and acceleration vectors $\{\{\ddot{D}_r\}\ \{\ddot{D}_b\}\}^T$.

(6) Construct all the vehicle matrices and vectors.

(7) For a new time $t + \Delta t$, re-calculate the global position x_{cj} of each wheelset and determine the contact elements. Compute the interpolation functions at the current contact points using equation (3.39) or (3.40). Use these interpolation functions and the track-bridge responses from previous time-step to compute the contact point displacement $\{d_c\}$ using equation (3.37) or (3.38); velocities $\{\dot{d}_c\}$ using equation (3.41) or (3.43); and accelerations $\{\ddot{d}_c\}$ using equation (3.42) or (3.44).

(8) With the computed contact point responses from Step (7), compute the wheel responses at each contact point using equations (3.34), (3.35) and (3.36) for vectors $\{d_w\}$, $\{\dot{d}_w\}$ and $\{\ddot{d}_w\}$ respectively.

(9) With the wheels' responses for the current time-step computed in step (8), the vehicle's upper part incremental displacement $\{\Delta d_u\}$ can be obtained with equation (3.27.8). The vehicle's responses can be computed using equations (3.27.4), (3.27.5) and (3.27.6) for vectors $\{d_u\}$, $\{\dot{d}_u\}$ and $\{\ddot{d}_u\}$ respectively.

(10) The contact forces $\{f_c\}$ are then computed using equation (3.28.1).

(11) Using interpolation functions and contact forces from Step (10), the nodal forces on the track-bridge subsystem are computed and the global track-bridge subsystem equation (3.45) is solve again using HHT α method to obtain new nodal displacement vectors $\{\{D_r\}\ \{D_b\}\}^T$, velocity vectors $\{\{\dot{D}_r\}\ \{\dot{D}_b\}\}^T$ and acceleration vectors $\{\{\ddot{D}_r\}\ \{\ddot{D}_b\}\}^T$ at the end of the current time-step.

(12) Repeat Step 7 until the last wheel of the last vehicle of the train convoy has left the track-bridge subsystem.

3.6 Model Verifications by Numerical Examples

To verify the accuracy of the numerical model discussed in this chapter, two numerical examples are evaluated. The first example is the model verification by a semi-analytical method based on modal superposition using a simply supported short span high speed rail bridge including the vehicle interaction and excluding the track structure. The second example is the model verification against a finite element model available in the literature using a vehicle-track-bridge interaction model therefore including the track contributions. Both examples use the same bridge data for comparison purposes. Track irregularities are ignored. Tables XIII, XIV, and XV show the properties of the vehicle, track and bridge. In the reference model (Lou and Zeng, 2005), the mass of the sleepers were not included. To use the model in this dissertation for simply supported bridges, the values of support vertical stiffness is given a very high value (i.e. 10^{12} for example) and the support rotational stiffness is given a very small value (i.e. 10^{-5}).

TABLE XIII PROPERTIES OF VEHICLE IN MODEL VERIFICATION

Parameter	Value	
	Metric (Units)	US Customary (Units)
M_c	41750 (kg)	238.4 (Ib_f-s^2/in)
J_c	2 080 000 (kg-m^2)	18 409 648 (Ib_f-s^2-in)
M_t	3 040 (kg)	17.36 (Ib_f-s^2/in)
J_t	3 930 (kg-m^2)	34 784 (Ib_f-s^2-in)
M_w	1 780 (kg)	10.16 (Ib_f-s^2/in)
k_p	1 180 (kN/m)	6738 (Ib_f/in)
c_p	39.2 (kN-s/m)	224 (Ib_f-s/in)
k_s	530 (kN/m)	3026 (Ib_f/in)
c_s	90.2 (kN-s/m)	515 (Ib_f-s/in)
L_c	8.75 (m)	344.5 (in)
L_t	1.25 (m)	49.21 (in)
v	27.78 (m/s)	1093.7 (in/s)

TABLE XIV PROPERTIES OF BRIDGE IN MODEL VERIFICATION

Parameter	Value	
	Metric (Units)	US Customary (Units)
L_b	30 (m)	1181.1 (in)
E_b	29 730 000 (kN/m^2)	4 311 988 (Ib_f/in^2)
ν_b	0.2	0.2
m_b	12 000 (kg/m)	1.74 (Ib_f-s^2/in)
I_b	2.80 (m^4)	6 726 973 (in^4)
ζ	2 %	2%

TABLE XV PROPERTIES OF TRACK IN MODEL VERIFICATION

Parameter	Value	
	Metric (Units)	US Customary (Units)
E_r	206 000 000 (kN/m^2)	4 311 988 (Ib_f/in^2)
ν_r	0.2	0.2
m_r [(1)]	51.5 (kg/m)	0.00747 (Ib_f-s^2/in)
I_r	0.00002037 (m^4)	48.94 (in^4)
k_{bv}	131 600 (kN/m^2)	19 087 (Ib_f/in/in)
c_{bv}	64.2 (kN-s/m)	9.31 (Ib_f-s/in/in)

(1) Value used by reference paper does not include mass of sleepers. It is included in present work.

3.6.1 Verification by semi-analytical method

In this first example, the finite element based method of this dissertation is compared with a semi-analytical solution method. The semi-analytical method consists of numerically solving the fully coupled equations of motion describing the vehicle and the bridge movements simultaneously. The 2D vehicle model with 10 degrees of freedom is used. After condensing the vehicle four wheels' displacements to the bridge displacements at the contact points, the vehicle's remaining 6 degrees of freedom are described by equations (3.3.1) through (3.3.6). Expressing the wheels' displacements in terms of the bridge displacements and substituting them into the vehicle's upper part equations mentioned above, the equations governing the fully coupled vehicle-bridge interaction in the time domain can be written as given in Appendix A.

The equation of motion of the bridge is based on the first mode of a modal superposition process. Using Matlab® program, the equations in Appendix A are solved simultaneously to obtain the time-histories of the vehicle's carbody vertical deflection and acceleration as well as the bridge mid-span vertical deflection and acceleration. These semi-analytical results are compared with results from the finite element program using the solution algorithms proposed in this dissertation as shown in Figure 3.9 for the vehicle responses and in Figure 3.10 for bridge mid-span vertical responses. It can be seen that there is an excellent agreement between the two methods. This clearly shows there is good validity of the finite element model described in this research with moving contact points that are formulated from the underlying structure based on its previous time-step responses in the incremental solutions. One observation to note is that the bridge's mid-span vertical accelerations obtained with the finite element method of this dissertation are higher than the semi-analytical method because the latter considers only one mode while the finite element program of this study considers all the modes of vibration in the system.

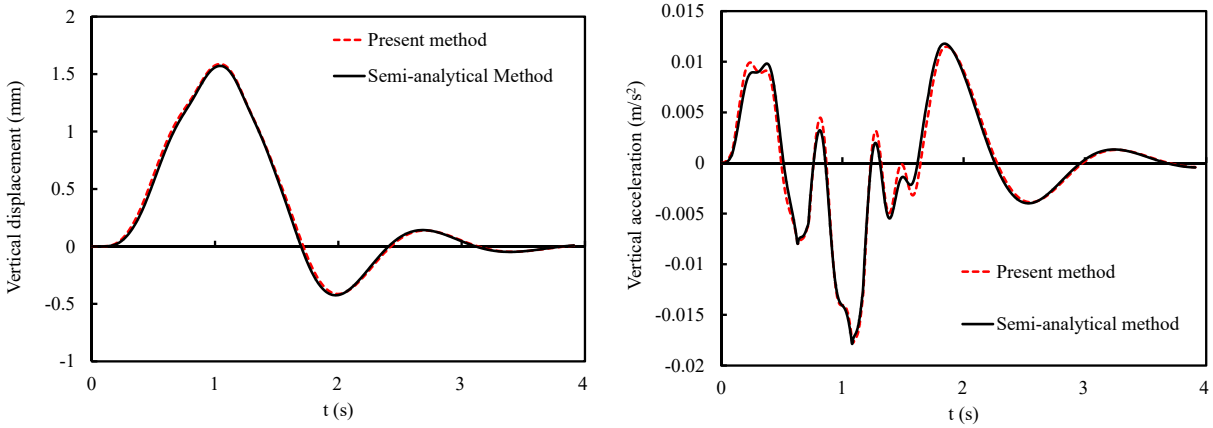

Figure 3.9 Results comparison of vehicle carbody vertical responses:
deflection (left), acceleration (right)

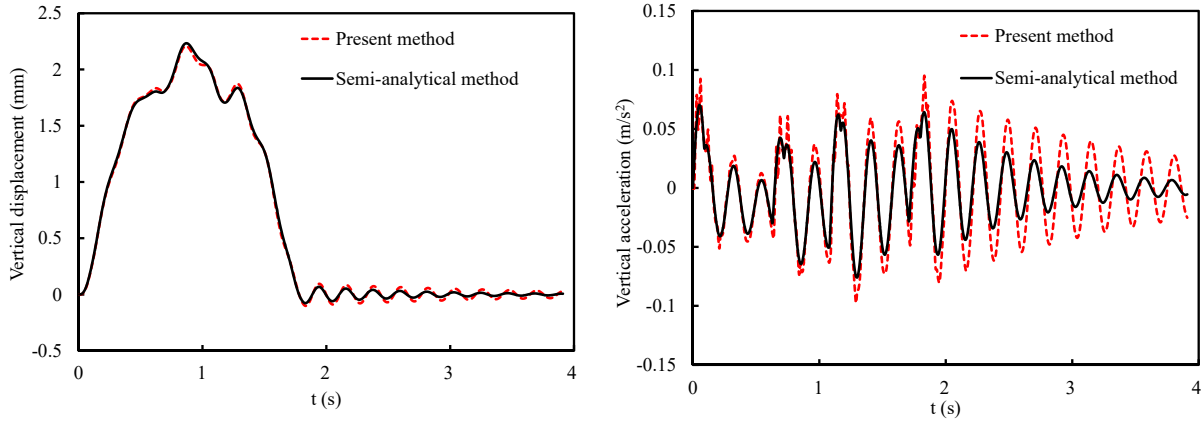

Figure 3.10 Results comparison of bridge mid-span vertical responses: deflection (left), acceleration (right)

3.6.2 Verification by finite element method with results in literature

In this second example, the solution method of this research is compared with results available in the literature. The excellent paper of (Lou and Zeng, 2004) is used a comparison basis. The authors of that paper performed dynamic analysis of a simply supported bridge using a numerical model that considers a fully coupled system. Their approach consisted of treating the vehicle, track and bridge as one whole system with a single equation of motion. Their formulation was based on the principle of a stationary value of total potential energy which treats the contact forces as internal forces. In their work, the entire system matrices and vectors in the direct time integration are time-dependent and must be updated at each increment, therefore, making the dynamic analysis computationally very expensive. In contrast, the solution method proposed in this dissertation decouples the vehicle subsystem from the track-bridge subsystem, therefore, considering the contact forces as external forces.

Results of the reference model and those from the work in this dissertation are shown in Figures 3.11 and 3.12 for the vehicle vertical deflection and acceleration respectively. The left graph is based on the present work and the right graph is based on the reference paper. It can be seen that the shapes of the graphs are similar and the magnitude is very close for the case with no track. In the case of including the track, the present work seems to give a slightly higher value but the orders of magnitude are nevertheless close.

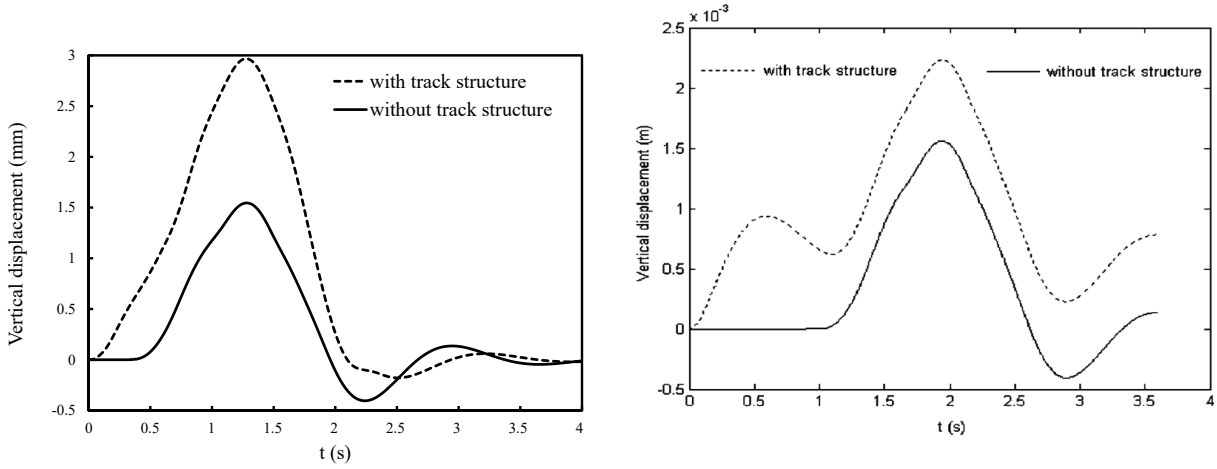

Figure 3.11 Result comparisons of vehicle carbody vertical displacement:
present study results (left graph); reference model results (right graph) (Lou and Zeng, 2005)

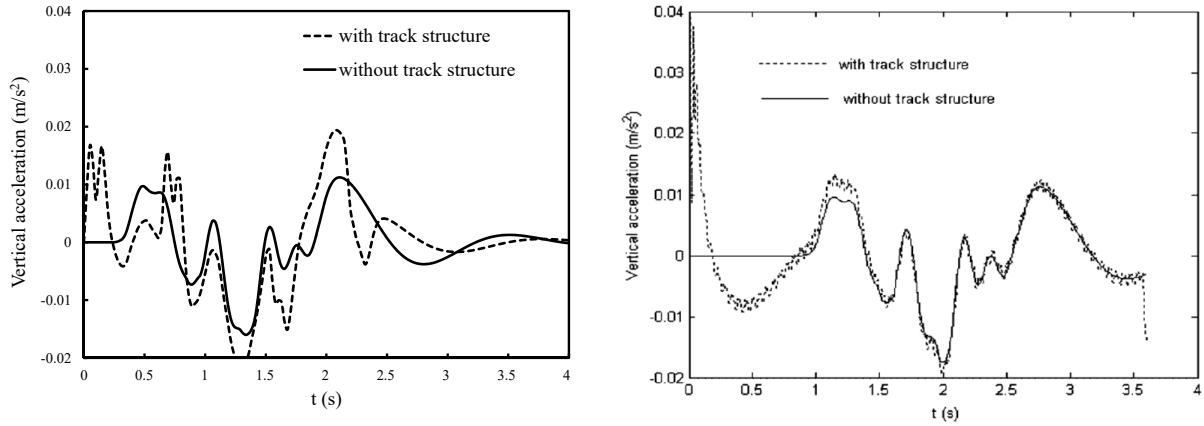

Figure 3.12 Result comparisons of vehicle carbody vertical acceleration:
present study results (left graph); reference model results (right graph) (Lou and Zeng, 2005)

Results of the reference model and those from the work in this dissertation are shown in Figures 3.13 and 3.14 for the bridge mid-span vertical deflection and acceleration respectively. For the bridge deflections the two set of results are practically identical. The present work has numerical damping built into the algorithms due to the HHT α method as shown in the accelerations while the reference paper used Newmark β method with no numerical damping.

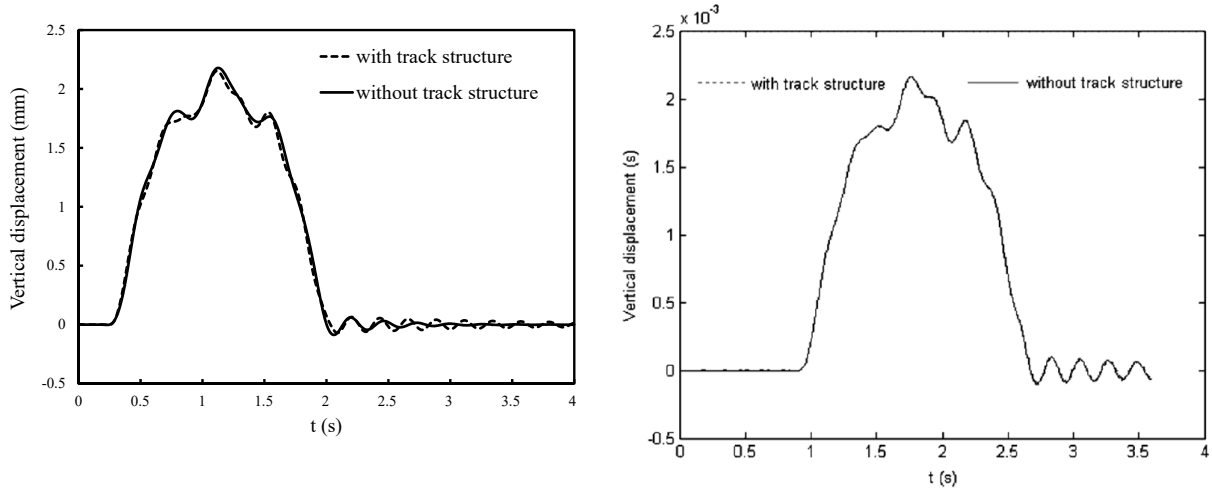

Figure 3.13 Result comparisons of bridge vertical displacement:
present study results (left graph); reference model results (right graph) (Lou and Zeng, 2005)

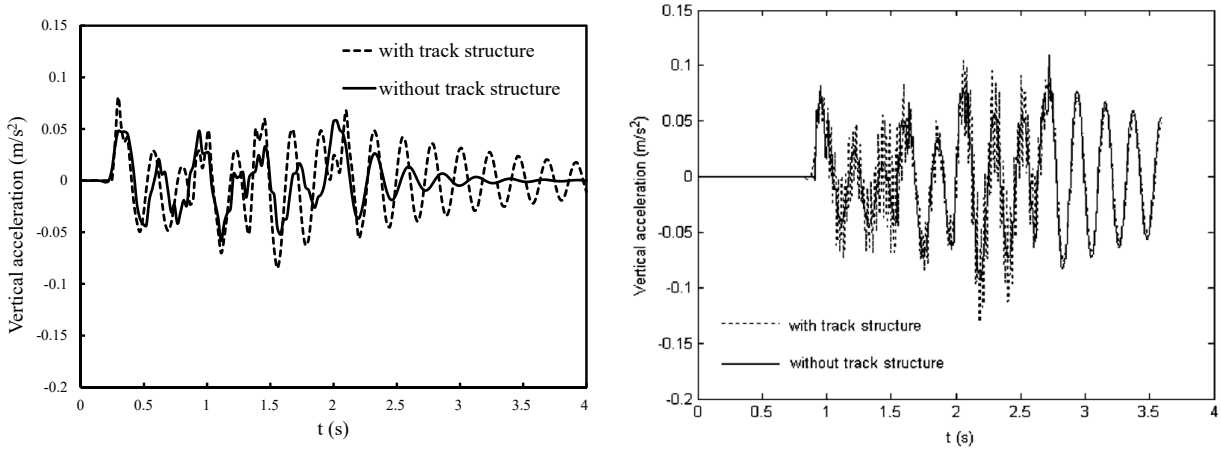

Figure 3.14 Result comparisons of bridge vertical acceleration:
present study results (left graph); reference model results (right graph) (Lou and Zeng, 2005)

Results of the reference model and those from the work in this dissertation are shown in Figure 3.15 for the track vertical deflection. It can be seen the two methods give the same results. The four peaks correspond to the four wheelset of the 10-DOF train vehicle used in the examples.

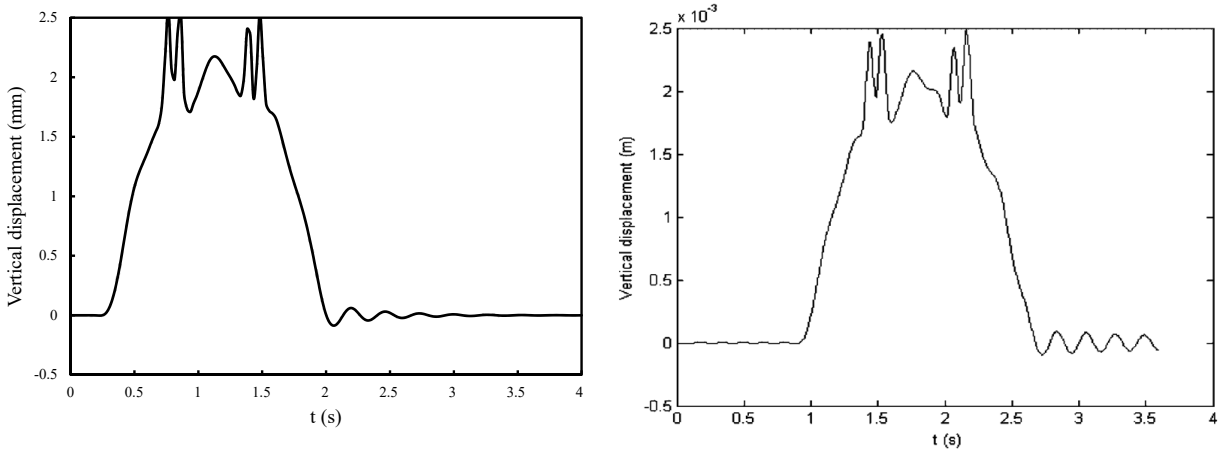

Figure 3.15 Results comparison for track vertical displacement:
present study results (left graph); reference model results (right graph) (Lou and Zeng, 2005)

CHAPTER 4

INVESTIGATION OF NATURAL FREQUENCIES

Parts of the material presented in this chapter are published in (Nour and Issa, 2015) and reproduced in this dissertation with permission which is listed in Appendix B. The author of this dissertation is a contributing co-author.

4.1 Introduction

A free vibration of any elastic body is called natural vibration and happens at a frequency called natural frequency. It is the frequency at which the structure would tend to oscillate in the absence of any driving or damping force. Natural vibrations are considered different from forced vibrations which happen at the frequency of applied force called forcing frequency. If the forcing frequency is equal to the natural frequency, the amplitude of vibrations increases many folds creating a phenomenon known as resonance. It is essential to estimate accurately natural frequencies of a structure undergoing dynamic loads.

In most international codes of railway bridge engineering (European Committee for Standardization, 2002; European Committee for Standardization, 2003), the natural frequency of the unloaded bridge is an important factor used in the serviceability limit check related to the verification of structural deformations and vibrations. The requirement for bridge dynamic analysis is a function of limits imposed on the fundamental frequency (UIC Leaflet 776-2, 2009). In the criteria for traffic safety, frequencies up to the frequency of the third mode of vibration are

included in the calculations of vertical bridge deck accelerations (UIC Leaflet 776-2, 2009). Regarding the dynamic enhancement due to real trains in the European Code, the factor representing the contribution of the track defects and vehicle imperfections is also a function of the first natural bending frequency of the bridge. In the selection of a critical universal train for dynamic analysis, the wavelength of excitation at the maximum design speed and the maximum value of aggressivity both require the fundamental frequency of the bridge in their computations. The speed at which resonance may occur is directly proportional to the first natural frequency (UIC Leaflet 776-2, 2009). Despite its importance as stated above, natural frequencies are however often obtained using simple basic models consisting of a simply supported bridge based on Euler-Bernoulli beam theory (UIC Leaflet 776-2, 2009), thus ignoring effects of other features of the structure such as boundary conditions and track properties.

Short span bridges traversed by a high speed train present a special challenge. According to (Timoshenko, 1921; Timoshenko, 1922), the application of Euler-Bernoulli beam theory may not be adequate for short span bridges as it neglects the effects of shear deformations and rotational inertia. High frequency excitations also require the use of Timoshenko beam theory. This chapter of the dissertation investigates the effects on the vibration natural frequencies of the track-bridge system features such as the stiffness of the bridge support elements, shear deformations and rotational inertia, and the vertical stiffness of the track structure. The combined effects of the bridge support vertical stiffness and rotational stiffness are also examined.

4.2 Effects of Bridge Support Vertical Stiffness

The effects of the elastomeric bearings and/or soil foundation on the bridge dynamic characteristics were studied by a number of researchers (Yang et al., 2004) with the introduction

of elastic springs at the bridge supports. Consider the beam shown in Figure 4.1. The beam is supported at each end by a vertical spring with a stiffness represented by the parameter k_v.

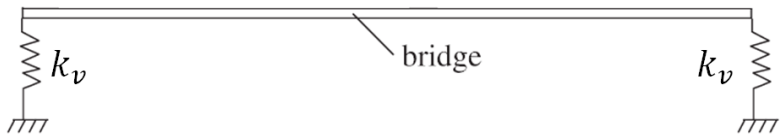

Figure 4.1 Elastically supported beam

A non-dimensional support vertical stiffness ratio κ can be defined as the ratio of the support vertical stiffness to bridge bending stiffness according to the following equation.

$$\kappa = \frac{k_v L^3}{EI} \tag{4.1}$$

The parameter k_v is the equivalent vertical stiffness of bridge supporting elements including elastomeric bearings, abutments and soil foundation. L is the bridge span length. E is the modulus of elasticity. The quantity I is the second moment of area.

In general, high speed rail bridges are required to be stiff in order to limit deflections and improve the riding comfort. As a result, for short span bridges, if all other parameters of equation (4.1) remain constant, the parameter κ decreases faster as the span L decreases. This may have important implications in the retrofitting of existing short span bridges being upgraded for high speed rail where bridge stiffening would increase the value of EI and therefore decreases the parameter κ. The effects of changes in this parameter on the natural frequencies are being investigated in this section.

4.2.1 Case of simply supported Euler-Bernoulli beam

Consider the free vibration of the elastically supported uniform beam shown in Figure 4.1. Assuming shear deformations and rotational inertia are ignored, this model reduces to the reference classic simple model of a pinned-pinned Euler-Bernoulli beam (i.e. $\kappa \rightarrow +\infty$).

Considering the mass m_b per unit length of the bridge, the natural angular frequency for this case is very easy to compute and given by

$$\omega_{n,ss,b} = (\lambda_{n,ss,b})^2 \sqrt{\frac{EI}{m_b L^4}} \tag{4.2}$$

The subscript n denotes the n[th] mode shape. The subscript *ss* denotes simply-supported and *b* represents Euler-Bernoulli beam theory.

The frequency parameter $\lambda_{n,ss,b}$ associated with the n^{th} mode shape of vibration is the solutions of the following characteristic equation

$$sin\lambda = 0 \tag{4.3}$$

Solutions are well known and can be written as in equation (4.4) where *n* is the mode number

$$\lambda_{n,ss,b} = n\pi\,, \quad n = 1, 2, 3, \ldots \tag{4.4}$$

In this chapter, this type of bridge modeling is used as a basic reference model with respect to which results of all other investigated models are normalized. Using equations (4.2) and (4.4), natural frequencies can be calculated without virtually any computational efforts. This model provides good results for simply supported slender beams only.

4.2.2 Case of elastically supported Euler-Bernoulli beam

Now consider the free vibration of the elastically supported uniform beam shown in Figure 4.1. Still assuming that shear deformations and rotational inertia are ignored, and the supports are flexible, this model is defined as an elastically supported Euler-Bernoulli beam. The natural angular frequency may be expressed as

$$\omega_{n,es,b} = (\lambda_{n,es,b})^2 \sqrt{\frac{EI}{m_b L^4}} \tag{4.5}$$

The subscript *es* denotes elastically supported.

The quantity $\lambda_{n,es,b}$ is the frequency parameter of the n^{th} mode shape of vibration for the elastically supported Euler-Bernoulli beam.

Dividing equation (4.5) by equation (4.2), the frequency ratio of an elastically supported beam to a simply supported Euler-Bernoulli beam can be written as

$$f_n(\kappa) = \frac{\omega_{n,es,b}}{\omega_{n,ss,b}} = \frac{(\lambda_{n,es,b})^2}{(\lambda_{n,ss,b})^2} \tag{4.6}$$

This frequency ratio $f_n(\kappa)$ depends on the parameter κ given by equation (4.1).

The frequency parameter $\lambda_{n,es,b}$ is obtained by solving the following characteristic equation of an elastically supported Euler-Bernoulli beam (Karnovsky and Lebed, 2000).

$$\lambda^6(1 - cos\,\lambda\, cosh\,\lambda) + 2\kappa\lambda^3(cos\,\lambda\, sinh\,\lambda - cosh\,\lambda\, sin\,\lambda) + 2\kappa^2 sin\lambda\, sinh\lambda = 0 \tag{4.7}$$

The quantity $\lambda_{n,es,b}$ is the solutions λ of the transcendental equation (4.7) which can only be obtained numerically. In the present research, an initial sensitivity study was performed to determine the relevant range of the parameter κ over which the frequency parameter changes significantly. A parametric sweep was then carried out to extract the frequency parameters for a wide range of κ values. The results are presented in the next section.

4.2.2.1 Development of empirical equations

Table XVI shows the normalized results $f_n(\kappa)$ of a sensitivity study for the first six natural frequencies of bending with values of the parameter κ between 10^{-6} corresponding to the free-free support condition and 10^{6} corresponding to the simply supported condition.

TABLE XVI VALUES OF $f_n(\kappa)$ FOR FIRST SIX NATURAL FREQUENCIES OF ELASTICALLY SUPPORTED EULER-BERNOULLI BEAM

κ	$Log_{10}(\kappa)$	$f_n(\kappa)$					
		$n=1$	$n=2$	$n=3$	$n=4$	$n=5$	$n=6$
10^{-6}	-6	0.000	0.000	0.252	0.391	0.490	0.562
10^{-5}	-5	0.000	0.000	0.252	0.391	0.490	0.562
10^{-4}	-4	0.001	0.001	0.252	0.391	0.490	0.562
10^{-3}	-3	0.005	0.002	0.252	0.391	0.490	0.562
10^{-2}	-2	0.014	0.006	0.252	0.391	0.490	0.563
10^{-1}	-1	0.045	0.020	0.252	0.391	0.490	0.563
1	0	0.142	0.062	0.254	0.391	0.490	0.563
10^{+1}	1	0.418	0.194	0.272	0.395	0.491	0.563
10^{+2}	2	0.839	0.551	0.416	0.434	0.504	0.568
10^{+3}	3	0.981	0.923	0.826	0.713	0.641	0.629
10^{+4}	4	0.998	0.992	0.982	0.967	0.946	0.918
10^{+5}	5	1.000	0.999	0.998	0.997	0.995	0.993
10^{+6}	6	1.000	1.000	1.000	1.000	1.000	0.999

As the supports of the bridge become softer (i.e. κ become smaller), the first two natural frequencies move quickly towards rigid body modes. For the free-free side of the spectrum, the 3rd mode of vibration becomes the fundamental frequency as can be seen in the above table. In the parametric study, it was found convenient to express the parameter κ in a logarithmic form to facilitate a small uniform stepping in the sweep. After the initial sensitivity study, further in-depth parametric sweep was performed to solve equation (4.7) for the frequency parameters λ to include all possible values of κ in the spectrum of bridge supports flexibility. As shown in Figure 4.2, a decrease in the parameter κ leads to a decrease in the bridge natural frequencies. The decrease follows smooth asymptotic sigmoid curves.

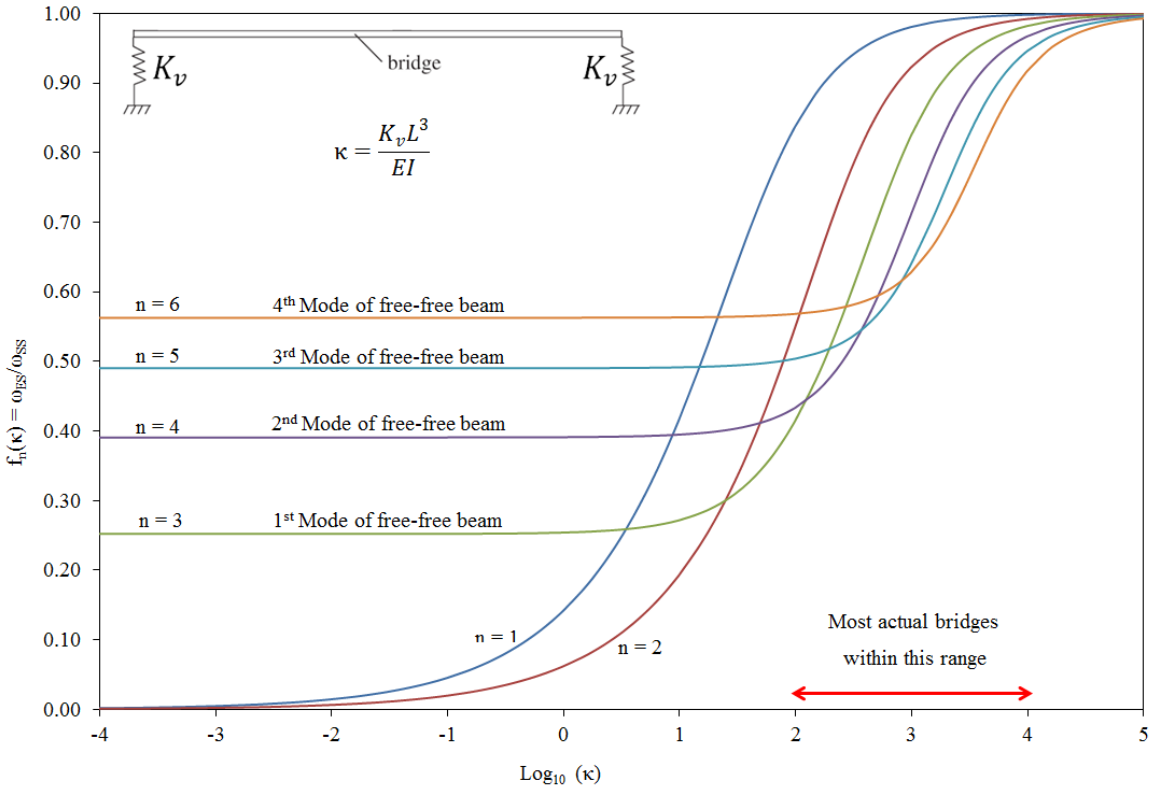

Figure 4.2 Plots of $f_n(\kappa)$ for the first six natural frequencies of Euler-Bernoulli beam

It is worth noting that actual field conditions of most bridges are such that the vertical support stiffness ratio defined by the parameter κ is between 100 and 10000 which correspond to logarithmic values of κ between 2 and 4 respectively.

Further processing of numerical results was performed to deduce empirical equations as given by equations (4.8a) through (4.8f) for the first six natural frequencies of an elastically supported beam using curve fitting techniques.

$$f_1(\kappa) = \left[\frac{1}{1 + 62\left(\frac{1}{\kappa}\right)^{1.07}}\right]^{0.47} \tag{4.8a}$$

$$f_2(\kappa) = \left[\frac{1}{1 + 668\left(\frac{1}{\kappa}\right)^{1.17}}\right]^{0.43} \tag{4.8b}$$

$$f_3(\kappa) = \left[\frac{0.724}{1 + 726\left(\frac{1}{\kappa}\right)^{1.10}}\right]^{0.89} + 0.25 \tag{4.8c}$$

$$f_4(\kappa) = \left[\frac{0.574}{1 + 6027\left(\frac{1}{\kappa}\right)^{1.25}}\right]^{0.89} + 0.39 \tag{4.8d}$$

$$f_5(\kappa) = \left[\frac{0.481}{1 + 30377\left(\frac{1}{\kappa}\right)^{1.35}}\right]^{0.92} + 0.49 \tag{4.8e}$$

$$\mathrm{f}_6(\kappa) = \left[\frac{0.418}{1 + 98845\left(\frac{1}{\kappa}\right)^{1.40}}\right]^{0.94} + 0.56 \tag{4.8f}$$

4.2.3 Case of elastically supported Timoshenko beam

Consider the free vibration of the elastically supported uniform beam shown in Figure 4.1 taking into account this time the shear deformations and rotational inertia. For time harmonic vibrations with angular frequency $\omega_{n,es,t}$ the two coupled dimensionless governing characteristic differential equations of motion describing Timoshenko beam theory are (Lee and Lin, 1995).

$$\begin{gathered} y''''(\xi) + \Omega^2(\delta + \mu)y''(\xi) + \Omega^2(\delta\mu\Omega^2 - 1)y(\xi) = 0, \\ \psi''''(\xi) + \Omega^2(\delta + \mu)\psi''(\xi) + \Omega^2(\delta\mu\Omega^2 - 1)\psi(\xi) = 0, \\ \xi \in (0,1) \end{gathered} \tag{4.9}$$

and the associated boundary conditions are,

at $\xi = 0$,

$$\kappa y = \left(\frac{1}{\delta}\right)(y' - \psi), \;\; \psi' = 0 \tag{4.10a}$$

at $\xi = 1$,

$$-\kappa y = \left(\frac{1}{\delta}\right)(y' - \psi), \;\; \psi' = 0 \tag{4.10b}$$

In equations (4.9) and (4.10), primes indicate differentiation with respect to the dimensionless spatial variable ξ. The variable y is the dimensionless flexural displacement and the variable ψ is the dimensionless angular rotation due to bending.

Additional dimensionless parameters for writing the characteristic equation of a uniform Timoshenko beam on elastic supports are defined in the following

$$\Omega^4 = \left(\omega_{n,es,t}\right)^2 \frac{m_b \mathrm{L}^4}{EI} \tag{4.11a}$$

$$\delta = \frac{EI}{k_s G A \mathrm{L}^2} \tag{4.11b}$$

$$\mu = \frac{I_b}{A\mathrm{L}^2} \tag{4.11c}$$

$$\alpha = \frac{\Omega}{\sqrt{2}} \sqrt{-(\delta+\mu) + \sqrt{\frac{4}{\Omega^2} + (\delta-\mu)^2}} \tag{4.11d}$$

$$\beta = \frac{\Omega}{\sqrt{2}} \sqrt{(\delta+\mu) + \sqrt{\frac{4}{\Omega^2} + (\delta-\mu)^2}} \tag{4.11e}$$

$$s = \frac{1}{\sqrt{\mu}} \tag{4.11f}$$

$$\gamma = \sqrt{\frac{\delta}{\mu}} \tag{4.11g}$$

$$\phi = \delta + \mu \tag{4.11h}$$

The quantity Ω is the frequency parameter, G is the shear modulus, k_s is the Timoshenko shear correction factor, and A is the cross-sectional area. The parameter μ accounts for the rotational inertia while the parameter δ accounts for the shear deformations. The parameter ϕ accounts for the combined effects of rotational inertia and shear deformations ($\phi = \delta + \mu$).

Together, equations (4.9) through (4.11) define the free vibration problem of an elastically supported uniform Timoshenko beam of Figure 4.1. Many researchers (Lee and Lin, 1995; Pielorz, A., 1996) have used similar formulation to solve special cases only of the boundary conditions such as free-free, free-clamped, etc. Other researchers (Maurizi et al., 1990) have gone as far as setting up the problem without proposing explicit form of the characteristic equation for an elastically supported uniform Timoshenko beam.

The author of this dissertation is making an attempt to write the explicit form of the characteristic equation for this problem and only the final result is presented in equation (4.12) as the intermediate mathematical derivations and manipulations are long and tedious.

$$
\begin{aligned}
&\alpha\beta(\alpha^2+\beta^2)\delta\Omega^2[\alpha^2-\beta^2+(\delta+\mu)\Omega^2]\{\alpha[\beta^2-\delta\Omega^2][\alpha^2+(\delta+\mu)\Omega^2]Cosh\alpha Sin\beta \\
&\quad+\{\beta[\alpha^2+\delta\Omega^2][-\beta^2+(\delta+\mu)\Omega^2]Cos\beta \\
&\quad+(\alpha^2+\beta^2)\kappa(-1+\delta\mu\Omega^2)Sin\beta\}Sinh\alpha\} \\
&\quad+\{\alpha\beta^3(\delta+\mu)\Omega^2(\alpha^2+\delta\Omega^2)Cosh\alpha \\
&\quad-\alpha^3(\beta^2-\delta\Omega^2)[\beta(\delta+\mu)\Omega^2Cos\beta+\kappa(-1+\delta\mu\Omega^2)Sin\beta] \\
&\quad+\beta^3\kappa(\alpha^2+\delta\Omega^2)(-1+\delta\mu\Omega^2)Sinh\alpha\}\{\alpha\beta[\beta^2-(\delta+\mu)\Omega^2]Cos\beta \\
&\quad+\alpha\beta[\alpha^2+(\delta+\mu)\Omega^2]Cosh\alpha+\kappa(-1+\delta\eta\Omega^2)(-\alpha Sin\beta+\beta Sinh\alpha)\} \\
&\quad-\{-\alpha\beta^3(\alpha^2+\delta\Omega^2)Cosh\alpha+\alpha(\beta^2-\delta\Omega^2)[\alpha^2\beta Cos\beta+\kappa(1-\delta\mu\Omega^2)Sin\beta] \\
&\quad-\beta\kappa(\alpha^2+\delta\Omega^2)(-1+\delta\mu\Omega^2)Sinh\alpha\}\{\alpha^3\beta[\beta^2-(\delta+\mu)\Omega^2]Cos\beta \\
&\quad-\alpha\beta^3[\alpha^2+(\delta+\mu)\Omega^2]Cosh\alpha-\kappa(-1+\delta\mu\Omega^2)(\alpha^3Sin\beta+\beta^3Sinh\alpha)\} \\
&\quad-\alpha\beta\{\alpha(\beta^2-\delta\Omega^2)[\alpha^2+(\delta+\mu)\Omega^2]Sin\beta \\
&\quad+\beta(\alpha^2+\delta\Omega^2)[-\beta^2+(\delta+\mu)\Omega^2]Sinh\alpha\}\{\beta^2\kappa(-1+\delta\mu\Omega^2)Cosh\alpha \\
&\quad+\alpha[\alpha\kappa(-1+\delta\mu\Omega^2)Cos\beta+\alpha\beta[\beta^2-(\delta+\mu)\Omega^2]Sin\beta \\
&\quad+\beta^2[\alpha^2+(\delta+\mu)\Omega^2]Sinh\alpha]\}=0
\end{aligned}
\tag{4.12}
$$

It is interesting to note that if the effects of rotational inertia are ignored (i.e. $\mu = 0$) and the shear deformations are ignored (i.e. $\delta = 0$), it implies that $\alpha = \beta$ and therefore equation (4.12) reduces to equation (4.7) which is the case of an elastically supported Euler-Bernoulli beam.

In order to study the effects of the parameter κ on the natural frequency of the bridge using Timoshenko beam theory, the parameter R is introduced and defined as the frequency ratio of an elastically supported Timoshenko beam to the simply supported Euler-Bernoulli beam as

$$R = \frac{\omega_{n,es,t}}{\omega_{n,ss,b}} = \frac{\Omega}{(\lambda_{n,ss,b})^2} \tag{4.13}$$

The subscript *t* denotes for Timoshenko.

Effects on the natural frequency of parameters such as the slenderness s defined by equation (4.11f), which is clearly the inverse of the rotational inertia and the parameter γ defined as the ratio of shear deformation to rotational inertia are investigated in the following. The combined effects ϕ of the shear deformations and rotatory inertia are also examined

4.2.3.1 Fundamental frequency of elastically supported Timoshenko beam

In this section of the dissertation, equation (4.12) is solved numerically for the frequency parameter Ω of the first natural frequency (i.e. fundamental frequency) and normalized with respect to the squared of the corresponding Euler-Bernoulli frequency parameter $\lambda_{n,ss,b}$.

The reduction *R* of the fundamental frequency with the support stiffness parameter κ and bridge slenderness *s* is shown in Figures 4.3 through 4.7 for five different values of the shear deformation parameter γ. These figures confirm that for slender bridges the shear deformations have no effects. Also, both shear deformations and slenderness effects become less significant as the bridge supports become more flexible.

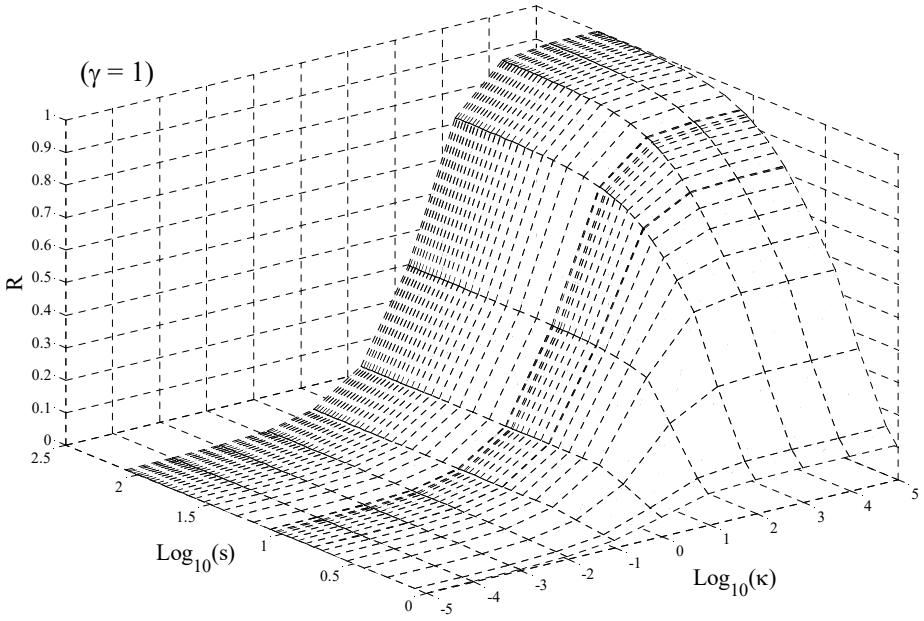

Figure 4.3 Ratio R of fundamental frequency for elastically supported Timoshenko beam with $\gamma = 1$

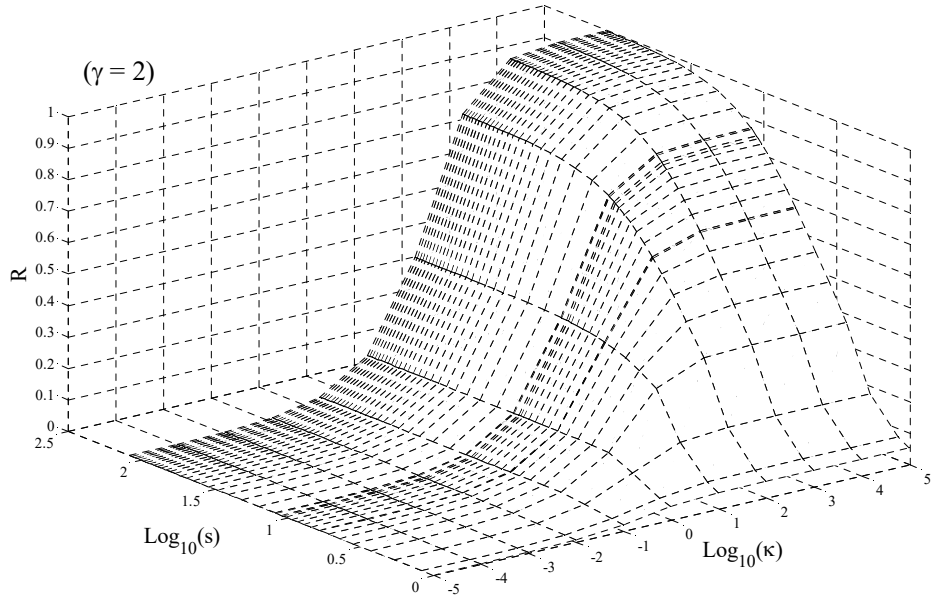

Figure 4.4 Ratio R of fundamental frequency for elastically supported Timoshenko beam with $\gamma = 2$

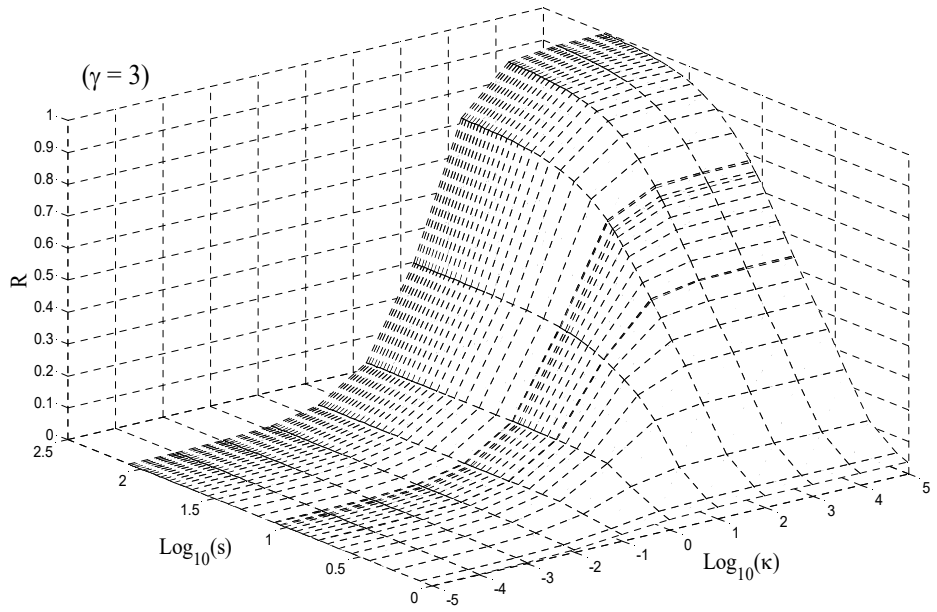

Figure 4.5 Ratio R of fundamental frequency for elastically supported Timoshenko beam with $\gamma = 3$

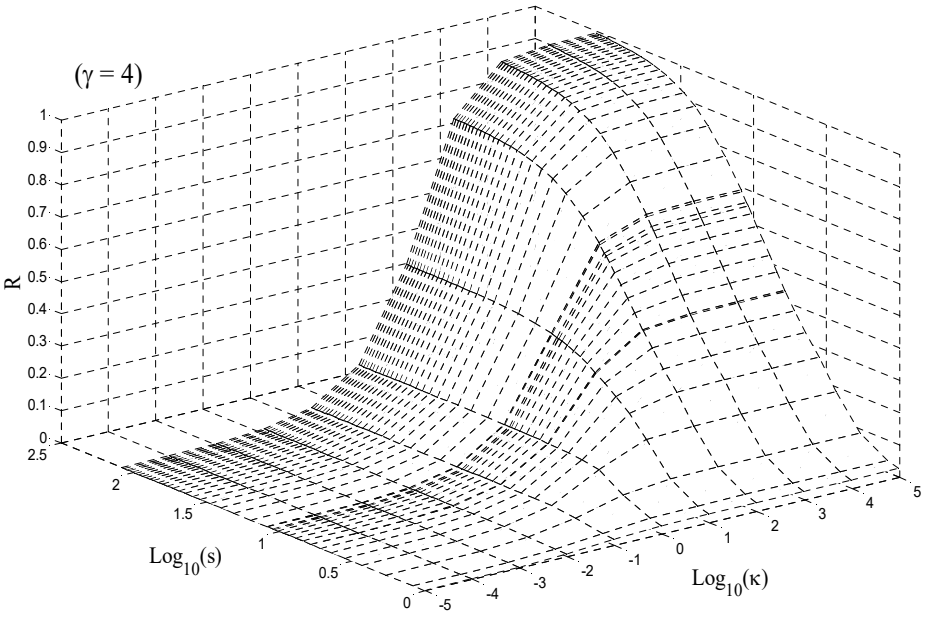

Figure 4.6 Ratio R of fundamental frequency for elastically supported Timoshenko beam with $\gamma = 4$

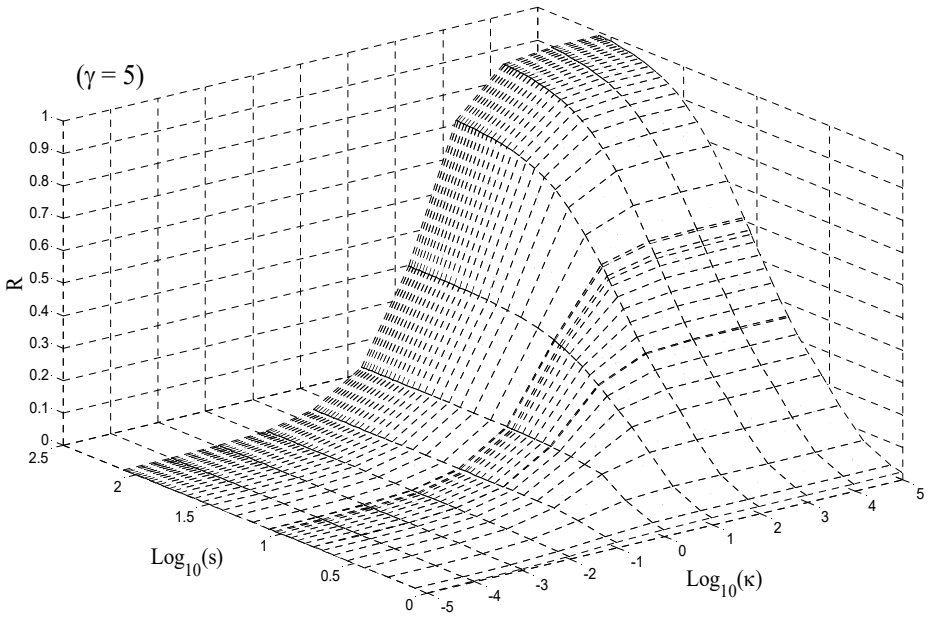

Figure 4.7 Ratio R of fundamental frequency for elastically supported Timoshenko beam with $\gamma = 5$

Another important physical parameter that can be used to trace the changes in the fundamental frequency is the combined effects of the shear deformations and rotational inertia (ϕ). Figure 4.8 shows the density plot of the fundamental frequency reduction R with the parameters κ and ϕ. The density of this figure shows again that the effects of shear deformations and rotational inertia become less significant as the bridge supports become more flexible.

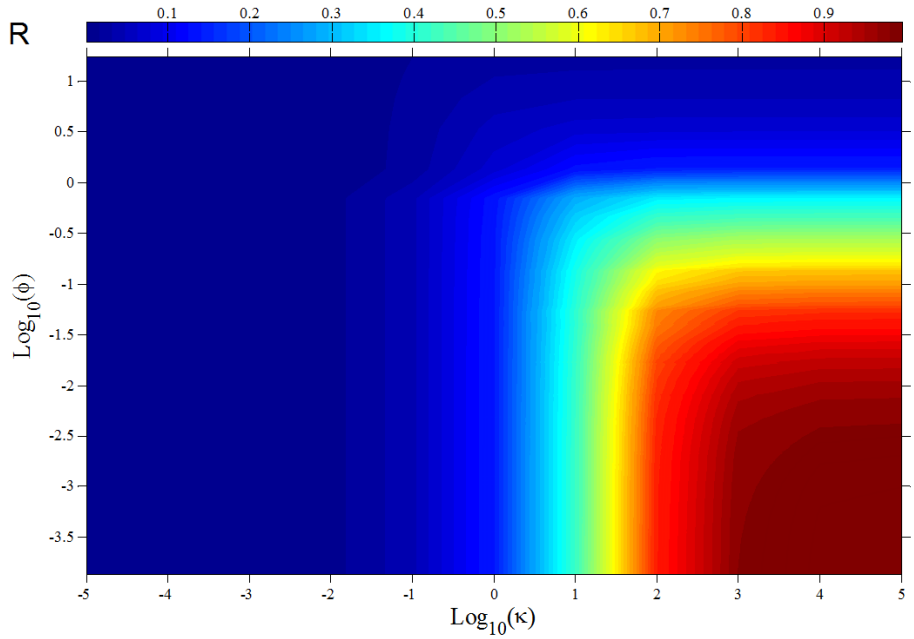

Figure 4.8 Density plot of ratio R as a function κ and ϕ

The contour plots of R values for the elastically supported uniform Timoshenko beam are shown in Figure 4.9. With the knowledge of the physical parameter ϕ and bridge support stiffness parameter κ, this figure can be used directly to estimate the fundamental frequency. It can be seen that the fundamental frequency of a simply supported bridge is always an upper bound value. The combined effects of supports flexibility as well as shear deformations and rotatory inertia reduce the bridge natural frequency.

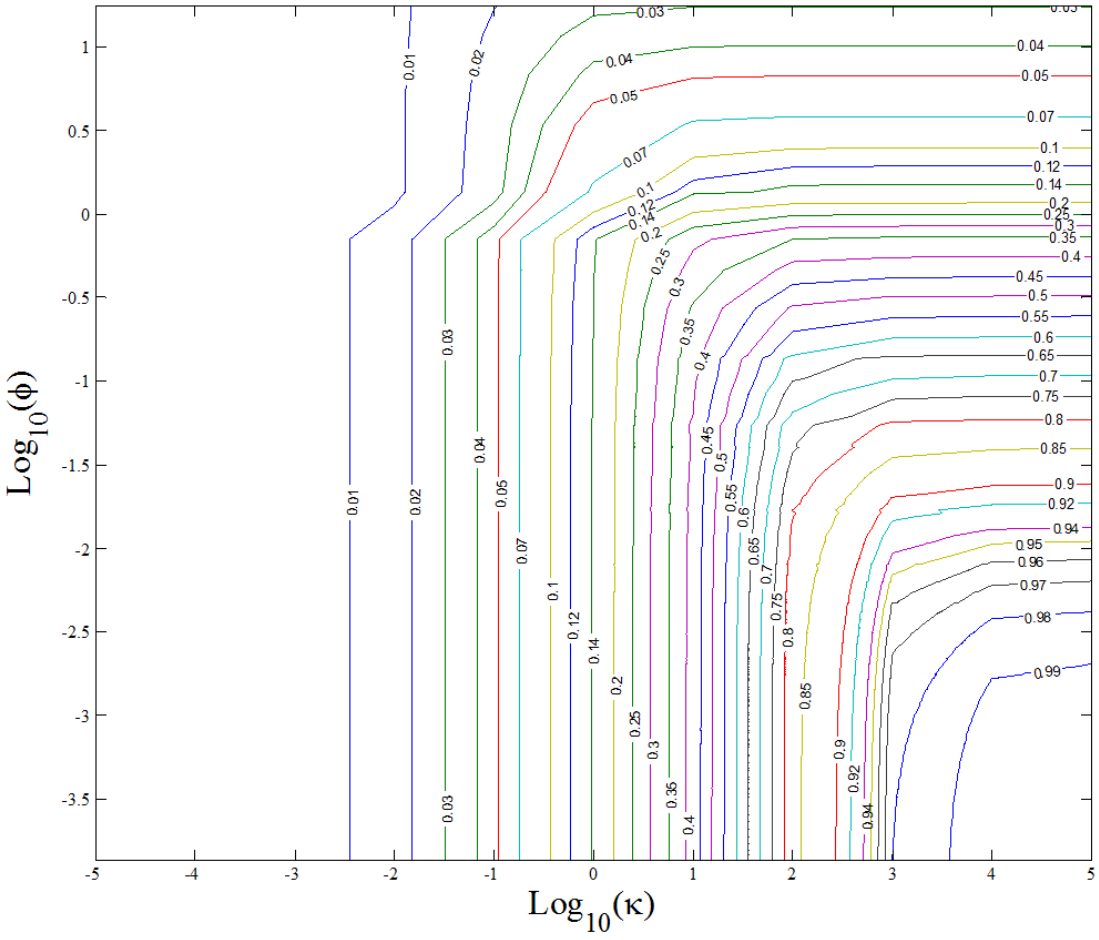

Figure 4.9 Contour plots of ratio R as a function κ and ϕ

4.3 Natural Frequency of Ballasted Track-Bridge System

Consider the track-bridge interaction as shown in Figure 4.10. The bridge is elastically supported with vertical springs. The track stiffness is represented by elastic springs with an equivalent vertical stiffness k_{bv} accounting for contributions of rail pads, sleepers and ballast. The mass of the bridge without any track structure is m_b and the mass of the ballast materials is m_{ba}.

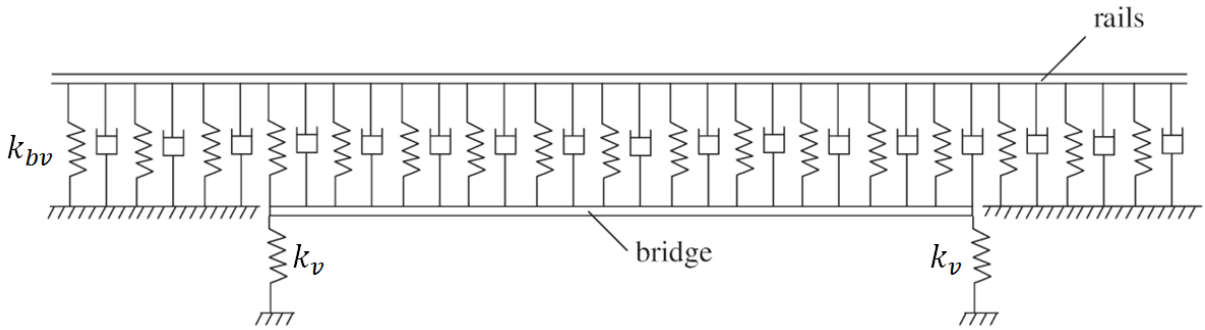

Figure 4.10 Ballasted track-bridge system with vertical flexible supports

In this case, the solutions are obtained by means of a finite element method. A two dimensional discretization of rail and beam elements is constructed. The rail is modeled with Timoshenko beam elements. The bridge is modeled using both Bernoulli and Timoshenko beam elements.

In addition to the vertical support stiffness parameter given in equation (4.1), a new parameter identified as the track stiffness parameter κ_b is introduced and defined as

$$\kappa_b = \frac{k_{bv}\mathrm{L}^4}{EI} \tag{4.14}$$

The quantity k_{bv} is the track vertical stiffness with units of force per unit length squared.

In the finite element formulation, consistent mass matrices are used. For the Timoshenko case, the mass matrix accounting for both the translational and rotational inertia is adopted. The track stiffness is added to the stiffness matrix of the bridge.

Let $\overline{\omega}_{n,es,b}$ be the natural frequency of the elastically supported track-bridge system without shear deformations or rotational inertia effects (i.e. Bernoulli beam theory), and defined as

$$\overline{\omega}_{n,es,b} = (\bar{\lambda}_{n,es,b})^2 \sqrt{\frac{EI}{m_b L^4}} \tag{4.15}$$

The quantity $\bar{\lambda}_{n,es,b}$ is the frequency parameter of the n^{th} mode shape of vibration of the elastically supported track-bridge system excluding shear deformations and rotational inertia effects.

Let $\bar{R}$ be the fundamental frequency ratio given by

$$\bar{R} = \frac{\overline{\omega}_{1,es,b}}{\omega_{1,ss,b}} \tag{4.16}$$

The quantity $\overline{\omega}_{1,es,b}$ is the first natural frequency of the elastically supported track-bridge system and $\omega_{1,ss,b}$ is the first natural frequency of the simply supported bridge without the track structure.

Similarly, let $\overline{\overline{\omega}}_{n,es,t}$ be the natural frequency of the elastically supported track-bridge system including shear deformations or rotational inertia effects (i.e. Timoshenko beam theory), and given by the following equation (4.17).

$$\bar{\bar{\omega}}_{n,es,t} = (\bar{\bar{\lambda}}_{n,es,t})^2 \sqrt{\frac{EI}{m_b L^4}} \tag{4.17}$$

The quantity $\bar{\bar{\lambda}}_{n,es,t}$ is the frequency parameter of the n^{th} mode shape of vibration of the elastically supported track-bridge system including shear deformations and rotational inertia effects.

Let $\bar{\bar{R}}$ be the fundamental frequency ratio given by

$$\bar{\bar{R}} = \frac{\bar{\bar{\omega}}_{1,es,t}}{\omega_{1,ss,b}} \tag{4.18}$$

The quantity $\bar{\bar{\omega}}_{1,es,t}$ is the first natural frequency associated with $\bar{\bar{\lambda}}_{n,es,t}$.

The ratio $\bar{R}$ considering the Bernoulli beam theory for the bridge in the track-bridge system and the ratio $\bar{\bar{R}}$ considering the Timoshenko beam theory for the bridge in the track-bridge system are evaluated for different values of the track vertical stiffness ratio, bridge support vertical stiffness ratio and mass ratio. Figure 4.11 shows the $\bar{R}$ contour maps for a small mass ratio of 1.72 and a large mass ratio of 7.22. Figure 4.12 shows the $\bar{\bar{\mathrm{R}}}$ contour maps for the same two mass ratios.

Figures 4.11(a) and 4.12(a) with small mass ratio represent short span bridges while Figures 4.11(b) and 4.12(b) represent longer span bridges. It can be observed that for short span bridges the stiffness of the ballast is significant for simply supported bridges and for bridges with very soft supports. For longer span bridges, the ballast stiffness is only significant in bridges with very soft supports. It is also interesting to note that including the shear deformations and rotational inertia effects in the bridge beam is less significant as the bridge supports become more flexible.

(a)

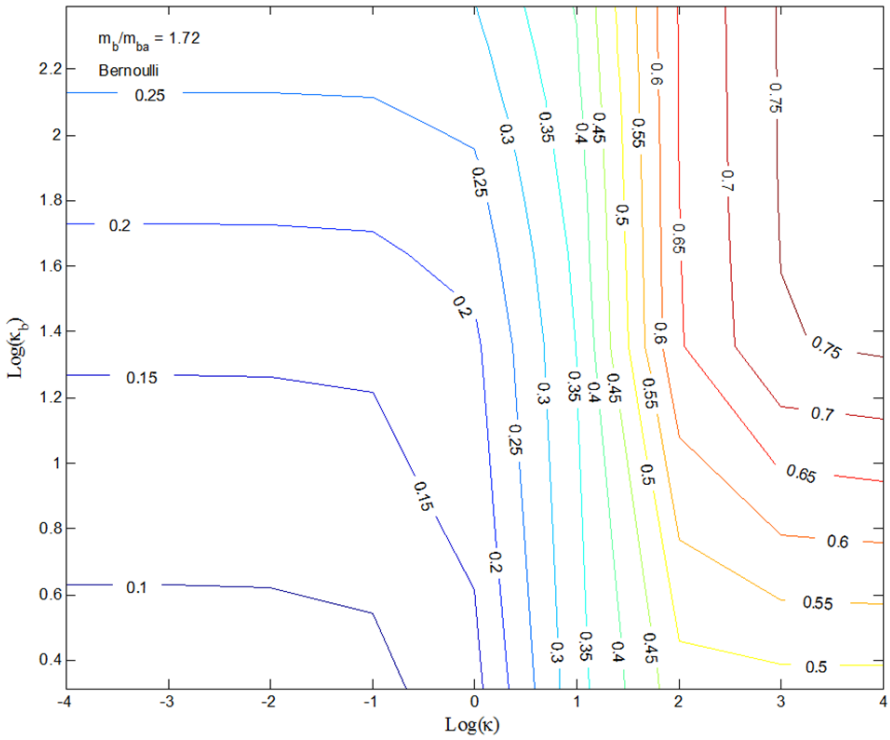

(b)

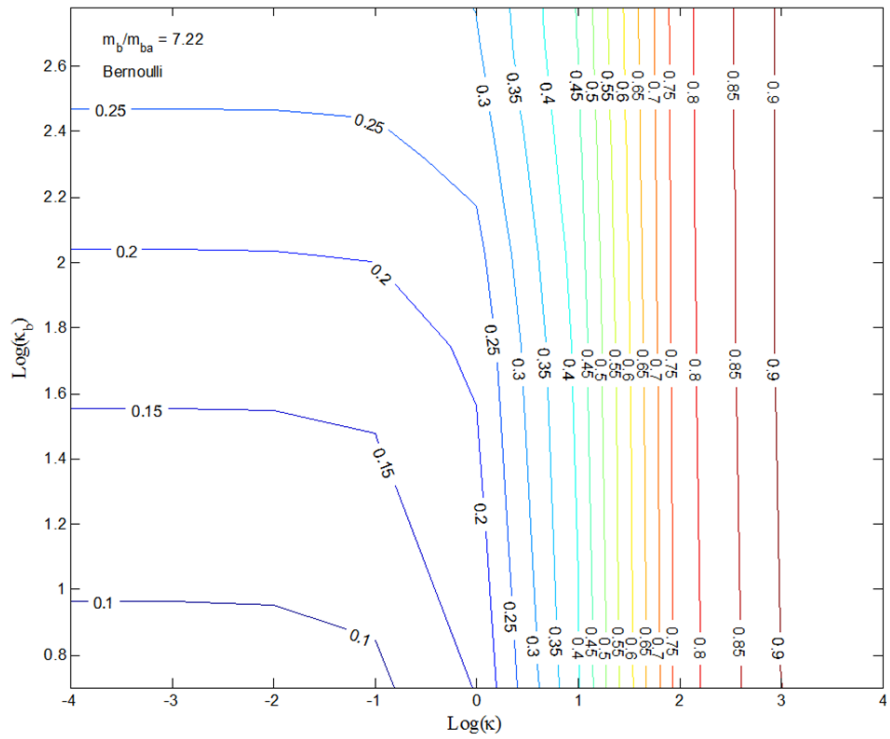

Figure 4.11 Fundamental frequency of elastically supported Bernoulli type of bridge: (a) $\bar{R}$ values for low mass ratio; (b) $\bar{R}$ values for high mass ratio

(a)

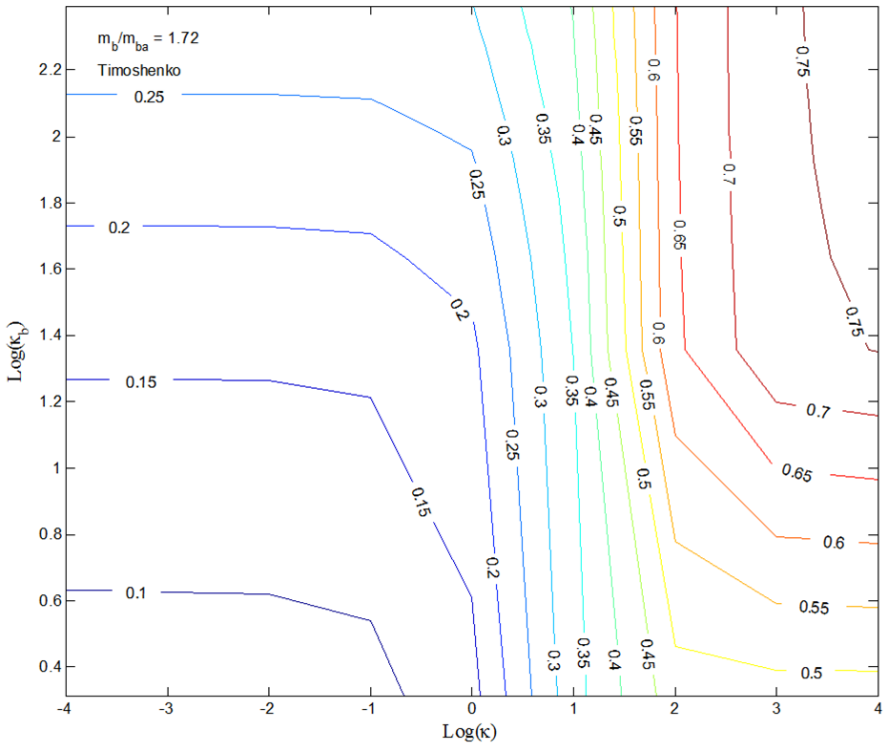

(b)

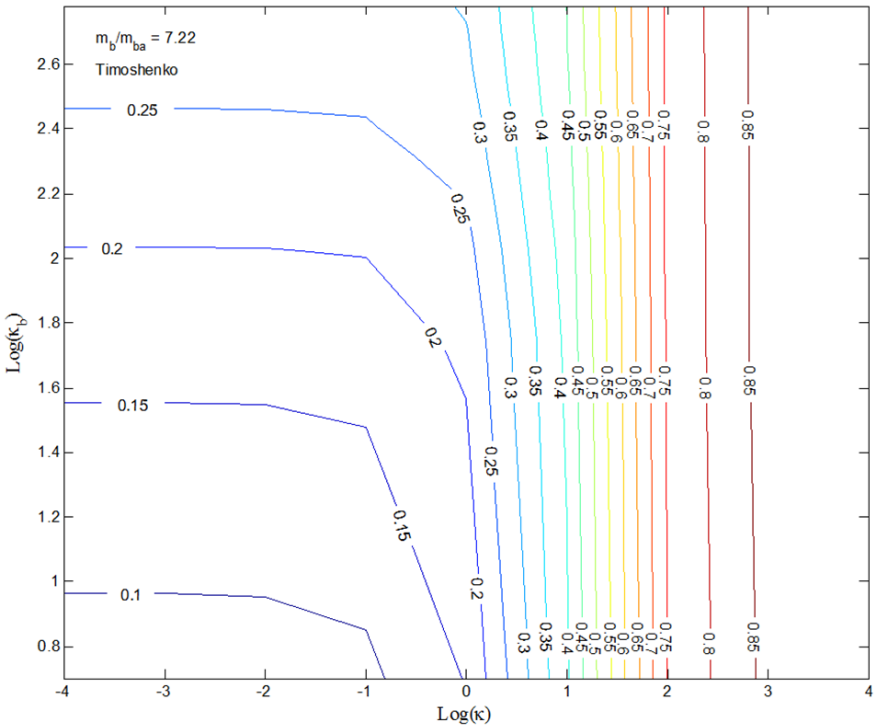

Figure 4.12 Fundamental frequency of elastically supported Timoshenko type of bridge: (a) $\bar{\bar{R}}$ values for low mass ratio; (b) $\bar{\bar{R}}$ values for high mass ratio

4.4 Vibration Mode Shapes of Elastically Supported Bridge

Figures 4.13 through 4.15 show the first three mode shapes of an Elastically Supported (ES) bridge supported by vertical springs having equal stiffness k_v at both ends. It can be seen clearly that the bridge modal characteristics change with the support vertical flexibility. For values of $Log_{10}(\kappa) \geq 4$, mode shapes are the same as in the case of $\kappa \to \infty$ which is the Simply-Supported (SS) bridge condition. The asymptotic limit of the first mode is the mode for a rigid body motion

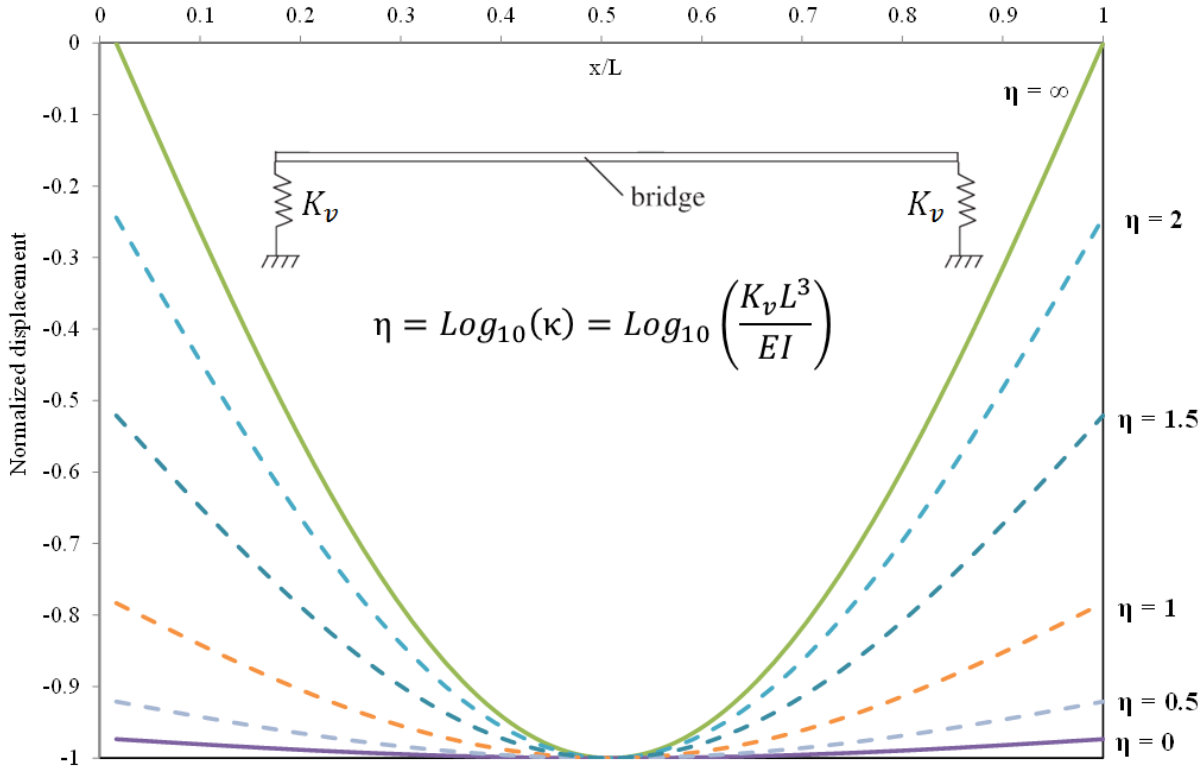

Figure 4.13 Plots of 1st mode shape for different ratios of κ

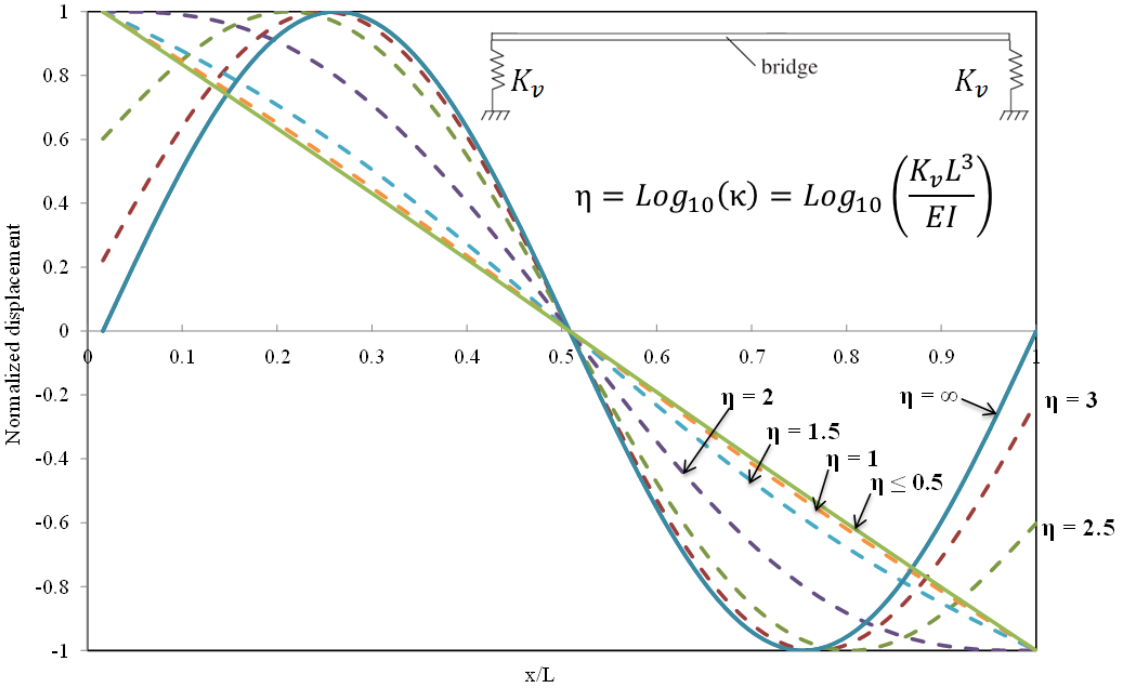

Figure 4.14 Plots of 2nd mode shape for different ratios of κ

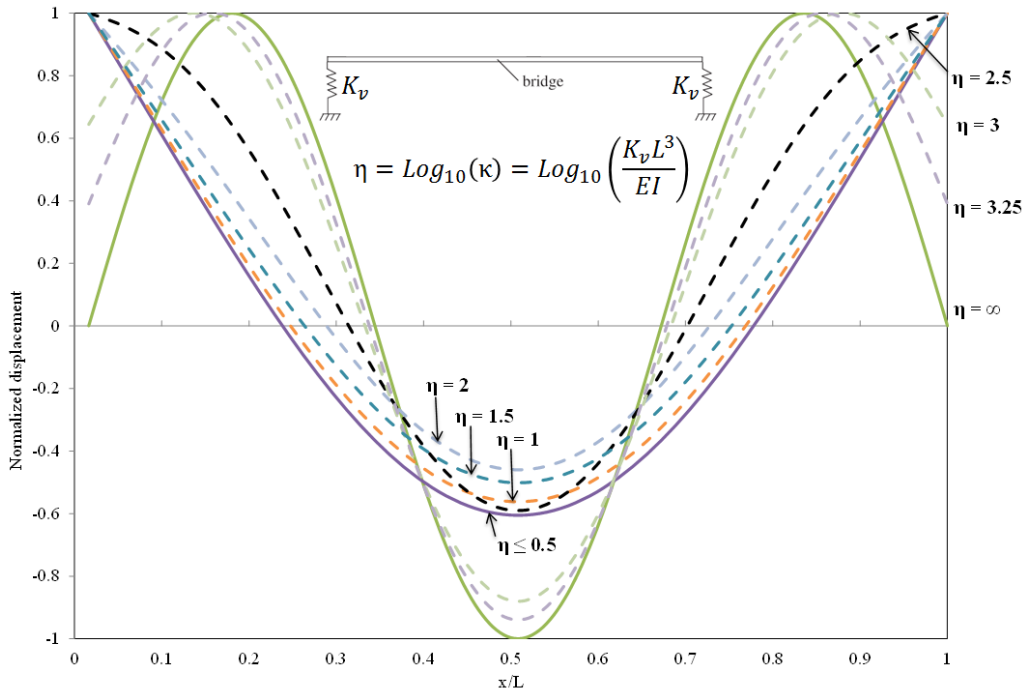

Figure 4.15 Plots of 3rd mode shape for different ratios of κ

4.5 Natural Frequency of Bridge with Vertical and Rotational Springs

In this section, the natural frequency of a bridge with boundary conditions as shown in Figure 4.16 is investigated. It is assumed that the boundary conditions are the same at both ends of the bridge. For the free vibration analysis of this system, the supports' damping is set to zero.

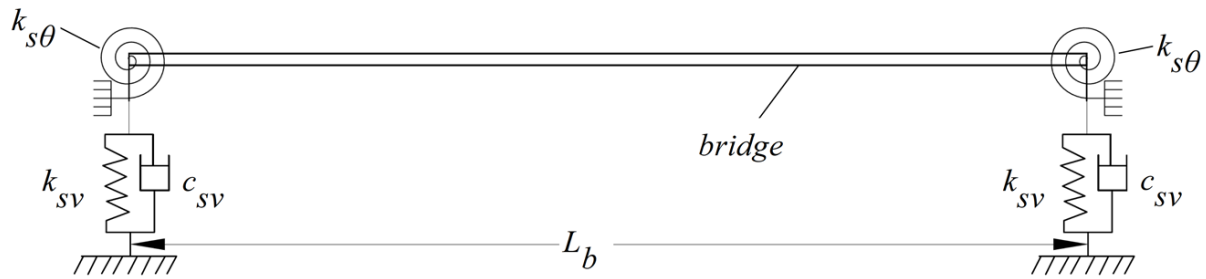

Figure 4.16 Bridge with vertical and rotational spring supports

The ratio η_{sv} of the bridge support's vertical stiffness to bridge flexural stiffness can be expressed as in equation (4.19). The ratio $\eta_{s\theta}$ of the bridge support's rotational stiffness to bridge flexural stiffness can be expressed as in equation (4.20).

$$\eta_{sv} = Log_{10}\left(\frac{k_{sv}L_b^3}{E_b I_b}\right) \tag{4.19}$$

$$\eta_{s\theta} = Log_{10}\left(\frac{k_{s\theta}L_b}{E_b I_b}\right) \tag{4.20}$$

Let $\bar{m} = m_b + m_{ba}$ be the sum of the mass of the bridge itself and the mass of the track structure. Let $\tilde{\omega}$ denote the natural angular frequency of the track-bridge system with vertical and

rotational springs as shown in the above figure. The frequency parameter Ψ of the system can be expressed as given by equation (4.21)

$$\Psi^4 = \widetilde{\omega}^2 \frac{\overline{m} L_b^4}{E_b I_b} \tag{4.21}$$

Let the frequency ratio R_{ω_n} be the ratio of natural frequency of system in Figure 4.16 to the natural frequency of a simply supported bridge with no track structure. The ratio R_{ω_n} can be expressed as given by equation (4.22).

$$R_{\omega_n} = \frac{\widetilde{\omega}}{\omega_{n,ss,b}} = \frac{\Psi}{(\lambda_{n,ss,b})^2} \tag{4.22}$$

The frequency equation of a bridge with the boundary conditions as shown in Figure 4.16 is synthesized in this dissertation and can be expressed in a compact format as shown in the following equation (4.23).

$$\begin{aligned}(100^{\eta_{sv}+\eta_{s\theta}} - 3 * 2^{1+\eta_{sv}+\eta_{s\theta}} * 5^{\eta_{sv}+\eta_{s\theta}} * \Psi^4 + \Psi^8) Cos\Psi Sin\Psi \\ + 2\Psi(10^{\eta_{sv}} + 10^{\eta_{s\theta}}\Psi^2)(-10^{\eta_{sv}+\eta_{s\theta}} + \Psi^4) Sin\Psi Cos\Psi \\ + 2\Psi(-10^{\eta_{sv}} + 10^{\eta_{s\theta}}\Psi^2)(-10^{\eta_{sv}+\eta_{s\theta}} + \Psi^4) Cos\Psi Sinh\Psi \\ + 2\Psi^2(-10^{\eta_{sv}} + 10^{\eta_{s\theta}}\Psi^2)(10^{\eta_{sv}} + 10^{\eta_{s\theta}}\Psi^2) Sin\Psi Sinh\Psi \\ - (10^{\eta_{sv}+\eta_{s\theta}} + \Psi^4)^2 = 0\end{aligned} \tag{4.23}$$

The solutions of the above frequency equation (4.23) are the frequency parameters Ψ and could not be solved analytically. The fundamental frequency is rather obtained numerically. The fundamental frequency ratio R_{ω_1} of the first natural frequency of the system is shown in Figure 4.17 for values of η_{sv} and $\eta_{s\theta}$ as indicated. It can be observed that the solutions of the frequency

parameter provide all possible conditions of the boundary conditions. The simply supported case is a special case with values $\eta_{sv} \geq 3$ and $\eta_{s\theta} \leq -3$ as indicated by "Hinge-Hinge" in Figure 4.17. The "clamped-clamped" is another special case with fully fixed boundary conditions. The parameter η_{sv} plays a relatively more important role that the parameter $\eta_{s\theta}$ in that the effects of the rotational stiffness at the supports becomes less significant as the bridge's vertical supports become more flexible. This means that, for modeling purposes, the bridge supports' rotational restraint can only be advantageous for relatively stiff vertical supports.

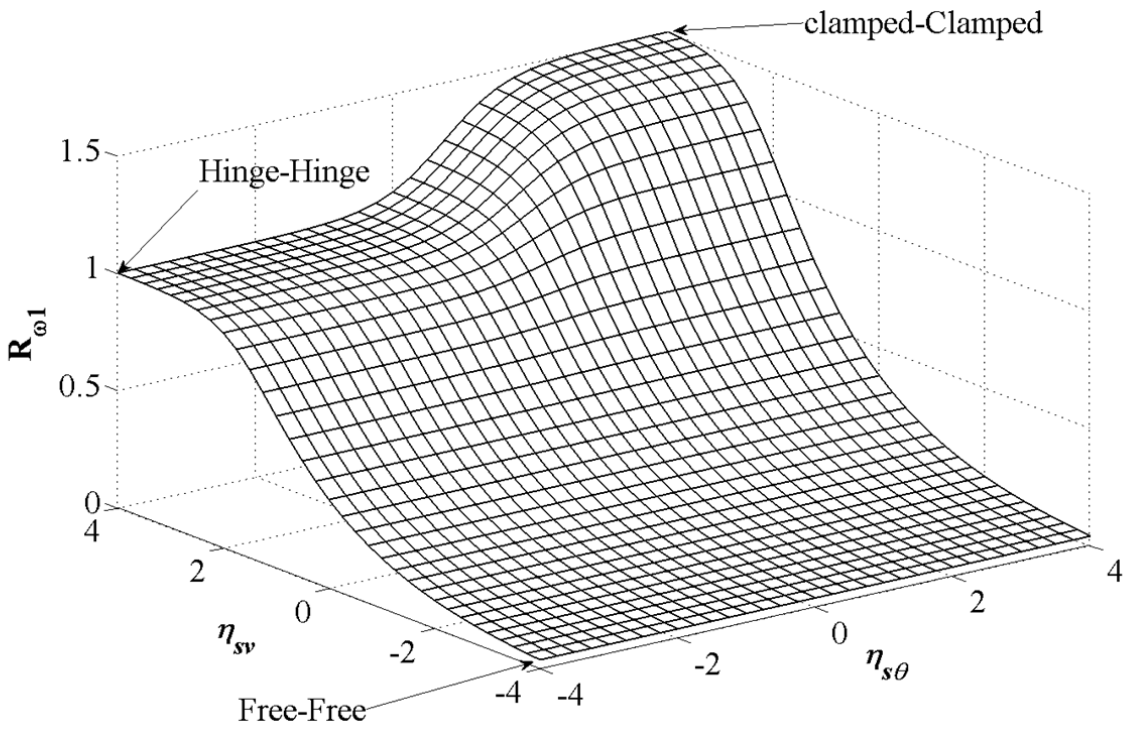

Figure 4.17 Frequency ratio R_{ω_1} for bridge with vertical and rotational spring supports

4.6 Concluding Remarks

As discussed in the introductory section of this chapter, the natural frequency of the structure is an important value used in many of the serviceability requirement checks related to short span high speed rail bridges. Based on the analyses performed in this chapter, the following concluding remarks can be made regarding the effects of each of the investigated parameter on the bridge natural frequencies:

- Shear deformations and rotational inertia effects. Natural frequencies of bending decrease when these effects are considered.
- Ratio of bridge mass to ballast mass. The shorter the bridge the more significant is the ballast mass in altering the natural frequency of the bridge. The natural frequency decreases with the additional mass of the ballast. For longer span bridges, the additional mass has no significant impact.
- Vertical stiffness of the bridge supports. The ratio of the support vertical stiffness to bridge flexural stiffness is an important parameter that determines the flexibility of the boundary conditions. The shorter the bridge the more significant is the effect of this parameter. The natural frequency of the bridge is reduced with a decrease of this parameter.
- Rotational stiffness of the bridge supports. Supports' rotational restraint increases the natural frequency. However, this effect is insignificant for soft vertical supports.
- The ballast vertical stiffness. For short span bridges with rigid supports, this parameter has minimal effects. However, for softer support bridges, the effects are more significant in further reducing the natural frequencies.
- Simply supported bare Bernoulli beam always provides an upper bound of frequency.

CHAPTER 5

NUMERICAL STUDIES OF SHORT SPAN HIGH SPEED RAIL BRIDGES

5.1. Dynamic Simulation Methodology

In this chapter of the dissertation, the numerical model and solution algorithms developed in Chapter 3 are used to investigate the dynamic behavior of short span high speed rail bridges. A finite element program is coded for this purpose using a combination of standard Excel® spreadsheet and Matlab® software. The spatial discretization of the track-bridge system is laid out in the first row of a worksheet in an excel workbook using finite beam elements of lengths equal or smaller than the spacing of the sleepers. The time steps are input in the first column of the same worksheet. The intersection cells of the rows and columns are activated or de-activated depending on the presence or absence of the train wheels on the interaction element. Matrices and other important system data are programmed in separate worksheets. An Excel® add-on for Matlab® is used to handle the complex matrix computations, particularly the inverse of large equivalent stiffness matrix. The vehicle equations of motion are solved using finite difference schemes of the numerical integration methods and the equations of the track-bridge subsystem are solved using the HHT alpha direct time integration methods. The focus in the bridge dynamic response is directed towards three general aspects of interest that are relevant to the behavior of short span bridges as explained below.

In the first part of the dynamic simulations, an examination is made regarding the effects of shear deformations and rotational inertia in the responses of simply supported bridges. The Timoshenko shear correction factor k_s and the bridge slenderness s are two parameters that are used to evaluate the influence of shear deformations and rotational inertia on dynamic behavior of short span high speed rail bridges. The shear correction factor is varied between the values of 0.233 and 0.833. The slenderness s is a non-dimensional parameter given by

$$s = L_b \sqrt{\frac{A_b}{I_b}} \tag{5.1}$$

In this equation, L_b is the bridge span, I_b is the bridge moment of inertia and A_b is the cross-sectional area. A total of 12 bridge models are investigated in this part of the chapter to gain a better understanding of the effects of the shear correction factor and the slenderness on dynamic responses of short span high speed rail bridges.

In the second part of the dynamic simulations, the bridges are assumed to be simply supported. The effects of the vehicle interaction and track elastic properties are investigated. A total of 4 different cases are examined. The first case ignores both the interaction and the track (i.e. No interaction + no track) which is equivalent to the basic moving force model on a single span simply supported bare beam. The second case considers the vehicle interaction with the track ignored (i.e. Interaction + no track). This case is the same as the vehicle-bridge interaction model on a single span simply supported bare beam. The third case ignores the vehicle interaction but considers the track structure (i.e. No interaction + track). The forth case includes both the vehicle interaction and the track structure (i.e. Interaction + track). The maximum vertical accelerations at mid-span of the bridges are examined. Also, in this part of the study: conditions that create resonance are examined; the effects of the track vertical stiffness are

investigated; the impact of the types of trainset on bridge and vehicle responses is evaluated; and the effects of the track irregularities are examined.

In the third part of the dynamic simulations, the effects of the bridge boundary conditions are investigated in-depth. The viscoelastic elements characterizing the flexibility of the bridge supports are chosen as linear spring-dampers representing the effective vertical stiffness and damping provided by the elastomeric bearings and/or soil foundation. Additionally, rotational springs are used at the ends of the bridge to account for any restraint against rotation at the supports. For the dynamic simulations, non-dimensional parameters are chosen to study the effects of the boundary conditions. The logarithmic expression of the ratio of support vertical stiffness to bridge flexural stiffness is given by

$$\eta_{sv} = Log_{10}\left(\frac{k_{sv}L_b^3}{E_b I_b}\right) \tag{5.2}$$

The logarithmic expression of the ratio of bridge support rotational stiffness to bridge rotational stiffness is given by

$$\eta_{s\theta} = Log_{10}\left(\frac{k_{s\theta}L_b}{E_b I_b}\right) \tag{5.3}$$

A parametric study is carried out in this part of the research within a range of values for η_{sv} and $\eta_{s\theta}$ given by

$$1.5 \leq \eta_{sv} \leq 3 \tag{5.4}$$

$$-3 \leq \eta_{s\theta} \leq 3 \tag{5.5}$$

For simply supported bridges, these parameters are such that $\eta_{sv} \to \infty$ and $\eta_{s\theta} = -3$.

The damping constant c_{sv} provided by the support structural elements and potentially additional external devices such as fluid viscous dampers can be related to the bridge's critical damping by the damping ratio defined as

$$\zeta_d = \frac{c_{sv}}{c_{cr}} \tag{5.6}$$

The dynamic simulations are carried out for different values of the damping constant between $c_{sv} = 0$ and $c_{sv} = 6.3$ MN-s/in (36000 Ib_f-s/in) with some combinations of stiffness ratios given by equations (5.4) and (5.5). Result discussions are provided in sections 5.3 through 5.9.

5.2. Description of Study Cases

In this section the properties of the bridge models, track structure and train rolling stock are described.

5.2.1 Bridge models

In this chapter, two groups of bridge models are evaluated, namely Group A and Group B bridge models. The properties of Group A bridge models are shown in Table XVII.

TABLE XVII PROPERTIES OF LOW MASS SHORT SPAN RAILWAY BRIDGES

Group A: Open deck steel plate girder bridges designed per AREMA [(1) (2)]								
Bridge ID	Bridge Span L_b		Moment of Inertia I_b		Cross-Section Area A_b		Bridge Mass m_b	
	(m)	(in)	(m^4)	(in^4)	(m^2)	(in^2)	(kg/m)	($Ib_f\ s^2/in^2$)
A7	4	157.5	0.00103	2451	0.00645	10	450.0	0.065
A8	8	315.0	0.00638	15337	0.02258	35	671.5	0.097
A9	12	472.4	0.01650	39631	0.04645	72	823.8	0.119
A10	16	629.9	0.03130	75198	0.07742	120	969.2	0.14
A11	20	787.4	0.05756	138287	0.12903	200	1094	0.158
A12	30	1181.1	0.18348	440809	0.25807	400	1509	0.218

[(1)]Poisson ratio of 0.2 and Modulus of elasticity of 29,000,000 psi (2 x 10^8 kN/m^2) are assumed
[(2)]Bridge plate-girder dimensioned per AREMA Chapter 15 to carry for E-Cooper 80 live load

Group A is a set of 6 bridge models representing short span steel open-deck railway bridges. Typically, they have a relatively low mass compared to concrete bridges and usually not used for high speed lines. In this study however, these light weight bridges are included for evaluation and comparison with heavier concrete bridges. They are supported by twin steel plate-girders dimensioned according to AREMA Chapter 15 provisions and designed to carry a slower moving train of the E-cooper 80 type.

Group B bridge models are based on the work performed by the ERRI D214 committee which has carried out simulations on a set of simply supported short span high speed rail bridge models, typically identified as the catalogue of benchmark bridges. Table XVIII shows the physical and mechanical properties of 6 of those bridge models. The bridges are assumed to be reinforced concrete. It is also assumed that the bridges are single span, homogenous and with no skew at the abutments. The 6 bridge models are identified as B1 through B6 in the rest of this dissertation.

TABLE XVIII PROPERTIES OF MODIFIED ERRI D214 BRIDGE PROTOTYPES

Bridge ID	Bridge Span L_b		Moment of Inertia I_b		Cross-Section Area A_b[(2)]		Bridge Mass m_b	
	(m)	(in)	(m^4)	(in^4)	(m^2)	(in^2)	(kg/m)	($Ib_f\ s^2/in^2$)
B1	5	196.85	0.014	33166	2.323	3600	7000	1.015
B2	10	393.7	0.079	189523	2.839	4400	10000	1.450
B3	15	590.6	0.234	562182	3.226	5000	15000	2.176
B4	20	787.4	0.631	1516180	3.871	6000	20000	2.901
B5	30	1181.1	2.246	5396951	5.032	7800	25000	3.626
B6	40	1574.8	8.520	20468432	8.710	13500	30000	4.351

(1) Poisson ratio of 0.3 and Modulus of elasticity of 4768962 psi (3.29 x 10^7 kN/m^2)
(2) Assumed cross-sectional area

The first natural frequency of bending n_0, the slenderness ratio s, the damping ratio ζ and the critical damping C_{cr} for both group A and group B bridges are shown in Table XIX.

TABLE XIX FREQUENCY, SLENDERNESS AND DAMPING OF BRIDGE MODELS

Bridge ID	First Frequency n_0 (Hz)	Slenderness ratio, s	Damping ratio ζ (%)	Critical damping, C_{cr} kN-s/m	Critical damping, C_{cr} Ib_f-s/in
A7	66	10	2.50	1492	8520
A8	34	15	2.00	2280	13018
A9	22	20	1.50	2706	15452
A10	16	25	1.00	3032	17315
A11	13	30	0.50	3495	19955
A12	9	36	0.50	4886	27901
B1	16	65	2.55	7036	40176
B2	8	60	2.20	10051	57395
B3	5	56	1.85	14137	80726
B4	4	50	1.50	20106	114806
B5	3	45	1.50	28275	161457
B6	3	40	1.50	45239	258319

The equations for the upper limit of the first natural frequency of bending n_0 (Hz) is given by

$$\begin{aligned} n_0 &= 94.76 L_b^{-0.748} \quad (L_b \text{ in m}) \\ n_0 &= 230.45 L_b^{-0.748} \quad (L_b \text{ in ft}) \end{aligned} \tag{5.7}$$

The equations for the lower limit of the first natural frequency of bending n_0 (Hz) is given by

$$\begin{aligned} n_0 &= 80/L_b \quad 4 \text{ m} \le L_b \le 20 \text{ m} \\ n_0 &= 262.47/L_b \quad 13.12 \text{ ft} \le L_b \le 65.12 \text{ ft} \end{aligned} \tag{5.8}$$

The first natural frequency of group A and B bridges along with the frequency's upper and lower limits of equations (5.7) and (5.8) are shown in the left graphs of Figures 5.1 and 5.2 respectively.

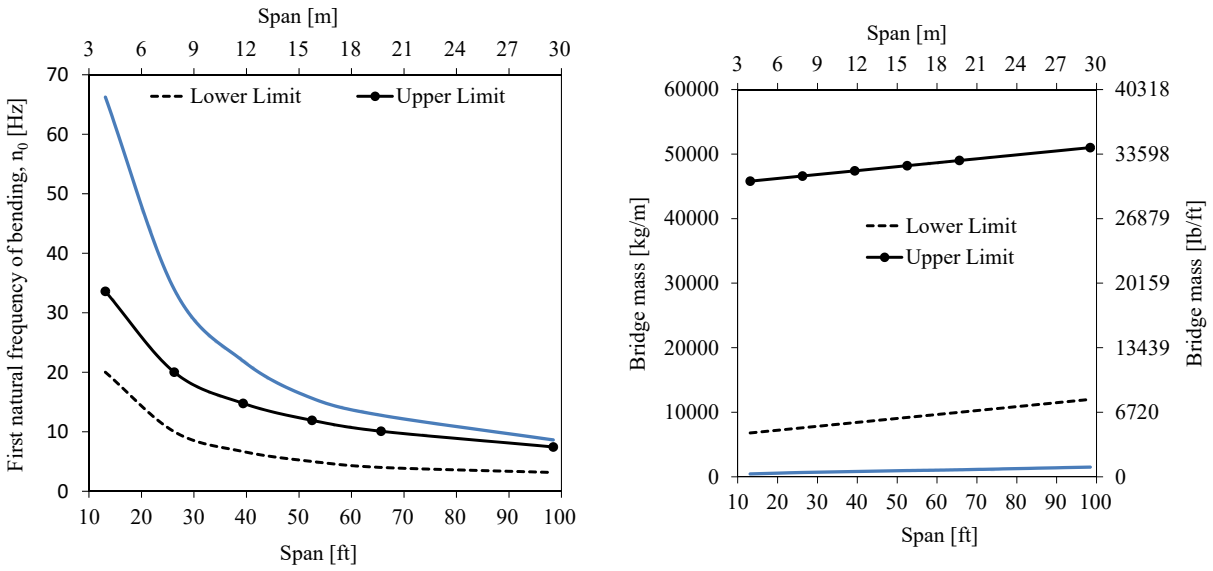

Fig.5.1 Frequency (left) and mass (right) versus span length of group A bridges

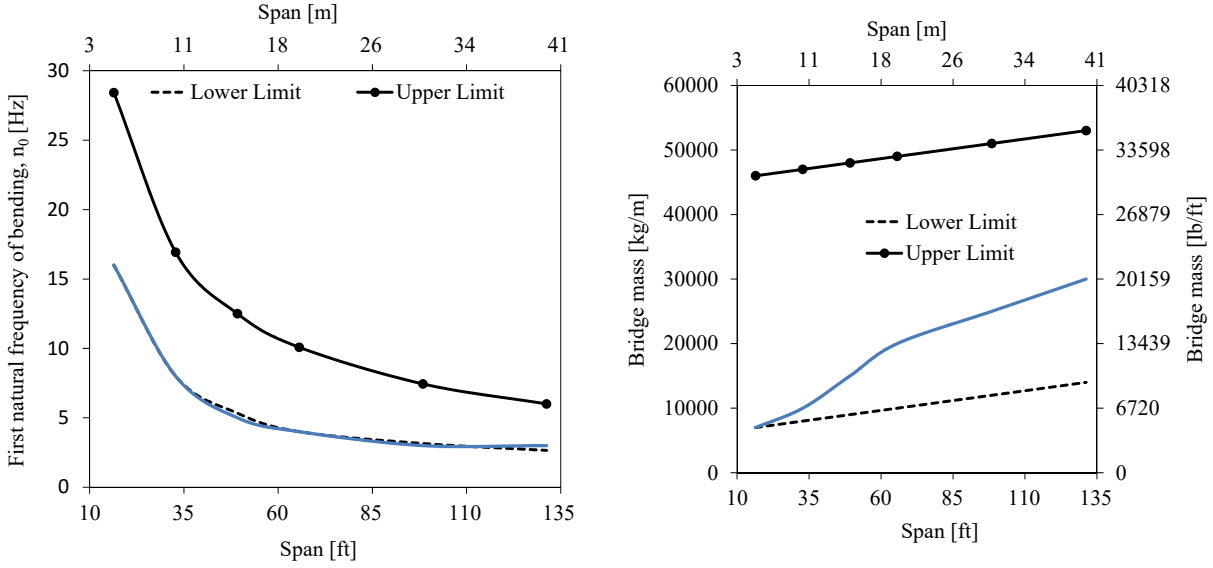

Fig.5.2 Frequency (left) and mass (right) versus span length of group B bridges

Based on the assumption that the bridge flexural stiffness is unchanged, the lower limit of the bridge mass in kg/m (Ib_m/ft) that would guarantee that the first natural frequency of bending would fall within the prescribed range can be computed and written as

$$\begin{aligned} m_b &= (6000L_b + 200L_b^2)/L_b \quad \text{(kg/m)} \\ m_b &= (4031.8L_b + 40.96L_b^2)/L_b \quad (\text{Ib}_m/\text{ft}) \end{aligned} \tag{5.9}$$

Similarly, the upper limit of the bridge mass in kg/m (Ib_m/ft) that would guarantee that the first natural frequency of bending would fall within the prescribed range can be computed and written as

$$\begin{aligned} m_b &= (45000L_b + 200L_b^2)/L_b \quad \text{(kg/m)} \\ m_b &= (30239L_b + 40.96L_b^2)/L_b \quad (\text{Ib}_m/\text{ft}) \end{aligned} \tag{5.10}$$

The mass of group A and B bridges along with the mass upper and lower limits of equations (5.9) and (5.10) are shown in the right graphs of Figures 5.1 and 5.2 respectively.

5.2.2 Track structure

The track model is considered to be a ballasted track. The rails are assumed to be an infinite long beam using AREMA RE141 rail profile. Concrete sleepers with 0.685m (2.25ft) spacing are used with their mass added to the mass of rails. Vertical linear spring and dampers connecting the rails and the bridge deck represent the elastic properties of the track components which include the rail pads and ballast material. The track parameters are assumed to remain constant along the track. The properties of the track in this study are shown in Table XX. The Poisson's ratio of the rails is assumed to be 0.3. The track represents the upper beam in the numerical model described in Chapter 3 of this dissertation. Therefore, the mass of the sleepers (crossties) are combined with the mass of the rails and smeared over the spacing of the sleepers (crossties). The mass of the ballast is included in the mass of the bridge.

TABLE XX PROPERTIES OF THE AREMA RE141 RAIL AND TRACK MODEL

Item Description	Item Notation	Values			
		Metric units		English units	
Young's modulus of rail[a]	E_r	210	GPa	30458041	Ib_f/in^2
Per unit length mass of rail[b]	m_r	299.5	kg/m	0.05691	$Ib_f\text{-}s^2/in/in$
Sectional area of rail	A_r	0.007686	m^2	11.91	in^2
Moment of inertia of rail	I_r	3.05×10^{-5}	m^4	73.4	in^4
Vertical stiffness of track	k_{bv}	240000	kN/m/m	34809	$Ib_f/in/in$
Vertical damping of track	c_{bv}	58.8	kN-s/m/m	8.5	$Ib_f\text{-}s/in/in$

[a] with a Poisson ratio of $\nu_r = 0.3$
[b] Including the mass of the sleeper.

5.2.3 Real high speed train models

The chosen train models in this research are 6 high speed trainsets with a convoy of 8-car configuration and distributed power among bogies as shown in Fig. 5.3.

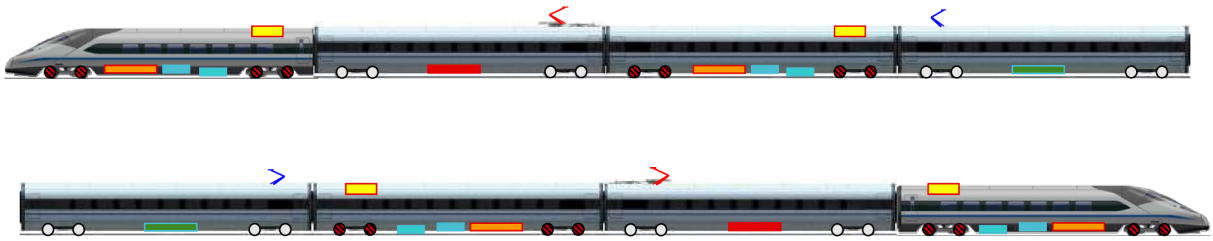

Figure 5.3 Typical high speed trains with 8-car convoy configuration

The 6 trainsets are the Bombardier Zefiro 380 with a maximum speed of 380 km/h (236 mph); the Chinese CRH380A train with a maximum speed of 380 km/h (236 mph); the Japanese series N700-I train intended for international markets with a cruising speed of 330 km/h (205 mph); the second generation of German Inter-City Express 2 (ICE-2) with a maximum speed of 280 km/h (174 mph); the third generation of German Inter-City Express 3 (ICE-3) with a maximum service speed of 320 km/h (199 mph) and design speed of 330 km/h (205 mph); and the American Amtrak Acela train with a maximum operating speed of 240 km/h (150 mph).

The trains are typical Electric Multiple Unit (EMU) composed of self-propelling cars with traction motorized bogies are distributed along the trainset. Table XXI shows distribution of Motorized and Trailer car coaches for the 6 different types of trains. The letter “M” means that the two bogies of the car have motors and the letter “T” means the car is a trailer car type with no

motorized bogies. With the symmetric distribution of power, the trains can move in either direction. The German ICE-2 and the American Amtrak Acela trains have one powered car at each end and the remainder coaches are trailer cars. The German ICE-3 and Bombardier Zefiro 380 trains have 4 powered cars positioned at the first, third, sixth and eight positions in the convoy. The Chinese CRH380A train has all its intermediate six cars powered. All 8 cars of the Japanese Series N700-I are powered.

TABLE XXI HIGH SPEED TRAINS DISTRIBUTED TRACTION CONFIGURATION

Car Number	Bombardier Zefiro 380	Chinese CRH380A	Japanese Series N700-I	German ICE-2	German ICE-3	Amtrak Acela Express
1	M	T	M	M	M	M
2	T	M	M	T	T	T
3	M	M	M	T	M	T
4	T	M	M	T	T	T
5	T	M	M	T	T	T
6	M	M	M	T	M	T
7	T	M	M	T	T	T
8	M	T	M	M	M	M

Note: M stands for Motorized coach and T for Trailer coach. Trailer coaches are not powered.

The physical and mechanical properties of the powered car and trailer car of each trainset are shown in Tables XXII and XXIII. Note that some trains have different properties of the powered and trailer cars while other trainset have the same properties.

TABLE XXII PROPERTIES OF HIGH SPEED TRAIN MOTORIZED COACHES

Parameter	Unit	Bombardier Zefiro 380	Chinese CRH380A	Japanese Series N700-I	German ICE-2	German ICE-3	Amtrak Acela Express
M_c	kg	49000	47476	32276	60768	49595	56250
	Ib_f-s^2/in	279.8	274.1	184.3	347	283.2	321.2
J_c	kg-m^2	2698656	2711622	2485653	1344000	2372669	1970000
	Ib_f-s^2-in	2.4 x 10^7	2.4 x 10^7	2.2 x 10^7	1.2 x 10^7	2.1 x 10^7	1.7 x 10^7
M_t	kg	5900	3200	3170	5600	4400	11923
	Ib_f-s^2/in	33.69	18.27	18.1	31.98	25.12	68.08
J_t	kg-m^2	8066	7200	3930	21840	5420	1476
	Ib_f-s^2-in	71390	63726	34784	193301	47971	13064
M_w	kg	1800	2400	1720	2000	2400	2662
	Ib_f-s^2/in	10.28	13.70	9.8	11.4	13.7	15.2
k_p	kN/m	2340	2080	2400	4800	1124	5200
	Ib_f/in	13362	11877	13704	27409	6418	29693
c_p	kN-s/m	21	60	80	108	8.76	100
	Ib_f-s/in	120	343	457	617	50	571
k_s	kN/m	886	800	600	1760	561	3000
	Ib_f/in	5059	4568	3426	10050	3203	17130
c_s	kN-s/m	63.75	90	100	152	27	400
	Ib_f-s/in	364	514	571	868	154	2284
L_c	m	8.7	8.75	8.75	5.75	8.688	5.372
	in	342.520	344.488	344.488	226.378	342.028	211.496
L_t	m	1.35	1.25	1.25	1.5	1.25	1.423
	in	53.150	49.213	49.213	59.055	49.213	56.004
Axle Load	kN	166.770	156.9	111.8	196.1	166.7	222.4
	Ib_f	37479	35273	25133	44082	37478	50000

TABLE XXIII PROPERTIES OF HIGH SPEED TRAIN TRAILER COACHES

Parameter	Unit	Bombardier Zefiro 380	Chinese CRH380A	Japanese Series N700-I	German ICE-2	German ICE-3	Amtrak Acela Express
M_c	kg	53200	44009	32276	33922	49000	46723
	lb_f-s^2/in	303.8	251.3	184.3	193.7	279.8	266.8
J_c	kg-m^2	2576400	2711622	2485653	2115000	2598637	1970000
	lb_f-s^2-in	2.3 x 10^7	2.4 x 10^7	2.2 x 10^7	1.9 x 10^7	2.3 x 10^7	1.7 x 10^7
M_t	kg	3800	2400	3240	2373	2700	5352
	lb_f-s^2/in	21.7	13.7	18.5	13.55	15.42	30.56
J_t	kg-m^2	3470	2200	3930	1832	3330	1476
	lb_f-s^2-in	30712	19472	34784	16215	29473	13064
M_w	kg	1800	2400	1720	1734	2400	1856
	lb_f-s^2/in	10.28	13.7	9.8	9.9	13.7	10.6
k_p	kN/m	550	1400	2400	1600	690	5200
	lb_f/in	3141	7994	13704	9136	3940	29693
c_p	kN-s/m	12	80	80	20	5.4	100
	lb_f-s/in	68.5	457	457	114	31	571
k_s	kN/m	400	600	600	300	603	3000
	lb_f/in	2284	3426	3426	1713	3443	17130
c_s	kN-s/m	80	80	80	6	29	400
	lb_f-s/in	457	457	571	34	166	2284
L_c	m	8.7	8.75	8.75	9.5	8.688	9.068
	in	342.520	344.488	344.488	374.015	342.028	357.008
L_t	m	1.35	1.25	1.25	1.5	1.25	1.5
	in	53.150	49.213	49.213	59.055	49.213	59.055
Axle Load	kN	166.770	143.2	111.8	111.8	156.9	159
	lb_f	37479	32185	25133	25133	35273	35750

The 8-car convoy configuration trainset have 16 bogies with 2 wheelsets per bogie for a total of 32 wheelsets. Considering the front wheelset as the reference wheelset, the distance of each subsequent wheelset from the front wheelset is shown in Tables XXIV and XXV for the imperial in inches and metric units in meters respectively.

TABLE XXIV AXLE DISTANCE FROM THE FRONT AXLE (INCHES)

Wheelset Coordinate	Bombardier Zefiro 380	Chinese CRH380A	Japanese Series N700-I	German ICE-2	German ICE-3	Amtrak Acela Express
1	0	0	0	0	0	0
2	106	98	98	118	98	112
3	685	689	689	451	684	423
4	791	787	787	569	782	535
5	1047	984	984	760	975	791
6	1154	1083	1083	859	1074	909
7	1732	1673	1673	1508	1659	1505
8	1839	1772	1772	1607	1758	1623
9	2094	1969	1969	1800	1951	1834
10	2201	2067	2067	1898	2049	1952
11	2780	2657	2657	2548	2635	2548
12	2886	2756	2756	2646	2733	2666
13	3142	2953	2953	2839	2926	2877
14	3248	3051	3051	2937	3025	2996
15	3827	3642	3642	3587	3610	3591
16	3933	3740	3740	3685	3709	3710
17	4189	3937	3937	3878	3902	3921
18	4295	4035	4035	3977	4000	4039
19	4874	4626	4626	4626	4586	4635
20	4980	4724	4724	4725	4684	4753
21	5236	4921	4921	4918	4877	4964
22	5343	5020	5020	5016	4975	5082
23	5921	5610	5610	5666	5561	5678
24	6028	5709	5709	5764	5659	5796
25	6283	5906	5906	5957	5852	6007
26	6390	6004	6004	6056	5951	6125
27	6969	6594	6594	6705	6536	6721
28	7075	6693	6693	6804	6635	6839
29	7331	6890	6890	6994	6828	7095
30	7437	6988	6988	7113	6926	7207
31	8016	7579	7579	7446	7512	7518
32	8122	7677	7677	7564	7610	7630

TABLE XXV AXLE DISTANCE FROM THE FRONT AXLE (METERS)

Wheelset Coordinate	Bombardier Zefiro 380	Chinese CRH380A	Japanese Series N700-I	German ICE-2	German ICE-3	Amtrak Acela Express
1	0.0	0.0	0.0	0.0	0.0	0.0
2	2.7	2.5	2.5	3.0	2.5	2.8
3	17.4	17.5	17.5	11.5	17.4	10.7
4	20.1	20.0	20.0	14.5	19.9	13.6
5	26.6	25.0	25.0	19.3	24.8	20.1
6	29.3	27.5	27.5	21.8	27.3	23.1
7	44.0	42.5	42.5	38.3	42.2	38.2
8	46.7	45.0	45.0	40.8	44.7	41.2
9	53.2	50.0	50.0	45.7	49.6	46.6
10	55.9	52.5	52.5	48.2	52.1	49.6
11	70.6	67.5	67.5	64.7	66.9	64.7
12	73.3	70.0	70.0	67.2	69.4	67.7
13	79.8	75.0	75.0	72.1	74.3	73.1
14	82.5	77.5	77.5	74.6	76.8	76.1
15	97.2	92.5	92.5	91.1	91.7	91.2
16	99.9	95.0	95.0	93.6	94.2	94.2
17	106.4	100.0	100.0	98.5	99.1	99.6
18	109.1	102.5	102.5	101.0	101.6	102.6
19	123.8	117.5	117.5	117.5	116.5	117.7
20	126.5	120.0	120.0	120.0	119.0	120.7
21	133.0	125.0	125.0	124.9	123.9	126.1
22	135.7	127.5	127.5	127.4	126.4	129.1
23	150.4	142.5	142.5	143.9	141.3	144.2
24	153.1	145.0	145.0	146.4	143.8	147.2
25	159.6	150.0	150.0	151.3	148.7	152.6
26	162.3	152.5	152.5	153.8	151.2	155.6
27	177.0	167.5	167.5	170.3	166.0	170.7
28	179.7	170.0	170.0	172.8	168.5	173.7
29	186.2	175.0	175.0	177.7	173.4	180.2
30	188.9	177.5	177.5	180.7	175.9	183.1
31	203.6	192.5	192.5	189.1	190.8	191.0
32	206.3	195.0	195.0	192.1	193.3	193.8

5.3. Effects of Shear Deformations and Rotational Inertia on Bridge Response

Generally, shear deformations and rotatory inertia may be neglected in many dynamic simulations where simply supported bridge modeled according to Euler-Bernoulli theory is enough. However, in many other situations, relying on such simplification may lead to erroneous results. This is the case for bridges with small slenderness ratio and high frequencies. The impact of shear deformations and rotatory inertia may be evaluated using the Timoshenko beam theory, known as the first-order shear deformation. Formulations based on the finite element are dependent on interpolation functions for the transverse deflection and rotation.

Figure 5.4 shows 6 graphs for the mid-span deflections of bridges A7 through A12 and 6 graphs for the mid-span deflections of bridges B1 through B6. The Timoshenko shear correction factor is taken as $k_s = 0.233$ and the slenderness ratio is varied from $s = 10$ to 65. It can be seen that the effects of shear deformations and rotatory inertia become less significant as the slenderness ratio increases. In terms of deflection magnitude, the shear deformations and rotatory inertia may be neglected for slenderness ratio s greater than 40. It can also be observed that their effects on deflections do not depend on train speed except at very high speed for very short light weight bridges. Figure 5.5 shows 6 graphs for the mid-span vertical accelerations of bridges A7 through A12 and 6 graphs for the mid-span vertical accelerations of bridges B1 through B6. Similarly, it can be observed that the effects of shear deformations and rotatory inertia become less significant as the slenderness ratio increases. In addition, the graphs show that for higher train speeds the effects of shear deformations and rotatory inertia are more significant in the low range of slenderness ratio s. The peaks corresponding to resonance speeds are shifted slightly to the left because the Timoshenko beam theory reduces the fundamental frequency of the bridge.

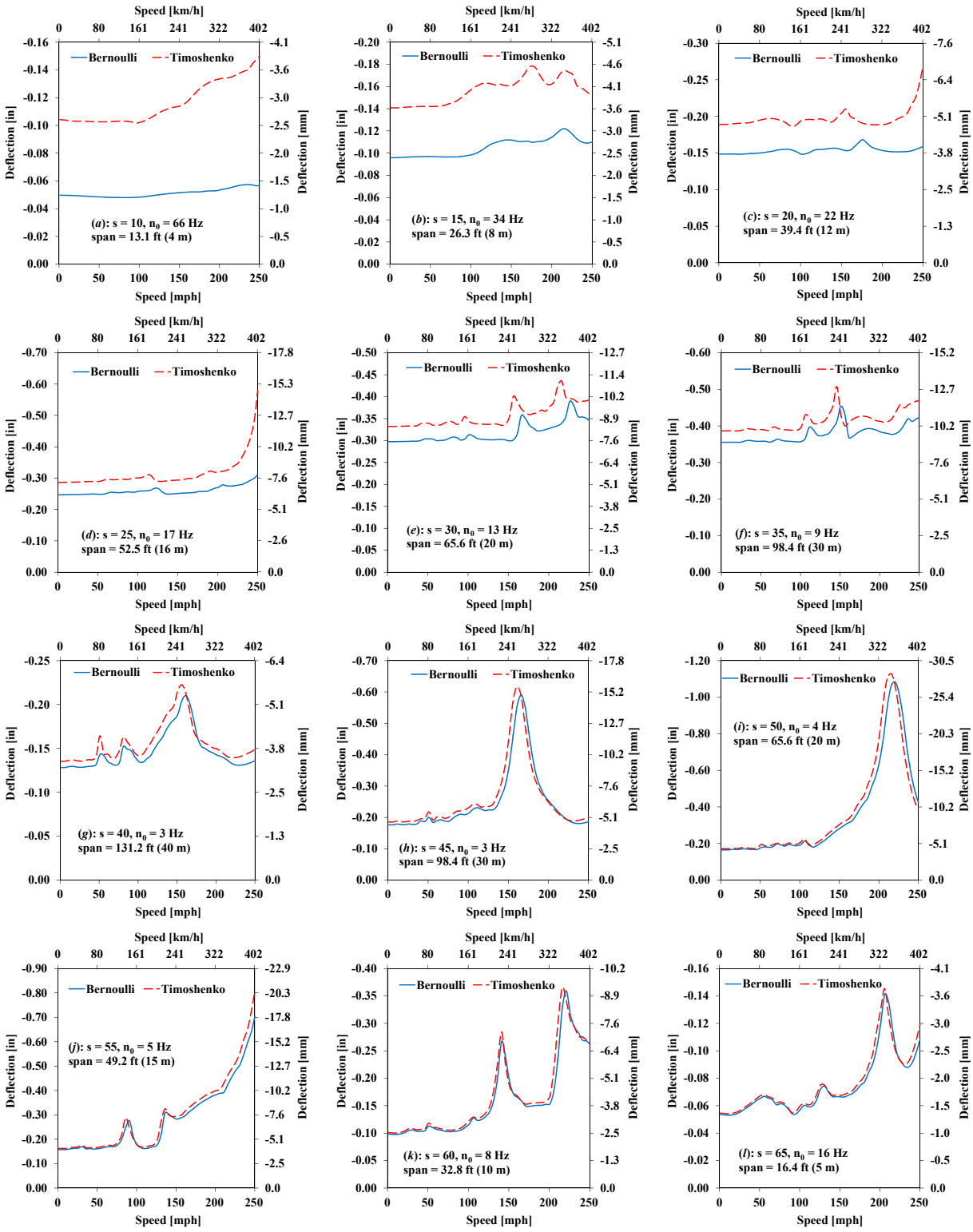

Figure 5.4 Effects of Shear deformations and rotational inertia on mid-span deflection of simply supported Group A (*a-f*) and Group B (*g-l*) bridge models

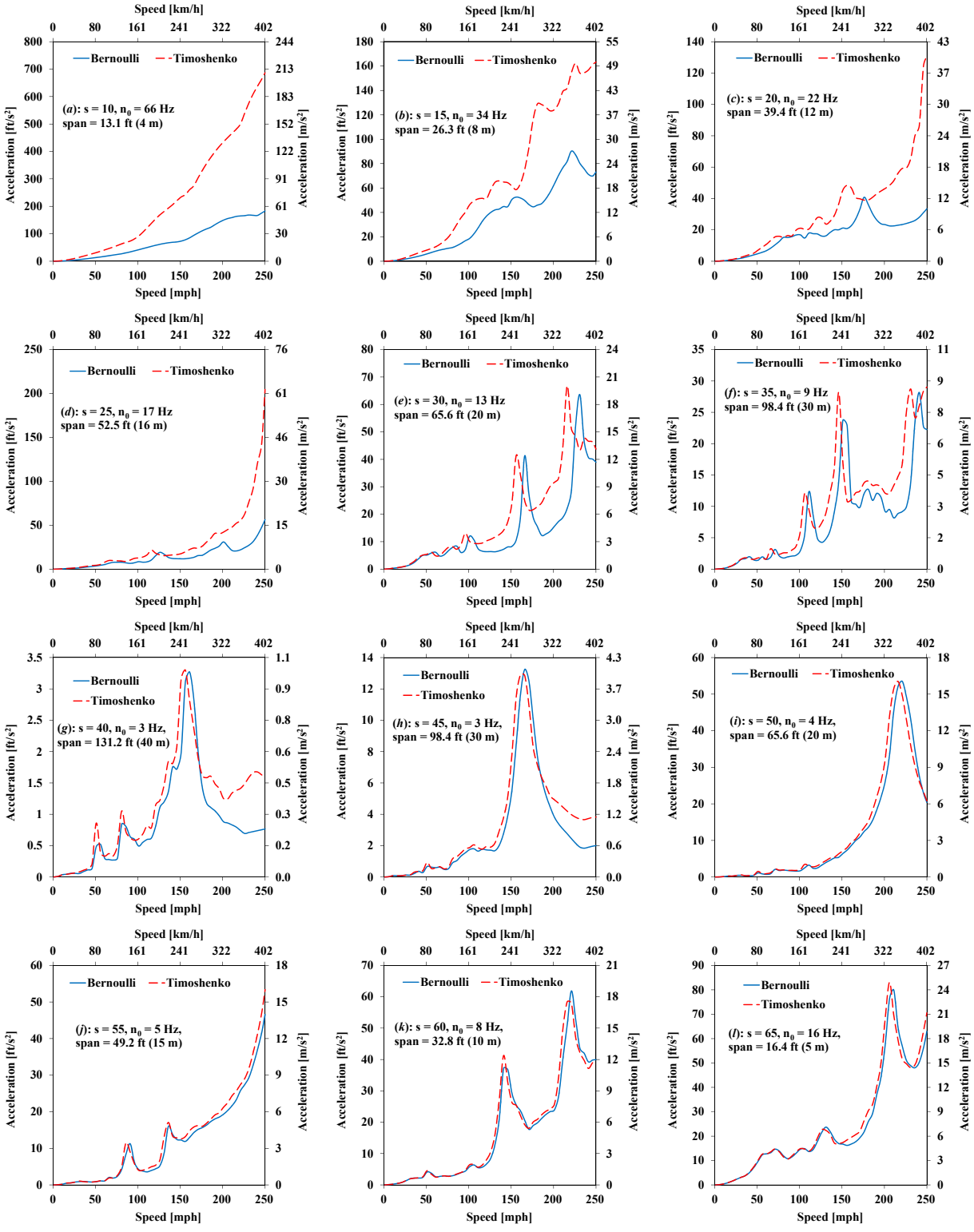

Figure 5.5 Effects of Shear deformations and rotational inertia on mid-span acceleration of simply supported Group A (*a-f*) and Group B (*g-l*) bridge models

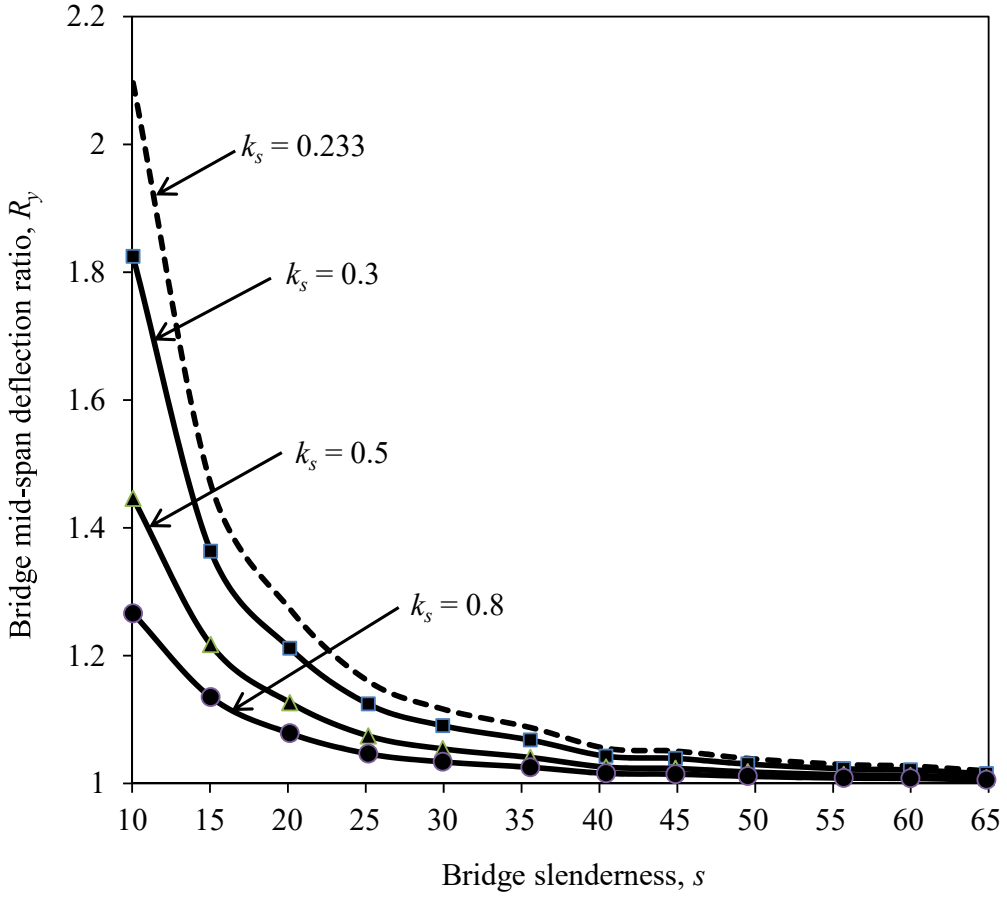

Figure.5.6 Ratio R_y of bridge mid-span static deflection for different shear factors k_s

Figure 5.6 shows the ratio R_y of Timoshenko theory to Bernoulli theory for the static bridge mid-span deflection in the range of slenderness ratio from 10 to 65 and shear factors from 0.233 to 0.8. This ratio can be as high as 2.1 for a combined low slenderness ratio and low shear factor. From the numerical results shown in Figure 5.6, an empirical relationship for the ratio R_y is developed and expressed as

$$R_y = \frac{25}{s^2 k_s} + 1 \tag{5.11}$$

5.4. Effects of Vehicle Interaction and Track Structure

Figures 5.7 and 5.8 show 6 graphs each corresponding to the 6 bridges B1 through B6. The bridges are simulated as simply supported. The loading is due to the passage of the ICE-3 high speed train. Each of the 6 graphs of Figures 5.7 and 5.8 shows 4 plots of the bridge mid-span vertical deflection and acceleration respectively for train speeds ranging from quasi-static to a maximum of 400 km/h (250 mph). A total of 4 separate dynamic simulation scenarios are considered, namely: (i) no interaction and no track; (ii) interaction and no track; (iii) no interaction and track; (iv) interaction and track.

It can be seen that there exists resonance conditions for bridge spans less than 30m (98.43ft) resulting in the bridge responses exceeding the code allowed maximum deflection or acceleration, particularly at high speeds over 200 km/h (124 mph). It is noticeable from the graphs that the train has the same signature on a given bridge regardless of whether the vehicle interaction and track contribution are considered or not. This is evidenced by the similar shape of the plots in each graph and for each bridge. Generally, the cumulative effects of the vehicle interaction and track contributions reduce the magnitude of the bridge responses at resonance speeds. This reduction is significant for shorter bridges. For example, for the cases in this, reductions of about 30-50% in the vertical acceleration are observed for all bridges when including both the vehicle interaction and the track structure compared to the model with no interaction and no track. For very short bridges like the 5m (16.4ft) span of bridge B1, the track contribution is more significant in reducing dynamic responses, even at lower train speeds.

Results presented in both Figures 5.7 and 5.8 also show that the curves shift slightly to the left at resonance speeds (i.e. lower speed) when elastic properties of the vehicle suspension

and track structure are taken into consideration, therefore implying a reduction in the speeds at which resonance is expected. For example, for the 10 m (32.8 ft) span of bridge B2, the resonance speed is reduced by 9% for vertical bridge deck acceleration when using an improved model considering both the vehicle interaction and track structure compared to the model which ignores both. Similar trend of resonance speed reduction is also noticed for other bridges as well as for deflection responses. This is due to a reduction in the fundamental frequency of the bridge provided by the consideration in the model of elastic elements of the vehicle suspension systems and track elastic properties.

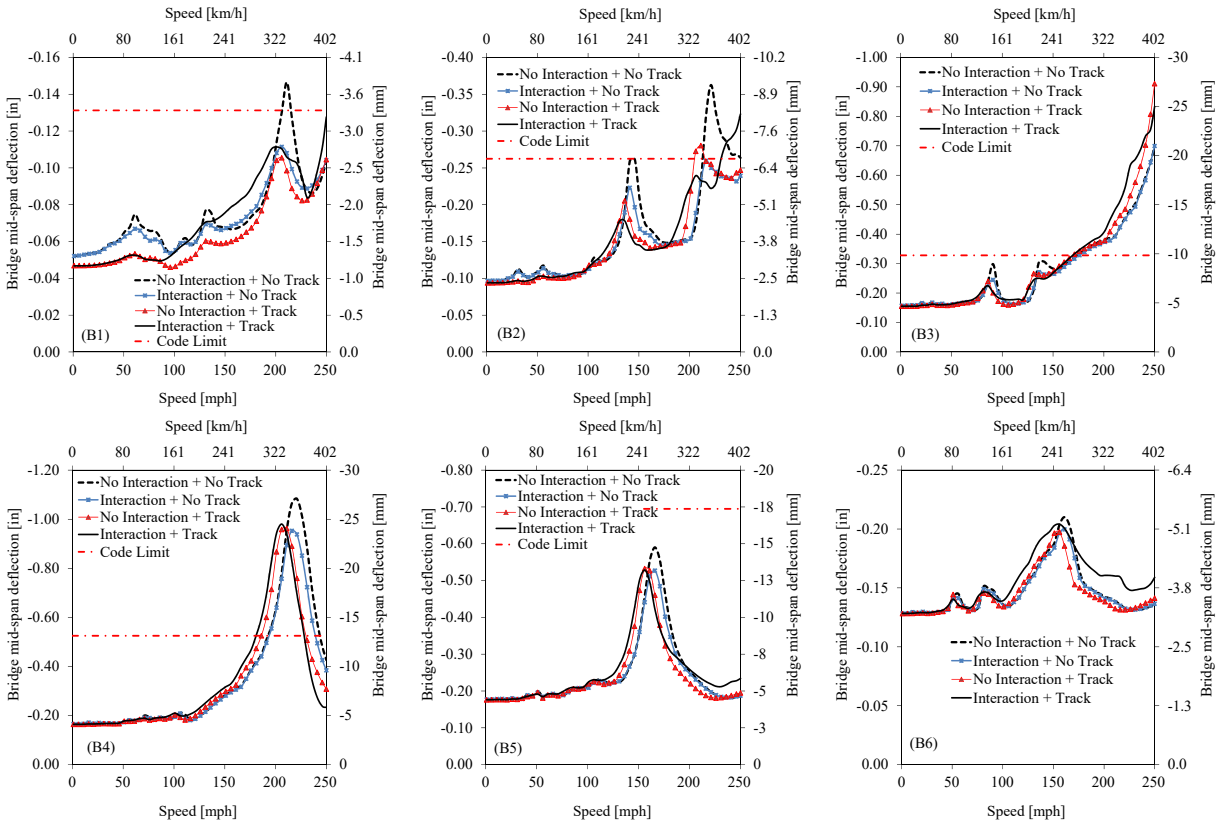

Figure 5.7 Mid-span vertical deflections of simply supported bridges B1 through B6

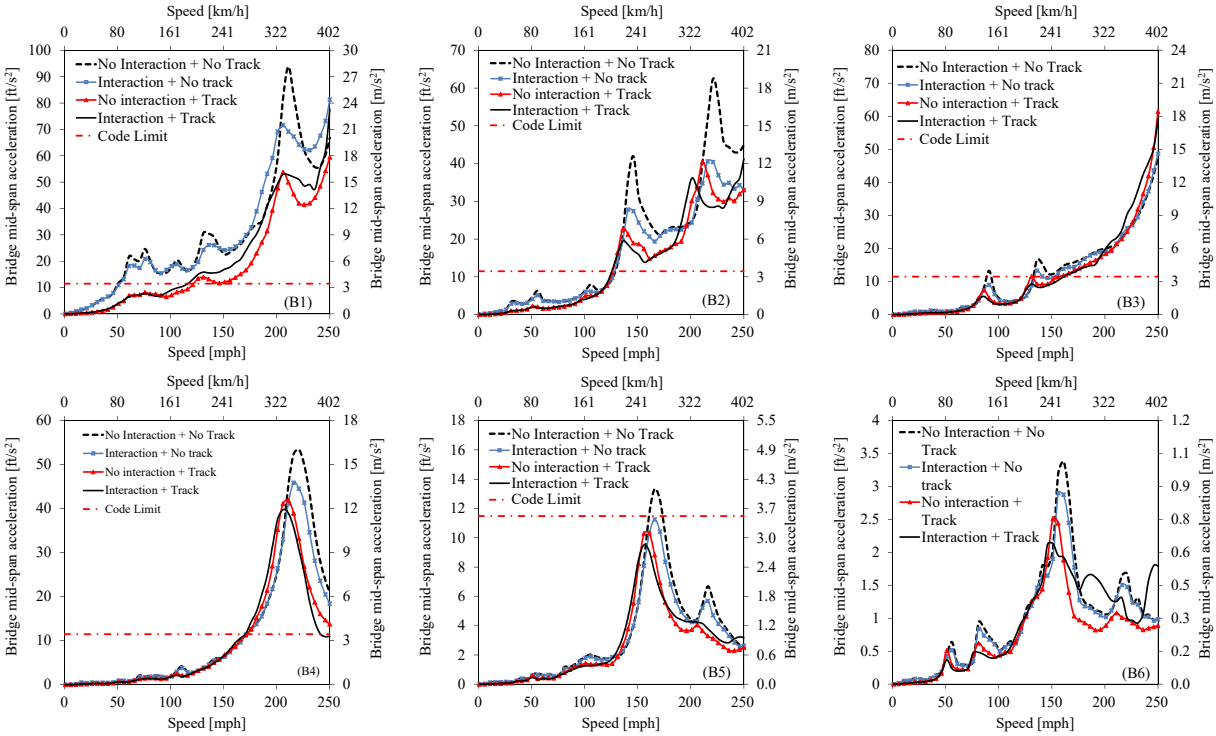

Figure 5.8 Mid-span vertical accelerations of simply supported bridges B1 through B6

5.5. Conditions of Resonance and Effects of Service Speed

The service speed of the ICE-3 train is 320 km/h (199 mph). Graphs in Figure 5.9 show the time-histories of mid-span vertical accelerations for simply supported bridges B1, B2, B4 and B5. The dynamic simulations in these cases include both the vehicle interaction and track structure. It can be seen that the resonance conditions occur at train speeds which are very close to the service speed for bridges B1, B2 and B4 where high vertical accelerations, exceeding the safe limit, are expected. For bridge spans less than 10 m (32.8 ft), accelerations could even exceed the ultimate limit of 0.7g, a situation that could destabilize the track.

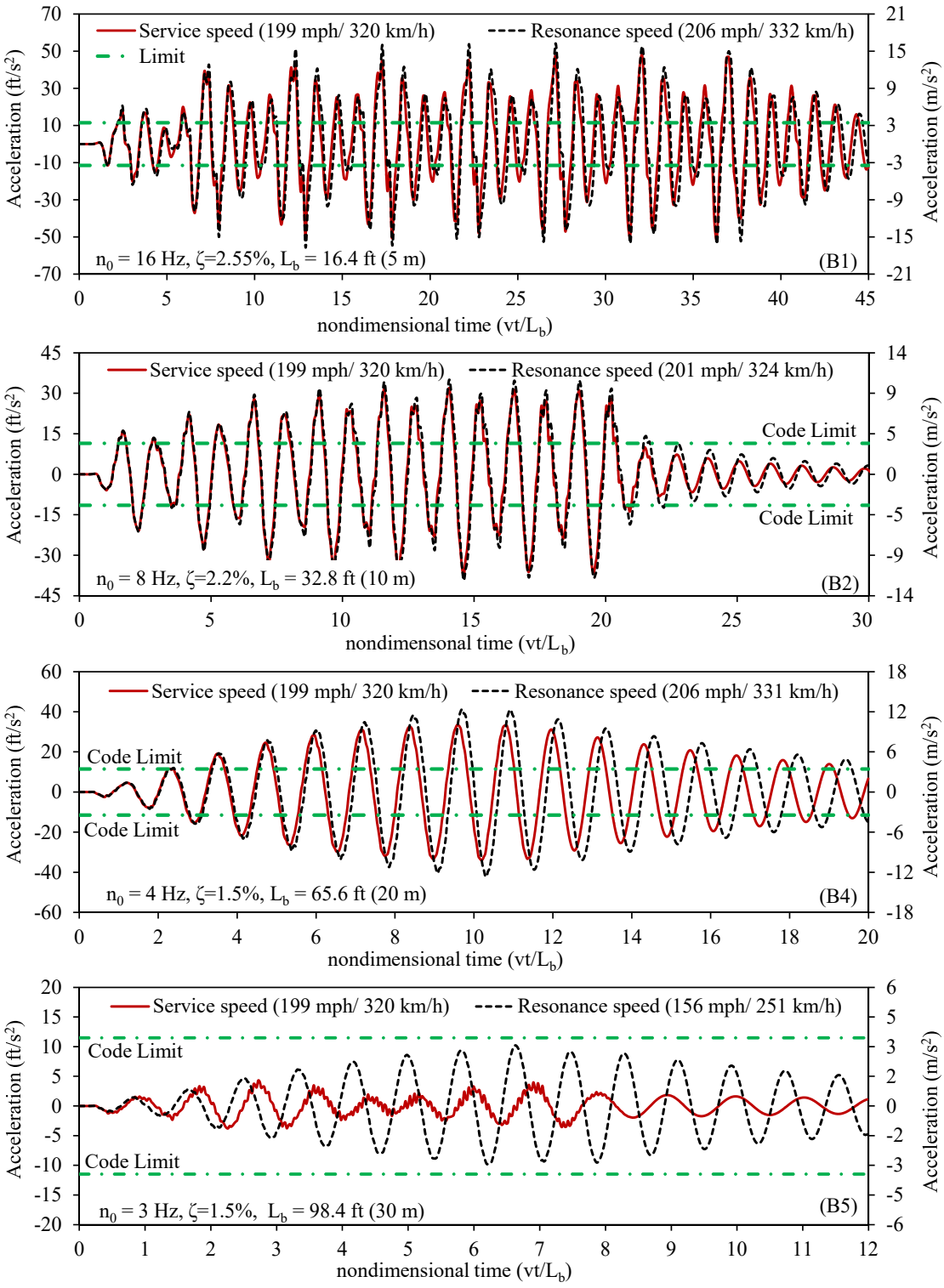

Figure 5.9 Mid-span vertical acceleration time-histories of bridge models B1, B2, B4 and B5 due to ICE-3 running at service and resonance speeds

It is interesting also to note that resonance may even occur at running speeds smaller than the service speed as shown in the acceleration plots for the case of 30 m (98.4 ft) span bridge B5 where resonance is predicted at a speed of 251 km/h (156 mph).

The time-histories of mid-span vertical deflection for simply supported bridges B1, B2 and B4 are shown in Figure 5.10 for the quasi-static case and resonance conditions. The solid lines of quasi-static speed, taken as 1.61 km/h (1 mph), represent the static deflection. Comparing the solid lines and the dashed lines it is easier to understand the components of the train vehicle that create the conditions of resonance on the bridge. For very short bridges like the 5 m (16.4 ft) span bridge B1, it can be seen that resonance occurs under the front bogie of the intermediate coaches. The bridge begins to vibrate freely when the front bogie leaves the bridge and the rear has not arrived yet. Observations indicate that the arrival of the rear bogie on the bridge creates a condition of cancellation of these free vibrations for the 5m span bridge.

In summary, the challenges with short span high speed rail bridges can be observed in Figures 5.7 through 5.10 where high vertical bridge responses, particularly accelerations, are problematic. For simple supported bridges with a span of 10 m (32.81 ft) to 20 m (65.62 ft), even a refined model both the vehicle interaction and track structure predicts vertical accelerations exceeding the safe limit. For bridges with a span of 40 m (131.23 ft) and longer, bridge vertical responses are not an issue. A situation where the beneficial effects of the vehicle interaction and track contributions can make a difference in the dynamic response prediction can be seen for the bridge B5 with a span of 30 m (98.43 ft). In this case, the moving load model on a simply supported bridge predicts vertical accelerations that exceed the safe limit of 3.5 m/s^2 (11.5 ft/s^2). A model that includes the track structure however predicts values below the safe limit. In this case therefore it would be sufficient to use a simply supported model with track contribution.

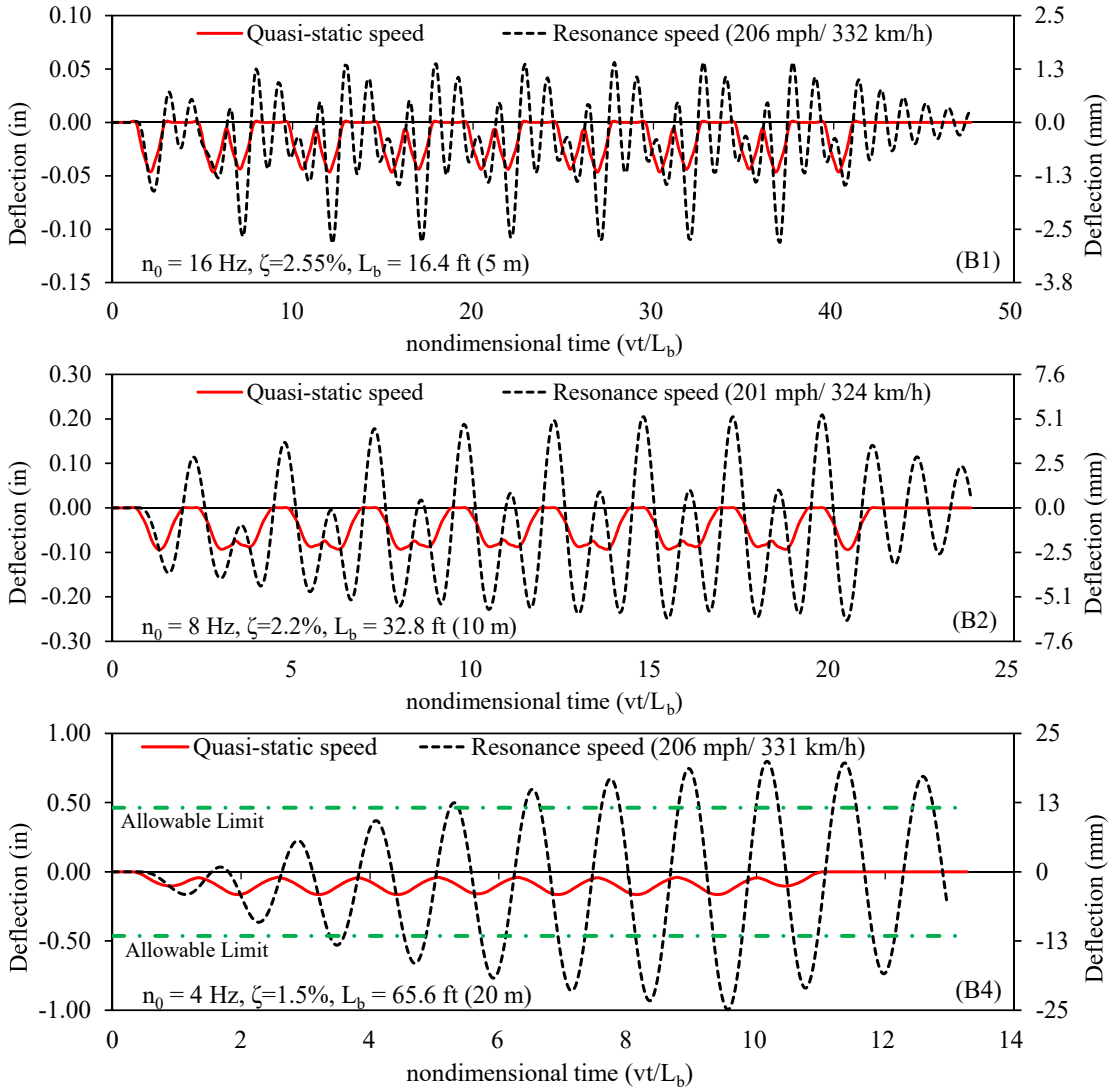

Figure 5.10 Mid-span vertical deflection time-histories of bridges B1 (top), B2 (middle) and B4 (bottom) due to ICE-3 train running at crawling and service speeds

5.6. Effects of Track Vertical Stiffness and Damping

The effects of the track vertical stiffness and damping on the dynamic response of the bridge, track and vehicle is investigated in this section. A total of 4 different cases are examined, namely: a low stiffness and low damping (LS + LD) condition; a low stiffness and a high damping (LS + HD) scenario; a high stiffness and low damping (HS + LD) situation; and a high stiffness and high damping (HS + HD) case. The 6 bridges B1 to B6 are simulated as simply supported. The value of the low track vertical stiffness is taken as 270000 Ib_f/in (47 MN/m) and the value of the high track vertical stiffness is set to 2160000 Ib_f/in (378 MN/m). The value of low track vertical damping is taken as 50 Ib_f-s/in (9 kN-s/m) and the value of high track vertical damping is chosen to be 400 Ib_f-s/in (70 kN-s/m). These extreme values of the track stiffness and damping are purposely chosen to be outside the typical values found in the literature (Arvidsson, 2014) in order to investigate the significance of their impact on the bridge, track or vehicle.

The dynamic simulations are carried out using the German ICE-3 trainset. The train speed was varied from the quasi-static speed of 1 mph (1.61 km/h) to a maximum speed of 250 mph (402 km/h) with a speed increment of 5 mph (8 km/h). The bridge mid-span vertical deflection, the track vertical acceleration over the bridge mid-span and the leading car vertical deflection are the chosen dynamic responses to evaluate the effects of the track vertical stiffness and damping on short span high speed rail bridges. Results are discussed below.

5.6.1 Bridge dynamic responses

Figure 5.11 shows the effect of the track vertical stiffness and damping on the mid-span vertical deflection of bridges B1 through B6. It can be seen that, although the consideration of the track elastic properties reduces the dynamic responses particularly at resonance as discussed

previously, the variations in magnitude of the track stiffness and damping within the considered ranges have no significant effects on the dynamic responses of bridges B2 to B6, and has a small noticeable effect with an insignificant magnitude difference on the very short 5 m (16.4ft) bridge B1. This observation indicates that the track transfers the loads to the bridge deck regardless of its properties notwithstanding the fact that changes in these properties can affect the responses of the track itself and the vehicle. The results in Figure 5.11 seem counter-intuitive in that they suggest that the magnitude of the track vertical stiffness and damping does not matter for the bridge deflection as long as there are elastic elements between the rails and the bridge deck since Figure 5.7 shows a reduction in deflection when taking the track into consideration. Perhaps further research in the future is needed to reconcile results of Figures 5.7 and 5.11.

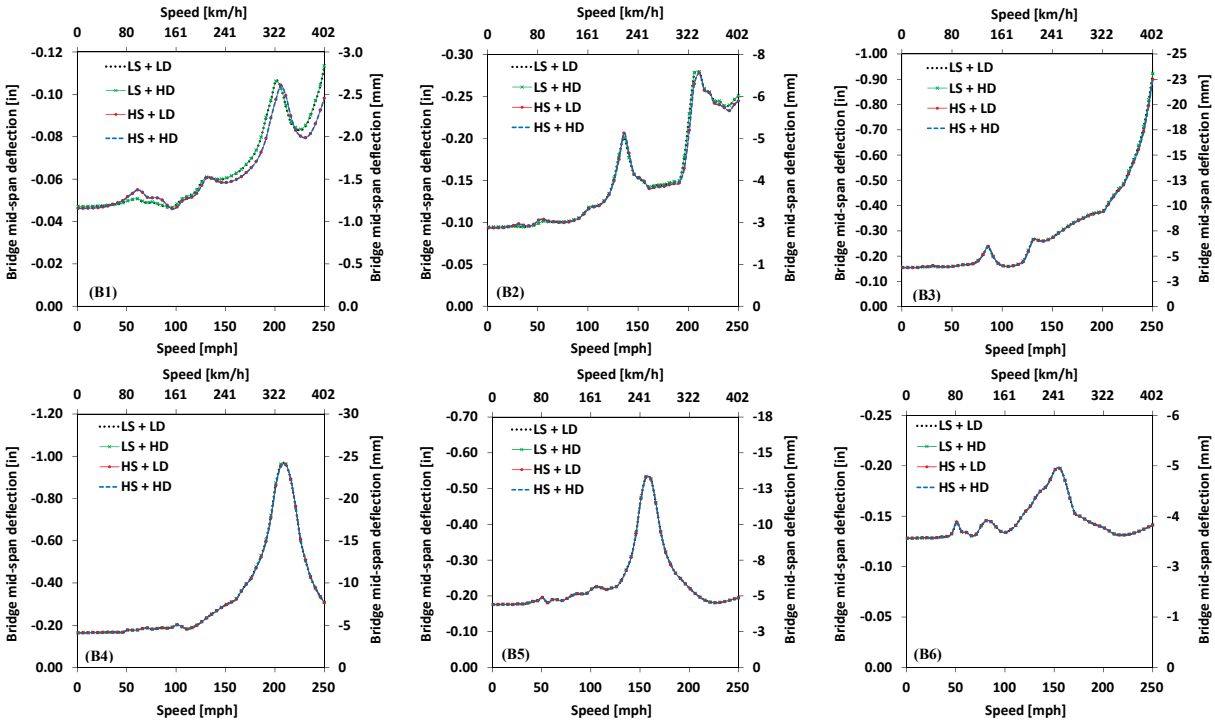

Figure 5.11 Effects of track Low Stiffness (LS), Low Damping (LD), High Stiffness (HS) and High Damping (HD) on vertical deflections of bridges B1 through B6

5.6.2 Track dynamic responses

Figure 5.12 shows the effects of the track vertical stiffness and damping on the vertical acceleration of the track for simply supported bridges B1 through B6 crossed by an ICE-3 train. Generally it can be observed that the track vertical acceleration increases with the increase in the train speed. The effects of the variations in track stiffness and damping are more significant at higher speeds and for shorter bridges. The damping of the track is more relevant in reducing the response for cases with low stiffness in the track. It can be deduced that the track stiffness plays a more important role in short span bridges. Large track stiffness can increase the dynamic loading and therefore precipitate the track deterioration. Low track stiffness may cause settlement of the track and create higher stress in the rails.

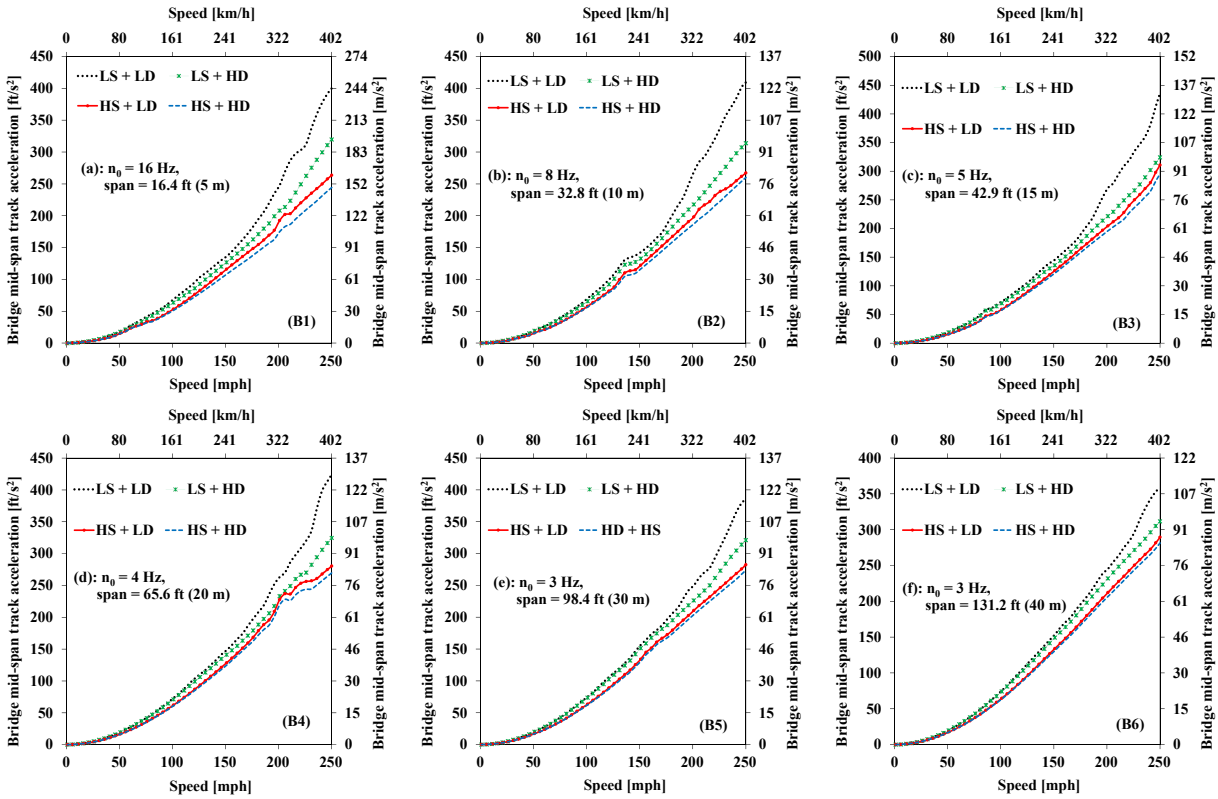

Figure 5.12 Effects of track Low Stiffness (LS), Low Damping (LD), High Stiffness (HS) and High Damping (HD) on rail accelerations over mid-span of bridges B1 through B6

5.6.3 Vehicle dynamic responses

Figure 5.13 shows the effects of the track vertical stiffness and damping on the vertical deflection of the leading car of the ICE-3 trainset crossing simply supported bridges B1 through B6. It can be observed that the damping value of the track has no impact on the vertical deflection of the carbody. However, the track stiffness has a more significant impact. The leading car deflection is greater with low track stiffness. This is because the track deflects more with low track stiffness and therefore so is the vehicle. For bridges with a span between 10 m (32.8ft) and 20 m (65.6ft), resonance condition with maximum vehicle deflection occurs at very low train speeds.

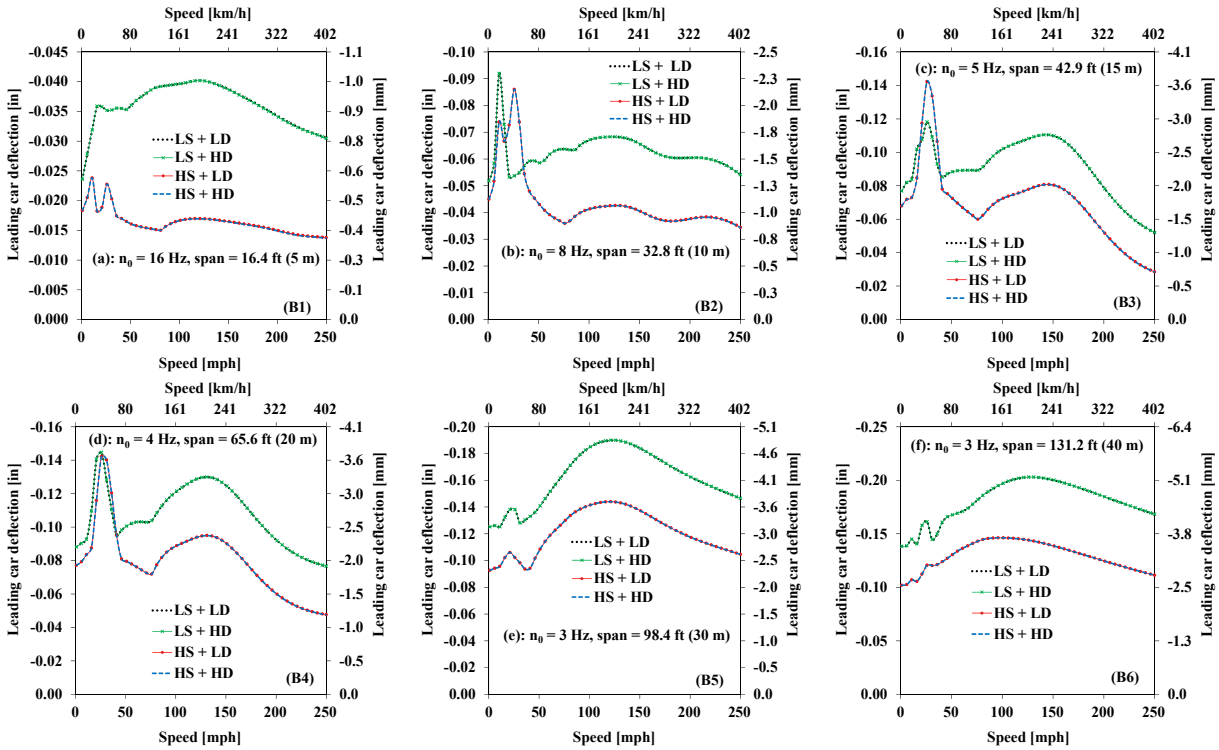

Figure 5.13 Effects of track Low Stiffness (LS), Low Damping (LD), High Stiffness (HS) and High Damping (HD) on vehicle deflections over bridges B1 through B6

5.7. Influence of Different Trainsets on Bridge and Vehicle Responses

Figure 5.14 shows the effects of 6 different trainset types on the vertical deflection at mid-span of simply supported bridges B1 through B6 with track structure included. The Japanese SKS N700-I with the smallest axle load and with all motorized bogies has the least impact on bridge responses. On the other hand, the Amtrak Acela, with the largest axle loads in the front and rear cars, has the largest impact on bridges B1, B2, B5 and B6. However, it should be noted that the maximum speed of the Acela train is 150 mph (240 km/h). For bridges B3 and B4, the effects are significant only at higher speeds.

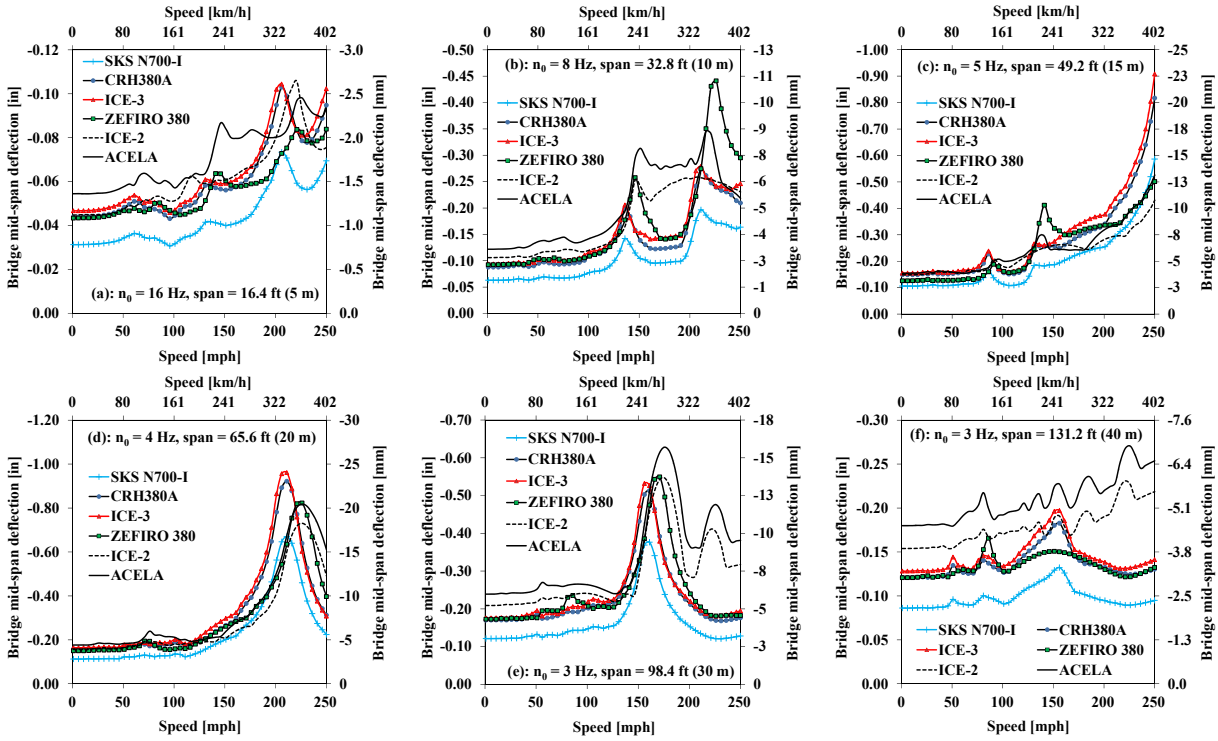

Figure 5.14 Effects of trainset type on vertical deflections of bridges B1 through B6

Figure 5.15 shows the effects of 6 different train types on the train leading car vertical acceleration over the mid-span of simply supported bridges B1 through B6 with track structure included. It can be noted that the Amtrak Acela has the highest leading car acceleration and the ICE-3 has the lowest leading car acceleration. The ICE-2 and Amtrak Acela have the heaviest axle loads resulting in their relative effects compared to other train types to be more pronounced in longer span bridges. The Japanese SKS N700-I, although with minimal effects on bridge responses, experience a higher leading car vertical accelerations than other train types with heavier axle loads such the ICE-3 train.

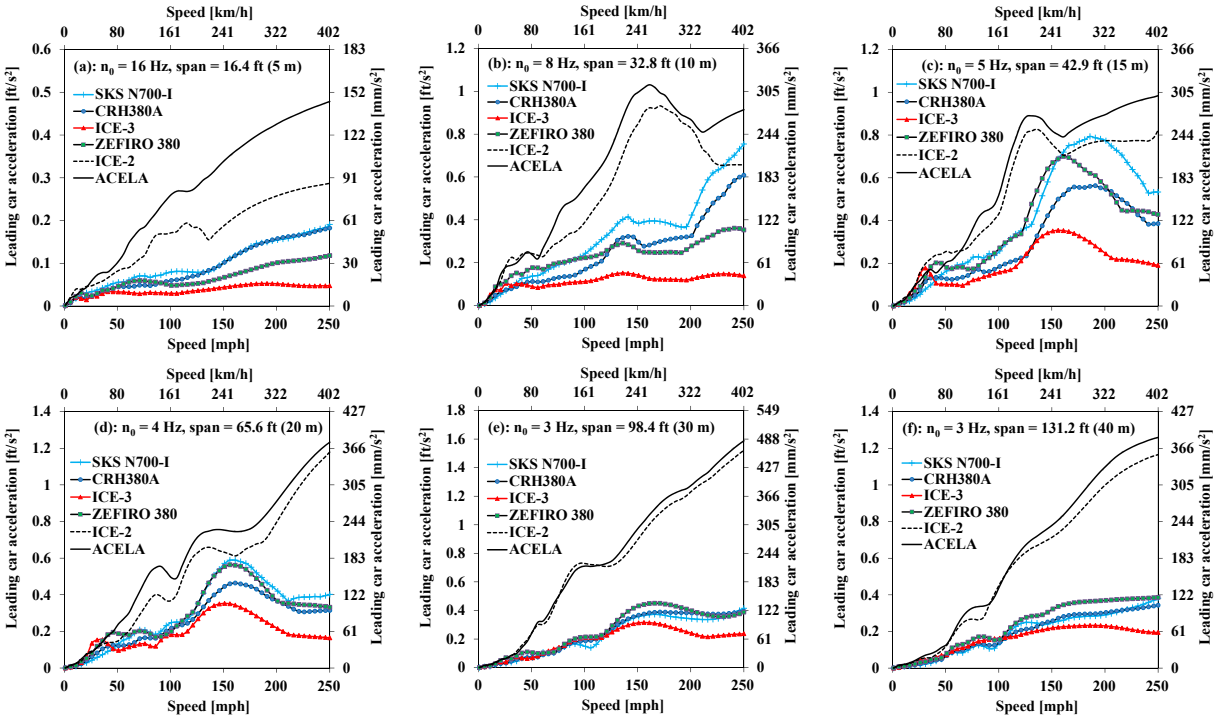

Figure 5.15 Effects of trainset type on leading car vertical accelerations over the mid-span of bridges B1 through B6

5.8. Effects of Track Irregularities on Bridge and Vehicle Responses

Track irregularities are considered to be a secondary source of bridge vibrations and a primary source of train vibrations. In order to evaluate the effect of track irregularities on the bridge and vehicle dynamic responses, a simply supported ballasted bridge with a span of 20 m (65.6 ft) and crossed by the ICE-3 trainset at its service speed of 320 km/h (199 mph) is simulated. A smooth track profile as well as FRA class 5 and class 6 track irregularities are investigated.

Figure 5.16 shows the time-histories of bridge mid-span vertical deflection and acceleration for the three types of track profile. It can be seen that there is a little differences in deflection responses between a smooth and a FRA class 6 track profiles. FRA class 5 however results in relatively more significant deflections. Track irregularities introduce higher frequency content in the accelerations response while the train is on the bridge as shown in Figure 5.17.

Figure 5.17 shows the time-histories of the leading car vertical deflection and acceleration for the three types of track profile. It can be observed that there is no significant differences in the deflection values between the smooth and FRA class 6 track profiles. FRA class 5 track profile however results in a more noticeable increase in deflection response. The acceleration is more sensitive to the track profile and increases with the track profile class. It is worth noting that in general the acceleration responses of both the bridge and the vehicle are more sensitive to the changes in track irregularities profiles.

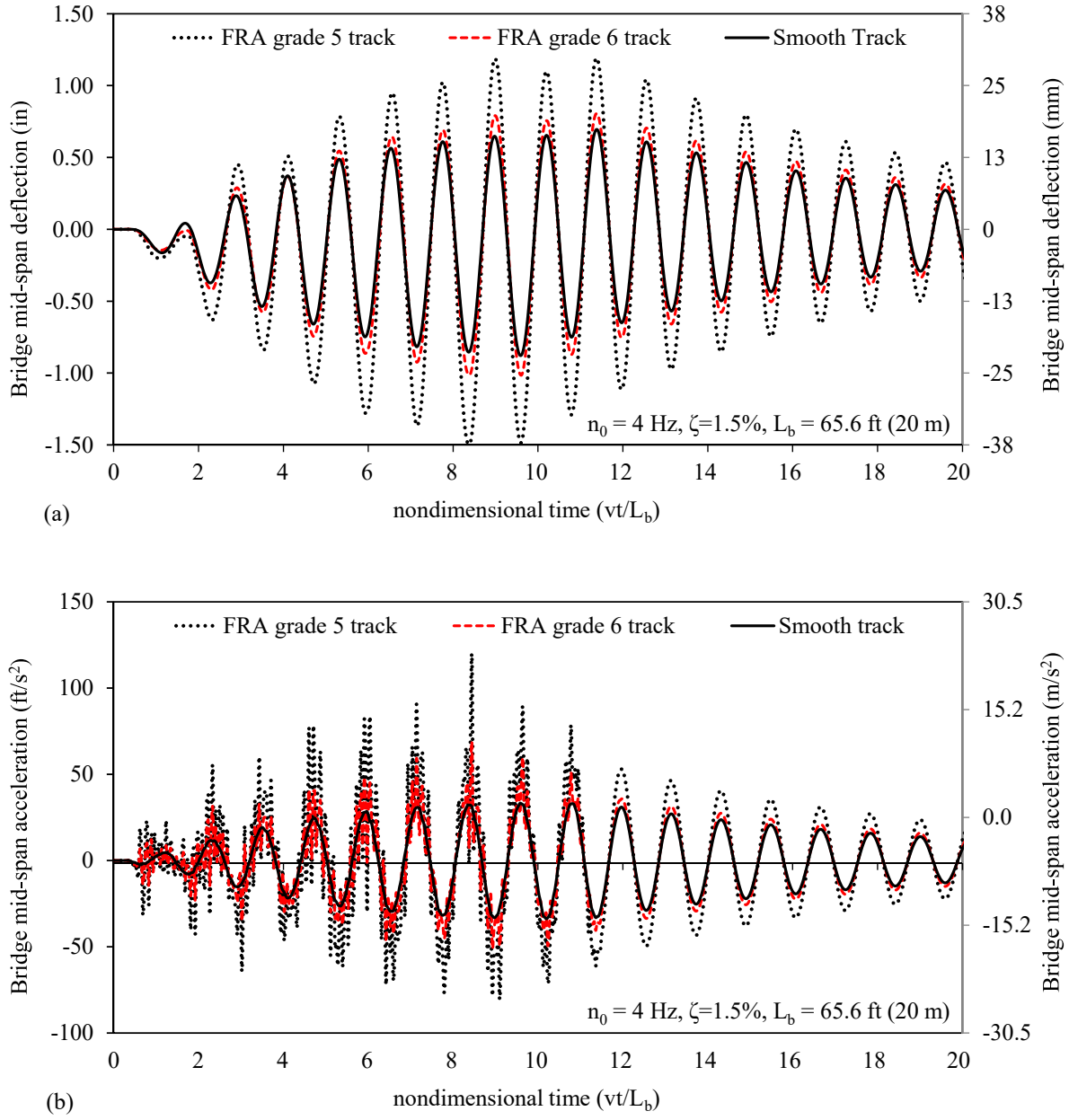

Figure 5.16 Effects of track irregularities on the dynamic response at mid-span of bridge B4 with ICE-3 at service speed: (a) deflection; (b) acceleration

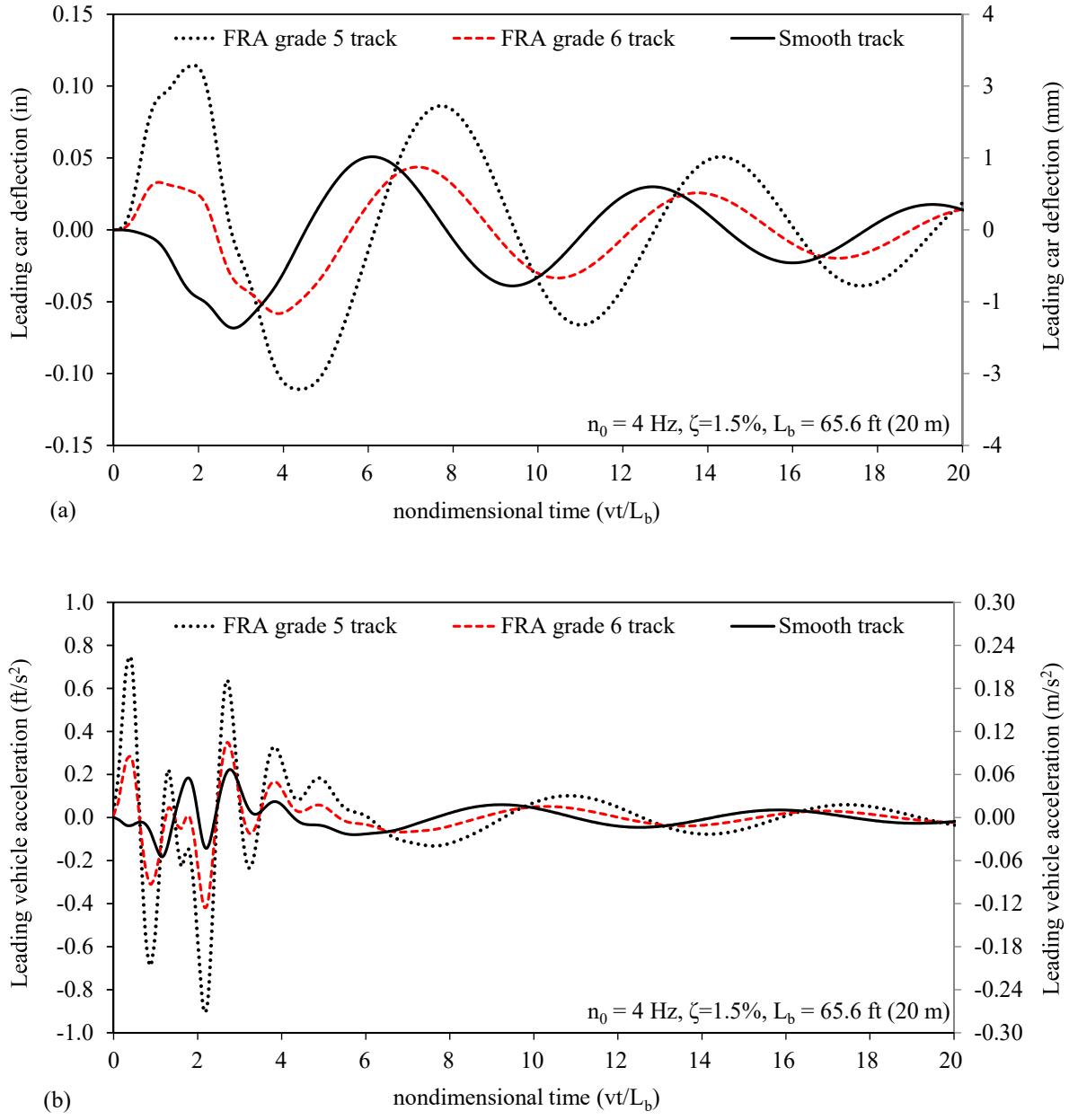

Figure 5.17 Effects of track irregularities on the vertical response of ICE-3 leading car over bridge B4 with ICE-3 at service speed: (a) deflection; (b) acceleration

5.9. Influence of Elastic Boundary Conditions on Dynamic Responses

The vertical stiffness ratio η_{sv} defined by equation (5.2) and the rotational stiffness ratio $\eta_{s\theta}$ defined by equation (5.3) are two significant parameters that can be used to assess the influence of the degree of flexibility in the bridge boundary conditions. The effects of these parameters on the bridge dynamic responses, with or without additional damping c_{sv} at the supports, are evaluated in this section. The vehicle interaction and track structure contributions are considered in the dynamic simulations. Parametric studies are performed considering 7 different scenarios for each of the bridges B1 through B6 with the following parameters.

1. $\eta_{s\theta}$ = -3, c_{sv} = 0, η_{sv} = 1.5, 2, 2.5, 3
2. $\eta_{s\theta}$ = 0, c_{sv} = 0, η_{sv} = 1.5, 2, 2.5, 3
3. $\eta_{s\theta}$ = 3, c_{sv} = 0, η_{sv} = 1.5, 2, 2.5, 3
4. $\eta_{s\theta}$ = -3, η_{sv} = 1.5, c_{sv} = 0, 9000 Ib_f-s/in (1.6 MN-s/m) to 18000 Ib_f-s/in (3.2 MN-s/m)
5. $\eta_{s\theta}$ = 0, η_{sv} = 1.5, c_{sv} = 0, 9000 Ib_f-s/in (1.6 MN-s/m) to 18000 Ib_f-s/in (3.2 MN-s/m)
6. $\eta_{s\theta}$ = -3, η_{sv} = 2, c_{sv} = 0, 9000 Ib_f-s/in (1.6 MN-s/m) to 18000 Ib_f-s/in (3.2 MN-s/m)
7. $\eta_{s\theta}$ = 0, η_{sv} = 2, c_{sv} = 0, 9000 Ib_f-s/in (1.6 MN-s/m) to 18000 Ib_f-s/in (3.2 MN-s/m)

In the dynamic simulations, the values of the damping constant c_{sv} in scenarios 4 to 7 above are taken in increments of 9000 Ib_f-s/in (1.6 MN-s/m). The case of Simply Supported (SS) condition is always considered in each scenario for comparison purposes. The ICE-3 with 8-car convoy configuration is used with speeds ranging crawling to 402 km/h (250 mph). Results for each of the above 7 scenarios are discussed below.

5.9.1 Case of free end rotations with no damping at bridge supports

Graphs in Figure 5.18 show the maximum vertical mid-span deflection of bridges B1 through B6 for 4 values of the vertical stiffness ratio η_{sv} between 1.5 and 3 with an increment of 0.5. The supports are assumed to have no additional damping in this case. The rotational stiffness ratio is set to $\eta_{s\theta}$ = -3 representing the case of free end rotation of the bridge. Graphs also show results of the simply supported (SS) case for comparison purposes. It is observed that for values of $\eta_{sv} > 3$ deflection curves are closer to the SS case. For the value of $\eta_{sv} = 1.5$ the supports can be considered very soft and deflection magnitudes are significantly higher, even exceeding allowable limits at very low train speeds for short span bridges.

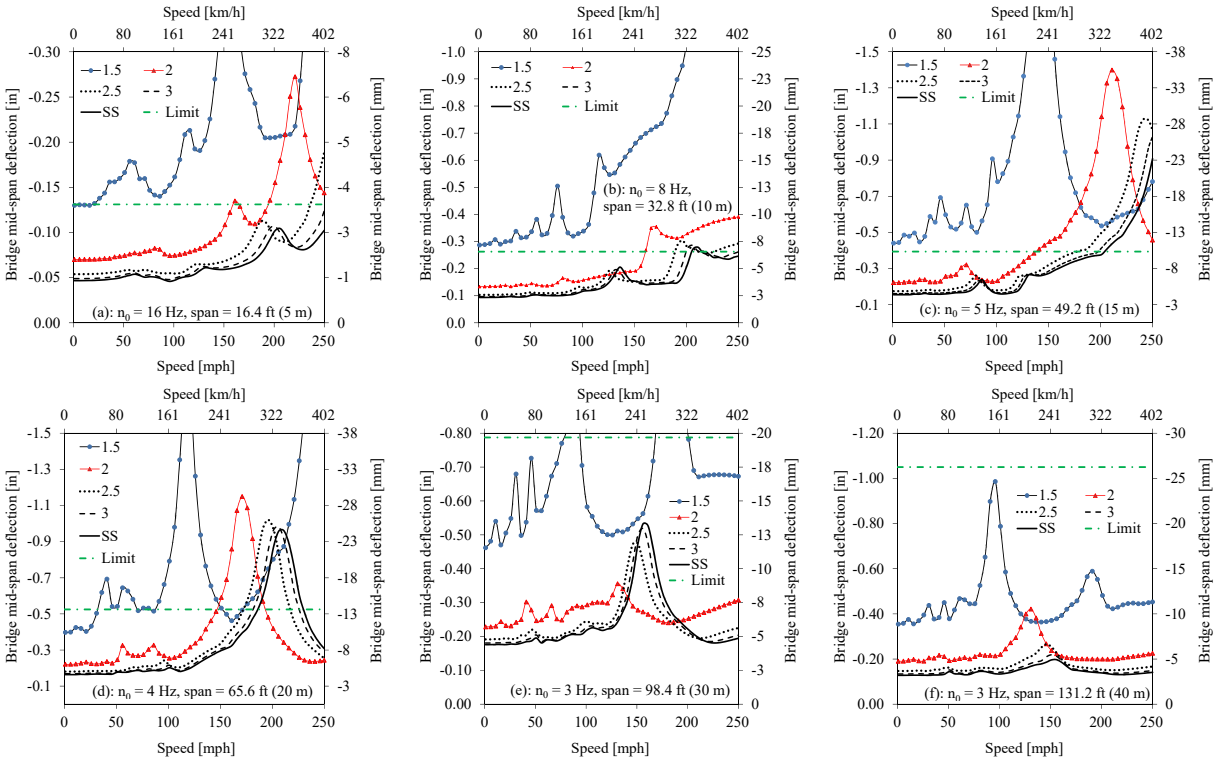

Figure 5.18 Mid-span vertical deflections of bridges B1 through B6 with vertical support stiffness ratios η_{sv} from 1.5 to 3 and SS for cases $\eta_{s\theta}$ = -3 and c_{sv} = 0

It can be seen that, in all bridges except bridge B5, for a decreasing value of η_{sv} from 3 to 2 the deflection magnitude increases rapidly and the resonance conditions appear at smaller speeds than the SS case.

Graphs in Figure 5.19 show the maximum vertical accelerations of bridges B1 through B6 for 4 values of the vertical stiffness ratio η_{sv} between 1.5 and 3 with an increment of 0.5. The supports are assumed to have no additional damping in this case. The rotational stiffness ratio is set to $\eta_{s\theta}$ = -3 representing the case of free end rotation of the bridge. Graphs also show results of the simply supported (SS) case for comparison purposes.

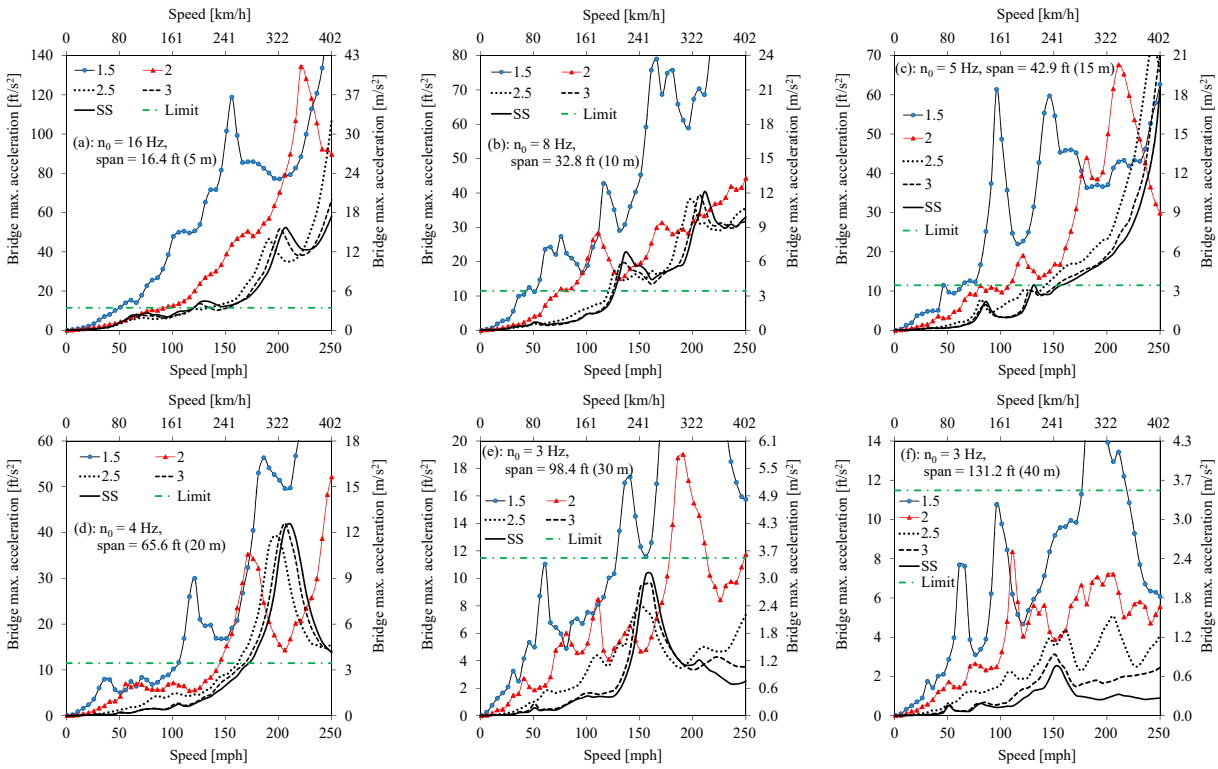

Figure 5.19 Maximum vertical accelerations of bridges B1 through B6 with vertical support stiffness ratios η_{sv} from 1.5 to 3 and SS for cases $\eta_{s\theta}$ = -3 and c_{sv} = 0

Results show that for values of η_{sv} equal to 1.5 and 2, bridge accelerations are significantly higher. For values of η_{sv} greater or equal to 2.5, there is a small noticeable differences with a decrease in acceleration at resonance. For values of η_{sv} > 3, it is expected that bridge vertical vibrations would be very close to the SS case.

5.9.2 Case of partial end rotations with no damping at bridge supports

Graphs in Figure 5.20 show the maximum vertical mid-span deflections of bridges B1 through B6 for 4 values of the vertical stiffness ratio η_{sv} between 1.5 and 3 with an increment of 0.5. The supports are assumed to have no additional damping in this case. The rotational stiffness ratio is set to $\eta_{s\theta}$ = 0 representing the case of partial restraint of bridge end rotations. Graphs also show results of the simply supported (SS) case for comparison purposes.

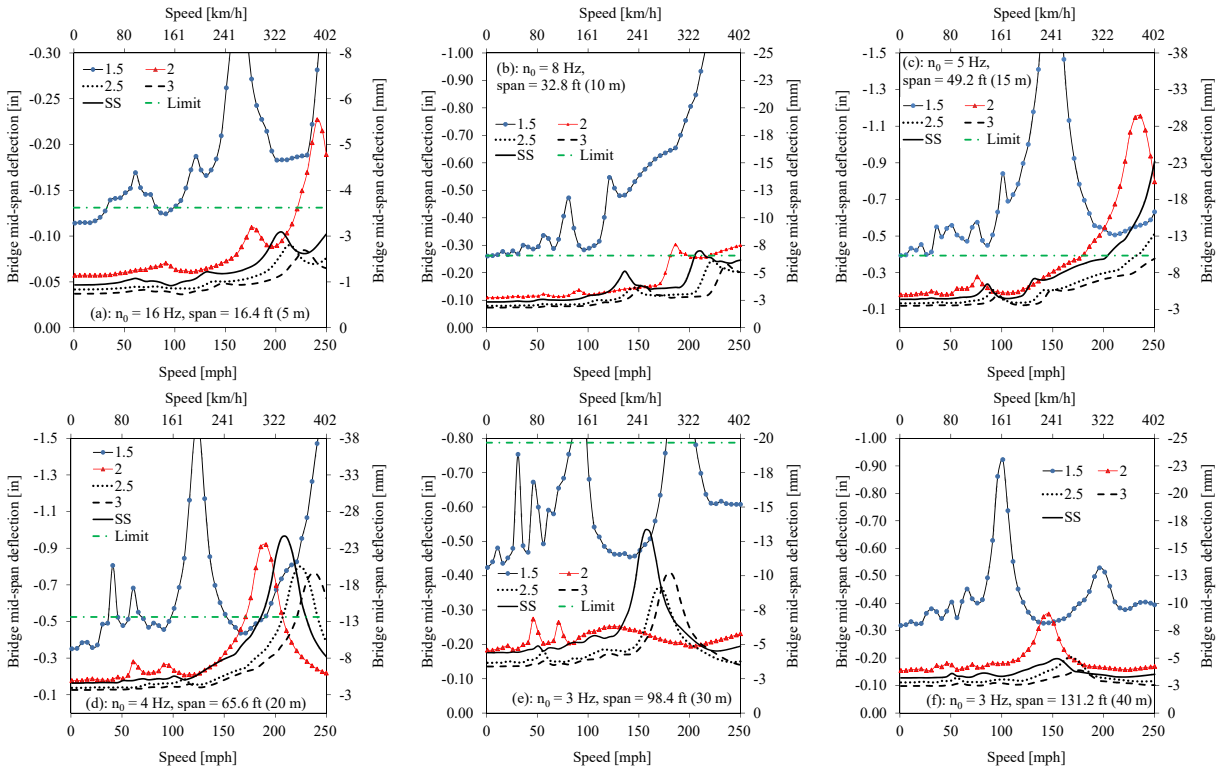

Figure 5.20 Mid-span vertical deflections of bridges B1 through B6 with vertical support stiffness ratios η_{sv} from 1.5 to 3 and SS for cases $\eta_{s\theta}$ = 0 and c_{sv} = 0

In this case of partial rotational restraint, it can be seen that for $\eta_{sv} \geq 2.5$ the mid-span deflections are less than the SS case and the resonance speeds are greater. But for $\eta_{sv} \leq 2$, it is the opposite in that the mid-span deflections are greater than the SS case and the resonance speeds are smaller. Therefore, It can be said that for $\eta_{s\theta} = 0$, the mid-span deflections of bridges, except Bridge B5, are the same as in the SS case for some values of the vertical support stiffness ratio η_{sv} between 2 and 2.5 as can be seen in the graphs. The deflection of Bridge B5 with $\eta_{sv} = 2$ at resonance speed is significantly suppressed.

Graphs in Figure 5.21 show the maximum vertical accelerations of bridges B1 through B6 for 4 values of the vertical stiffness ratio η_{sv} between 1.5 and 3 with an increment of 0.5. The supports are assumed to have no additional damping in this case. The rotational stiffness ratio is set to $\eta_{s\theta}$ = 0 representing the case of partial restraint of bridge end rotations. Graphs also show results of the simply supported (SS) case for comparison purposes.

It can be observed that there is a benefit in considering the rotational restraint of bridge ends for values of the vertical stiffness ratio $\eta_{sv} \geq 2.5$ as it results in higher speeds for which the maximum allowable acceleration is exceeded and also increases the speed at which resonance may be expected. However, for values of the support vertical stiffness ratio $\eta_{sv} \leq 2$ these benefits are reversed and acceleration responses are significantly higher.

Generally, comparing Figures 5.19 and 5.21, it can be seen that for values of vertical stiffness ratio $\eta_{sv} \leq 2$, the acceleration response curves have similar shapes and magnitudes for values of $\eta_{s\theta}$ of -3 and 0, thus indicating that the bridge end partial restraint of rotation has no effect in the dynamic responses in that range of support vertical stiffness ratios.

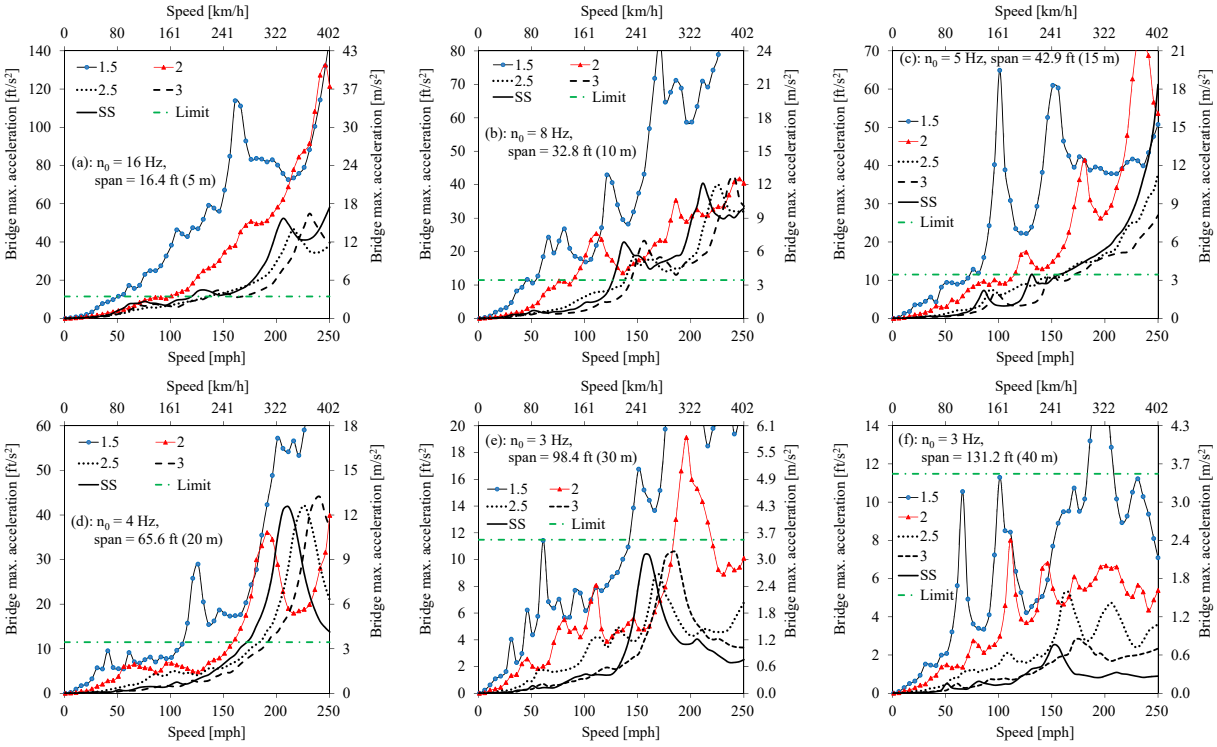

Figure 5.21 Maximum vertical accelerations of bridges B1 through B6 with vertical support stiffness ratios η_{sv} from 1.5 to 3 and SS for cases $\eta_{s\theta} = 0$ and $c_{sv} = 0$

5.9.3 Case of fixed end rotations with no damping at bridge supports

Graphs in Figure 5.22 show the maximum mid-span vertical deflections of bridges B1 through B6 for 4 values of the vertical stiffness ratio η_{sv} between 1.5 and 3 with an increment of 0.5. The supports are assumed to have no additional damping in this case. The rotational stiffness ratio is set to $\eta_{s\theta} = 3$ representing the case of fully restrained end rotations. Graphs also show results of the simply supported (SS) case for comparison purposes. It can be seen that for fixed-fixed boundary conditions where both the vertical translation and rotations at bridge ends are zero, bridge deflections are nearly constant across all speeds and always below the serviceability limits. For η_{sv} =2, deflection in short span bridges is smaller than the SS case. However, for the

condition of η_{sv} < 2, rotational restraint of bridge ends do not provide any significant difference and deflections are excessively high.

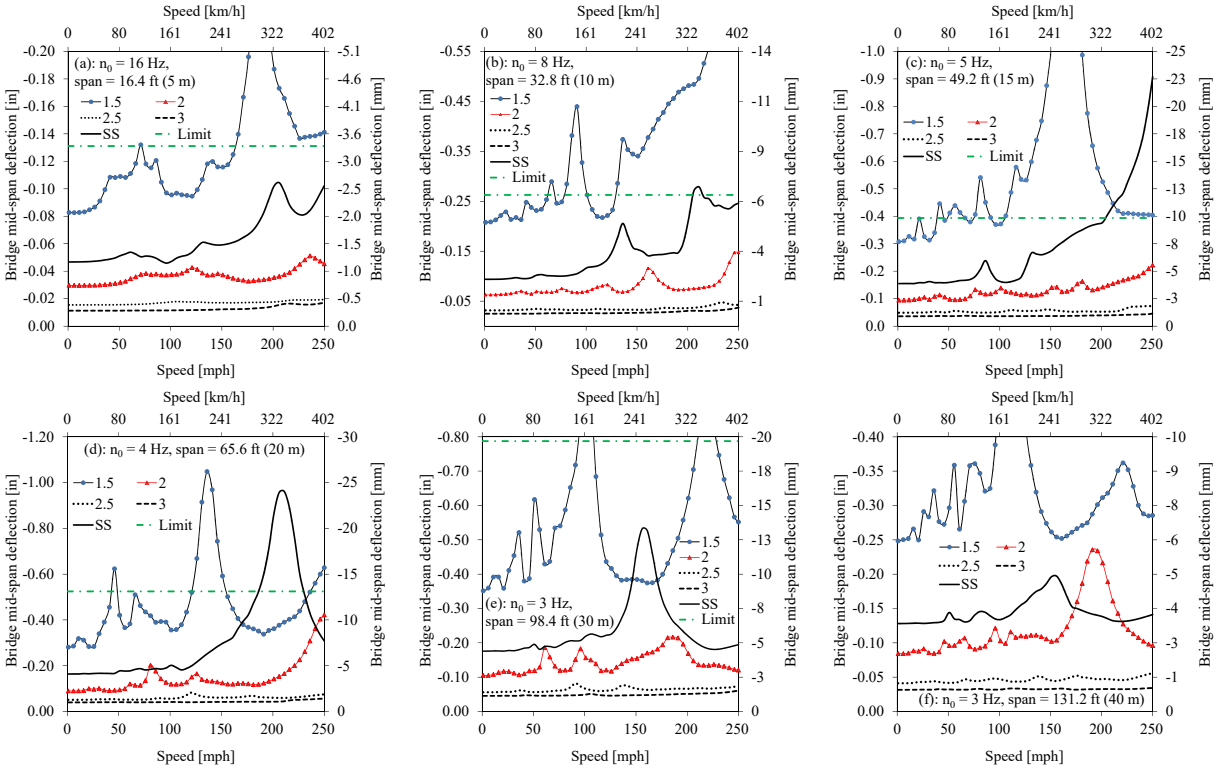

Figure 5.22 Mid-span vertical deflections of bridges B1 through B6 with vertical support stiffness ratios η_{sv} from 1.5 to 3 and SS for cases $\eta_{s\theta}$ = 3 and c_{sv} = 0

Graphs in Figure 5.23 show the maximum vertical accelerations of bridges B1 through B6 for 4 values of the vertical stiffness ratio η_{sv} between 1.5 and 3 with an increment of 0.5. The supports are assumed to have no additional damping in this case. The rotational stiffness ratio is set to $\eta_{s\theta}$ = 3 representing the case of fully restrained end rotations. Graphs also show results of the simply supported (SS) case for comparison purposes.

It can be noted that, even without damping at supports, restraining both translation and rotation at bridge ends leads to significantly reduced bridge vibrations compared to the SS case. However, even with full rotational restraint at bridge supports, the accelerations increase for when the support vertical stiffness ratio η_{sv} decreases. For values $\eta_{sv} \geq 2.5$ accelerations are smaller than in the case of simply supported case. For values $\eta_{sv} \leq 2$, accelerations are significantly increased compared to the SS case.

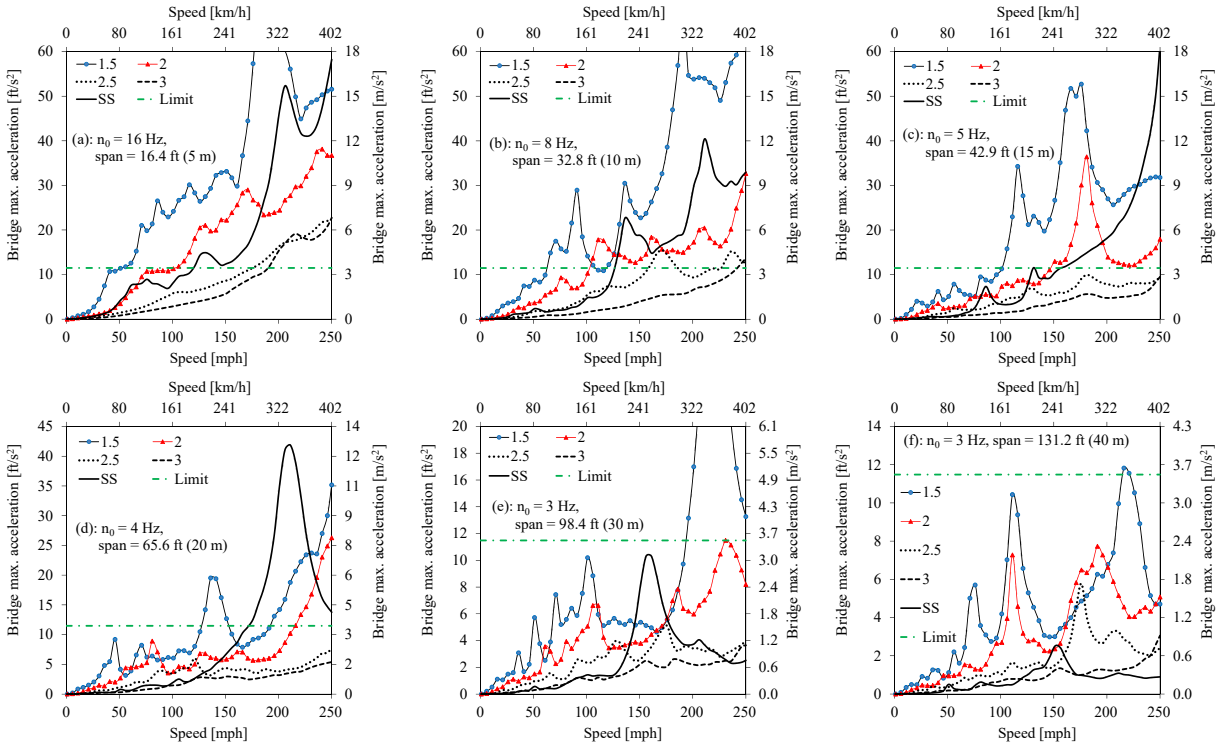

Figure 5.23 Maximum vertical accelerations of bridges B1 through B6 with vertical support stiffness ratios η_{sv} from 1.5 to 3 and SS for cases $\eta_{s\theta}$ = 3 and c_{sv} = 0

5.9.4 Case of free rotation with very soft springs and damping at supports

Graphs in Figure 5.24 show the maximum mid-span vertical deflections of bridges B1 through B6 for different damping ratios ζ_d (%) of the bridge supports corresponding to the selected support damping constants c_{sv}; and for values of η_{sv} = 1.5 representing very soft vertical supports and $\eta_{s\theta}$ = -3 representing free rotation of bridge ends. Generally, it can be seen that damping has a significant effect in reducing the deflections. Due to the low value of η_{sv} the deflections in bridges B2 and B3 exceed serviceability limits even at static loads. This is due to excessive deflections at the supports. For bridges with spans less than 15 m (49.2 ft), it would require a relatively high damping at supports to reduce deflections below the allowable limits.

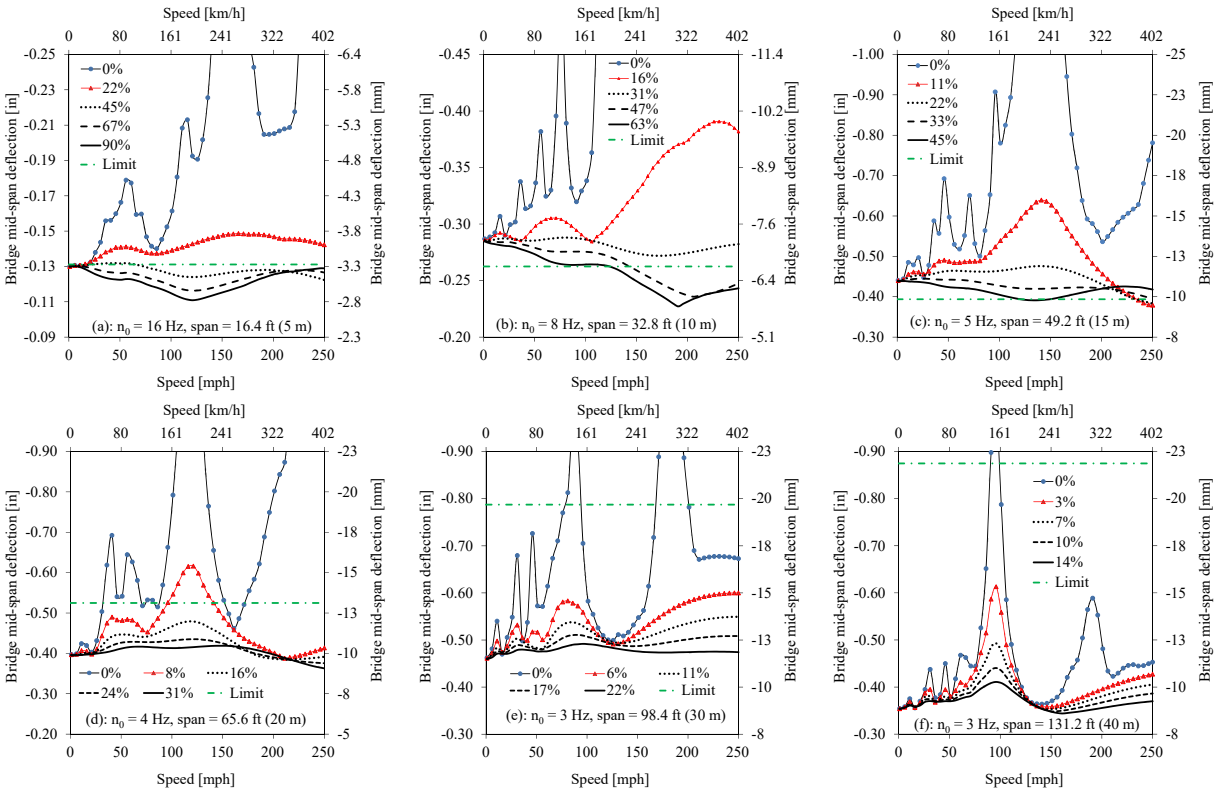

Figure 5.24 Mid-span vertical deflection of bridges B1 through B6 with different vertical supports damping ratios ζ_d(%) for cases η_{sv} = 1.5 and $\eta_{s\theta}$ = -3

Graphs in Figure 5.25 show the maximum vertical accelerations of bridges B1 through B6 for different damping ratios ζ_d (%) of the bridge supports corresponding to the selected support damping constants c_{sv}; and for values of η_{sv} = 1.5 representing very soft vertical supports and $\eta_{s\theta}$ = -3 representing free rotation of bridge ends. Again, generally, damping at supports reduces significantly the bridge accelerations. The required damping to achieve this reduction can be very high for very short bridges. For bridges with spans of 10 m (32.8 ft) or longer, it is even possible to limit the accelerations to values below the safe limit with additional damping at supports. The available damping in the structure or in the supports (i.e. bearings and foundation) may not sufficient to provide the amount of damping needed to achieve the significant reductions. For this reason, it is possible to use external dampers for this purpose.

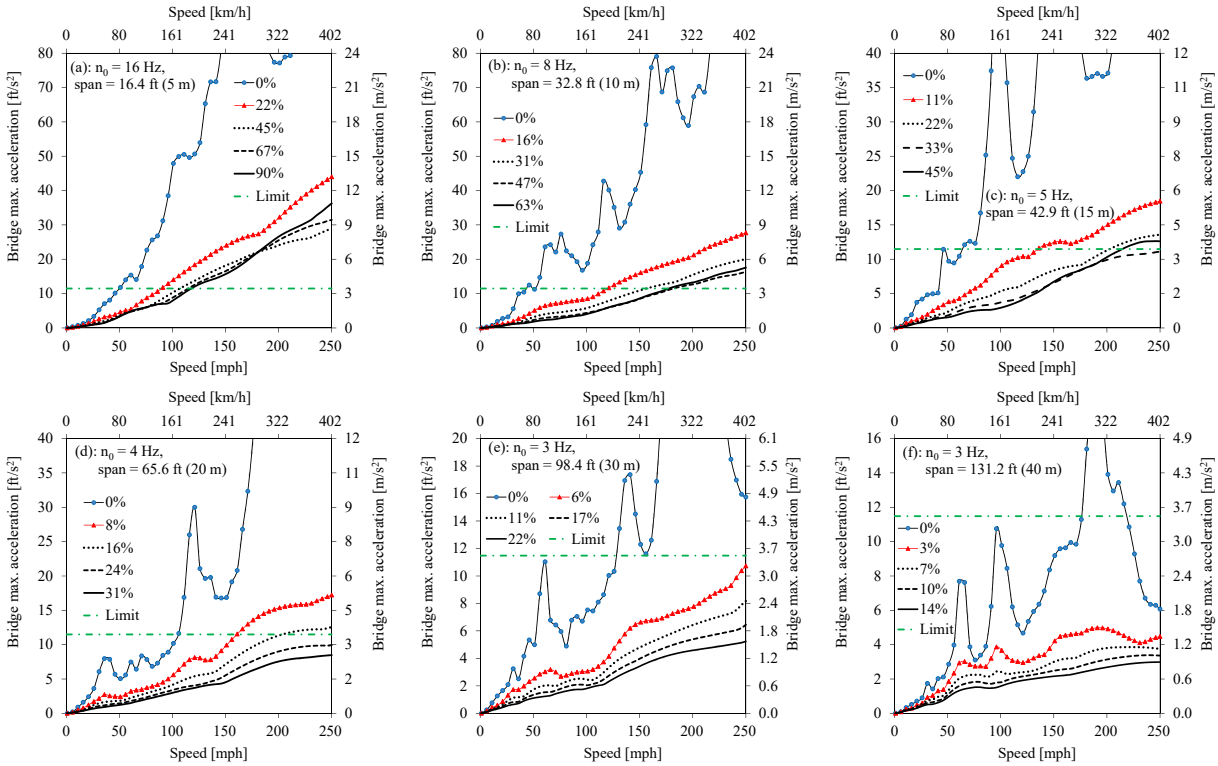

Figure 5.25 Maximum vertical acceleration of bridges B1 through B6 with different vertical supports damping ratios ζ_d(%) for cases η_{sv} = 1.5 and $\eta_{s\theta}$ = -3

5.9.5 Case of partial rotation with very soft springs and damping at supports

Graphs in Figures 5.26 and 5.27 show the maximum mid-span vertical deflections and maximum accelerations respectively of bridges B1 through B6 for different damping ratios ζ_d (%) of the bridge supports corresponding to the selected support damping constants c_{sv}; and for values of η_{sv} = 1.5 representing very soft vertical supports and $\eta_{s\theta}$ = 0 representing partial restraint of bridge end rotations. It can be seen that for very soft vertical supports, reasonable amount of damping that can be provided by external dampers can reduce deflections significantly when taking advantage of the rotational restraints at bridge ends as shown in Figure 5.26.

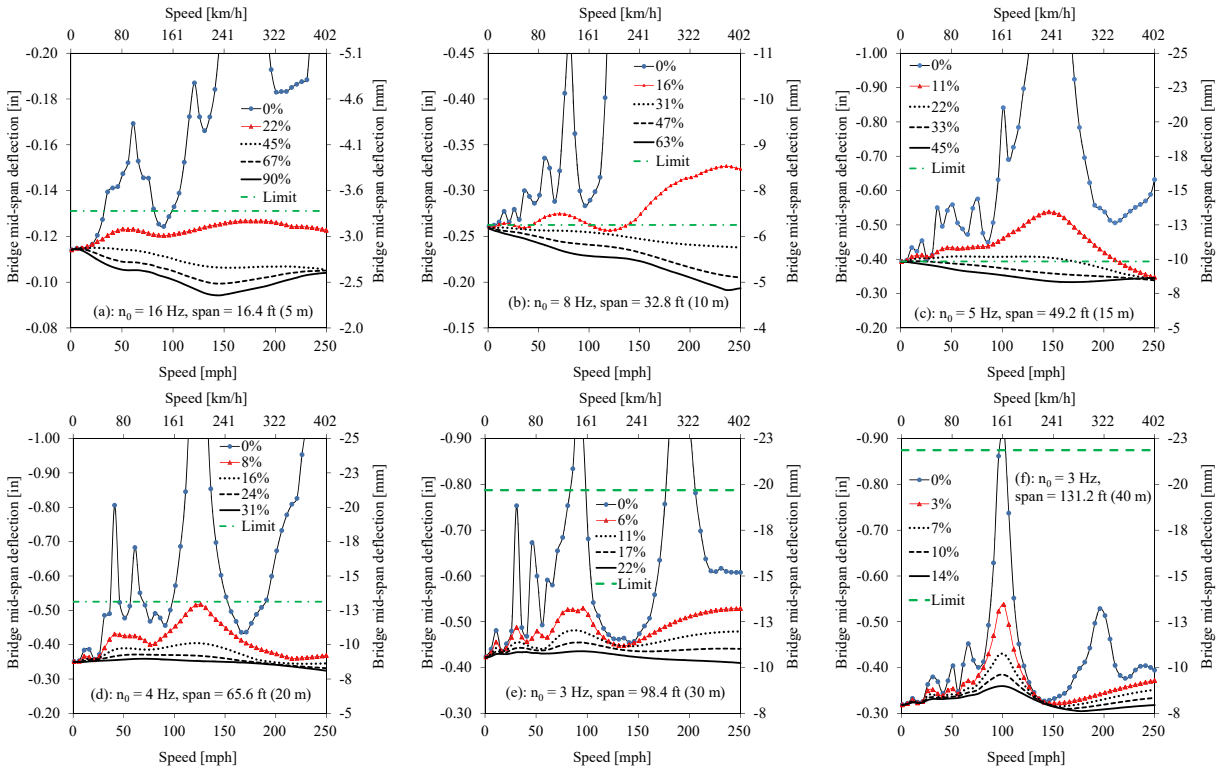

Figure 5.26 Mid-span vertical deflections of bridges B1 through B6 with different vertical supports damping ratios ζ_d(%) for cases η_{sv} = 1.5 and $\eta_{s\theta}$ = 0

Regarding the maximum vertical accelerations, it can be seen that support damping suppresses significantly the vibrations as shown in Figure 5.27. In addition, damping at supports increase the critical train speeds at which the safe limits may be exceeded. Generally, considering the bridge end rotation restraints make damping of supports more effective in reducing the dynamic responses.

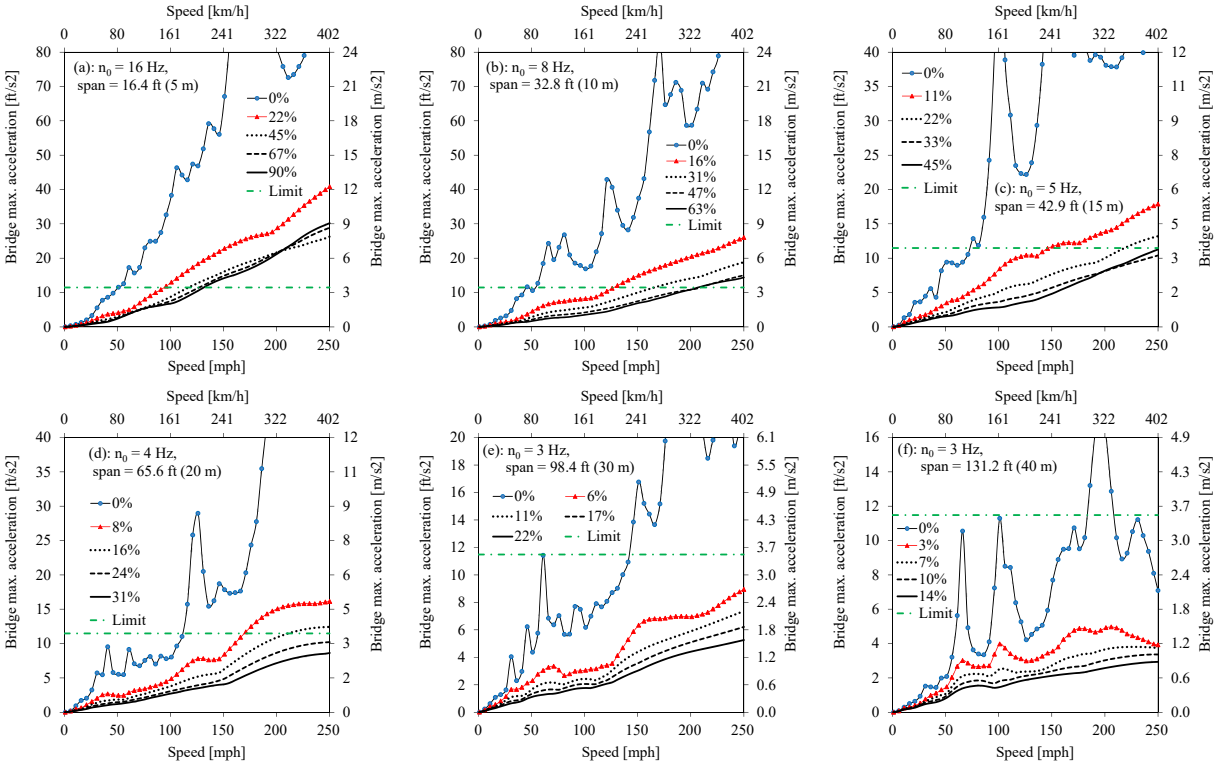

Figure 5.27 Maximum vertical accelerations of bridges B1 through B6 with different vertical supports damping ratios $\zeta_d(\%)$ for cases η_{sv} = 1.5 and $\eta_{s\theta}$ = 0

5.9.6 Case of free rotation with soft springs and damping at supports

Graphs in Figures 5.28 and 5.29 show the maximum mid-span vertical deflections and maximum accelerations respectively of bridges B1 through B6 for different damping ratios ζ_d (%) of the bridge supports corresponding to the selected support damping constants c_{sv}; and for values of η_{sv} = 2 representing soft vertical supports and $\eta_{s\theta}$ = -3 representing free rotation of bridge ends. It can be observed that, unlike very soft support conditions, soft supports may be mitigated more easily because the amount of damping needed to reduce the dynamic responses considerably are not as high as in the case of very soft supports. It appears that deflections are easier to control than vertical bridge deck accelerations using damping at the supports.

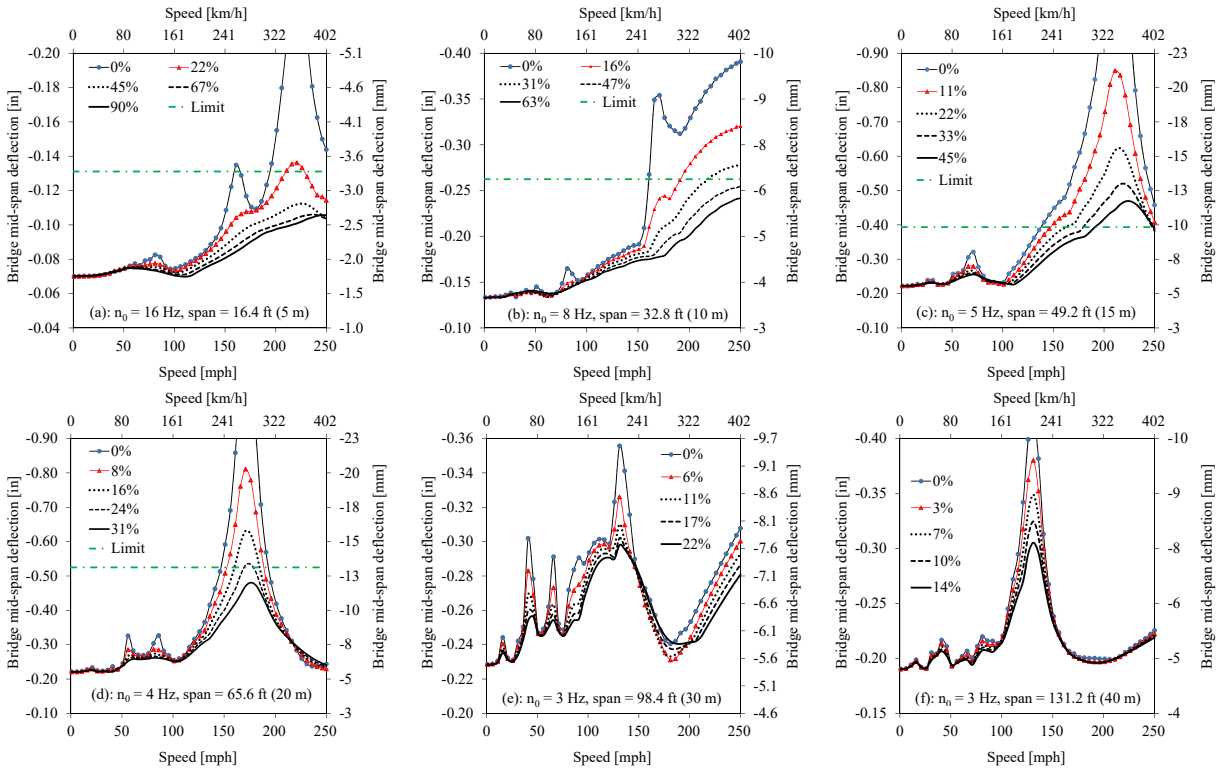

Figure 5.28 Mid-span vertical deflection of bridges B1 through B6 with different vertical supports damping ratios ζ_d(%) for cases η_{sv} = 2 and $\eta_{s\theta}$ = -3

For bridge spans less than 15m (49.2 ft), as shown in Figure 5.29, it may not possible to successfully reduce vertical bridge accelerations to values below the safe limits. However, taking into account the damping at the supports increase the train speed at which the safe limit is expected to be exceeded.

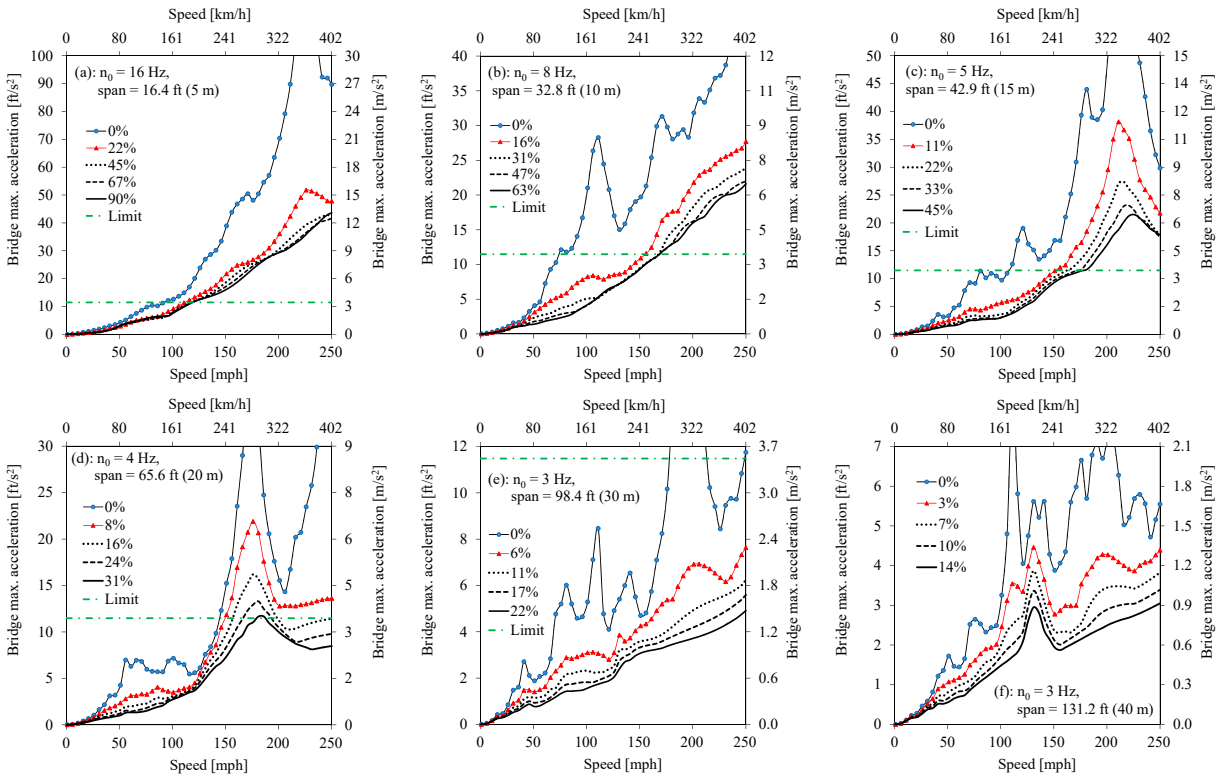

Figure 5.29 Maximum vertical acceleration of bridges B1 through B6 with different vertical supports damping ratios $\zeta_d(\%)$ for cases η_{sv} = 2 and $\eta_{s\theta}$ = -3

5.9.7 Case of partial rotation with soft springs and damping at supports

Graphs in Figures 5.30 and 5.31 show the maximum mid-span vertical deflections and maximum accelerations respectively of bridges B1 through B6 for different damping ratios ζ_d (%) of the bridge supports corresponding to the selected support damping constants c_{sv}; and for values of η_{sv} = 2 representing soft vertical supports and $\eta_{s\theta}$ = 0 representing partial end restraint of rotations at bridge ends.

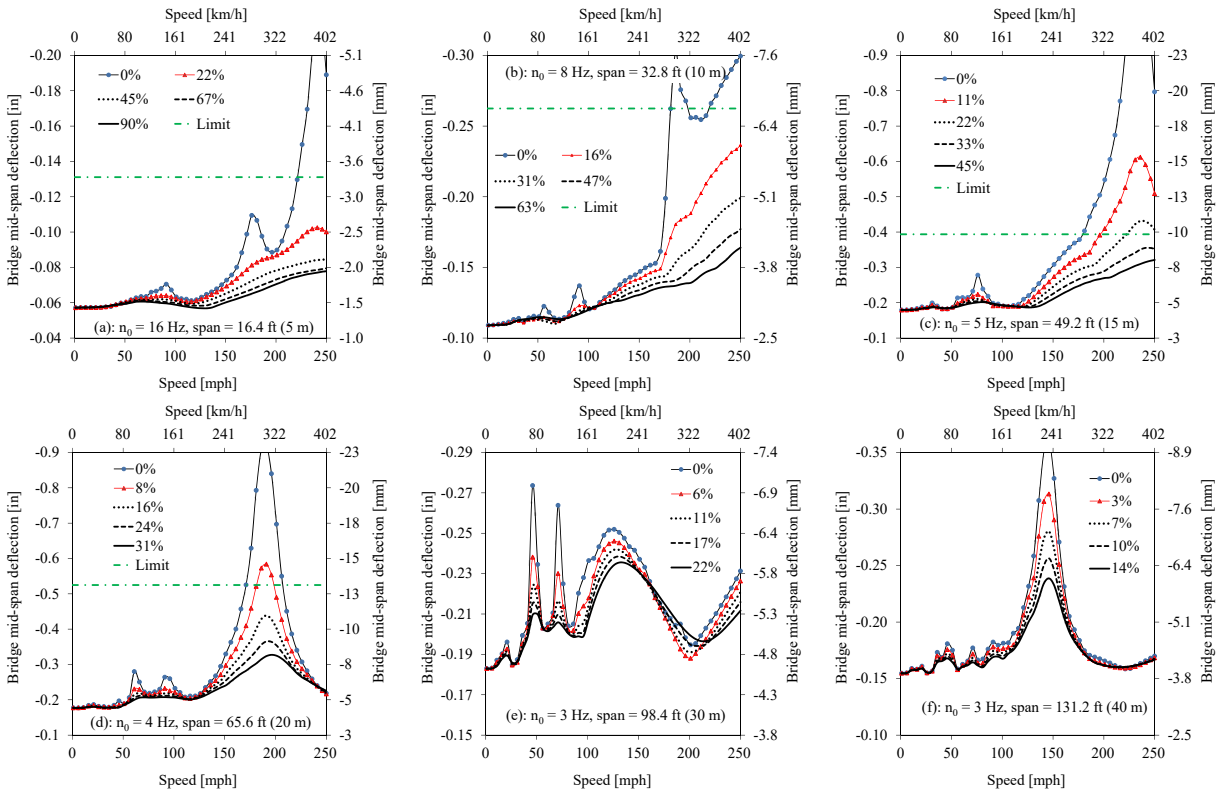

Figure 5.30 Mid-span vertical deflection of bridges B1 through B6 with different vertical supports damping ratios ζ_d(%) for cases η_{sv} = 2 and $\eta_{s\theta}$ = 0

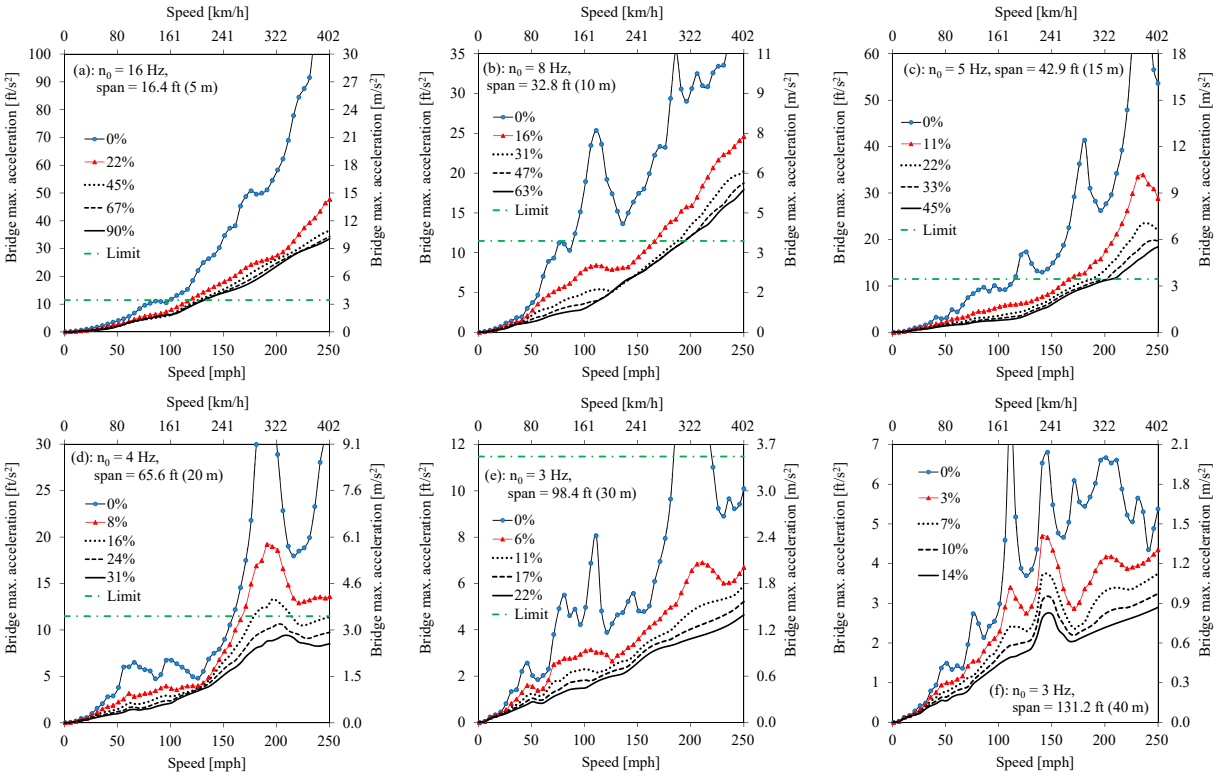

Figure 5.31 Maximum vertical acceleration of bridges B1 through B6 with different vertical supports damping ratios $\zeta_d(\%)$ for cases $\eta_{sv} = 2$ and $\eta_{s\theta} = 0$

CHAPTER 6

CONCLUSIONS

6.1. General Conclusions

The objective of this research has been to investigate short span bridges used in high speed rail networks. These types of structures have been known to cause problems associated with resonance effects resulting in excessive vibrations. Accurate predictions of responses are particularly challenging as the behavior is affected by the bridge dynamic properties while at the same time it is susceptible to the train and track dynamic properties. Theoretical methods used to carry out dynamic calculations require a balance between simplicity of models and accuracy of numerical results. Dynamic responses obtained with simple models do not correlate with experimental results in the analysis of short span high speed rail bridges. Errors are typically associated with simplistic assumptions in the model, geometric uncertainties, boundary conditions, variations in the material properties and the interactions between system components.

The author of this dissertation has been motivated by the renewed interest in High Speed Rail (HSR) in the United States where the National University Rail (NuRail) Center is currently leading a federally funded study in railway engineering that includes research on potential networks and possible increase of train speeds on shared corridors. Assessment of existing bridges which were not initially designed for high speed trains and construction of new bridges would both require proper theoretical models to predict their dynamic behavior. Within this

context in conjunction with the ongoing challenges, this research focused on the investigation of the dynamic behavior of short single span high speed rail bridges subjected to vertical loading due to a train travelling at a constant speed. The emphasis was placed on the modeling aspect of the bridge systems as well as study of its modal characteristics and dynamic simulation through numerical examples.

Chapter 2 focused entirely on a comprehensive review of available literature in this field. The review showed that many researchers carried out extensive studies related to dynamics of railway bridges, particularly in Europe. Recent Chinse efforts in their development of high speed rail networks resulted in an increase of research work related to bridges. Some of the main findings in the literature dealing with the short span high speed rail bridges are summarized below

- Numerical studies done by previous researchers showed that short span high speed rail bridges are susceptible to resonance effects particularly for speeds over 200 km/h (124 mph). This phenomenon is due to high loading frequency matching a multiple of bridge fundamental frequency. Vertical accelerations at resonance speeds are significantly amplified and may possibly exceed safe limits of 3.5 m/s^2 for short span bridges.
- Analysis and design of short span high speed rail bridges are primarily based on the work of ERRI D214 committee who proposed a set of procedures to follow in the determination of dynamic calculation requirements and serviceability limit checks related to bridge deformations. However, these guidelines are limited to simply supported bridges and simplified load models were used in the work of the committee.
- It is documented in the literature that moving load models are not well suited in the study of short span bridges since numerical results from previous studies showed that these

models overestimate the dynamic response at resonance regime compared to models incorporating the vehicle interaction. International codes recommend the use of an additional fictitious damping for the bridge to account for the effects of vehicle interaction. However, many researchers found this to be too simplistic and not widely applicable to most real structures.

- Recent studies incorporating the track structure in the numerical models reported some contradicting conclusions. As discussed in Chapter 2, some authors indicated the track has no effects on bridge responses while other authors observed the opposite. A model including both the track and the train has unique challenges. In some short bridges, it is believed that the track plays some role in the load distribution and therefore results in lower dynamic responses. However, there is no widespread use of the train-track-bridge interaction model and its effects on the overall bridge dynamic responses at resonance speeds have not been fully studied yet.
- There is a lack of extensive work on the effects of boundary conditions on short span high speed rail bridges. Some previous partial work concluded that flexible supports in the vertical direction reduce bridge natural frequencies. However, there is little research focused on the impact of bridge supports flexibility considering both the vertical stiffness and rotational stiffness as well as the effects of damping at the supports.

Chapter 3 was dedicated to the development of a numerical model that takes into account the interactions between the train travelling at a constant speed, the track structure and the bridge supports. The Train-Track-Bridge Interaction (TTBI) system was treated as two separate subsystems. The equations of motion of the train vehicle as a moving subsystem and the equations of motion of the underlying stationary train-bridge subsystem were formulated

independently. The interaction between the two subsystems was assumed to occur at the contact interface where a no-separation condition between the wheels and the rails was enforced through constraint equations. The track-bridge finite elements were assumed to consist of contact elements impacted by the wheels and non-contact elements free of wheels. Using dynamic condensation and Hermitian cubic interpolation functions, the wheels' degrees of freedom at the contact points were related to the global nodal displacement vector of the rail beam. Velocity and acceleration vectors of the contact points were then formulated with the first and second derivatives respectively of the displacement vector. After the wheels' displacement, velocity and acceleration vectors were computed using the global deformations of the underlying structure from the previous time step the vehicle's equations of motion were solved using modified Newmark finite difference schemes using HHT alpha method. From the vehicle's equations of motion, contact forces were obtained which were then used to solve the track-bridge equations of motion for the next time step in the direct time integration algorithms. The bridge supports conditions have been included using vertical spring-damper elements and rotational springs. The developed model was validated comparing results with those obtained using a semi-analytical method in Section 3.6.1 and with results of previous researchers in Section 3.6.2. Both sets of results showed very good agreement of results thus indicating that the formulated contact algorithms perform well in the dynamic calculations.

Chapter 4 was dedicated to the evaluation of natural frequencies of track-bridge systems used in high speed rail. The objective was to understand the effects of model aspects and parameters on the free vibration responses of the structure. The bridge without the track structure was evaluated as a simply supported beam or as a beam on vertical elastic supports. Influence of the shear deformation and rotational inertia was examined. Effects of the track structure on a

simply supported bridge were then investigated. The combined effects of vertical spring and rotational spring at supports were studied. Proper estimation of natural frequencies of high speed rail bridges is necessary since dynamic responses strongly depend on this parameter. The following conclusions can be drawn from the work presented in Chapter 4 regarding the influences of model characteristics on the natural frequencies.

- Natural frequencies of the bridge decrease when shear deformations and rotational inertia effects are considered. The decrease is more significant with the decrease of the slenderness ratio of equation (4.11f) and increase of the shear deformation parameter of equation (4.11g). Generally the analysis using Timoshenko beam theory is more accurate than Euler-Bernoulli beam theory, particularly at high speed and for shorter bridges.
- The vertical stiffness of supports at the two ends of the bridge, assumed to be equal, has a significant effect on the natural frequencies of the bridge. The vertical stiffness ratio, which is a ratio of the vertical stiffness of supports to bridge flexural stiffness, determines the degree of flexibility in the boundary conditions. The natural frequencies of the bridge are reduced when this ratio decreases. For a given value of this ratio, the decrease is more significant in the frequencies of higher modes. Also, for constant support conditions, the decrease in natural frequencies is more significant as the bridge span decreases.
- The ballast mass is usually within a narrow range of practical values. Therefore, because short span high speed rail bridges have relatively lower total mass than longer bridges, the additional ballast mass decreases the natural frequencies. For the logarithmic value of the vertical stiffness ratio, equation (4.14), less than 2, the ballast mass has no significant effect on the fundamental frequency. The mass of the ballast should be considered in the calculation of natural frequencies for short span bridges.

- For short span bridges with rigid supports, the vertical stiffness of the ballast has negligible effects on the natural frequencies. However, the effects become more significant in decreasing the natural frequency for bridges with flexible supports.
- An increase in the rotational restraint of the bridge supports leads to an increase of the natural frequencies. Values of the fundamental frequency for a bridge with rotational flexible at the supports are between 1 and 1.5 times the fundamental frequency of the simply supported bridge.

In Chapter 5, the numerical model developed in Chapter 3 was used to carry out dynamic simulations on two sets of Group A and Group B bridges. The group A bridges were low mass steel open-deck plate-girder short bridges designed according to AREMA specifications. Group B bridges were reinforced concrete short span high speed rail bridges adopted from the ERRI D 214 catalogue of benchmark bridges. Group A bridges were used in conjunction with Group B bridges in the first part of the simulations to investigate the influence of the shear deformations and rotational inertia on short span bridges. Later, group B bridges were used to study the effects of vehicle interaction, track structure, trainset types, track irregularities and boundary conditions. The following general conclusions can be drawn based on the results of dynamic simulations carried out in Chapter 5.

- Effects of shear deformations and rotational inertia can be ignored in the dynamic analysis of short span high speed rail bridges when the slenderness ratio as defined by equation (5.1) is greater than 50. However, the dynamic responses grow larger as the slenderness ratio becomes smaller. Also the speed at which resonance occurs is smaller when these effects are included because the natural frequencies are reduced. For shorter and stocky types of bridges, the responses due to these effects are

significantly amplified, particularly in acceleration magnitudes at higher train speeds. The combined effects of the slenderness ratio and shear correction factors on the static deflection of the bridge can be approximate in a preliminary design or analysis using the proposed equation (5.11) which leads to an increase of as much as twice for a slenderness ratio of 10.

- In General, taking into account both the vehicle interaction and track structure is beneficial in improving accuracy of dynamic responses. Results of the numerical simulations in short span high speed rail bridges showed that the vehicle interaction decreases the responses at resonance speeds. Results also showed that the track structure reduces also the peak dynamic responses at resonance. This reduction is significant for shorter bridges. For example, for the cases of this study, reductions of about 30-50% in the vertical acceleration were observed for all simulated bridges.
- For very short bridges less than 5 m (16.4 ft) span, resonance occurs under the front bogie of the intermediate coaches. The bridge vibrates freely between the departure of the front bogie and the arrival of the rear bogie.
- Resonance conditions occur at train speeds which are very close to the service speed for the studied 5 m (16.4 ft), 10 m (32.81 ft) and 20 m (65.62 ft) bridges resulting in high vertical accelerations exceeding the safe limit of 3.5 m/s^2 (11.3 ft/s^2). For bridge spans less than 10 m (32.8ft), accelerations could even exceed the ultimate limit of 0.7g, a situation that could destabilize the track.
- The changes in magnitudes of the track vertical stiffness and damping do not have any effects on the dynamic responses of bridges with span greater than 10 m (32.81 ft) and minimal effects on very short bridges less than 10 m (32.81 ft). Both the track

vertical stiffness and damping have effects on the response of the track itself. A combination of low stiffness and low damping increases the track response particularly at higher speeds. The damping of the track has no effects on the responses of the vehicle while a low stiffness increases the vehicle responses.

- Among the six different types of trainset that were investigated, it was found that the Japanese SKS N700-I has the least impact on the bridge responses due to its lower axle loads. However, the passenger comfort in its leading car is not necessarily the best among the studied trainset since the leading car vertical acceleration is more than some other heavier car like the ICE-3 which has the least vertical acceleration in the leading car. This is due to the fact that, despite its higher axle load, the ICE-3 has better suspension systems. The Amtrak Acela, with a leading car having twice the axle load of SKS N700-I, has the most negative impact on bridge deflections except on the 15 m (49.2 ft) and 20 m (65.62 ft) bridges. The vertical acceleration of the leading car is also the highest for Amtrak Acela.
- Elastic properties of the boundary conditions have significant effects on bridge dynamic responses. The logarithmic value (η_{sv}) of the support vertical stiffness to bridge flexural stiffness given by equation (5.2) and the logarithmic value ($\eta_{s\theta}$) of the support rotational stiffness to bridge rotational stiffness given by equation (5.3) are two important non-dimensional parameters that can be used to make a rough assessment of the degree of flexibility in the bridge boundaries. Generally dynamic bridge responses increase when η_{sv} decreases; and they increase when $\eta_{s\theta}$ increases. However, The ratio η_{sv} is more critical than the ratio $\eta_{s\theta}$.

- For values of $\eta_{sv} > 3$, the bridge can be modeled as a simply supported structure since there are no significant differences. For values $\eta_{sv} \leq 3$, the fundamental frequency is reduced and the mode shapes become a combination of rigid modes and flexural modes. For very soft vertical supports with values $\eta_{sv} < 2$, rigid mode dominates.

- For values of $\eta_{sv} \leq 2.5$ dynamic responses are significantly amplified and the consideration of the damping in the bridge supports becomes critical. It was found that damping is more effective for smaller η_{sv} ratios. In flexible supports with $\eta_{sv} \leq 2$, the available structural damping in elastomeric bearings and soil foundation may not be sufficient to obtain an acceptably reduced response. In that case, additional damping in the form of external devices such as Fluid Viscous Dampers (FVD) installed at the supports may be an efficient method in controlling the high vertical accelerations in high speed rail short span bridges.

6.2. Practical Recommendations

Single span short bridges typically used in crossing urban roads, creeks, rivers or wildlife trails are usually considered to have a relatively low budget compared to larger viaducts, signature bridges or iconic structures such as cable-stayed bridges or suspension bridges. Consequently, they are assigned a correspondingly low budget for engineering which necessitates often times the use of simple methods of modeling to predict the dynamic responses. Although this philosophy may be acceptable in highway bridges which are mostly governed by the strength ultimate limit state criteria, it becomes problematic for high speed rail bridges where high frequency loading may cause resonance with dynamic responses approaching or exceeding

the safe limits in the serviceability limit state. Within this context the lessons learnt from this research can be viewed in terms of the engineer's decisions regarding the numerical modeling approach that needs to be taken and whether this approach is adequate for the design of a new bridge or the assessment of an existing bridge. Therefore, based on the knowledge gained in this research, the author of this dissertation is making the following general practical recommendations related to short span high speed rail bridges:

- The concept of "service provider" is useful to visualize the entire system of the train-track-bridge interaction problem from the bottom up. For example, the bridge supports consisting of the bearings and soil foundation can be viewed as providing a "service" to the bridge; in turn, the bridge is providing a "service" to the track structure; and the track is providing a "service" to the train. The elastic properties between these different subsystems should not be ignored as the dynamic responses are reduced when energy dissipation elements are included in the modeling. This is particularly necessary for the capacity assessment of existing bridges where neither too much overestimation nor too much underestimation of dynamic responses is acceptable.
- The boundary conditions can be considered rigid and therefore the bridge analyzed as a simply supported structure if the ratio $\eta_{sv} > 3$, see equation (5.2). However, if the value of this ratio is such that $2.5 \leq \eta_{sv} \leq 3$, the bridge may be analyzed as a simply supported structure with the expectations that the peak dynamic responses would be 3% to 7% higher than the simply supported case which should be taken into consideration. If the ratio $\eta_{sv} < 2.5$, the bridge boundary conditions should be considered flexible and the numerical model should include spring-damper elements at the bridge boundaries.

- The considerations of rotational restraints in the bridge boundaries are always beneficial and shall be included if refined dynamic calculations are desired.
- If the objective is to study the effects of vertical loading only, 2D numerical model is generally sufficient.
- When dynamic responses of the bridge are above the safe limits in accelerations and deflections, the track structure should be first considered before including the vehicle interaction since the track-bridge finite element is easier than the analysis of the train-track-bridge interaction problems. However, if refined dynamic calculations are required, particularly if responses in the vehicle are needed, the effects of the train interaction should be included.
- When the objective of the analysis includes a check for passenger comfort, both the track structure and the train interaction should be considered.
- The assessment of existing short span bridges shall always consider the effects of boundary conditions with at least linear viscoelastic elements as well as the track structure and train interaction. When the boundary conditions are estimated to be soft with $\eta_{sv} < 2.5$ in existing bridges, retrofit with external dampers shall be considered to reduce excessive vibrations.

6.3. Suggestions for Further Research

The following are suggestions for future research work related to the numerical modeling and dynamic behavior of short span high speed rail bridges.

1. Development of a 3D numerical model of the train-track-bridge interaction problems which would encourage more research in the following :

- Investigation of bridge torsional vibration due to train running off the center-line of the structure.
- Effects of lateral interaction of wheels and rails on the overall bridge dynamic responses including transverse external loadings such as cross-winds on the train coaches.
- Impact of different random irregularity profiles on the two tracks of a double-track bridge.
- Dynamic response of a bridge with a double-track crossed by two high speed trains simultaneously running in opposite directions.

2. Effects of train longitudinal acceleration and deceleration on the dynamic response of short span high speed rail bridges.
3. Bridges studied in this research were single span bridges. Similar research on the dynamic responses of continuous bridges would be interesting.
4. It is suggested that further studies be undertaken regarding the analysis of the train-track-bridge-support interaction problems including the non-linearity of system elastic properties.
5. The numerical results in this research showed that increasing damping at the bridge supports significantly reduces bridge dynamic responses. However, in short and very short bridges the required damping could be high in some cases. This could be further investigated with an experimental work, particularly the possibility of adding external vertical and horizontal dampers at bridge abutments to handle both vertical vibrations due to traffic as well as horizontal loading due to seismic events.

CITED LITERATURE

Akin, J.E. and Mofid, M.: Analytical Numerical Solution for Response of Beams with Moving Mass. Journal of Structural Engineering, ASCE 115(1):120-131, 1989.

Alvarez, R.: Dynamic Interaction of Vehicle-Track-Structure in Railway Bridges. PhD Thesis, Polytechnic University of Madrid, Madrid, 1984.

Araujo, N.M.F.: High-speed trains on ballasted railway track: dynamic stress field analysis. PhD Thesis, Universidade do Minho, Portugal, 2011.

AREMA 136-Ib/yd Rail, Retrieved 1/1/2016, http://harmersteel.com/catalog/tee-rails/136-lbyd-arema-rail/

AREMA 141-Ib/yd Rail, Retrieved 1/1/2016, http://harmersteel.com/catalog/tee-rails/141-lbyd-arema-rail/

Bathe, K.J.: Finite element procedures. Upper Saddle River, NJ, USA, Prentice-Hall, 1996.

Biggs, J.M.: Introduction to Structural Dynamics. New York, McGraw-Hill, 1964.

Biondi, B., Muscolino, G. and Sofi, A.: A Substructure Approach for the Dynamic Analysis of Train-Track-Bridge System. Computers & Structures, 83:2271–2281, 2005.

Bleich, F.: Theorie und Berechnung der Eisernen Brücken. Springer, 1924.

Brady, S.P., O'Brien, E.J. and Znidaric, A.: Effect of vehicle velocity on the dynamic amplification of a vehicle crossing a simply supported bridge. Journal of Bridge Engineering, ASCE 11(2):241-249, 2006.

California High-speed Train Project (CHSTP): Design Criterial Manual, Rev.2, California, USA, 2014.

Casal, H: Comportamento Dinâmico de Pontes Ferroviárias de Alta Velocidade: efeito da via não balastrada. MSc Thesis, Universidade Técnica de Lisboa, Lisboa, Portugal, 2010

Chen, Y.H. and Li, C.Y.: Dynamic response of elevated high-speed railway. Journal of Bridge Engineering, ASCE 5(2):124-130, 2000.

Cheng, Y.S., Au, F.T.K. and Cheung, Y.K.: Vibration of railway bridges under a moving train by using bridge-track-vehicle element. Engineering Structures, 23(12):1597-1606, 2001.

Cheung, Y.K., Au, F.T.K., Zheng, D.Y., and Cheng, Y.S.: Vibration of multi-span non-uniform bridges under moving vehicles and trains by using modified beam vibration functions. Journal of Sound and Vibration, 228(3):611-628, 1999.

China High Speed Rail. Retrieved January 1, 2016, from http://www.chinadiscovery.com/china-high-speed-train-tours/china-high-speed-rail.html

Chu, K.H., Garg, V.K., and Dhar, C.L.: Railway-bridge impact: simplified train and bridge model. Journal of the Structural Division, 105:1823-1844, September 1979.

Chu, K.H., Garg, V.K., and Wiriyachai, A.: Dynamic interaction of railway train and bridges. Vehicle System Dynamics, 9:207-236, 1980.

Chu, K.H., Garg, V.K., and Wang, T.L.: Impact in railway prestressed concrete bridges. Journal of Structural Engineering, 112(5):1036-1051, 1986.

Clark, R.A., Dean, P.A., Elkins, J.A., and Newton, S.G.: An investigation into the dynamic effects of railway vehicles running on corrugated rails. Journal of Mechanical Engineering Science, 24(2):65-76, 1982.

Delgado, R. and Santos, S.M.: Modelling of railway bridge-vehicle interaction on high speed tracks. Computers & Structures, 63 (3):511-523. 1997.

Duffy, D.G.: The response of an infinite railroad track to a moving, vibrating mass. Journal of Applied Mechanics, 57:66-73, 1990.

Dugush, Y.A. and Eisenberger, M.: Vibrations of non-uniform continuous beams under moving loads. Journal of Sound and Vibration 254(5):911-926, 2002.

European Committee for Standardization (CEN): Eurocode 1 – Basis of structural design. European Committee for Standardization (CEN), Brussels, 2002.

European Committee for Standardization (CEN): Eurocode - Actions on structures - Part2: Traffic loads on bridges. European Committee for Standardization (CEN), Brussels, 2003.

European Rail Research Institute (ERRI): Rail bridges for speeds over 200 km/h. Final Report. ERRI D214/RP 9, Brussels, 1999.

Fournol, A., and Dieleman, L.: Comportement dynamique de pont-rails courts. Revue européenne de génie civil, 9(1-2): 215-232, 2005.

Fries, R. H. and Coffey, B. M.: A state-space approach to the synthesis of random vertical and crosslevel rail irregularities. J. Dyn. Syst., Measurement, and Control, 112(1):83–87, 1990.

Frýba, L.: The dynamic influence of wheel flats on railway bridges. Intl. Railway Congr. Assoc. Bullet., 477-512, 1967.

Frýba, L.: Vibration of Solids and Structures under Moving Loads. Groningen, Netherlands, Noordhoff International Publishing, 1972.

Frýba, L.: Dynamics of Railway Bridges. London, Thomas Telford, 1996.

Frýba, L. and Naprstek, J.: Appearance of resonance vibration on railway bridges. In "Advances in Civil and Structural Engineering Computing for Practice", 377-382. Civil-Comp Press, 1998.

Frýba, L.: Vibration of Solids and Structures Under Moving Loads. 3rd Ed.. Thomas Telford, 1999.

Frýba, L.: A rough assessment of railway bridges for high-speed lines. Engineering Structures, 23:548-556, 2001.

Frýba, L.: Dynamics of bridges under moving loads (past, present and future). In: Dynamics of High-Speed Railway Bridges, eds. Delgado, R., Calcada, R.,Goicolea, J.M., and Gabaldon, F., pp. 19-34, 2009.

Garg, V.K. and Dukkipati, R.V.: Dynamics of Railway Vehicle Systems. Toronto, Canada, Academic Press, 1984.

Gbadeyan, J.A. and Oni, S.T.: Dynamic behaviour of beams and rectangular plates under moving loads. Journal of Sound and Vibration 182(5):677-695, 1995.

Genin, J., Ting, E.C., and Vafa, Z.: Curved bridge response to moving vehicle. J. Sound and Vibration, 81(4):469-475, 1982.

Green, M.F. and Cebon, D.: Dynamic response of highway bridges to heavy vehicle loads: Theory and experimental validation. Journal of Sound and Vibration 170(1):51-78, 1994.

High Speed Rail in China. In Wikipedia. Retrieved January 1, 2016, from https://en.wikipedia.org/wiki/High-speed_rail_in_China

High-Speed Rail in Europe. In Wikipedia. Retrieved January 1, 2016, from https://en.wikipedia.org/wiki/High-speed_rail_in_Europe

Hilber, H.M., Hughes, T.J.R and Taylor, R.L.: Improved numerical dissipation for time integration algorithms in structural dynamics. Earthquake Engineering and Structural Dynamics, 5:283-292, 1977.

Humar, J.L. and Kashif, A.M.: Dynamic response of bridges under travelling loads. Can. J. Civ. Eng. 20:287-298, 1993.

Hutton, S.G. and Cheung, Y.K.: Dynamic response of single span highway bridges. Earthquake Engineering and Structural Dynamics, 115(1):120-131, 1979.

Hwang, E.S. and Nowak, A.S.: Simulation of dynamic load for bridges. Journal of Structural Engineering, ASCE 117(5):1413-1434, 1991.

Infraspeed: High Speed in the Low Lands. Infraspeed, Zoetermeer, 2006.

Inglis, C. E.: A Mathematical Treatise on Vibrations in Railway Bridges. Cambridge University Press, 1934.

Karnovsky, I. A. and Lebed, O. I.: Formulas for Structural Dynamics: Tables, Graphs, and Solutions. New York, NY, McGraw-Hill Professional Publishing, 2000.

Kawazoe, K., Kono, I., Aida, T., Aso, T. and Eibisuda, K.: Beam-type Dynamic Vibration Absorber Compromised of free-free Beam. Journal of Engineering Mechanics, 124(4):476–479, 1998.

Klasztorny, M., and Langer, J.: Dynamic response of single-span beam bridges to a series of moving loads. Earthquake Engineering and Structural Dynamics, 19:1107-1124, 1990.

Le, R., Ripke, B. and Zacher, M.: Ballast mats on high speed bridges. Proceedings of the fourth European Conference on Structural Dynamics (Eurodyn '99), volume 2, pp 699-703. A.A. Balkema, 1999.

Lee, Y.S. and Kimb, S.H.: Structural analysis of 3D high-speed train–bridge interactions for simple train load models. Vehicle System Dynamics, 48 (2):263-281, 2010.

Lee, S. Y. and Lin, S. M.: Vibrations of elastically restrained non-uniform Timoshenko beams. Journal of Sound and Vibration, 183(3):403-415, 1995.

Lei, X. and Noda, N.A.: Analyses of dynamic response of vehicle and track coupling system with random irregularity of track vertical profile. Journal of Sound and Vibration, 258 (1):147-165, 2002.

Lin, Y.H. and Trethewey, M.W.: Finite element analysis of elastic beams subjected to moving dynamic loads. Journal of Sound and Vibration, 136(2):323-342, 1990.

Lou, P.: A vehicle-track-bridge interaction element considering vehicle's pitching effect. Finite Elements in Analysis and Design, 41(4):397-427, 2005.

Lou, P. and Zeng, Q.: Formulation of equations of motion of finite element form for vehicle-track-bridge interaction system with two types of vehicle model. International journal for numerical methods in engineering, 62:435-474, 2005.

Lou, P., Dai, G.L. and Zeng, Q.Y.: Dynamic analysis of a Timoshenko beam subjected to moving concentrated forces using the finite element method. Shock and Vibration, 14:459-468, 2006.

Majka, M. and Hartnett, M.: Effects of Speed, Load and Damping on the Dynamic Response of Railway Bridges and Vehicles. Computers & Structures, 86(6):556–572, 2008.

Man, A.: A survey of dynamic railway track properties and their quality. PhD thesis, TU Delft, DUP–Science, Delft, 2002.

Maunder, L.: On the work of a force crossing a beam. Quarterly Journal of Applied Mathematics, 17(4):437-440, 1960.

Maurizi, M. J., Ross, R. E. and Belles, P. M.: Free vibrations of uniform Timoshenko beams with ends elastically restrained against rotation and translation. Journal of Sound and Vibration, 141(2):359-362, 1990.

Negrut, D., Ottarsson, G., Rampalli, R., and Sajdak, A.: On an implementation of the Hilber-Hughes-Taylor method in the context of index 3 differential-algebraic equations of multibody dynamics (DETC2005-85096). Journal of Computational and Nonlinear Dynamics, 2(1):73-85, 2007.

Neves, S.G.M., Azevedo, A.F.M. and Calçada, R.: A direct method for analyzing the vertical vehicle-structure interaction. Engineering Structures, 34:414-420, 2012.

Neves, S.G.M., Montenegro, P.A., Azevedo, A.F.M. and Calçada, R.: A direct method for analyzing the nonlinear vehicle–structure interaction. Engineering Structures, 69:83-89, 2014.

Newmark, N.M.: A method of computation for structural dynamics. Proc. Am. Soc. Civil Eng., 85(3):67-94, 1959.

Nguyen, D.V., Kim, K.D. and Warnitchai, P.: Dynamic analysis of three-dimensional bridge-high-speed train interactions using a wheel-rail contact model. Engineering Structures, 31 (12):3090-3106, 2009a.

Nguyen, D.V., Kim, K.D. and Warnitchai, P.: Simulation procedure for vehicle–substructure dynamic interactions and wheel movements using linearized wheel–rail interfaces. Finite Elements in Analysis and Design, 45 (5):341-356, 2009b.

Nour, S.I. and Issa, M.A.: Effects of Different Models on Natural Frequencies of Short Span Bridges Used in High Speed Rail. Proceedings of the ASME 2015 Joint Rail Conference, JRC2016-5772, San Jose, CA, USA, March 23-26, 2015.

Nour, S.I. and Issa, M.A.: High Speed Rail Short Bridge-Track-Train Interaction Based on the Decoupled Equations of Motion in the Finite Element Domain. Proceedings of the ASME 2016 Joint Rail Conference, JRC2016-5785, Columbia, SC, USA, April 12-15, 2016.

Olsson, M.: On the fundamental moving load problem. Journal of Sound and Vibration, 145(2):299-307, 1991.

Oniszczuk, Z.: Transverse Vibrations of Elastically Connected Double-String System", Parts I, II. Journal of Sound and Vibration, 232(2):355–386, 2000.

Oscarsson, J., and Dahlberg, T.: Dynamic train/track/ballast interaction – computer models and full-scale experiments. Vehicle System Dynamics Supplement, 28:73-84, 1998.

Owen, D.R.J. and Hinton, E.: Finite Elements in Plasticity: Theory and Practice. Swansea, UK, Pineridge Press Limited, 1980.

Pesterev, A.V., yang, B., Bergman, L.A. and Tan, C.A.: Response of elastic continuum carrying multiple moving oscillators. J. Eng. Mech., ASCE 127(3):260-265, 2001.

Pesterev, A.V., Bergman, L.A., Tan, C.A., Tsao, T.C., Yang, B.: On asymptotics of the solution of the moving oscillator problem. Journal of sound and Vibration 260:519-536, 2003.

Pielorz, A.: Nonlinear discrete-continuous models in the analysis of low structures subject to kinematic excitations caused by transversal waves. Journal of Theoretical and Applied Mechanics, 36(4):979-999, 1998.

Podworna, M.: Modelling of random vertical irregularities of railway tracks. Int. J. of Applied Mechanics and Engineering, 20(3):647-655, 2015.

Proença, J. M., Casal, H. and Neves, M.: Effect of the type of track on the dynamic behaviour of high speed railway brigdes. In: 3rd ECCOMAS Thematic Conference on Computational Methods in Structural Dynamics and Earthquake Engineering, eds. M. Papadrakakis, M. Fragiadakis, V. Plevris, COMPDYN 2011, Corfu, Greece, 2011.

Rail.One: Rheda 2000® Ballastless Track System. Railone.com. Retrieved 3/4/2016, http://www.railone.com/fileadmin/daten/05-presse-medien/downloads/broschueren/en/Rheda2000_EN_2011_ebook.pdf

Rail Technical Guide, Retrieved 1/1/2016, www.tatasteeleurope.com/static_files/Downloads/Rail/Rail%20technical%20guide%20Eng.pdf

Rao, G.V.: Linear dynamics of an elastic beam under moving loads. J. Vibr. & Acous., ASME 122(7):281-289, 2000.

Reckmann, H.: Aktive Schwingungsreduktion an einem elastischen Fahrweg unter bewegter Masse. Fortschritte-Berichte VDI, Reihe 11, No. 309, VDI Verlag, 2002.

Richardson, H.H. and Wormley, D.N.: Transportation vehicle/beam-elevated guideway dynamic interactions, a state-of-the art review. J. Dynamics Systems Measurement and Control, 96:169-179, 1974.

Sadiku, S. and Leipholz, H.H.E.: On the dynamics of elastic systems with moving concentrated masses. Ingenieur-Archiv 57:223-242, 1987.

Shinkansen Route Map. Retrieved January 1, 2016, from http://www.nippon.com/en/features/h00077/

Song, M.K., Noh, H.C. and Choi, C.K.: A new three-dimensional finite element analysis model of high-speed train–bridge interactions. Engineering Structures, 25:1611–626, 2003.

Stanišić, M.M. and Hardin, J.C.: On the response of beams to an arbitrary number of concentrated moving masses. J. Franklin Inst. 287:115-123, 1969.

Stanišić, M.M.: On a new theory of the dynamic behavior of the structures carrying moving masses. Ingenieur-Archiv 55:176-185, 1985.

Stokes, G. G.: Mathematical and Physical Papers. Vol.2, Cambridge, 1847.

Tartary, J.P. and Fournol, A.: Railway bridges damping identification using traffic induced vibration. Proceedings of the fourth European Conference on Structural Dynamics (Eurodyn '99), volume 2, pp 705-710. A.A. Balkema, 1999.

Taylor, W.: Iron, Engineering and Architectural History in Crisis: Following the Case of the River Dee Bridge Disaster, 1847. Architectural Histories, 1(1):13, 2013.

Teixeira, P.F.: Contribución a la Reducción de los costes de Mantenimiento de Vías de Alta Velocidad Mediante la Optimización de su Rigidez Vertical. PhD Thesis, Universidade Politécnica de Catalunha, Barcelona, 2003.

Thambiratnam, D.P., and Zhuge, Y.: Dynamic analysis of beams on an elastic foundation subjected to moving loads. Journal of Sound and Vibration, 198(2):149-169, 1996.

Timoshenko, S.P.: On the forced vibrations of bridges. Philosophical Magazine Series 6, 43(257):1018-1019, 1922.

Timoshenko, S.P.: Vibration of Bridges. American Society of Mechanical Engineers, Transactions, Vol.53, 1928. In "Vibration Problems in Engineering", D. Van Nostrand, 3rd Ed., 1955.

Timoshenko, S.P. and Young, D.H.: Vibration Problems in Engineering, 3rd Edition. New York, D. Van Nostrand, 1955.

Ting, E.C., Genin, J. and Ginsberg, J.H.: A general algorithm for the moving mass problems. Journal of Sound and Vibration 33(1):49-58, 1974.

Ting, E.C. and Genin, J.: Dynamics of bridge structures. Struct. Mech. Archives, 5(3):217-252, 1980.

Tünnissen, Joep T. F. M.: Dynamic aspects of the high-speed railway bridge across the Hollandsch Diep. In: Workshop Track-Bridge Interaction on High-Speed Railways. FEUP, Universidade do Porto, Porto, 2007.

US High Speed Rail Map. Retrieved January 1, 2016, from http://www.ushsr.com/ushsrmap.html

Union International de Chemin de fer (UIC) Leaflet 776-2, (2nd Edition): Design requirements for rail-bridges based on interaction phenomena between train, track and bridge. UIC, Paris, 2009.

Veletsos, A.S. and Huang, T.: Analysis of dynamic response of highway bridges. J. Eng Mech Div, Proc ASCE; 96(EM5):593-620, 1970.

Vu-Quoc, L. and Olsson, M.: A computational procedure for interaction of high-speed vehicles on flexible structures without assuming known vehicle nominal motion. Computer Methods in Applied Mechanics and Engineering, 76:207-244, 1989.

Wang, R.T.: Vibration of multi-span Timoshenko beams to a moving force. Journal of Sound and Vibration 207(5):731-742, 1997.

Weaver, W., Timoshenko, S.P. and Young, D.H.: Vibration problems in engineering, 5th edition. New York, John Wiley & Sons, 1990.

Willis, R.: Appendix to the Report of the Commissions Appointed to Inquire into the Application of Iron to Railway Structures. H. M. Stationery Office, 1849.

Wiriyachai A., Chu, K.H., and Garg, V.K.: Bridge impact due to wheel and track irregularities. Journal of Engineering Mechanics, 108(4):648-666, 1982.

Wu, J.S. and Dai, C.W.: Dynamic responses of multi-span non-uniform beam due to moving loads. Journal of Structural Engineering, ASCE 113(3):458-474, 1987.

Wu, Y.S., Yang, Y.B. and Yau, J.D.: Three-dimensional analysis of train-rail-bridge interaction problems. Vehicle System Dynamics, 36 (1):1-35, 2001.

Wu, Y.S. and Yang, Y.B.: Steady-state response and riding comfort of trains moving over a series of simply supported bridges. Engineering Structures 25:251-265, 2003.

Xia, H., De Roeck, G., Zhang, H.R. and Zhang, N.: Dynamic analysis of train-bridge system and its application in steel girder reinforcement. Computers & Structures 79(21–22):1851–1860, 2001.

Xia, H., Zhang, N. and De Roeck, G.: Dynamic analysis of high speed railway bridge under articulated trains. Computers & Structures 81(26-27):2467-2478, 2003.

Xia, H., Guo, W., Wu, X., Pi, Y.L., and Bradford, M.A.: Lateral dynamic interaction analysis of a train–girder–pier system. Journal of Sound and Vibration, 318 (4-5):927-942, 2008.

Yang, F. and Fonder, G.: An iterative solution method for dynamic response of bridge-vehicles systems. Earthquake Engineering and Structural Dynamics, 25 (2):195-215, 1996.

Yang, Y.B. and Lin, B.H.: Vehicle-bridge interaction analysis by dynamic condensation method. Journal of Structural Engineering, 121(11):1636-1643, 1995.

Yang, Y.B. and Yau, J.D.: Vehicle-bridge interaction element for dynamic analysis. Journal of Structural Engineering, 123(11):1512-1518, 1997.

Yang, Y.B., Yau, J.D. and Hsu, L.C.: Vibration of simple beams due to trains moving at high speeds. Engineering Structures, 19(11):936-944, 1997.

Yang, Y.B., Chang, C.H. and Yau, J.D.: An element for analyzing vehicle-bridge systems considering vehicle's pitching effect. Int. J. Num. Meth. Eng. 46:1031-1047, 1999.

Yang, Y.B. and Wu, Y.S.: A versatile element for analyzing vehicle-bridge interaction response. Engineering Structures, 23 (5):452-469, 2001.

Yang, Y.B., Yau, J.D. and Wu, Y.S.: Vehicle-bridge interaction dynamics with applications to high- speed railways. Singapore, World Scientific Publishing Co., 2004.

Yau, J.D., Wu, Y.S. and Yang, Y.B.: Impact responses of bridges with elastic bearings to moving loads. Journal of Sound and Vibration, 248(1):9-30, 2001.

Zhai, W., and Cai, Z.: Dynamic interaction between a lumped mass vehicle and a discretely supported continuous rail track. Computers and Structures, 63(5):987-997, 1997.

Zhai, W., Wang, K. and Cai, C.: Fundamentals of vehicle-track coupled dynamics. Vehicle System Dynamics 47 (11):1349-1376, 2009.

Zhang, Q.L., Vrouwenvelder, A. and Wardenier, J.: Numerical simulation of train-bridge interactive dynamics. Computers & Structures, 79:1059-1075, 2001.

Zheng, D.Y., Cheung, Y.K., Au, F.T.K. and Cheng, Y.S.: Vibration of multi-span non-uniform bridge under moving loads by using modified beam vibration functions. Journal of Sound and Vibration 212:455-467, 1998.

APPENDICES

Appendix A

SEMI-ANALYTICAL EQUATIONS OF VEHICLE-BRIDGE INTERACTION

A.1 Equations Relating Responses of Wheel *j* and Bridge at contact Points

With no-jump condition, the equations, in function of time, relating the wheels' vertical deflection, velocity and accelerations given by

$$y_{wj}(t) = y_b(t)\text{Sin}\left[\frac{\pi(vt - x_j)}{L}\right] \tag{A.1}$$

$$\dot{y}_{wj}(t) = y_b(t)\left(\frac{\pi v}{L}\right)\text{Cos}\left[\frac{\pi(vt - x_j)}{L}\right] + \dot{y}_b(t)\text{Sin}\left[\frac{\pi(vt - x_j)}{L}\right] \tag{A.2}$$

$$\begin{aligned}\ddot{y}_{wj}(t) = {} & \ddot{y}_b(t)\text{Sin}\left[\frac{\pi(vt - x_j)}{L}\right] + 2\dot{y}_b(t)\left(\frac{\pi v}{L}\right)\text{Cos}\left[\frac{\pi(vt - x_j)}{L}\right] \\ & - y_b(t)\left(\frac{\pi v}{L}\right)^2\text{Sin}\left[\frac{\pi(vt - x_j)}{L}\right]\end{aligned} \tag{A.3}$$

The position x_j of the wheel j is measured from the first leading wheel.

A.2 Differential Equations of Motion of the Vehicle in the Time-Domain

Substituting equations (A.1) through (A.2) into equations (3.3.1) through (3.3.6), the following equations in the time domain describe the motion of the vehicle's remaining 6 degrees of freedom after condensing the wheels' degrees of freedom to the bridge's degree of freedom at the contact points.

APPENDIX (Continued)

$$m_c\ddot{y}_c(t) + 2c_s\dot{y}_c(t) - c_s\dot{y}_{t1}(t) - c_s\dot{y}_{t2}(t) + 2k_s y_c(t) - k_s y_{t1}(t) - k_s y_{t2}(t) = 0 \tag{A.4}$$

$$\begin{aligned} J_c\ddot{\theta}_c(t) &+ 2c_s L_c^2\dot{\theta}_c(t) - c_s L_c\dot{y}_{t1}(t) + c_s L_c\dot{y}_{t2}(t) + 2k_s L_c^2\theta_c(t) - k_s L_c y_{t1}(t) \\ &+ k_s L_c y_{t2}(t) = 0 \end{aligned} \tag{A.5}$$

$$\begin{aligned} m_t\ddot{y}_{t1}(t) &- c_s\dot{y}_c(t) - c_s L_c\dot{\theta}_c(t) + \left(c_s + 2c_p\right)\dot{y}_{t1}(t) - k_s y_c(t) - k_s L_c\theta_c(t) \\ &+ \left(k_s + 2k_p\right)y_{t1}(t) \\ &- c_p\sum_{j=1}^{2}\left(y_b(t)\left(\frac{\pi v}{L}\right)\mathrm{Cos}\left[\frac{\pi\left(vt - x_j\right)}{L}\right]\right. \\ &\left. + \dot{y}_b(t)\mathrm{Sin}\left[\frac{\pi\left(vt - x_j\right)}{L}\right]\right)\left[H\left(t - \frac{x_j}{v}\right) - H\left(t - \frac{x_j + L}{v}\right)\right] \\ &- k_p\sum_{j=1}^{2}\left(y_b(t)\mathrm{Sin}\left[\frac{\pi\left(vt - x_j\right)}{L}\right]\right)\left[H\left(t - \frac{x_j}{v}\right) - H\left(t - \frac{x_j + L}{v}\right)\right] = 0 \end{aligned} \tag{A.6}$$

$$\begin{aligned} J_t\ddot{\theta}_{t1}(t) &+ 2c_p L_t^2\dot{\theta}_{t1}(t) + 2k_p L_t^2\theta_{t1}(t) \\ &+ c_p L_t\sum_{j=1}^{2}\left((-1)^j y_b(t)\left(\frac{\pi v}{L}\right)\mathrm{Cos}\left[\frac{\pi\left(vt - x_j\right)}{L}\right]\right. \\ &\left. + \dot{y}_b(t)\mathrm{Sin}\left[\frac{\pi\left(vt - x_j\right)}{L}\right]\right)\left[H\left(t - \frac{x_j}{v}\right) - H\left(t - \frac{x_j + L}{v}\right)\right] \\ &+ k_p L_t\sum_{j=1}^{2}\left((-1)^j y_b(t)\mathrm{Sin}\left[\frac{\pi\left(vt - x_j\right)}{L}\right]\right)\left[H\left(t - \frac{x_j}{v}\right) - H\left(t - \frac{x_j + L}{v}\right)\right] \\ &= 0 \end{aligned} \tag{A.7}$$

APPENDIX (Continued)

$$
\begin{aligned}
&m_t\ddot{y}_{t2}(t) - c_s\dot{y}_c(t) + c_sL_c\dot{\theta}_c(t) + \left(c_s + 2c_p\right)\dot{y}_{t2}(t) - k_sy_c(t) + k_sL_c\theta_c(t) \\
&\quad + \left(k_s + 2k_p\right)y_{t2}(t) \\
&\quad - c_p\sum_{j=3}^{4}\left(y_b(t)\left(\frac{\pi v}{L}\right)\mathrm{Cos}\left[\frac{\pi\left(vt - x_j\right)}{L}\right]\right. \\
&\quad \left. + \dot{y}_b(t)\mathrm{Sin}\left[\frac{\pi\left(vt - x_j\right)}{L}\right]\right)\left[H\left(t - \frac{x_j}{v}\right) - H\left(t - \frac{x_j + L}{v}\right)\right] \\
&\quad - k_p\sum_{i=3}^{4}\left(y_b(t)\mathrm{Sin}\left[\frac{\pi\left(vt - x_j\right)}{L}\right]\right)\left[H\left(t - \frac{x_j}{v}\right) - H\left(t - \frac{x_j + L}{v}\right)\right] = 0
\end{aligned}
\tag{A.8}
$$

$$
\begin{aligned}
&J_t\ddot{\theta}_{t2}(t) + 2c_pL_t^2\dot{\theta}_{t2}(t) + 2k_pL_t^2\theta_{t2}(t) \\
&\quad + c_pL_t\sum_{j=3}^{4}\left((-1)^j y_b(t)\left(\frac{\pi v}{L}\right)\mathrm{Cos}\left[\frac{\pi\left(vt - x_j\right)}{L}\right]\right. \\
&\quad \left. + \dot{y}_b(t)\mathrm{Sin}\left[\frac{\pi\left(vt - x_j\right)}{L}\right]\right)\left[H\left(t - \frac{x_j}{v}\right) - H\left(t - \frac{x_j + L}{v}\right)\right] \\
&\quad + k_pL_t\sum_{j=3}^{4}\left((-1)^j y_b(t)\mathrm{Sin}\left[\frac{\pi\left(vt - x_j\right)}{L}\right]\right)\left[H\left(t - \frac{x_j}{v}\right) - H\left(t - \frac{x_j + L}{v}\right)\right] \\
&\quad = 0
\end{aligned}
\tag{A.9}
$$

A.2 Differential Equations of Motion of the Bridge Mid-span in the Time-Domain

The simply supported bridge mid-span vertical motion is described by the following modal superposition equation with the first mode considered.

APPENDIX (Continued)

$$\left(\frac{m_b L}{2} + m_w \sum_{j=1}^{4} Sin^2\left[\frac{\pi(vt - x_j}{L}\right]\left[H\left(t - \frac{x_j}{v}\right) - H\left(t - \frac{x_j + L}{v}\right)\right]\right)\ddot{y}_b(t) + c_b\dot{y}_b(t)$$

$$+ \left(\frac{m_b L\omega_1^2}{2}\right) y_b(t)$$

$$= -\sum_{j=1}^{2}\Bigg(f_{stj}$$

$$+ m_w\left(\ddot{y}_b(t)\text{Sin}\left[\frac{\pi(vt - x_j)}{L}\right] + 2\dot{y}_b(t)\left(\frac{\pi v}{L}\right)\text{Cos}\left[\frac{\pi(vt - x_j)}{L}\right]\right.$$

$$\left. - y_b(t)\left(\frac{\pi v}{L}\right)^2 \text{Sin}\left[\frac{\pi(vt - x_j)}{L}\right]\right) - c_p\dot{y}_{t1}(t) + (-1)^j c_p L_t\dot{\theta}_{t1}(t) - k_p y_{t1}(t)$$

$$+ (-1)^j k_p L_t\theta_{t2}(t) + c_p\left(y_b(t)\left(\frac{\pi v}{L}\right)\text{Cos}\left[\frac{\pi(vt - x_j)}{L}\right] + \dot{y}_b(t)\text{Sin}\left[\frac{\pi(vt - x_j)}{L}\right]\right)$$

$$\left. + k_p\left(y_b(t)\text{Sin}\left[\frac{\pi(vt - x_j)}{L}\right]\right)\right)\text{Sin}\left[\frac{\pi(vt - x_j)}{L}\right]\left[H\left(t - \frac{x_j}{v}\right) - H\left(t - \frac{x_j + L}{v}\right)\right] \quad \text{(A.10)}$$

$$-\sum_{j=3}^{4}\Bigg(f_{stj}$$

$$+ m_w\left(\ddot{y}_b(t)\text{Sin}\left[\frac{\pi(vt - x_j)}{L}\right] + 2\dot{y}_b(t)\left(\frac{\pi v}{L}\right)\text{Cos}\left[\frac{\pi(vt - x_j)}{L}\right]\right.$$

$$\left. - y_b(t)\left(\frac{\pi v}{L}\right)^2 \text{Sin}\left[\frac{\pi(vt - x_j)}{L}\right]\right) - c_p\dot{y}_{t2}(t) + (-1)^j c_p L_t\dot{\theta}_{t2}(t) - k_p y_{t2}(t)$$

$$+ (-1)^j k_p L_t\theta_{t2}(t) + c_p\left(y_b(t)\left(\frac{\pi v}{L}\right)\text{Cos}\left[\frac{\pi(vt - x_j)}{L}\right] + \dot{y}_b(t)\text{Sin}\left[\frac{\pi(vt - x_j)}{L}\right]\right)$$

$$\left. + k_p\left(y_b(t)\text{Sin}\left[\frac{\pi(vt - x_j)}{L}\right]\right)\right)\text{Sin}\left[\frac{\pi(vt - x_j)}{L}\right]\left[H\left(t - \frac{x_j}{v}\right) - H\left(t - \frac{x_j + L}{v}\right)\right]$$

$$\{f_{st}\} = \left(\frac{1}{4}m_c + \frac{1}{2}m_t + m_w\right) g\langle 1 \;\; 1 \;\; 1 \;\; 1\rangle^T \quad \text{(A.11)}$$

and the parameter g is the gravitational constant.

Appendix B

Permission to re-use author's previously published ASME conference papers in this dissertation.

Beth Darchi <DarchiB@asme.org> Thu, Oct 13, 2016 at 2:55 F
To: Said Nour <snour2@uic.edu>

Dear Prof. Nour,
It is our pleasure to grant you permission to **use all or any part of** the following ASME papers:

- Effects of Different Models on Natural Frequencies of Short Span Bridges Used in High Speed Rail, by Said I. Nour and Mohsen A. Issa, Paper No. JRC2015-5772
- High Speed Rail Short Bridge-Track-Train Interaction Based on the Decoupled Equations of Motion in the Finite Element Domain, by Said I. Nour and Mohsen A. Issa, Paper No. JRC2016-5785

cited in your letter for inclusion in your PhD Dissertation entitled Numerical Model of Interaction and Behavior of Short Span High Speed Rail Bridge on Viscoelastic Supports to be published by University of Illinois at Chicago.

Permission is granted for the specific use as stated herein and does not permit further use of the materials without proper authorization. Proper attribution must be made to the author(s) of the materials. **Please note:** if any or all of the figures and/or Tables are of another source, permission should be granted from that outside source or include the reference of the original source. ASME does not grant permission for outside source material that may be referenced in the ASME works.

As is customary, we request that you ensure full acknowledgment of this material, the author(s), source and ASME as original publisher. Acknowledgment must be retained on all pages printed and distributed.

Many thanks for your interest in ASME publications.

Sincerely,

Beth Darchi
Publishing Administrator
ASME
2 Park Avenue, 6th Floor
New York, NY 10016-5990
Tel 1.212.591.7700
darchib@asme.org

VITA

Said Ibrahim Nour

EDUCATION

DOCTOR OF PHILOSOPHY | EXPECTED GRADUATION: 2016 | UNIVERSITY OF ILLINOIS AT CHICAGO

- Field: Civil Engineering
- Dissertation: Numerical Model of Interaction and Behavior of Short Span High Speed Rail Bridge on Viscoelastic Supports

MASTER OF SCIENCE | 2001 | UNIVERSITY OF WINDSOR

- Field: Civil Engineering
- Thesis: Load Distribution in Curved Composite Concrete Deck-Steel Multiple-Spine Box Girder Bridges
- Coursework: Structural Design, Foundation Design, Soil Analysis, Earthquake Engineering, Wind Loading.

MASTER OF ENGINEERING | 1999 | UNIVERSITY OF TORONTO

- Field: Civil Engineering
- Coursework: Bridge Engineering, Structural Dynamics, Steel Design, Rock Mechanics, earthwork stabilization

BACHELOR OF ENGINEERING | 1998 | RYERSON POLYTECHNIC UNIVERSITY

- Field: Civil Engineering
- Thesis: Analysis of Coupled Reinforced Concrete Shear Walls.
- Coursework: Environmental Engineering, Finite Element Analysis, Concrete Mix and Design, Soil Investigation, Hydrology, Engineering Economy, Transportation Infrastructures, Marine Structure Analysis and Design

SPECIALIZED TRAINING AND CERTIFICATIONS

NEW DIRECTIONS FOR FLORIDA POST-TENSIONED BRIDGES: FINAL PHASE OF IMPLEMENTATION

July 2003. Florida Department of Transportation, Tallahassee, Florida, USA.

STRUCTURAL STRENGTHENING USING CARBON FIBER REINFORCED POLYMERS (CFRP)

June 2004. SIKA Corporation Inc., Lyndhurst, New Jersey, USA.

NON-DESTRUCTIVE TESTING OF CONCRETE STRUCTURES

December 2004. Geophysical Survey Systems Inc., North Salem, New Hampshire, USA

BRIDGE REHABILITATION

February 2005. American Society of Civil Engineers, Amarillo, Texas, USA.

CORROSION ENGINEER CERTIFICATION

June 2005. National Association of Corrosion Engineers, Houston, Texas, USA.

PROFESSIONAL EXPERIENCE

SENIOR CIVIL ENGINEER | DYWIDAG SYSTEMS INTERNATIONAL USA INC. | APRIL 2010-CURRENT

- Engineering tasks in the analysis and design of assigned infrastructure components. Special projects expert.
- Supervision of shop drawing preparation and submittal; Research, Development and Testing of Construction Systems
- Resolution of Technical Issues with Contractors and Client Engineers.

CIVIL ENGINEER | DYWIDAG SYSTEMS INTERNATIONAL USA INC. | MARCH 2003-APRIL 2010

- Technical Assistance to Sales Personnel and Project Managers
- Design Calculations related to assigned projects.
- Participation in Industry Conferences and occasional presentation of case studies with unique value engineering.

DESIGN ENGINEER | CARL WALKER INC. | FEBRUARY 2002-DECEMBER 2002

- Analysis/Design of High Rise Buildings and Parking Garages
- Preparation of Project Specification. Approval of Shop Drawings and Construction Documents..

PROJECT ENGINEER | VSTRUCTURAL, LLC | JANUARY 2001-FEBRUARY 2002

- Design and Analysis of Post-Tensioned Concrete Buildings, Tanks and Bridges.
- Construction material take-off, Proposal and Bid Preparation. Managing Small Jobs.

RESEARCH AND TEACHING ASSISTANT| UNIVERSITY OF WINDSOR | SEPTEMBER 1999-DECEMBER 2000

- Assisted in teaching undergraduate courses: Highway Design, Soil Mechanics, Plastic Design, Engineering Economy
- Developed bridge design procedures for curved composite concrete-steel box girder bridges.

PUBLICATION AUTHORSHIP

HIGH SPEED RAIL SHORT BRIDGE-TRACK-TRAIN INTERACTION BASED ON THE DECOUPLED EQUATIONS OF MOTION IN THE FINITE ELEMENT DOMAIN

ASME 2016 Joint Rail Conference Proceedings, Paper No. JRC2015-5785, Columbia, SC, USA, April 12-15, 2016

EFFECTS OF DIFFERENT MODELS ON NATURAL FREQUENCIES OF SHORT SPAN BRIDGES USED IN HIGH SPEED RAIL

ASME 2015 Joint Rail Conference Proceedings, Paper No. JRC2015-5772, San Jose, CA, USA, March 23-26, 2015

ANTI-SUFFOCATION INCLINED SLEEP AID FOR INFANTS WITH REFLUX OR VOMITING

United States Patent Number US 8082614 B2, December 2011.

GUIDE FOR THE SELECTION OF STRENGTHENING SYSTEMS FOR CONCRETE STRUCTURES

International Concrete Repair Institute (ICRI), February 2006.

TESTING/EVALUATION AND GROUT REMEDIATION OF POST-TENSIONING TENDONS FOR BRIDGES

Post-Tensioning Institute (PTI), July 2006.

DESIGN FOR SHEAR IN CURVED COMPOSITE MULTIPLE STEEL BOX GIRDER BRIDGES

Journal of Bridge Engineering, Volume 8, Issue 3, pp. 144-152, May 2003.